

Neuroimaging study of post-stroke cerebral edema

Edited by

Sheng Zhang, Peiyu Huang, Gabriel Broocks,
Chengcheng Zhu and Christopher Blair

Published in

Frontiers in Neurology



FRONTIERS EBOOK COPYRIGHT STATEMENT

The copyright in the text of individual articles in this ebook is the property of their respective authors or their respective institutions or funders. The copyright in graphics and images within each article may be subject to copyright of other parties. In both cases this is subject to a license granted to Frontiers.

The compilation of articles constituting this ebook is the property of Frontiers.

Each article within this ebook, and the ebook itself, are published under the most recent version of the Creative Commons CC-BY licence. The version current at the date of publication of this ebook is CC-BY 4.0. If the CC-BY licence is updated, the licence granted by Frontiers is automatically updated to the new version.

When exercising any right under the CC-BY licence, Frontiers must be attributed as the original publisher of the article or ebook, as applicable.

Authors have the responsibility of ensuring that any graphics or other materials which are the property of others may be included in the CC-BY licence, but this should be checked before relying on the CC-BY licence to reproduce those materials. Any copyright notices relating to those materials must be complied with.

Copyright and source acknowledgement notices may not be removed and must be displayed in any copy, derivative work or partial copy which includes the elements in question.

All copyright, and all rights therein, are protected by national and international copyright laws. The above represents a summary only. For further information please read Frontiers' Conditions for Website Use and Copyright Statement, and the applicable CC-BY licence.

ISSN 1664-8714
ISBN 978-2-83251-972-1
DOI 10.3389/978-2-83251-972-1

About Frontiers

Frontiers is more than just an open access publisher of scholarly articles: it is a pioneering approach to the world of academia, radically improving the way scholarly research is managed. The grand vision of Frontiers is a world where all people have an equal opportunity to seek, share and generate knowledge. Frontiers provides immediate and permanent online open access to all its publications, but this alone is not enough to realize our grand goals.

Frontiers journal series

The Frontiers journal series is a multi-tier and interdisciplinary set of open-access, online journals, promising a paradigm shift from the current review, selection and dissemination processes in academic publishing. All Frontiers journals are driven by researchers for researchers; therefore, they constitute a service to the scholarly community. At the same time, the *Frontiers journal series* operates on a revolutionary invention, the tiered publishing system, initially addressing specific communities of scholars, and gradually climbing up to broader public understanding, thus serving the interests of the lay society, too.

Dedication to quality

Each Frontiers article is a landmark of the highest quality, thanks to genuinely collaborative interactions between authors and review editors, who include some of the world's best academicians. Research must be certified by peers before entering a stream of knowledge that may eventually reach the public - and shape society; therefore, Frontiers only applies the most rigorous and unbiased reviews. Frontiers revolutionizes research publishing by freely delivering the most outstanding research, evaluated with no bias from both the academic and social point of view. By applying the most advanced information technologies, Frontiers is catapulting scholarly publishing into a new generation.

What are Frontiers Research Topics?

Frontiers Research Topics are very popular trademarks of the *Frontiers journals series*: they are collections of at least ten articles, all centered on a particular subject. With their unique mix of varied contributions from Original Research to Review Articles, Frontiers Research Topics unify the most influential researchers, the latest key findings and historical advances in a hot research area.

Find out more on how to host your own Frontiers Research Topic or contribute to one as an author by contacting the Frontiers editorial office: frontiersin.org/about/contact

Neuroimaging study of post-stroke cerebral edema

Topic editors

Sheng Zhang — Zhejiang Provincial People's Hospital, China

Peiyu Huang — Zhejiang University, China

Gabriel Broocks — University of Hamburg, Germany

Chengcheng Zhu — University of Washington, United States

Christopher Blair — Liverpool Hospital, Australia

Citation

Zhang, S., Huang, P., Broocks, G., Zhu, C., Blair, C., eds. (2023). *Neuroimaging study of post-stroke cerebral edema*. Lausanne: Frontiers Media SA.
doi: 10.3389/978-2-83251-972-1

Table of contents

- 05 **Editorial: Neuroimaging study of post-stroke cerebral edema**
Sheng Zhang, Chengcheng Zhu, Gabriel Broocks, Peiyu Huang and Christopher Blair
- 08 **Evaluation and Prediction of Post-stroke Cerebral Edema Based on Neuroimaging**
Xiaocheng Zhang, Peiyu Huang and Ruiting Zhang
- 18 **Evaluation of Intracranial Hypertension in Patients With Hypertensive Intracerebral Hemorrhage Using Texture Analysis**
Yingchi Shan, Yihua Li, Xiang Wu, Jiaqi Liu, Guoqing Zhang, Yajun Xue and Guoyi Gao
- 25 **Impaired Glymphatic Transport Kinetics Following Induced Acute Ischemic Brain Edema in a Mouse pMCAO Model**
Jianying Zhang, Hongchen Zhao, Yang Xue, Yiqi Liu, Guohang Fan, He Wang, Qiang Dong and Wenjie Cao
- 38 **Early Edema Within the Ischemic Core Is Time-Dependent and Associated With Functional Outcomes of Acute Ischemic Stroke Patients**
Qing Han, Jianhong Yang, Xiang Gao, Jichuan Li, Yuefei Wu, Yao Xu, Qing Shang, Mark W. Parsons and Longting Lin
- 47 **Filling Defect of Ipsilateral Transverse Sinus in Acute Large Artery Occlusion**
Yi Chen, Sheng Zhang, Shenqiang Yan, Meixia Zhang, Ruiting Zhang, Feina Shi, David S. Liebeskind, Mark Parsons and Min Lou
- 56 **The Recipient Vessel Hemodynamic Features Affect the Occurrence of Cerebral Edema in Moyamoya Disease After Surgical Revascularization: A Single-Center Retrospective Study**
Liang Xu, Yin Li, Yun Tong, Jun-wen Hu, Xu-chao He, Xiong-jie Fu, Guo-Yang Zhou, Yang Cao, Xiao-bo Yu, Hang Zhou, Chao-ran Xu and Lin Wang
- 64 **Automated Measurement of Net Water Uptake From Baseline and Follow-Up CTs in Patients With Large Vessel Occlusion Stroke**
Atul Kumar, Yasheng Chen, Aaron Corbin, Ali Hamzehloo, Amin Abedini, Zeynep Vardar, Grace Carey, Kunal Bhatia, Laura Heitsch, Jamal J. Derakhshan, Jin-Moo Lee and Rajat Dhar
- 75 **Association Between Post-procedure Cerebral Blood Flow Velocity and Severity of Brain Edema in Acute Ischemic Stroke With Early Endovascular Therapy**
Jie Pan, Huadong Wu, Tingting Wu, Yu Geng and Ruozhen Yuan

- 84 **Net water uptake, a neuroimaging marker of early brain edema, as a predictor of symptomatic intracranial hemorrhage after acute ischemic stroke**
Tianqi Xu, Jianhong Yang, Qing Han, Yuefei Wu, Xiang Gao, Yao Xu, Yi Huang, Aiju Wang, Mark W. Parsons and Longting Lin
- 93 **The application value of CT radiomics features in predicting pressure amplitude correlation index in patients with severe traumatic brain injury**
Jiaqi Liu, Yingchi Shan and Guoyi Gao
- 100 **Risk factors of late lesion growth after acute ischemic stroke treatment**
Praneeta Konduri, Amber Bucker, Anna Boers, Bruna Dutra, Noor Samuels, Kilian Treurniet, Olvert Berkhemer, Albert Yoo, Wim van Zwam, Robert van Oostenbrugge, Aad van der Lugt, Diederik Dippel, Yvo Roos, Joost Bot, Charles Majoie, Henk Marquering and the MR CLEAN Trial Investigators (Multicenter Randomized Clinical Trial of Endovascular Treatment for Acute Ischemic Stroke in the Netherlands)
- 108 **Bloody fluids located between the temporal muscle and targeted cerebral cortex affect the establishment of indirect collaterals in Moyamoya disease with surgical bypass: A case-control study**
Yin Li, Jun-wen Hu, Xu-chao He, Yang Cao, Xiao-bo Yu, Xiong-jie Fu, Hang Zhou, Li-bin Hu, Liang Xu, Chao-ran Xu, Yong-jie Wang and Lin Wang
- 117 **Radiomics features from perihematoma edema for prediction of prognosis in the patients with basal ganglia hemorrhage**
Peng Zhou, Quanye Sun, Gesheng Song, Zexiang Liu, Jianfeng Qi, Xuhui Yuan, Xu Wang, Shaofeng Yan, Jianyang Du, Zhengjun Dai, Jianjun Wang and Shaoshan Hu
- 128 **Quantitative pupillometry and radiographic markers of intracranial midline shift: A pilot study**
Ivy So Yeon Kim, Oluwafemi O. Balogun, Brenton R. Prescott, Hanife Saglam, DaiWai M. Olson, Kinley Speir, Sonja E. Stutzman, Nathan Schneider, Veronica Aguilera, Bethany L. Lussier, Stelios M. Smirnakis, Josée Dupuis, Asim Mian, David M. Greer and Charlene J. Ong
- 139 **Large mismatch profile predicts rapidly progressing brain edema in acute anterior circulation large vessel occlusion patients undergoing endovascular thrombectomy**
Yanqi Shao, Xinyi Chen, Huiyuan Wang, Yafei Shang, Jie Xu, Jinshi Zhang, Peng Wang and Yu Geng



OPEN ACCESS

EDITED AND REVIEWED BY

Brunno Machado De Campos,
State University of Campinas, Brazil

*CORRESPONDENCE

Sheng Zhang
✉ zhangsheng@hmc.edu.cn

SPECIALTY SECTION

This article was submitted to
Applied Neuroimaging,
a section of the journal
Frontiers in Neurology

RECEIVED 16 February 2023

ACCEPTED 23 February 2023

PUBLISHED 07 March 2023

CITATION

Zhang S, Zhu C, Brooks G, Huang P and
Blair C (2023) Editorial: Neuroimaging study of
post-stroke cerebral edema.
Front. Neurol. 14:1167275.
doi: 10.3389/fneur.2023.1167275

COPYRIGHT

© 2023 Zhang, Zhu, Brooks, Huang and Blair.
This is an open-access article distributed under
the terms of the [Creative Commons Attribution
License \(CC BY\)](#). The use, distribution or
reproduction in other forums is permitted,
provided the original author(s) and the
copyright owner(s) are credited and that the
original publication in this journal is cited, in
accordance with accepted academic practice.
No use, distribution or reproduction is
permitted which does not comply with these
terms.

Editorial: Neuroimaging study of post-stroke cerebral edema

Sheng Zhang^{1*}, Chengcheng Zhu², Gabriel Brooks³,
Peiyu Huang⁴ and Christopher Blair⁵

¹Department of Neurology, Center for Rehabilitation Medicine, People's Hospital of Hangzhou Medical College, Zhejiang Provincial People's Hospital, Hangzhou, China, ²Department of Radiology, University of Washington, Seattle, WA, United States, ³Department of Diagnostic and Interventional Neuroradiology, University Medical Center Hamburg-Eppendorf, Hamburg, Germany, ⁴Department of Radiology, School of Medicine, The Second Affiliated Hospital of Zhejiang University, Hangzhou, China, ⁵Sydney Brain Centre, Ingham Institute for Applied Medical Research Senior Lecturer SWS Clinical Campus, Faculty of Medicine and Health, UNSW Sydney, Sydney, NSW, Australia

KEYWORDS

stroke, edema, imaging, identification, prediction

Editorial on the Research Topic

Neuroimaging study of post-stroke cerebral edema

Stroke is a leading cause of death and long-term disability worldwide, affecting 10 million people each year (1, 2). Brain edema is one of the most harmful complications of stroke and can lead to further ischemic damage of brain tissue. Therefore, it is of great clinical importance to understand the causes of brain edema and identify biomarkers that can predict its occurrence. Imaging plays a crucial role in studying brain edema *in vivo*.

Multi-modal CT scans

Non-contrast CT scan

Since Brooks et al. developed quantitative net water uptake (NWU) based on non-contrast brain CT scans, several studies have been conducted on NWU in the field of brain edema (3). Two studies from Ningbo First People's Hospital (by Han et al. and Xu T. et al.) found that the occurrence of early edema in the ischemic core, as quantified by NWU, was time-dependent and correlated with the functional outcome of acute ischemic stroke patients. In addition, the NWU core/NWU penumbra ratio had good predictive power for the occurrence of symptomatic intracranial hemorrhage after endovascular therapy. Kumar et al. developed a method to automatically quantify the infarct area and NWU from brain non-contrast CT scans using deep learning, which may aid in exploring the factors influencing edema evolution in stroke patients in large-scale studies in the future.

In addition to NWU-related studies, Zhou et al. compiled a clinical-radiomics nomogram to characterize the relationship between brain edema and prognosis in patients with basal ganglia hemorrhage. They found that the radiomics features of peripheral hemorrhagic edema on non-contrast CT scans in patients with basal ganglia hemorrhage predicted patient outcomes. Application of this clinical-radiomic nomogram may therefore assist with individualizing clinical treatment decisions for these patients.

CT perfusion (CTP) and CTP-derived 4-dimensional CT angiography (4D-CTA)

Shao et al. found that in patients who underwent successful endovascular therapy, a large mismatch ratio at baseline was a protective factor for rapidly progressive brain edema. Konduri et al. observed that collateral volume was the key factor affecting midline shift. Using CTP-reconstructed 4D-CTA, Chen et al. showed that an ipsilateral transverse sinus filling defect was related to the progression of brain edema and poor prognosis after stroke. Li et al. found that the volume of bloody fluids located between the temporal muscle and the targeted cerebral cortex, as calculated using 3D slicer software on non-contrast CT or CTA performed within 3 days post-surgery, affected the establishment of indirect collaterals in patients with moyamoya disease undergoing surgical bypass.

Contrast-enhanced brain MRI

Intraventricular injection of a contrast agent and observation of cerebrospinal fluid metabolism by enhanced MRI is a recently validated method for evaluating glymphatic transport function in recent years. Zhang et al. studied glymphatic function using enhanced MRI (11.7T) by injecting gadolinium benzoate (BOPTA Gd) into the cistern magna of mice. They showed that the decrease in glymphatic clearance after stroke was related to cytotoxic edema caused by middle cerebral artery occlusion (MCAO), and that, the cytotoxic edema was related to the depolarization of aquaporin-4 in both the parenchyma PVSs and periventricular zone.

Hemodynamics imaging

Pan et al. found that the affected-to-contralateral ratio of systolic cerebral blood flow velocity (CBFV) and mean CBFV were both independently associated with severe brain edema. They concluded that the affected-to-contralateral ratio of CBFV after endovascular treatment (EVT) may be a promising predictor of brain edema severity in patients who received EVT. Xu L. et al. found that cerebral vascular hemodynamic characteristics based on digital subtraction angiography (DSA), including flow direction and hemodynamic sources, can predict post-operative brain edema in surgically-managed Moyamoya disease.

Texture analysis and machine learning

Shan et al. performed an in-depth analysis of CT images based on texture analysis, demonstrating its great potential in the non-invasive assessment of intracranial hypertension. Liu et al. established a machine learning model based on CT radiomic features and verified that it can predict the pressure amplitude correlation index (RAP) level of patients with severe traumatic brain injury, also providing a non-invasive method for intracranial pressure monitoring.

Other research

Making ingenious use of the well-established clinical observation that pupil size reflects midbrain compression and midline shift in patients with ischemic stroke, Kim et al. used automatic infrared pupillary instruments to perform quantitative pupil observations on NICU patients and developed the neuropupillary index (NPI). Their results showed that the NPI had the potential to correlate with the degree of midline/pineal shift, suggesting that this technology could be used to monitor the occurrence and progression of brain edema in a high-dependency setting.

Future directions

Brain edema after stroke is an active area of research that has seen increasing attention in recent years. In this Research Topic, 15 articles were published, including 1 review and 14 original studies. Based on these studies, we aim to further investigate the mechanism of brain edema and the clinical applications of imaging markers in the future, with the following core objectives. Firstly, most current studies are cross-sectional and have limited sample sizes, so future longitudinal studies and randomized controlled trials are needed to establish imaging markers that can predict brain edema in stroke patients. Secondly, as well as having a short scan time multi-model CT has the advantage of providing ample information about brain tissue and vessels, making it useful for evaluating brain edema in the early stages of stroke. However, most of these markers have not been prospectively verified. The same issue applies to the study of hemodynamic imaging using DSA and transcranial Doppler (TCD). Despite the great potential of hemodynamics analysis based on DSA and TCD, additional hemodynamic-related markers need to be developed and validated in future studies. Machine learning has great potential for accelerating imaging analysis, reconstructing images, and automating image analysis, but it is likely to have the greatest utility when applied to imaging markers that have been prospectively verified or have high consistency in manual measurement. Finally, research into the relationship between post-stroke glymphatic clearance and brain edema has become popular since 2020 (4). In this Research Topic, one study showed that post-stroke brain edema is related to the decline of glymphatic clearance function. Currently, there are very few imaging markers (especially non-invasive imaging) that can directly measure glymphatic function. Technical advancement in this field may provide tools for understanding the association between glymphatic function and brain edema. In particular, adjuvant treatment strategies for ischemic stroke beyond reperfusion are of significant clinical interest. To fully realize the potential of neuroprotectants and anti-edema drugs currently being tested in clinical trials neuroimaging tools, like those described here, are likely to be instrumental in assessing treatment effects and guiding optimal use in clinical practice.

Author contributions

SZ was responsible for writing the editorial. CZ, GB, PH, and CB were responsible for proofreading, editing, and reviewing. All authors contributed to the article and approved the submitted version.

Funding

SZ was supported by the Zhejiang Provincial Natural Science Foundation of China Grants No. LGF22H090020 and the Medical Health Science and Technology Project of Zhejiang Provincial Health Commission Grants No. 2022KY600.

Acknowledgments

I would like to thank Prof. Ruiting Zhang and Prof. Longting Lin for their help in recruiting editors and establishing this

Research Topic. Dr. Zheyu Zhang for her assistance in the process of draft preparation.

Conflict of interest

The authors declare that the research was conducted in the absence of any commercial or financial relationships that could be construed as a potential conflict of interest.

Publisher's note

All claims expressed in this article are solely those of the authors and do not necessarily represent those of their affiliated organizations, or those of the publisher, the editors and the reviewers. Any product that may be evaluated in this article, or claim that may be made by its manufacturer, is not guaranteed or endorsed by the publisher.

References

1. Benjamin EJ, Muntner P, Alonso A, Bittencourt MS, Callaway CW, Carson AP, et al. Heart disease and stroke statistics-2019 update: a report from the American Heart Association. *Circulation*. (2019) 139:e56–528. doi: 10.1161/CIR.0000000000000659
2. Iadecola C, Anrather J. Stroke research at a crossroad: asking the brain for directions. *Nat Neurosci*. (2011) 14:1363–8. doi: 10.1038/nn.2953
3. Broocks G, Flottmann F, Scheibel A, Aigner A, Faizy TD, Hanning U, et al. Quantitative lesion water uptake in acute stroke computed tomography is a predictor of malignant infarction. *Stroke*. (2018) 49:1906–12. doi: 10.1161/STROKEAHA.118.020507
4. Mestre H, Du T, Sweeney AM, Liu G, Samson AJ, Peng W, et al. Cerebrospinal fluid influx drives acute ischemic tissue swelling. *Science*. (2020) 367:eaax7171. doi: 10.1126/science.aax7171



Evaluation and Prediction of Post-stroke Cerebral Edema Based on Neuroimaging

Xiaocheng Zhang, Peiyu Huang and Ruiting Zhang*

Department of Radiology, School of Medicine, The Second Affiliated Hospital of Zhejiang University, Hangzhou, China

OPEN ACCESS

Edited by:

Volker Rasche,
University of Ulm, Germany

Reviewed by:

J. Marc Simard,
University of Maryland, Baltimore,
United States
Qi Li,
The First Affiliated Hospital of
Chongqing Medical University, China

*Correspondence:

Ruiting Zhang
zhangruitong@zju.edu.cn

Specialty section:

This article was submitted to
Applied Neuroimaging,
a section of the journal
Frontiers in Neurology

Received: 23 August 2021

Accepted: 06 December 2021

Published: 11 January 2022

Citation:

Zhang X, Huang P and Zhang R
(2022) Evaluation and Prediction of
Post-stroke Cerebral Edema Based
on Neuroimaging.
Front. Neurol. 12:763018.
doi: 10.3389/fneur.2021.763018

Cerebral edema is a common complication of acute ischemic stroke that leads to poorer functional outcomes and substantially increases the mortality rate. Given that its negative effects can be reduced by more intensive monitoring and evidence-based interventions, the early identification of patients with a high risk of severe edema is crucial. Neuroimaging is essential for the assessment and prediction of edema. Simple markers, such as midline shift and hypodensity volume on computed tomography, have been used to evaluate edema in clinical trials; however, advanced techniques can be applied to examine the underlying mechanisms. In this study, we aimed to review current imaging tools in the assessment and prediction of cerebral edema to provide guidance for using these methods in clinical practice.

Keywords: ischemic stroke, edema, mechanism, imaging evaluation, predictors

INTRODUCTION

Cerebral edema is a severe complication of acute ischemic stroke; it results in poorer functional outcomes and significantly increases the rate of mortality. During ischemia, excessive fluid accumulates in the intracellular or extracellular spaces of the brain because of the failure of energy-dependent ion transport (1–3) and the destruction of the blood–brain barrier (BBB) (4–6), which leads to tissue swelling and the elevation of intracranial pressure. Cerebral edema can appear several hours after ischemia and may progress over the first few days of stroke onset (7).

Patients with mild to moderate edema can be treated with medication (3, 8, 9). However, for those with malignant edema (ME), the mortality rate can increase up to 80% with conservative treatment (10–12). Timely surgical treatment by early decompressive craniectomy is recommended to reduce mortality (9, 13–15). Thus, the accurate assessment and early prediction of edema can benefit patients by more intensive monitoring and evidence-based interventions.

Neuroimaging examination is essential for the assessment of edema. Midline shift (MLS) has long been established as a marker of severe edema and is known to correlate with clinical deterioration (16–18). However, MLS is insensitive to mild to moderate edema and is thus an unsuitable index for monitoring the condition of patients. Recently, new methods, such as cerebrospinal fluid (CSF) displacement (19, 20) and net water uptake (NWU) (12, 21), have been developed to quantify brain edema at an early stage. Furthermore, magnetic resonance imaging

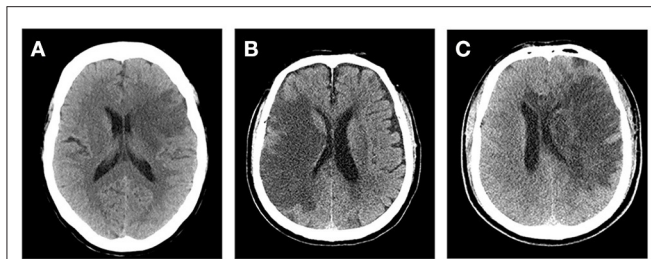


FIGURE 1 | Cerebral edema grades. **(A)** Left frontal lobe and basal ganglia brain swelling, $<1/3$ of the hemisphere. **(B)** Right frontal and parietal lobe brain swelling, $>1/3$ of the hemisphere and without midline shift (MLS). **(C)** Left cerebral hemisphere swelling, $>1/3$ of the hemisphere with MLS.

(MRI) can distinguish cytotoxic edema from ionic edema and vasogenic edema (22, 23), and advanced MRI techniques, such as diffusion tensor imaging, can detect subtle structural changes in brain edema (24). These new methods can be used to quantify less severe edema and may serve as early imaging markers in clinical practice.

Imaging is important in the prediction of edema. Previous research has shown that infarct volume, collateral status, and CSF volume (CSV), among other factors, are closely related to the development of edema (11, 18, 25, 26). However, the predictive values of these indicators often vary across studies (18, 27); moreover, the optimal timing and modality of imaging exams are also under debate.

There have been numerous reviews on post-stroke edema, of which most have focused on the mechanisms of edema with an emphasis on scientific discoveries rather than on clinical applications. In this review, we briefly discuss the mechanisms of post-stroke edema and focus more on current edema assessment methods and neuroimaging predictors.

Our aim was to provide a comprehensive review of imaging tools for the management of edema and provide guidance for clinical practice.

MECHANISM OF EDEMA

Traditionally, cerebral edema after an ischemic stroke includes cytotoxic edema, ionic edema, and vasogenic edema (7). These three processes occur in sequence and are closely interrelated. Cytotoxic edema is the earliest manifestation of brain hydromineral disturbance as a result of changes in ion channel and transporter (e.g., $\text{Na}^+ - \text{K}^+ - 2\text{Cl}^-$ cotransporter and Na-H exchangers) activity during a stroke event (3, 28–31). It attracts ions and water into neurons or astrocytes, which causes intracellular water accumulation and extracellular space reduction without increasing brain tissue volume. Because of the changes in ion concentrations on both sides of the BBB, new gradients are formed; this generates a driving force for an influx of water and ion across the intact BBB into the depleted extracellular space, resulting in ionic edema (32–34). Ischemia can also activate inflammatory mediators and increase oxidative stress (35, 36), both of which lead to BBB disruption. This

event allows plasma proteins and other macromolecules to pass through the BBB from the intravascular space into brain tissue, which further aggravates water influx and results in vasogenic edema. Recently, studies have shown that post-stroke cerebral edema can also be driven by CSF influx through perivascular spaces (37, 38). Although this has not been confirmed clinically, the related mechanisms underlying the structural and functional abnormalities of the brain's glymphatic system following stroke have gathered the interest of researchers.

IMAGING EVALUATION OF CEREBRAL EDEMA

Computed Tomography

Computed tomography (CT) is the most frequently used diagnostic procedure in acute stroke. It is sensitive to net water changes but not fluid shifts among tissue compartments within the brain parenchyma. Therefore, CT is sensitive to ionic and vasogenic edema but not cytotoxic edema because fluid shifts from the vascular to interstitial spaces during the first two processes (22, 39, 40). Experimental models have demonstrated a linear relationship between CT attenuation and hemispheric tissue water content (39–41). Within the first few hours following stroke onset, CT shows attenuation of gray matter, which results in the loss of gray/white matter contrast in the cortex, indistinct basal ganglia, and an insular ribbon. With the development of edema, cortical sulci may disappear, and hypoattenuation develops in white matter. During the late stages, ventricles may shrink because of increased parenchymal volume, and MLS occurs.

Midline Shift and Volume of Infarct-Related Hypodensity

MLS and the volume of infarct-related hypodensity are two commonly used imaging markers of edema based on CT images (16–18). MLS describes the degree of displacement of the septum pellucidum, which is a thin membrane between the frontal horns of the lateral ventricles, relative to the ideal midline on CT images. An MLS of over 5 mm is usually considered malignant cerebral edema (18, 42). Edema in a temporal lobe infarction can cause uncal herniation with severe symptoms despite minimal MLS.

The volume of infarct-related hypodensity has also been widely used to evaluate edema (22, 25), and it can be manually outlined on each CT slice. However, quantifying hypodensity on CT during the acute phase when infarcts are subtle can sometimes be difficult; moreover, distinguishing edema from infarct growth in follow-up studies is also challenging.

At present, several comprehensive scores are based on the above methods, such as cerebral edema grading (grade 1 = focal brain swelling of $\leq 1/3$ of the hemisphere, grade 2 = $> 1/3$ of the hemisphere, grade 3 = edema with MLS; Figure 1). These scores are used widely in clinical studies (43–45). However, this semi-quantitative method can only be applied to roughly assess the degree of edema, and it is insufficient for evaluating patients with mild edema.

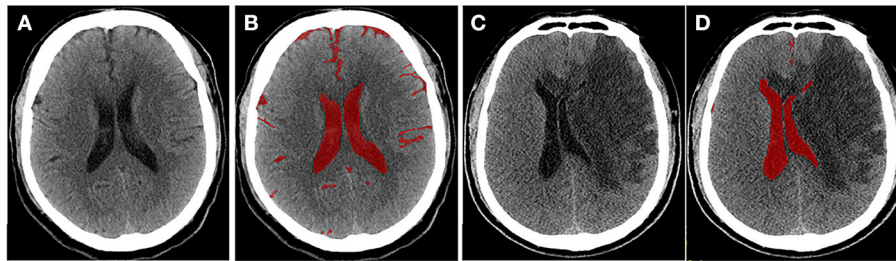


FIGURE 2 | Quantitative cerebrospinal fluid (CSF) shifts. Baseline (A) and 24 h (C) follow-up CTs after ischemic stroke, respectively. CSF spaces are outlined on a CT scan slice at baseline (B) and follow-up (D). Supratentorial CSF and basal cisterns were outlined on each slice, and Δ CSF was subsequently calculated.

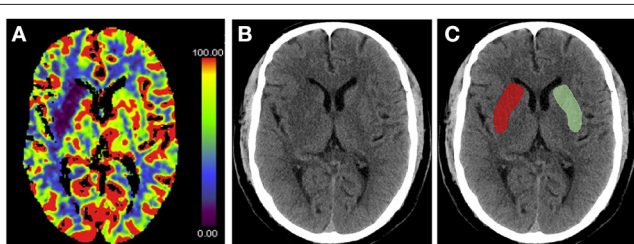


FIGURE 3 | Measurement of % net water uptake (NWU) per volume on admission. (A) The initial ischemic core is identified by the initial relative cerebral blood flow (CBF) volume using a threshold of $<30\%$ in CBF maps. (B) Non-enhanced computed tomography shows a slight decrease in the density of the right basal ganglia region. (C) The mean density of the initial core (D_{Ischemic}) (red) was calculated in relation to the normal density (D_{Normal}) (green) in the homotopic contralateral region. $NWU = 1 - D_{\text{Ischemic}}/D_{\text{Normal}}$.

Displacement of Cerebrospinal Fluid

To quantify the severity of edema more accurately, Dhar et al. proposed a CT-based volumetric measure of CSF shifts over time (19). As ionic and vasogenic edemas develop, the CSF is progressively displaced from the sulci and ventricles of the cerebral hemispheres to compensate for the increased brain tissue volume in the fixed cranial cavity. Supratentorial CSF spaces (sulci and ventricles ipsilateral and contralateral to the stroke and the third ventricle) and basal cisterns are outlined on each slice, and the volume of CSF is quantified (Figure 2). The CSF can be pushed out of the hemispheric sulci, cerebral ventricles, and basal cisterns as edema develops in the hours or days following the stroke. Studies have shown that, compared with MLS, the reduction in CSV (Δ CSF) from baseline to follow-up CT is an earlier and more sensitive indicator of edema severity across a broader dynamic range (46, 47). Furthermore, the authors developed an automated algorithm to segment the CSF from the CT scans of stroke patients (46) to facilitate and scale up such approaches. However, their method measures changes in the brain volume (BV); thus, it cannot distinguish edema from infarct growth or hemorrhagic transformation. Moreover, it is not suitable for patients with stroke in the brainstem or cerebellum.

Net Water Uptake

Recent studies have proposed the use of NWU within the lesion area to determine the volume of edema (12, 48–50). NWU is

calculated using the equation $NWU = 1 - D_{\text{Ischemic}}/D_{\text{Normal}}$, where D_{Ischemic} (Hounsfield Unit, HU) is the density of the ischemic core with hypoattenuation, and D_{Normal} is the density of the same area in the contralateral normal tissue (21, 49, 51) (Figure 3). This quantitative method is based on a physical principle in which the product between the volume of a body and its mean CT density remains constant, regardless of the volume of water uptake (49). Therefore, the increased water content is proportional to the NWU, and the edematous component of the infarct lesion can be quantified using CT densitometry according to the following equation: edema volume = lesion volume \times NWU.

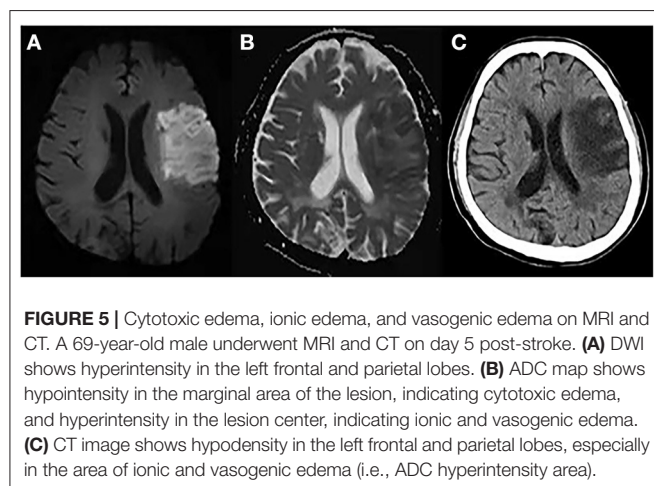
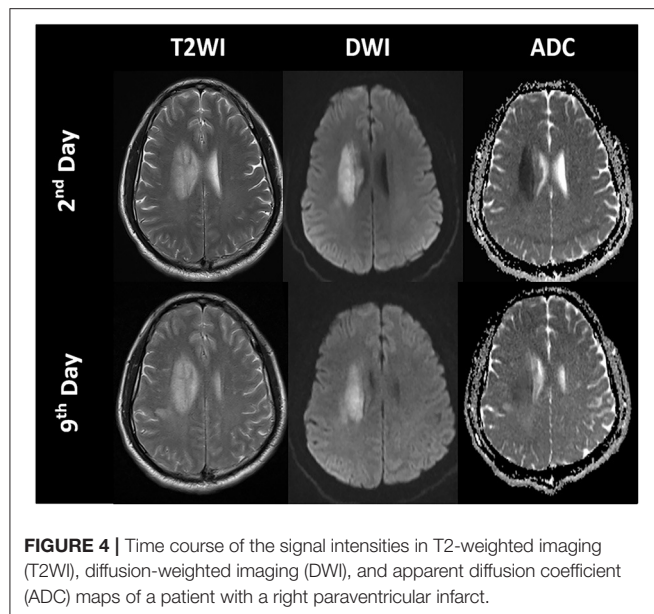
CT-based NWU quantification has been described as a precise method to determine the individual volume of edema (21). A previous study demonstrated that it is related to histopathological measurements of the volume of water uptake (52). Fu et al. proposed a new image patch-based NWU procedure that only uses non-enhanced admission CT without the need for lesion segmentation (53). However, this approach has other limitations; for example, patients with pre-existing stroke or significant carotid stenosis may have hypodense lesions, which affect NWU measurement.

Magnetic Resonance Imaging

Similar to CT, cerebral edema can also be assessed by MLS and change in CSV on MRI because BV increases as edema progresses. Moreover, the intensity characteristics of MRI reflect the tissue composition, and some sequences are particularly sensitive to changes in water content.

T2 and T2 Fluid-Attenuated Inversion Recovery

T2 prolongation is commonly observed hours after stroke and is considered to be related to increased water content in ischemic tissue, which represents ionic and vasogenic edema (54, 55). Gerriets et al. found that a significant T2 signal increase is detectable as early as 20–45 min following middle cerebral artery occlusion in rats (56). However, in the early phase of stroke, a slightly increased T2 signal intensity may be masked by high CSF signal. Therefore, T2-weighted fluid-attenuated inversion recovery (FLAIR) sequences can be more sensitive because of the inhibition of CSF signals. In several studies, FLAIR hyperintensity has been measured by calculating the intensity ratio between the stroke lesion and the corresponding normal



contralateral hemisphere as a marker to quantify vasogenic edema (57–59).

Diffusion Magnetic Resonance Imaging

Diffusion MRI is sensitive to the diffusion of water molecules in biological tissue and plays a critical role in the research and clinical management of acute stroke. Diffusion-weighted imaging (DWI) is the most frequently used technique to detect cytotoxic edema. An increase in DWI and a decrease in apparent diffusion coefficient (ADC) can be observed several hours after acute ischemia because of extracellular fluid loss and swelling of various cellular compartments, which are proportionate to the degree of intracellular water accumulation (60, 61). ADC declines immediately when the cerebral blood flow (CBF) falls below 20 to 40 ml/100 g/min in animals and humans (22), and the most dominant decay occurs within the first hours (1–1.5 h) (57, 61, 62). Subsequently, ADC values increase in the days following

stroke because of progressive ionic and vasogenic edema and cell lysis, which results in a phenomenon called *ADC pseudo-normalization* (63) (Figures 4, 5). Therefore, timely imaging (24–48 h after stroke onset) is essential to evaluate the process of cytotoxic edema.

However, DWI provides relatively limited quantitative information regarding the microstructural features of brain tissue. Recently, several advanced diffusion techniques have been proposed, such as the ball-and-stick model, q-ball imaging, diffusion spectrum imaging, composite hindered and restricted models of diffusion, and neurite orientation dispersion and density imaging (NODDI) (64–67). Among these, NODDI provides quantification of the relative contribution of the three diffusion compartments (CSF-like, extra-neurite, and intra-neurite) to the total diffusion signal in each voxel (65). NODDI parameters can be used to further elaborate microstructural changes within ischemic tissue and may disentangle the confounding factors behind cerebral edema.

NEUROIMAGING PREDICTORS OF EDEMA

The measurement methods of edema have been described above. Because edema strongly influences patient prognoses, predicting its occurrence in the early stages is vital to provide timely intervention. To date, various clinical and imaging markers have been developed to predict edema. In this review, we focus on neuroimaging predictors.

Infarction Volume

A large ischemic core is considered a key risk factor for ME. Occlusion of both the middle cerebral (MCA) and internal carotid arteries (ICA) is a strong predictor of MLS (11, 18, 68, 69). For patients with MCA occlusion, over 50% of the MCA territory infarction on initial CT predicts ME (18, 70), whereas an acute DWI volume of >80 ml on MRI acquired within 6 h of stroke onset and that of >145 ml when imaged 14 h from stroke onset have been shown to predict rapid early neurological deterioration and the need for neurosurgery (11, 71–74).

A large cerebellar hemisphere infarction is the major cause of severe edema in infra-tentorial infarcts and results in acute obstructive hydrocephalus and potentially fatal tonsillar herniation. Decompressive suboccipital craniectomy with dural expansion with or without ventriculostomy leads to acceptable functional outcomes in most patients. However, cerebellar infarction volume that is predictive of the need for decompression has not yet been established (75, 76).

The early development of a large ischemic area suggests extensive cytotoxic edema. Because this may be associated with a proximal clot, in combination with a poor leptomeningeal collateral status, it can further lead to prominent vasogenic edema.

Intracranial Volume Reserve

Intracranial volume reserve is represented by the space occupied by the CSF, which is mainly determined by pre-existing brain atrophy. A larger intracranial volume reserve provides space

to compensate for the increased BV and can alleviate early neurological deterioration.

The assessment of BV and/or CSV can quantify the degree of brain atrophy (72, 77, 78). The DWI high-intensity volume/BV ratio and cerebral blood volume lesion volume/CSV ratio have been demonstrated as reliable predictive markers for malignant MCA infarction, with a cut-off value of 0.078 (sensitivity 86%, specificity 87%) and 0.92 (sensitivity 96.2%, specificity 96.2%), respectively (72, 79). However, BV information is not readily available to clinicians during the management of acute stroke patients because traditional image processing methods involve sophisticated post-processing steps and are thus relatively slow. However, the application of deep learning-based segmentation methods can provide fast and accurate results (47), which offers great potential for future clinical practice.

Intercaudate distance (ICD) is considered a convenient and practical marker for brain atrophy (80), and a higher ICD has been shown to be a protective factor against malignant infarction (74, 78, 80). Lee et al. demonstrated that an ICD ≥ 20 mm in the non-infarcted hemisphere has an independent protective effect against malignant clinical outcomes during admission to hospital. However, it is also negatively associated with a modified Rankin Scale score of <4 at 6 months (80). These studies indicate that although intracranial volume reserve can compensate for the space-occupying edema during the early phase of stroke, it also represents a pre-existing neurodegenerative process that affects patients' long-term outcomes.

Blood–Brain Barrier Permeability

The BBB is the interface between blood circulation and brain tissue; it consists of a continuous endothelial membrane within brain microvessels and is sheathed by mural vascular cells and perivascular astrocyte end-feet. During ischemia, several pathological mechanisms, such as inflammation and oxidative stress, can disrupt BBB integrity and increase paracellular permeability, which contributes to vasogenic edema (81, 82).

In clinical studies, the permeability of the BBB (BBBP) is usually measured by the amount of contrast agent that leaks into the extravascular space (83, 84). Hom et al. analyzed 32 patients with acute anterior circulation stroke within 12 h of stroke onset and found that BBBP > 7 ml/100 g/min at admission is 100% sensitive and 79% specific in predicting symptomatic hemorrhagic transformation and ME. Moreover, specificity further increases to 100% after adding age (≥ 65 years) and tissue plasminogen activator (tPA) administration (81). Compared with cerebral hemorrhage, cerebral edema may have a lesser degree of BBB disruption because it only needs to be permeable to small molecules, such as albumin, rather than blood cells. Unfortunately, the clinical application of BBBP measurement is limited by the use of contrast agents. Recently, a new MRI method based on diffusion-weighted arterial spin labeling (ASL) was proposed as a method to quantify the rate of water exchange across the BBB; it has the advantages of repeatable measurement for longitudinal monitoring and being exempt from the need for a contrast agent (85, 86).

Collateral Status

Robust pial arterial collaterals may temporarily preserve blood flow during stroke, and collateral status has been shown to be related to post-stroke cerebral edema. Various methods have been proposed to evaluate collateral status based on different imaging models, such as the American Society of Interventional and Therapeutic Neuroradiology or Thrombolysis in Cerebral Infarction grades on digital subtraction angiography (87), as well as the Alberta Stroke Program Early CT Score based on CT angiography (88) or CT perfusion (89). Additionally, new methods, such as ASL, have also been introduced (90).

Collateral status has been demonstrated to be a predictor of cerebral edema in ischemic stroke (91, 92). Jo et al. reported that a collateral status score of <2 strongly predicts malignant cerebral edema [odds ratio (OR): 0.165, 95% confidence interval (CI): 0.064–0.426] (92). Poor collateral status is known to augment the progression of the infarct core and induce more proximal vascular occlusion, which are both associated with brain edema (93, 94).

In patients undergoing recanalization, those with initially poor collaterals may develop greater early brain edema and have a higher early edema progression rate (EPR) (1.6% EPR per one collateral status point) 24 h after acute ischemic stroke (25, 95). This may result in elevated interstitial pressure, increased resistance of collateral arterioles, and downstream perforating arterioles in the hypoperfused area. Subsequently, ischemic edema may be further aggravated, which results in adverse functional outcomes. Huang et al. found that a low collateral score may be an independent risk factor for the development of malignant cerebral edema after mechanical thrombectomy, especially in patients with successful reperfusion (93).

Therefore, collateral status could be used for the early stratification of adjuvant treatment options after successful vessel recanalization, especially anti-edematous treatment.

Cerebral Veins

Venous changes in the affected hemisphere after acute ischemic stroke may play a crucial role in determining clinical outcomes (94, 96), given that the venous system is responsible for ~ 70 –80% of the cerebral blood volume. Zhang et al. suggested that a lack of superficial middle cerebral vein filling contributes to poor outcomes following thrombolysis and that this indicator predicts edema progression within 24 h in non-reperfusion patients (97, 98). Xia et al. assessed cortical veins (Labbe, sphenoparietal sinus, and the superficial middle cerebral vein) and found that the absence of cortical venous filling is associated with increased brain edema and a higher risk of malignant cerebral edema (OR, 14.68; 95% CI, 4.03–53.45) (94) regardless of whether patients received reperfusion therapy. The likely pathophysiologic mechanism of these signs is the elevation of venous pressure caused by micro-thrombotic occlusion in venules or endothelium swelling after ischemia (99, 100), which may increase fluid leakage into the perivascular space, resulting in brain edema (101).

Recanalization and Reperfusion

Recanalization therapies in the hyperacute phase following ischemic stroke, such as intravenous thrombolysis with tPA and endovascular thrombectomy, aim to reopen the occluded artery, which has been unequivocally shown to restore CBF in salvageable ischemic tissue and reduce patient disability (102, 103). However, pre-clinical data using rodent and primate models have indicated that tPA facilitates the development of BBB damage in acute ischemic stroke by inducing phasic secretion of matrix metalloproteinase-9, and reperfusion injury is observed after the restoration of vascular supply to ischemic lesions. Both of these conditions may augment the development of edema following recanalization therapy (104, 105). On the contrary, several studies have demonstrated that thrombolytic therapy and recanalization in the hyperacute phase reduce brain edema by arresting infarct growth and rescuing at-risk ischemic tissue (18, 45, 93, 106, 107). Thorén et al. analyzed 22,184 patients who underwent recanalization therapies (intravenous thrombolysis and thrombectomy with or without intravenous thrombolysis) and found that patients who had successful recanalization had a lower cerebral edema grade at 24–36 h than that of those who did not undergo recanalization (13 vs. 23.6%; OR: 0.52) (45). Additionally, *post-hoc* analysis of the Echoplanar Imaging Thrombolytic Evaluation Trial and Mechanical Retrieval and Recanalization of Stroke Clots Using Embolectomy cohorts found that increasing reperfusion is associated with and independently predicts less MLS and a lower swelling volume 3–8 days after stroke onset (107). However, downstream reperfusion is not always achieved even after complete recanalization (called futile recanalization), which is likely related to microvascular obstruction. Nawabi et al. reported that futile recanalization after receiving successful endovascular recanalization (thrombolysis in cerebral infarction scale 2b/3) is associated with an elevated edema volume in the follow-up CT 24 h later (12).

ARTIFICIAL INTELLIGENCE IN THE ASSESSMENT AND PREDICTION OF EDEMA

Artificial intelligence has been widely used in the segmentation of intracranial tissues. Following the theory that CSF displacement reflects the extent of edema, Chen et al. developed a computer algorithm capable of automatically segmenting CSF from standard clinical CT images to evaluate edema and further

refined this algorithm by training a fully convolutional neural network. This new method automatically performs segmentation of clinical CT images with high concordance to manually obtained measurements and takes <1 min per scan (108).

Different types of neural network algorithms have been introduced in the past several decades to predict cerebral edema (109, 110). Compared with traditional regression models, these new methods have higher accuracy. However, studies that investigated these models are often conducted in a single center with relatively small sample sizes. Thus, further research is needed to validate these methods.

CONCLUSION

Severe cerebral edema following ischemic stroke is associated with a poor prognosis if timely intervention is not provided. Neuroimaging is important in the assessment of edema and can be used to evaluate the degree of cerebral edema and quantify edema volume. Using different imaging modalities, a range of neuroimaging indicators to predict edema progression have been offered, although their predictive value varies between studies. Therefore, further research is required to establish evaluation and prediction models of cerebral edema and improve their clinical applicability.

AUTHOR CONTRIBUTIONS

XZ conceived and drafted the review with guidance from RZ. RZ and PH critically revised the manuscript. All authors carefully reviewed the content and approved the final manuscript version for publication.

FUNDING

This study was supported by the National Natural Science Foundation of China (Grant Nos. 81771820 and 82101987), the Natural Science Foundation of Zhejiang Province (Grant Nos. LSZ19H180001 and LQ20H180015), the China Post-doctoral Science Foundation (Grant No. 2019M662083), the Office of China Post-doctoral Council (Grant No. PC2020117), and the Post-doctoral Science Foundation of Zhejiang Province.

ACKNOWLEDGMENTS

We thank Sarina Iwabuchi, PhD, from Liwen Bianji (Edanz) (www.liwenbianji.cn) for editing a draft of this manuscript.

REFERENCES

1. Kahle KT, Simard JM, Staley KJ, Nahed BV, Jones PS, Sun D, et al. Molecular mechanisms of ischemic cerebral edema: role of electroneutral ion transport. *Physiology (Bethesda)*. (2009) 24:257–65. doi: 10.1152/physiol.00015.2009
2. Hu HJ, Song M. Disrupted ionic homeostasis in ischemic stroke and new therapeutic targets. *J Stroke Cerebrovasc Dis*. (2017) 26:2706–19. doi: 10.1016/j.jstrokecerebrovasdis.2017.09.011
3. Stokum JA, Gerzanich V, Simard JM. Molecular pathophysiology of cerebral edema. *J Cereb Blood Flow Metab*. (2016) 36:513–38. doi: 10.1177/0271678X15617172
4. Abdullahi W, Tripathi D, Ronaldson PT. Blood-brain barrier dysfunction in ischemic stroke: targeting tight junctions and transporters for vascular protection. *Am J Physiol Cell Physiol*. (2018) 315:C343–56. doi: 10.1152/ajpcell.00095.2018

5. Nian K, Harding IC, Herman IM, Ebong EE. Blood-brain barrier damage in ischemic stroke and its regulation by endothelial mechanotransduction. *Front Physiol.* (2020) 11:605398. doi: 10.3389/fphys.2020.605398
6. Jiang X, Andjelkovic AV, Zhu L, Yang T, Bennett MVL, Chen J, et al. Blood-brain barrier dysfunction and recovery after ischemic stroke. *Prog Neurobiol.* (2018) 163–164:144–71. doi: 10.1016/j.pneurobio.2017.10.001
7. Liebeskind DS, Juttler E, Shapovalov Y, Yegin A, Landen J, Jauch EC. Cerebral edema associated with large hemispheric infarction. *Stroke.* (2019) 50:2619–25. doi: 10.1161/STROKEAHA.118.024766
8. Alquisiras-Burgos I, Ortiz-Plata A, Franco-Perez J, Millan A, Aguilera P. Resveratrol reduces cerebral edema through inhibition of *de novo* SUR1 expression induced after focal ischemia. *Exp Neurol.* (2020) 330:113353. doi: 10.1016/j.expneurol.2020.113353
9. Powers WJ, Rabinstein AA, Ackerson T, Adeoye OM, Bambakidis NC, Becker K, et al. Guidelines for the early management of patients with acute ischemic stroke: 2019 update to the 2018 guidelines for the early management of acute ischemic stroke: a guideline for healthcare professionals from the American Heart Association/American Stroke Association. *Stroke.* (2019) 50:e344–418. doi: 10.1161/STR.0000000000000211
10. Kim H, Jin ST, Kim YW, Kim SR, Park IS, Jo KW. Predictors of malignant brain edema in middle cerebral artery infarction observed on CT angiography. *J Clin Neurosci.* (2015) 22:554–60. doi: 10.1016/j.jocn.2014.08.021
11. Wu S, Yuan R, Wang Y, Wei C, Zhang S, Yang X, et al. Early prediction of malignant brain edema after ischemic stroke. *Stroke.* (2018) 49:2918–27. doi: 10.1161/STROKEAHA.118.022001
12. Nawabi J, Flottmann F, Hanning U, Bechstein M, Schon G, Kemmling A, et al. Futile recanalization with poor clinical outcome is associated with increased edema volume after ischemic stroke. *Invest Radiol.* (2019) 54:282–7. doi: 10.1097/RLI.0000000000000539
13. Hofmeijer J, Kappelle LJ, Algra A, Amelink GJ, van Gijn J, van der Worp HB, et al. Surgical decompression for space-occupying hemispheric infarction: a systematic review and individual patient meta-analysis of randomized clinical trials. *JAMA Neurol.* (2021) 78:208–16. doi: 10.1001/jamaneurol.2020.3745
14. Stokum JA, Gerzanich V, Sheth KN, Kimberly WT, Simard JM. Emerging pharmacological treatments for cerebral edema: evidence from clinical studies. *Annu Rev Pharmacol Toxicol.* (2020) 60:291–309. doi: 10.1146/annurev-pharmtox-010919-023429
15. Reinink H, Juttler E, Hacke W, Hofmeijer J, Vicaut E, Vahedi K, et al. Surgical decompression for space-occupying cerebral infarction (the Hemispherectomy After Middle Cerebral Artery infarction with Life-threatening Edema Trial [HAMLET]): a multicentre, open, randomised trial. *Lancet Neurol.* (2009) 8:326–33. doi: 10.1016/S1474-4422(09)70047-X
16. Barber PA, Demchuk AM, Zhang J, Kasner SE, Hill MD, Berrouschot J, et al. Computed tomographic parameters predicting fatal outcome in large middle cerebral artery infarction. *Cerebrovasc Dis.* (2003) 16:230–5. doi: 10.1159/000071121
17. Ong CJ, Gluckstein J, Laurido-Soto O, Yan Y, Dhar R, Lee JM. Enhanced detection of edema in malignant anterior circulation stroke (EDEMA) score: a risk prediction tool. *Stroke.* (2017) 48:1969–72. doi: 10.1161/STROKEAHA.117.016733
18. Miao J, Song X, Sun W, Qiu X, Lan Y, Zhu Z. Predictors of malignant cerebral edema in cerebral artery infarction: a meta-analysis. *J Neurol Sci.* (2020) 409:116607. doi: 10.1016/j.jns.2019.116607
19. Dhar R, Yuan K, Kulik T, Chen Y, Heitsch L, An H, et al. CSF volumetric analysis for quantification of cerebral edema after hemispheric infarction. *Neurocrit Care.* (2016) 24:420–7. doi: 10.1007/s12028-015-0204-z
20. Kauw F, Bennink E, de Jong HWAM, Kappelle LJ, Horsch AD, Velthuis BK, et al. Intracranial cerebrospinal fluid volume as a predictor of malignant middle cerebral artery infarction. *Stroke.* (2019) 50:STROKEAHA119024882. doi: 10.1161/STROKEAHA.119.026853
21. Brooks G, Flottmann F, Ernst M, Faizy TD, Minnerup J, Siemonsen S, et al. Computed tomography-based imaging of voxel-wise lesion water uptake in ischemic brain: relationship between density and direct volumetry. *Invest Radiol.* (2018) 53:207–13. doi: 10.1097/RLI.0000000000000430
22. von Kummer R, Dzialowski I. Imaging of cerebral ischemic edema and neuronal death. *Neuroradiology.* (2017) 59:545–53. doi: 10.1007/s00234-017-1847-6
23. Obenaus A, Badaut J. Role of the noninvasive imaging techniques in monitoring and understanding the evolution of brain edema. *J Neurosci Res.* (2021). doi: 10.1002/jnr.24837. [Epub ahead of print].
24. Zhang LJ, Zhong J, Lu GM. Multimodality MR imaging findings of low-grade brain edema in hepatic encephalopathy. *AJNR Am J Neuroradiol.* (2013) 34:707–15. doi: 10.3174/ajnr.A2968
25. Galego O, Jesus-Ribeiro J, Baptista M, Sargento-Freitas J, Martins AI, Silva F, et al. Collateral pial circulation relates to the degree of brain edema on CT 24 hours after ischemic stroke. *Neuroradiol J.* (2018) 31:456–63. doi: 10.1177/1971400918769912
26. Dhar R, Chen Y, Hamzehloo A, Kumar A, Heitsch L, He J, et al. Reduction in cerebrospinal fluid volume as an early quantitative biomarker of cerebral edema after ischemic stroke. *Stroke.* (2020) 51:462–7. doi: 10.1161/STROKEAHA.119.027895
27. Muscari A, Faccioli L, Lega MV, Lorusso A, Trossello MP, Puddu GM, et al. Predicting cerebral edema in ischemic stroke patients. *Neurol Sci.* (2019) 40:745–52. doi: 10.1007/s10072-019-3717-y
28. Zhao YX, Cui M, Chen SF, Dong Q, Liu XY. Amelioration of ischemic mitochondrial injury and Bax-dependent outer membrane permeabilization by Mdivi-1. *CNS Neurosci Ther.* (2014) 20:528–38. doi: 10.1111/cns.12266
29. Yan Y, Dempsey RJ, Flemmer A, Forbush B, Sun D. Inhibition of Na(+)-K(+)-Cl(-) cotransporter during focal cerebral ischemia decreases edema and neuronal damage. *Brain Res.* (2003) 961:22–31. doi: 10.1016/S0006-8993(02)03832-5
30. O'Donnell ME, Chen YJ, Lam TI, Taylor KC, Walton JH, Anderson SE. Intravenous HOE-642 reduces brain edema and Na uptake in the rat permanent middle cerebral artery occlusion model of stroke: evidence for participation of the blood-brain barrier Na/H exchanger. *J Cereb Blood Flow Metab.* (2013) 33:225–34. doi: 10.1038/jcbfm.2012.160
31. Vella J, Zammit C, Di Giovanni G, Muscat R, Valentino M. The central role of aquaporins in the pathophysiology of ischemic stroke. *Front Cell Neurosci.* (2015) 9:108. doi: 10.3389/fncel.2015.00108
32. O'Donnell ME, Tran L, Lam TI, Liu XB, Anderson SE. Bumetanide inhibition of the blood-brain barrier Na-K-Cl cotransporter reduces edema formation in the rat middle cerebral artery occlusion model of stroke. *J Cereb Blood Flow Metab.* (2004) 24:1046–56. doi: 10.1097/01.WCB.0000130867.32663.90
33. Yuen N, Lam TI, Wallace BK, Klug NR, Anderson SE, O'Donnell ME. Ischemic factor-induced increases in cerebral microvascular endothelial cell Na/H exchange activity and abundance: evidence for involvement of ERK1/2 MAP kinase. *Am J Physiol Cell Physiol.* (2014) 306:C931–42. doi: 10.1152/ajpcell.00021.2013
34. Jia SW, Liu XY, Wang SC, Wang YF. Vasopressin hypersecretion-associated brain edema formation in ischemic stroke: underlying mechanisms. *J Stroke Cerebrovasc Dis.* (2016) 25:1289–300. doi: 10.1016/j.jstrokecerebrovasdis.2016.02.002
35. Khatri R, McKinney AM, Swenson B, Janardhan V. Blood-brain barrier, reperfusion injury, and hemorrhagic transformation in acute ischemic stroke. *Neurology.* (2012) 79(Suppl. 1):S52–7. doi: 10.1212/WNL.0b013e3182697e70
36. Yang C, Hawkins KE, Dore S, Candelario-Jalil. Neuroinflammatory mechanisms of blood-brain barrier damage in ischemic stroke. *Am J Physiol Cell Physiol.* (2019) 316:C135–53. doi: 10.1152/ajpcell.00136.2018
37. Liff JJ, Wang M, Liao Y, Plogg BA, Peng W, Gundersen GA, et al. A paravascular pathway facilitates CSF flow through the brain parenchyma and the clearance of interstitial solutes, including amyloid beta. *Sci Transl Med.* (2012) 4:147ra111. doi: 10.1126/scitranslmed.3003748
38. Mestre H, Du T, Sweeney AM, Liu G, Samson AJ, Peng W, et al. Cerebrospinal fluid influx drives acute ischemic tissue swelling. *Science.* (2020) 367:eaax7171. doi: 10.1126/science.aax7171
39. Dzialowski I, Weber J, Doerfler A, Forsting M, von Kummer R. Brain tissue water uptake after middle cerebral artery occlusion assessed with CT. *J Neuroimaging.* (2004) 14:42–8. doi: 10.1111/j.1552-6569.2004.tb00214.x
40. Dzialowski I, Klotz E, Goericke S, Doerfler A, Forsting M, von Kummer R. Ischemic brain tissue water content: CT monitoring during middle

- cerebral artery occlusion and reperfusion in rats. *Radiology*. (2007) 243:720–6. doi: 10.1148/radiol.2432060137
41. Nemoto EM, Mendez O, Kerr ME, Firlik A, Stevenson K, Jovin T, et al. CT density changes with rapid onset acute, severe, focal cerebral ischemia in monkeys. *Transl Stroke Res*. (2012) 3:369–74. doi: 10.1007/s12975-012-0193-6
 42. Du M, Huang X, Li S, Xu L, Yan B, Zhang Y, et al. A nomogram model to predict malignant cerebral edema in ischemic stroke patients treated with endovascular thrombectomy: an observational study. *Neuropsychiatr Dis Treat*. (2020) 16:2913–20. doi: 10.2147/NDT.S279303
 43. Strbian D, Meretoja A, Putaala J, Kaste M, Tatlisumak T. Cerebral edema in acute ischemic stroke patients treated with intravenous thrombolysis. *Int J Stroke*. (2013) 8:529–34. doi: 10.1111/j.1747-4949.2012.00781.x
 44. Thoren M, Azevedo E, Dawson J, Egido JA, Falcou A, Ford GA, et al. Predictors for cerebral edema in acute ischemic stroke treated with intravenous thrombolysis. *Stroke*. (2017) 48:2464–71. doi: 10.1161/STROKEAHA.117.018223
 45. Thoren M, Dixit A, Escudero-Martinez I, Gdovinova Z, Klecka L, Rand VM, et al. Effect of recanalization on cerebral edema in ischemic stroke treated with thrombolysis and/or endovascular therapy. *Stroke*. (2020) 51:216–23. doi: 10.1161/STROKEAHA.119.026692
 46. Dhar R, Chen Y, An H, Lee JM. Application of machine learning to automated analysis of cerebral edema in large cohorts of ischemic stroke patients. *Front Neurol*. (2018) 9:687. doi: 10.3389/fneur.2018.00687
 47. Dhar R. Automated quantitative assessment of cerebral edema after ischemic stroke using CSF volumetrics. *Neurosci Lett*. (2020) 724:134879. doi: 10.1016/j.neulet.2020.134879
 48. Minnerup J, Brooks G, Kalkoffen J, Langner S, Knauth M, Psychogios MN, et al. Computed tomography-based quantification of lesion water uptake identifies patients within 4.5 hours of stroke onset: a multicenter observational study. *Ann Neurol*. (2016) 80:924–34. doi: 10.1002/ana.24818
 49. Brooks G, Flottmann F, Scheibel A, Aigner A, Faizy TD, Hanning U, et al. Quantitative lesion water uptake in acute stroke computed tomography is a predictor of malignant infarction. *Stroke*. (2018) 49:1906–12. doi: 10.1161/STROKEAHA.118.020507
 50. Foroushani HM, Hamzehloo A, Kumar A, Chen Y, Heitsch L, Slowik A, et al. Quantitative serial CT imaging-derived features improve prediction of malignant cerebral edema after ischemic stroke. *Neurocrit Care*. (2020) 33:785–92. doi: 10.1007/s12028-020-01056-5
 51. Brooks G, Hanning U, Faizy TD, Scheibel A, Nawabi J, Schon G, et al. Ischemic lesion growth in acute stroke: Water uptake quantification distinguishes between edema and tissue infarct. *J Cereb Blood Flow Metab*. (2020) 40:823–32. doi: 10.1177/0271678X19848505
 52. Flottmann F, Brooks G, Faizy TD, Ernst M, Forkert ND, Grosser M, et al. CT-perfusion stroke imaging: a threshold free probabilistic approach to predict infarct volume compared to traditional ischemic thresholds. *Sci Rep*. (2017) 7:6679. doi: 10.1038/s41598-017-06882-w
 53. Fu B, Qi S, Tao L, Xu H, Kang Y, Yao Y, et al. Image patch-based net water uptake and radiomics models predict malignant cerebral edema after ischemic stroke. *Front Neurol*. (2020) 11:609747. doi: 10.3389/fneur.2020.609747
 54. Ayata AH, Ropper C. Ischaemic brain oedema. *J Clin Neurosci*. (2002) 9:113–24. doi: 10.1054/jocn.2001.1031
 55. Neumann-Haefelin T, Kastrup A, de Crespigny A, Yenari MA, Ringer T, Sun GH, et al. Serial MRI after transient focal cerebral ischemia in rats: dynamics of tissue injury, blood-brain barrier damage, edema formation. *Stroke*. (2000) 31:1965–72; discussion 1972–63. doi: 10.1161/01.STR.31.8.1965
 56. Gerriets T, Walberer M, Ritschel N, Tschernatsch M, Mueller C, Bachmann G, et al. Edema formation in the hyperacute phase of ischemic stroke. Laboratory investigation. *J Neurosurg*. (2009) 111:1036–42. doi: 10.3171/2009.3.JNS081040
 57. Schaefer PW. Diffusion-weighted imaging as a problem-solving tool in the evaluation of patients with acute stroke-like syndromes. *Top Magn Reson Imaging*. (2000) 11:300–309. doi: 10.1097/00002142-200010000-00006
 58. Kimberly WT, Battery TW, Pham L, Wu O, Yoo AJ, Furie KL, et al. Glyburide is associated with attenuated vasogenic edema in stroke patients. *Neurocrit Care*. (2014) 20:193–201. doi: 10.1007/s12028-013-9917-z
 59. Chang PD, Malone HR, Bowden SG, Chow DS, Gill BJA, Ung TH, et al. A multiparametric model for mapping cellularity in glioblastoma using radiographically localized biopsies. *AJNR Am J Neuroradiol*. (2017) 38:890–8. doi: 10.3174/ajnr.A5112
 60. Liu KF, Li F, Tatlisumak T, Garcia JH, Sotak CH, Fisher M, et al. Regional variations in the apparent diffusion coefficient and the intracellular distribution of water in rat brain during acute focal ischemia. *Stroke*. (2001) 32:1897–905. doi: 10.1161/01.STR.32.8.1897
 61. Kuroiwa T, Miyasaka N, Fengyo Z, Yamada I, Nakane M, Nagaoka T, et al. Experimental ischemic brain edema: morphological and magnetic resonance imaging findings. *Neurosurg Focus*. (2007) 22:E11. doi: 10.3171/foc.2007.22.5.12
 62. Kucinski T, Vaterlein O, Glauche V, Fiehler J, Klotz E, Eckert B, et al. Correlation of apparent diffusion coefficient and computed tomography density in acute ischemic stroke. *Stroke*. (2002) 33:1786–91. doi: 10.1161/01.STR.0000019125.80118.99
 63. Ng FC, Campbell BCV. Imaging after thrombolysis and thrombectomy: rationale, modalities and management implications. *Curr Neurol Neurosci Rep*. (2019) 19:57. doi: 10.1007/s11910-019-0970-7
 64. Yang S, Ghosh K, Sakaie K, Sahoo SS, Carr SJA, Tatsuoka C. A simplified crossing fiber model in diffusion weighted imaging. *Front Neurosci*. (2019) 13:492. doi: 10.3389/fnins.2019.00492
 65. Kamiya K, Hori M, Aoki S. NODDI in clinical research. *J Neurosci Methods*. (2020) 346:108908. doi: 10.1016/j.jneumeth.2020.108908
 66. Caiazzo G, Trojsi F, Cirillo M, Tedeschi G, Esposito F. Q-ball imaging models: comparison between high and low angular resolution diffusion-weighted MRI protocols for investigation of brain white matter integrity. *Neuroradiology*. (2016) 58:209–15. doi: 10.1007/s00234-015-1616-3
 67. Assaf Y, Basser J. Composite hindered and restricted model of diffusion (CHARMED) MR imaging of the human brain. *Neuroimage*. (2005) 27:48–58. doi: 10.1016/j.neuroimage.2005.03.042
 68. Shimoyama T, Kimura K, Uemura J, Yamashita S, Saji N, Shibasaki K, et al. The DASH score: a simple score to assess risk for development of malignant middle cerebral artery infarction. *J Neurol Sci*. (2014) 338:102–6. doi: 10.1016/j.jns.2013.12.024
 69. Song SY, Ahn SY, Rhee JJ, Lee JW, Hur JW, Lee HK. Extent of contrast enhancement on non-enhanced computed tomography after intra-arterial thrombectomy for acute infarction on anterior circulation: as a predictive value for malignant brain edema. *J Korean Neurosurg Soc*. (2015) 58:321–7. doi: 10.3340/jkns.2015.58.4.321
 70. Hofmeijer J, Algra A, Kappelle LJ, van der Worp HB. Predictors of life-threatening brain edema in middle cerebral artery infarction. *Cerebrovasc Dis*. (2008) 25:176–84. doi: 10.1159/000113736
 71. Thomalla G, Hartmann F, Juettler E, Singer OC, Lehnhardt FG, Kohrmann M, et al. Prediction of malignant middle cerebral artery infarction by magnetic resonance imaging within 6 hours of symptom onset: a prospective multicenter observational study. *Ann Neurol*. (2010) 68:435–45. doi: 10.1002/ana.22125
 72. Minnerup J, Wersching H, Ringelstein EB, Heindel W, Niederstadt T, Schilling M, et al. Prediction of malignant middle cerebral artery infarction using computed tomography-based intracranial volume reserve measurements. *Stroke*. (2011) 42:3403–9. doi: 10.1161/STROKEAHA.111.619734
 73. Park J, Goh DH, Sung JK, Hwang YH, Kang DH, Kim Y, et al. Timely assessment of infarct volume and brain atrophy in acute hemispheric infarction for early surgical decompression: strict cutoff criteria with high specificity. *Acta Neurochir (Wien)*. (2012) 154:79–85. doi: 10.1007/s00701-011-1178-z
 74. Park JH, Hwang J. Where are we now with decompressive hemicraniectomy for malignant middle cerebral artery infarction? *J Cerebrovasc Endovasc Neurosurg*. (2013) 15:61–6. doi: 10.7461/jcen.2013.15.2.61
 75. Ayling OGS, Alotaibi NM, Wang JZ, Fatehi M, Ibrahim GM, Benavente O, et al. Suboccipital decompressive craniectomy for cerebellar infarction: a systematic review and meta-analysis. *World Neurosurg*. (2018) 110:450–9.e455. doi: 10.1016/j.wneu.2017.10.144
 76. Wijdevicks EF, Sheth KN, Carter BS, Greer DM, Kasner SE, Kimberly WT, et al. Recommendations for the management of cerebral and cerebellar infarction with swelling: a statement for healthcare

- professionals from the American Heart Association/American Stroke Association. *Stroke*. (2014) 45:1222–38. doi: 10.1161/01.str.0000441965.15164.d6
77. Beck C, Krutzmann A, Forkert ND, Juettler E, Singer OC, Kohrmann M. A simple brain atrophy measure improves the prediction of malignant middle cerebral artery infarction by acute DWI lesion volume. *J Neurol*. (2014) 261:1097–103. doi: 10.1007/s00415-014-7324-9
 78. Tschirret O, Moreno Legast G, Mansuy A, Mewton N, Buisson M, Hannoun S, et al. Impact of brain atrophy on early neurological deterioration and outcome in severe ischemic stroke treated by intravenous thrombolysis. *Eur Neurol*. (2018) 79:240–6. doi: 10.1159/000487668
 79. Goto Y, Kumura E, Watabe T, Nakamura H, Nishino A, Koyama T, et al. Prediction of malignant middle cerebral artery infarction in elderly patients. *J Stroke Cerebrovasc Dis*. (2016) 25:1389–95. doi: 10.1016/j.jstrokecerebrovasdis.2015.12.034
 80. Lee SH, Oh CW, Han JH, Kim CY, Kwon OK, Son YJ, et al. The effect of brain atrophy on outcome after a large cerebral infarction. *J Neurol Neurosurg Psychiatry*. (2010) 81:1316–21. doi: 10.1136/jnnp.2009.197335
 81. Hom J, Dankbaar JW, Soares BP, Schneider T, Cheng SC, Bredno J, et al. (2011) Blood-brain barrier permeability assessed by perfusion CT predicts symptomatic hemorrhagic transformation and malignant edema in acute ischemic stroke. *AJNR Am J Neuroradiol* 32:41–8. doi: 10.3174/ajnr.A2244
 82. Bektas H, Wu TC, Kasam M, Harun N, Sitton CW, Grotta JC, et al. Increased blood-brain barrier permeability on perfusion CT might predict malignant middle cerebral artery infarction. *Stroke*. (2010) 41:2539–44. doi: 10.1161/STROKEAHA.110.591362
 83. Kim T, Koo J, Kim SH, Song IU, Chung SW, Lee KS. Blood-brain barrier permeability assessed by perfusion computed tomography predicts hemorrhagic transformation in acute reperfusion therapy. *Neurol Sci*. (2018) 39:1579–84. doi: 10.1007/s10072-018-3468-1
 84. Suh CH, Jung SC, Cho SJ, Kim D, Lee JB, Woo DC, et al. Perfusion CT for prediction of hemorrhagic transformation in acute ischemic stroke: a systematic review and meta-analysis. *Eur Radiol*. (2019) 29:4077–87. doi: 10.1007/s00330-018-5936-7
 85. Shao X, Ma SJ, Casey M, D'Orazio L, Ringman JM, Wang DJJ. Mapping water exchange across the blood-brain barrier using 3D diffusion-prepared arterial spin labeled perfusion MRI. *Magn Reson Med*. (2019) 81:3065–79. doi: 10.1002/mrm.27632
 86. Tiwari YV, Lu J, Shen Q, Cerqueira B, Duong TQ. Magnetic resonance imaging of blood-brain barrier permeability in ischemic stroke using diffusion-weighted arterial spin labeling in rats. *J Cereb Blood Flow Metab*. (2017) 37:2706–15. doi: 10.1177/0271678X16673385
 87. Singer OC, Berkefeld J, Nolte CH, Bohner G, Reich A, Wiesmann M, et al. Collateral vessels in proximal middle cerebral artery occlusion: the ENDOSTROKE study. *Radiology*. (2015) 274:851–8. doi: 10.1148/radiol.14140951
 88. Seker F, Potreck A, Mohlenbruch M, Bendszus M, Pham M. Comparison of four different collateral scores in acute ischemic stroke by CT angiography. *J Neurointerv Surg*. (2016) 8:1116–8. doi: 10.1136/neurintsurg-2015-012101
 89. Consoli A, Andersson T, Holmberg A, Verganti L, Saletti A, Vallone S, et al. CT perfusion and angiographic assessment of pial collateral reperfusion in acute ischemic stroke: the CAPRI study. *J Neurointerv Surg*. (2016) 8:1211–6. doi: 10.1136/neurintsurg-2015-012155
 90. Lou X, Yu S, Scalzo F, Starkman S, Ali LK, Kim D, et al. Multi-delay ASL can identify leptomeningeal collateral perfusion in endovascular therapy of ischemic stroke. *Oncotarget*. (2017) 8:2437–43. doi: 10.18632/oncotarget.13898
 91. Flores A, Rubiera M, Ribo M, Pagola J, Rodriguez-Luna D, Muchada M, et al. Poor collateral circulation assessed by multiphase computed tomographic angiography predicts malignant middle cerebral artery evolution after reperfusion therapies. *Stroke*. (2015) 46:3149–53. doi: 10.1161/STROKEAHA.115.010608
 92. Jo K, Bajgur SS, Kim H, Choi HA, Huh PW, Lee K, et al. A simple prediction score system for malignant brain edema progression in large hemispheric infarction. *PLoS ONE*. (2017) 12:e0171425. doi: 10.1371/journal.pone.0171425
 93. Huang X, Yang Q, Shi X, Xu X, Ge L, Ding X, et al. Predictors of malignant brain edema after mechanical thrombectomy for acute ischemic stroke. *J Neurointerv Surg*. (2019) 11:994–8. doi: 10.1136/neurintsurg-2018-14650
 94. Xia H, Sun H, He S, Zhao M, Huang W, Zhang Z, et al. Absent cortical venous filling is associated with aggravated brain edema in acute ischemic stroke. *AJNR Am J Neuroradiol*. (2021) 42:1023–9. doi: 10.3174/ajnr.A7039
 95. Brooks G, Kemmling A, Meyer L, Nawabi J, Schon G, Fiehler J, et al. Computed tomography angiography collateral profile is directly linked to early edema progression rate in acute ischemic stroke. *Stroke*. (2019) 50:3424–30. doi: 10.1161/STROKEAHA.119.027062
 96. Chen CY, Chen CI, Tsai FY, Tsai PH, Chan WP. Prominent vessel sign on susceptibility-weighted imaging in acute stroke: prediction of infarct growth and clinical outcome. *PLoS ONE*. (2015) 10:e0131118. doi: 10.1371/journal.pone.0131118
 97. Zhang S, Lai Y, Ding X, Parsons M, Zhang JH, Lou M. Absent filling of ipsilateral superficial middle cerebral vein is associated with poor outcome after reperfusion therapy. *Stroke*. (2017) 48:907–14. doi: 10.1161/STROKEAHA.116.016174
 98. Zhang S, Lin L, Zhang R, Wang M, Yu Y, Shi Z, et al. Absent contrast filling of ipsilateral superficial middle cerebral vein predicts midline shift in acute middle cerebral artery occlusion. *Front Neurol*. (2020) 11:570844. doi: 10.3389/fneur.2020.570844
 99. Zhou Y, Wang Y, Wang J, Anne Stetler R, Yang QW. Inflammation in intracerebral hemorrhage: from mechanisms to clinical translation. *Prog Neurobiol*. (2014) 115:25–44. doi: 10.1016/j.pneurobio.2013.11.003
 100. Schwarzmair SM, Kim SW, Trabold R, Plesnila N. Temporal profile of thrombogenesis in the cerebral microcirculation after traumatic brain injury in mice. *J Neurotrauma*. (2010) 27:121–30. doi: 10.1089/neu.2009.1114
 101. Alperin N. MR-intracranial compliance and pressure: a method for noninvasive measurement of important neurophysiologic parameters. *Methods Enzymol*. (2004) 386:323–49. doi: 10.1016/S0076-6879(04)86016-6
 102. Emberson J, Lees KR, Lyden P, Blackwell L, Albers G, Bluhmki E, et al. Effect of treatment delay, age, and stroke severity on the effects of intravenous thrombolysis with alteplase for acute ischaemic stroke: a meta-analysis of individual patient data from randomised trials. *Lancet*. (2014) 384:1929–35. doi: 10.1016/S0140-6736(14)60584-5
 103. Goyal M, Menon BK, van Zwam WH, Dippel DW, Mitchell PJ, Demchuk AM, et al. Endovascular thrombectomy after large-vessel ischaemic stroke: a meta-analysis of individual patient data from five randomised trials. *Lancet*. (2016) 387:1723–31. doi: 10.1016/S0140-6736(16)00163-X
 104. Ning M, Furie KL, Koroshetz WJ, Lee H, Barron M, Lederer M, et al. Association between tPA therapy and raised early matrix metalloproteinase-9 in acute stroke. *Neurology*. (2006) 66:1550–5. doi: 10.1212/01.wnl.0000216133.98416.b4
 105. Pillai DR, Dittmar MS, Baldranov D, Heidemann RM, Henning EC, Schuierer G, et al. Cerebral ischemia-reperfusion injury in rats—a 3 T MRI study on biphasic blood-brain barrier opening and the dynamics of edema formation. *J Cereb Blood Flow Metab*. (2009) 29:1846–55. doi: 10.1038/jcbfm.2009.106
 106. Kimberly WT, Dutra BG, Boers AMM, Alves H, Berkhemer OA, et al. Association of reperfusion with brain edema in patients with acute ischemic stroke: a secondary analysis of the MR CLEAN trial. *JAMA Neurol*. (2018) 75:453–61. doi: 10.1001/jamaneurol.2017.5162
 107. Irvine HJ, Ostwaldt AC, Bevers MB, Dixon S, Battey TW, Campbell BC, et al. Reperfusion after ischemic stroke is associated with reduced brain edema. *J Cereb Blood Flow Metab*. (2018) 38:1807–17. doi: 10.1177/0271678X17720559
 108. Chen Y, Dhar R, Heitsch L, Ford A, Fernandez-Cadenas I, Carrera C, et al. Automated quantification of cerebral edema following hemispheric infarction: application of a machine-learning algorithm to evaluate CSF shifts on serial head CTs.

- Neuroimage Clin.* (2016) 12:673–80. doi: 10.1016/j.nicl.2016.09.018
109. Wei H, Tang X, Zhang M, Li Q, Xing X, Sean Zhou X, et al. The delineation of largely deformed brain midline using regression-based line detection network. *Med Phys.* (2020) 47:5531–42. doi: 10.1002/mp.14302
 110. Foroushani HM, Hamzehloo A, Kumar A, Chen Y, Heitsch L, Slowik A, et al. Accelerating prediction of malignant cerebral edema after ischemic stroke with automated image analysis and explainable neural networks. *Neurocrit Care.* (2021). 20:1–2. doi: 10.1007/s12028-021-01325-x

Conflict of Interest: The authors declare that the research was conducted in the absence of any commercial or financial relationships that could be construed as a potential conflict of interest.

Publisher's Note: All claims expressed in this article are solely those of the authors and do not necessarily represent those of their affiliated organizations, or those of the publisher, the editors and the reviewers. Any product that may be evaluated in this article, or claim that may be made by its manufacturer, is not guaranteed or endorsed by the publisher.

Copyright © 2022 Zhang, Huang and Zhang. This is an open-access article distributed under the terms of the Creative Commons Attribution License (CC BY). The use, distribution or reproduction in other forums is permitted, provided the original author(s) and the copyright owner(s) are credited and that the original publication in this journal is cited, in accordance with accepted academic practice. No use, distribution or reproduction is permitted which does not comply with these terms.



Evaluation of Intracranial Hypertension in Patients With Hypertensive Intracerebral Hemorrhage Using Texture Analysis

Yingchi Shan^{1†}, Yihua Li^{1†}, Xiang Wu¹, Jiaqi Liu¹, Guoqing Zhang², Yajun Xue^{1*} and Guoyi Gao^{1*}

¹ Department of Neurosurgery, Shanghai General Hospital, Shanghai Jiao Tong University School of Medicine, Shanghai, China, ² Department of Neurosurgery, The People's Hospital of Qiannan, Guizhou, China

OPEN ACCESS

Edited by:

Sheng Zhang,
Zhejiang Provincial People's
Hospital, China

Reviewed by:

Wang Binli,
Nanxun People's Hospital of
Huzhou, China
Sui Sum Kung,
Kaohsiung Medical University
Hospital, Taiwan

*Correspondence:

Yajun Xue
xue_yj@163.com
Guoyi Gao
gao3@sina.com

[†]These authors have contributed
equally to this work

Specialty section:

This article was submitted to
Stroke,
a section of the journal
Frontiers in Neurology

Received: 09 December 2021

Accepted: 21 February 2022

Published: 16 March 2022

Citation:

Shan Y, Li Y, Wu X, Liu J, Zhang G,
Xue Y and Gao G (2022) Evaluation of
Intracranial Hypertension in Patients
With Hypertensive Intracerebral
Hemorrhage Using Texture Analysis.
Front. Neurol. 13:832234.
doi: 10.3389/fneur.2022.832234

Purpose: Texture analysis based on clinical images had been widely used in neurological diseases. This study aimed to achieve depth information of computed tomography (CT) images by texture analysis and to establish a model for noninvasive evaluation of intracranial pressure (ICP) in patients with hypertensive intracerebral hemorrhage (HICH).

Methods: Forty-seven patients with HICH were selected. Related CT images and ICP value were collected. The morphological features of hematoma volume, midline shift, and ventriculocranial ratio were measured. Forty textural features were extracted from regions of interest. Four models were established to predict intracranial hypertension with morphological features, textural features of anterior horn, textural features of temporal lobe, and textural features of posterior horn.

Results: Model of posterior horn had the highest ability to predict intracranial hypertension (AUC = 0.90, F1 score = 0.72), followed by model of anterior horn (AUC = 0.70, F1 score = 0.53) and model of temporal lobe (AUC = 0.70, F1 score = 0.58), and model of morphological features displayed the worst performance (AUC = 0.42, F1 score = 0.38).

Conclusion: Texture analysis can realize interpretation of CT images in depth, which has great potential in noninvasive evaluation of intracranial hypertension.

Keywords: hypertensive intracerebral hemorrhage, computed tomography, texture analysis, noninvasive evaluation, intracranial hypertension

INTRODUCTION

Hypertensive intracerebral hemorrhage (HICH) is one of the most common critical diseases in neurosurgery, with high morbidity, disability, mortality, and recurrence rates (1–3). The increase of intracranial pressure (ICP) after intracerebral hemorrhage directly causes the decrease of cerebral perfusion pressure, and finally leads to cerebral ischemia, hypoxia, and even cerebral hernia (4). Timely and efficient monitoring of ICP plays an important role in identifying intracranial physiological and pathological changes (5). In recent years, various methods of noninvasive ICP monitoring have been used in clinical practice, with the characteristics of low cost, wide range of use and fewer complications (6–8). Computed tomography (CT) image, as one of the most commonly

used clinical examination, plays an essential role in the evaluation of patients' condition (9). In addition, relatively perfect scoring scales and guidelines have been formed for the morphological analysis of CT images, which can be used for the evaluation of ICP to a certain extent, but it largely depends on the clinical experiences of doctors and is difficult to be accurate and quantitative (10, 11). This study aims to analyze nonvisual features of CT images by texture analysis, with machine learning being used to capture ICP signals, and then the performance of predicting ICP by CT can be improved.

MATERIALS AND METHODS

Study Design and Setting

Clinical data of patients with HICH admitted to the Department of Neurosurgery, Shanghai General Hospital from January 2019 to December 2020 were collected and analyzed. Inclusion criteria were as follows: (1) patients admitted to emergency department for spontaneous intracranial hemorrhage, with a history of hypertension; (2) with the main lesion of intracerebral hematoma; (3) received invasive ICP monitoring according to the guidelines (12) for the management of HICH; (4) received emergency cranial CT scan within 60 min of ICP monitoring. Exclusion criteria were as follows: (1) patients with a history of traumatic brain injury, cerebral infarction, brain tumor, or other neurological diseases or cranial surgical interventions that might result in an abnormal anatomical structure; (2) with previous coagulopathy and blood system related diseases; (3) a large amount of subarachnoid hemorrhage or ventricular hemorrhage being showed on CT images, with aneurysms, moyamoya disease, vascular malformations, or other vascular anatomical abnormalities detected by cranial CTA or angiography in follow-up treatment. The study protocol conformed to the ethical guidelines of the Declaration of Helsinki, and this study was approved by the Ethics Committee of Shanghai General Hospital, Shanghai Jiao Tong University School of Medicine. Participants' right to know was fully guaranteed and indicated in the ethical approval document.

Data Sources and Measurements

In addition to the baseline characteristics, we collected and analyzed the last cranial CT before the surgery and the initial ICP value immediately after ICP sensor (Integra, USA) insertion. In this study, the ICP sensor was inserted into the ventricle before performing a craniotomy for hematoma removal, and the location of the sensor was verified by cranial CT after surgery. The CT related features were acquired from the Digital Imaging and Communications in Medicine (DICOM) file of the last cranial CT before ICP monitoring using a 64-slice spiral CT machine (General Electric Medical Systems, USA). As per the routine protocol of a CT scan, the CT slices were parallel to the orbitomeatal plane from the foramen magnum to the vertex. The scanning slice thickness was 1 mm.

In this study, hematoma volume, midline shift, and ventriculocranial ratio (VCR) were included in the morphological features, and the final results were the average of the measurements by two clinical experts. The specific measuring

method is as follows: (1) the DICOM files of CT were imported into 3D slicer software, using the Threshold function under the Editor module to complete the 3D reconstruction of the hematoma and obtain the hematoma volume; (2) the slice with maximum midline shift was selected, and the perpendicular distance between the septum pellucidum and cranial midline (median ridge of the fronto-parietal bone) was measured at the level of Monroe's foramen; (3) the lateral ventricle width between the heads of the caudate nuclei and the width of the same horizontal cranial cavity were measured at the slice which was 5 cm above the orbitomeatal plane; ratio of the two width was VCR. These three morphological features were then included into random forest model to evaluate the probability of intracranial hypertension ($ICP \geq 20$ mmHg) (12) as the morphological features related model (MF model).

The slice with upper part of the third ventricle (about 6 cm above the orbitomeatal plane) was selected for the extraction of textural features. "Pydicom" module in Python 3.8 was used to extract six rectangular regions of interest (ROI) with size of 20 pixels \times 20 pixels from the bilateral anterior horn of lateral ventricle, bilateral temporal lobe and bilateral posterior horn of lateral ventricles (the bilateral ROI is symmetrical as shown in **Figure 1**). On the one hand, the ROIs were selected according to CT values (the threshold of CT value was set to ≤ 50 HU and ≥ 0 HU, HU was short for Hounsfield Unit); on the other hand, manual verification was carried out to avoid ROIs falling into the hematoma or the ventricle. "Radiomics" module was used to extract a total of 40 textural features including gray level cooccurrence matrix (GLCM, 24 features) and gray level run

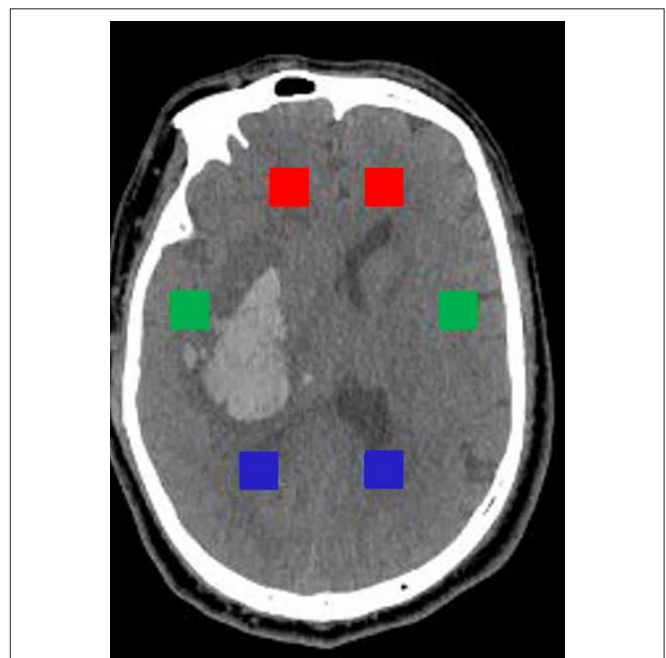


FIGURE 1 | Selection of six rectangular ROI with size of 20 pixels \times 20 pixels. The red, green, and blue rectangles, respectively, represent ROI of the anterior horn, the temporal lobe, and the posterior horn.

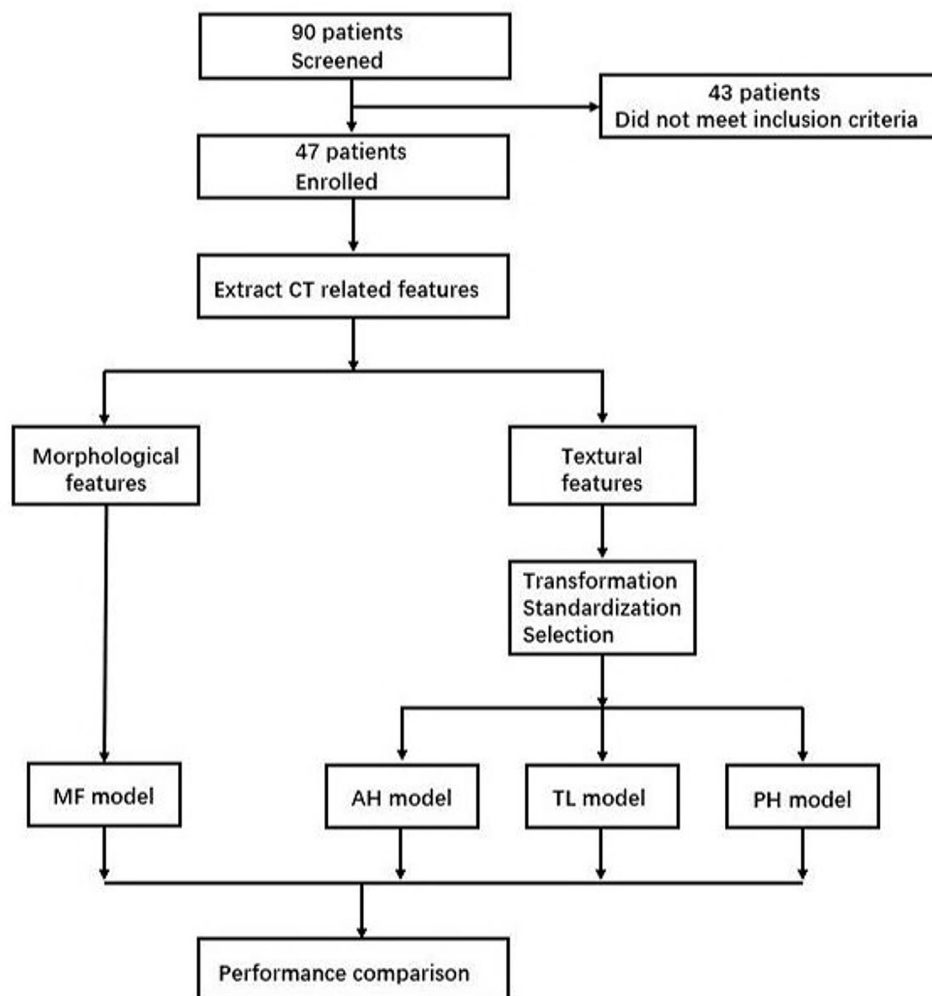


FIGURE 2 | Model establishment and analysis process. MF, morphological features; AH, anterior horn; TL, temporal lobe; PH, posterior horn.

length matrix (GLRLM, 16 features) from six ROI, respectively. Next, there were three steps for processing textural features. Firstly, the value of features from six ROI were transformed into variation rate related to three areas (anterior horn of lateral ventricle, temporal lobe, and posterior horn of lateral ventricle). The formula was as follows:

$$R = \left| \frac{F_{Hemorrhagic\ lateral} - F_{Contralateral}}{F_{Hemorrhagic\ lateral}} \right|$$

Secondly, the variation rate of three groups were standardized. The formula was as follows:

$$R_{new} = \frac{R - R_{min}}{R_{max} - R_{min}}$$

Thirdly, recursive feature elimination method (RFE) was used for feature selection in three groups, respectively. The importance of each feature was obtained by random forest classifier, the least

important feature was removed from the current feature set, and this step was repeated on the feature set. To avoid overfitting, cross validation (RFECV) was used to find the optimal number of features. According to the features selected for three groups, three random forest models were established to evaluate the probability of intracranial hypertension ($ICP \geq 20$ mmHg), including anterior horn model (AH model), temporal lobe model (TL model), and posterior horn (PH model). The establishment and analysis process of above models are shown in **Figure 2**.

Statistical Analysis

Python 3.8 was used for statistical analysis of the data. Numpy module and Pandas module were used for data operation and sorting, RFECV module of Sklearn was used for feature selection, RandomForestClassifier module of Sklearn was used for model establishment, and Matplotlib module is used for drawing. Continuous variables subject to normal distribution were expressed as the mean (M) \pm standard deviation (SD),

TABLE 1 | Initial ICP and morphological features of patients.

	Patients with HICH (<i>n</i> = 47)
Systolic pressure (mmHg)	146 (135–157)
GCS score	6 (4–7)
Initial ICP (mmHg)	25 (15–30)
>20 mmHg	32 (68.09%)
Location of hemorrhage	
<i>Thalamus</i>	5 (10.64%)
<i>Basal ganglia</i>	35 (74.47%)
<i>Cerebral cortex</i>	7 (14.89%)
With subarachnoid hemorrhage	6 (12.77%)
Hematoma volume (ml)	52.40 (37.25–78.94)
Midline shift (mm)	6.61 (3.95–9.21)
Ventriculocranial ratio	0.24 (0.16–0.30)

continuous variables not subject to normal distribution were expressed as the median and interquartile range (IQR), and categorical variables were expressed as the frequency and percentage. Accuracy, precision, recall, and F1 score were used to evaluate the performance of each model. The area under the receiver operator characteristic (ROC) curve was used in all four models to assess discrimination.

RESULTS

As shown in **Table 1**, a total of 47 patients with HICH were included in this study, among which 30 were males (63.83%) and 17 were females (36.17%). Bleeding sites include basal ganglia (35, 74.47%), thalamus (5, 10.64%) and cerebral cortex (7, 14.89%), and six cases (12.77%) were accompanied by a small amount of subarachnoid hemorrhage. The median Glasgow Coma Score (GCS) was 6 (IQR: 4–7) at the time of emergency admission. Median systolic pressure was 146 mmHg (IQR: 135–157) upon arrival. The median ICP of all patients was 25 mmHg (IQR: 15–30), and 32 patients (68.09%) were diagnosed with intracranial hypertension. Median hematoma volume was 52.40 mL (IQR: 37.25–78.94 mL), median midline shift was 6.61 mm (IQR: 3.95–9.21 mm), and median ventriculocranial ratio was 0.24 (IQR: 0.16–0.30).

The selected textural features and variation rate of anterior horn, temporal lobe, and posterior horn are shown in **Table 2**. After RFECV selection, a total of 12 features were extracted from the anterior horn of the lateral ventricle, and the cross-validation score was the highest at this time. As above, 10 features were extracted from temporal lobe and 12 features were extracted from posterior horn of lateral ventricle. The illustration of all features extracted was added in the **Supplementary Material**.

The performance of the MF, AH, TL, and PH models in predicting intracranial hypertension is shown in **Table 3** and **Figure 3**. PH model had the strongest prediction ability of intracranial hypertension, TL model and AH model had the same prediction ability and were inferior to PH

TABLE 2 | Selected features and their variation rate.

Selected features	Variation rate
Anterior horn (12 features)	
Autocorrelation	0.09 (0.05~0.16)
Cluster shade	0.71 (0.46~1.66)
Idm	0.05 (0.03~0.07)
Joint average	0.05 (0.02~0.09)
Joint energy	0.27 (0.16~0.40)
Maximum probability	0.16 (0.10~0.24)
Sum average	0.05 (0.02~0.09)
Gray level variance	0.47 (0.24~0.75)
High gray level run emphasis	0.59 (0.32~0.79)
Run length nonuniformity	0.22 (0.10~0.34)
Short run emphasis	0.20 (0.09~0.45)
Short run low gray level emphasis	0.25 (0.13~0.39)
Temporal lobe (10 features)	
Cluster prominence	0.65 (0.32~0.91)
Id	0.05 (0.02~0.08)
Idm	0.05 (0.02~0.08)
Joint average	0.06 (0.03~0.12)
Maximum probability	0.11 (0.06~0.23)
Gray level nonuniformity	0.12 (0.05~0.23)
High gray level run emphasis	0.22 (0.13~0.38)
Long run high gray level emphasis	0.49 (0.22~0.85)
Run length nonuniformity	0.26 (0.14~0.52)
Run percentage	0.22 (0.09~0.40)
Posterior horn (12 features)	
Cluster prominence	0.40 (0.23~0.88)
Cluster shade	0.82 (0.34~2.37)
Correlation	0.92 (0.57~1.75)
Imc1	0.45 (0.25~0.79)
Imc2	0.32 (0.14~0.56)
MCC	0.42 (0.15~0.60)
Sum squares	0.33 (0.13~0.73)
Long run emphasis	0.26 (0.16~0.45)
Run entropy	0.15 (0.09~0.23)
Run length nonuniformity normalized	0.34 (0.18~0.55)
Run percentage	0.12 (0.07~0.23)
Short run low gray level emphasis	0.17 (0.07~0.26)

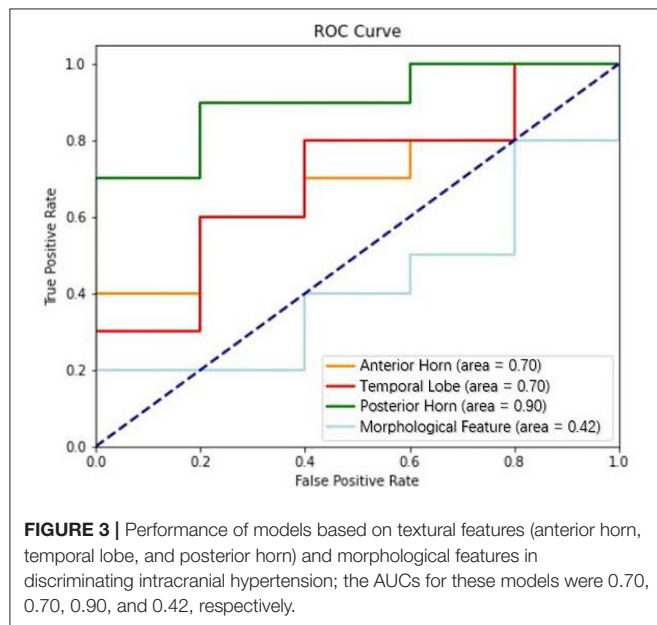
model, and MF model had the worst prediction ability of intracranial hypertension.

DISCUSSION

This study retrospectively analyzed the preoperative CT images of patients with HICH, conducted texture analysis, predicted intracranial hypertension according to the textural features obtained, and compared them with traditional morphological features. The results showed that texture features had better prediction ability than morphological features, and the prediction ability of textural features varied in different regions.

TABLE 3 | Performance of models based on textural features and morphological features.

	Textural features (anterior horn)	Textural features (temporal lobe)	Textural features (posterior horn)	Morphological features
Accuracy	66.67%	73.33%	80.00%	60.00%
Precision	59.62%	85.71%	88.46%	32.14%
Recall	55.00%	60.00%	70.00%	45.00%
F1 score	0.53	0.58	0.72	0.38
AUC	0.70	0.70	0.90	0.42



With the promotion of noninvasive concept, CT image-based ICP evaluation has been carried out. Clinically, it is commonly used to evaluate ICP based on visual features, including midline shift, width of third ventricle, change of basal cistern, and optic nerve sheath diameter. These radiological findings are regarded as morphological features and a prognostic evaluation system such as Marshall classification and Rotterdam classification has been formed, which is a concentrated manifestation of the clinical application of these features. Oliveira et al. (13) evaluated intracranial conditions by measuring the width of the third ventricle, peri-mesencephalic cistern, and sylvian fissure. Optic nerve sheath diameter had also been measured on preoperative brain CT, which predicted increased ICP with good discrimination and high inter-observer reliability (14). Rotterdam classification is a new CT scoring method proposed by Mass et al. (10) on the basis of Marshall classification, which was scored on the shape of basal cistern, midline shift, presence of the hematoma or contusion and presence of intraventricular hemorrhage or subarachnoid hemorrhage; the score indicated the severity of the brain injury (15). The above methods can predict ICP to a certain extent, but they are highly subjective, highly affected by the heterogeneity of the disease, and difficult

to be accurately quantified (hematoma volume, midline shift, and ventricle cisternal size are currently measured by different methods and most of them are manually measured). In addition, most studies on morphological features were focused on individual correlation analysis, and comprehensive assessment models are rarely reported.

Currently, the main trend of texture analysis is to judge or predict the outcome of a clinical event through the extraction and deep learning of textural features of selected lesions. For example, a study extracted textural features to predict ICP level (elevated ICP with ICP > 12 mm Hg and normal ICP with ICP ≤ 12 mm Hg) in patients with traumatic brain injury (16). Shen et al. (17) filtered the CT images in different degree, and the gray related parameters (average gray intensity, variance, and uniformity) of hematoma sites on images with different texture thickness were extracted, so as to predict the possibility of early hematoma enlargement in patients with ICH. Texture features generally include first-order features, second-order features and higher-order features according to the current study of radiomics (18–20). CT value is the expression form of gray value on CT image, which describes distribution of the intensities of voxels within the ROI by entropy, mean value, range, root mean square, skewness, standard deviation, consistency, variance, and other parameters (known as first-order features). As mentioned above, CT value can be used to predict clinical events under certain conditions, but it has limitations for the assessment of ICP discussed in this study. For example, high CT value area caused by small amount of subarachnoid hemorrhage and low CT value area caused by brain edema existed around hematoma after ICH, both of which were under intracranial hypertension. These differences of CT value could cause effective visual impact, but they could not explain the same situation of intracranial hypertension caused by different CT values. Therefore, first order features were not included in this study.

The second-order features (known as textural features in a narrow sense) which described the spatial distribution of voxel intensity levels were obtained by GLCM and GLRLM. Guan et al. had showed the judgement ability of textural features. They selected 38 infarcted areas and 38 symmetrical non-infarcted areas of contralateral cerebral hemisphere from CT images by matching the lesion areas displayed on MRI images, extracted textural features, and established classifiers through computer deep learning method to verify its effectiveness. The results showed that there were differences in textural features between the two types of regions, which could be helpful for early clinical assessment of acute ischemic stroke and quantification of affected regions (21). However, the results of studies on the predictive ability of textural features were not always positive. Nawabi et al. (22) indicated that machine learning-based evaluation of filter- and texture-derived high-end image features provided the same discriminatory power in predicting functional outcome as multidimensional clinical scoring systems. In summary, most textural analysis based on second-order features at present focuses on selecting hematoma or the local lesion, while multi-area comparative analysis of surrounding tissues is rarely reported. This study aims to explore the differences in the degree of compression of local brain tissue after HICH by comparing

the textural features of the brain tissue in bilateral symmetric regions without lesion, and to explore the relationship between these differences and ICP.

HICH is usually unilateral, and the main bleeding sites are basal ganglia, thalamus, ventricle, cerebellum and brain stem (23, 24). Patients with hemorrhage of ventricle, cerebellum, and brainstem were excluded in this study, so as to reflect the pressure changes in bilateral brain tissues caused by intracerebral hematoma. After the ICH, compression of hematoma and swelling of brain tissue result in the disruption of cranial cavity, such as midline deviation to the healthy side, ventricle compression, and decrease of VCR. Therefore, the average CT value of brain tissue on the bleeding side is higher than that on the opposite side. In clinical practice, doctors often judge the degree of increased ICP according to the “density” of brain tissue, but it is greatly affected by anatomical factors and blood flow effects, and there are many application restrictions. The second-order textural features obtained by GLCM and GLRLM describe the relative positions of the two voxels. By comparing the textural features at the same position on the bleeding side and the contralateral side, the differences in the internal structure changes of the bilateral brain tissues after hematoma compression and brain tissue swelling can be reflected. In this study, variation rate was used to quantify the difference. The results showed that the three models of textural feature are superior to the MF model. The parameters included by the morphological model were commonly used in clinical practice to roughly evaluate intracranial hypertension, and their measurements were greatly affected by clinical experience, so the performance of the MF model is poor. In addition, the performance of PH model was better than that of AH model and TL model. The reason may lie in: the anterior horn and temporal lobe were close to the hematoma; due to the relative smaller space of the frontal lobe and temporal lobe compared with the occipital lobe, and the mass effect of hematoma, although the increase of hematoma would lead to the displacement of internal structures, the deformation space of the frontal or temporal brain tissue was limited, and was not as large as that of the occipital lobe. Therefore, the PH model has the best judgement ability.

In summary, the value and potential of textural analysis in the prediction of intracranial hypertension had been proved, but this study also had some limitations. Firstly, the sample size was relatively small and from a single center. Secondly, there are strict requirements on the inclusion data of texture analysis. In this study, hemorrhage of ventricle, cerebellum and brainstem were excluded, and the study coverage was narrow. Thirdly, as different observers have different perceptions of lesions in ROI delineation, manual segmentation would cause certain interference to experimental results, increase inaccuracy and lead to certain errors. Fourthly, the ICP value acquired from the intraventricular ICP sensor could not represent the actual ICP of different regions. Fifthly, this study was conducted only from the perspective of CT image; many objective factors including age, preoperative medication, and time of onset were not considered. Lastly, the HU method evaluated ICP values in

a semiquantitative way, without providing a continuous value. These flaws need to be addressed in subsequent research.

CONCLUSIONS

In summary, texture analysis, which is known for high-throughput, obtain a large amount of additional quantitative data that cannot be observed by eyes through parameterization of CT images, which can be used for the prediction and avoidance of adverse clinical events. In this study, compared with traditional morphological analysis, this novel method can distinguish intracranial hypertension more accurately, and has an extensive application prosperity for noninvasive filed.

DATA AVAILABILITY STATEMENT

The original contributions presented in the study are included in the article/**Supplementary Material**, further inquiries can be directed to the corresponding author/s.

ETHICS STATEMENT

The studies involving human participants were reviewed and approved by the Ethics Committee of Shanghai General Hospital, Shanghai Jiao Tong University School of Medicine. The patients/participants provided their written informed consent to participate in this study.

AUTHOR CONTRIBUTIONS

GG, YS, YL, and XW conceived the study. GG and YX supervised and coordinated all aspects of the work. YS, YL, XW, and GZ collected and analyzed the data. YS, YL, XW, and GG wrote the paper. GG and YX acquired the funding and administrated the project. All authors contributed to the article and approved the submitted version.

FUNDING

This study was supported by the National Natural Science Foundation of China (Grant Nos. 81671198 and 81971699) and the Clinical Research Innovation Plan of Shanghai General Hospital.

ACKNOWLEDGMENTS

We would like to thank all colleagues in the department of neurosurgery for their work.

SUPPLEMENTARY MATERIAL

The Supplementary Material for this article can be found online at: <https://www.frontiersin.org/articles/10.3389/fneur.2022.832234/full#supplementary-material>

REFERENCES

- Ikram MA, Wieberdink RG, Koudstaal PJ. International epidemiology of intracerebral hemorrhage. *Curr Atheroscler Rep.* (2012) 14:300–6. doi: 10.1007/s11883-012-0252-1
- Dastur CK, Yu W. Current management of spontaneous intracerebral haemorrhage. *Stroke Vasc Neurol.* (2017) 2:21–9. doi: 10.1136/svn-2016-000047
- Marcolini E, Stretz C, DeWitt KM. Intracranial hemorrhage and intracranial hypertension. *Emerg Med Clin North Am.* (2019) 37:529–44. doi: 10.1016/j.emc.2019.04.001
- Naranjo D, Arkuszewski M, Rudzinski W, Melhem ER, Krejza J. Brain ischemia in patients with intracranial hemorrhage: pathophysiological reasoning for aggressive diagnostic management. *Neuroradiol J.* (2013) 26:610–28. doi: 10.1177/197140091302600603
- Harary M, Dolmans RGF, Gormley WB. Intracranial pressure monitoring-review and avenues for development. *Sensors (Basel).* (2018) 18:465. doi: 10.3390/s18020465
- Canac N, Jalaieddini K, Thorpe SG, Thibeault CM, Hamilton RB. Review: pathophysiology of intracranial hypertension and noninvasive intracranial pressure monitoring. *Fluids Barriers CNS.* (2020) 17:40. doi: 10.1186/s12987-020-00201-8
- Zhang X, Medow JE, Iskandar BJ, Wang F, Shokouinejad M, Koueik J, et al. Invasive and noninvasive means of measuring intracranial pressure: a review. *Physiol Meas.* (2017) 38:R143–R82. doi: 10.1088/1361-6579/aa7256
- Nag DS, Sahu S, Swain A, Kant S. Intracranial pressure monitoring: gold standard and recent innovations. *World J Clin Cases.* (2019) 7:1535–53. doi: 10.12998/wjcc.v7.i13.1535
- Fernando SM, Tran A, Cheng W, Rochwerf B, Taljaard M, Kyeremanteng K, et al. Diagnosis of elevated intracranial pressure in critically ill adults: systematic review and meta-analysis. *BMJ.* (2019) 366:l4225. doi: 10.1136/bmj.l4225
- Maas AI, Hukkelhoven CW, Marshall LF, Steyerberg EW. Prediction of outcome in traumatic brain injury with computed tomographic characteristics: a comparison between the computed tomographic classification and combinations of computed tomographic predictors. *Neurosurgery.* (2005) 57:1173–82. doi: 10.1227/01.NEU.0000186013.63046.6B
- Mohammadifard M, Ghaemi K, Hanif H, Sharifzadeh G, Haghparast M. Marshall and Rotterdam Computed Tomography scores in predicting early deaths after brain trauma. *Eur J Transl Myol.* (2018) 28:7542. doi: 10.4081/ejtm.2018.7542
- Hemphill JC 3rd, Greenberg SM, Anderson CS, Becker K, Bendok BR, Cushman M, et al. Guidelines for the management of spontaneous intracerebral hemorrhage: a guideline for healthcare professionals from the American Heart Association/American Stroke Association. *Stroke.* (2015) 46:2032–60. doi: 10.1161/STR.0000000000000069
- Oliveira RA, de Oliveira Lima M, Paiva WS, de Sa Malbouisson LM, Teixeira MJ, Bor-Seng-Shu E. Comparison between brain computed tomography scan and transcranial sonography to evaluate third ventricle width, perimesencephalic cistern, and sylvian fissure in traumatic brain-injured patients. *Front Neurol.* (2017) 8:44. doi: 10.3389/fneur.2017.00044
- Lee HC, Lee WJ, Dho YS, Cho WS, Kim YH, Park HP. Optic nerve sheath diameter based on preoperative brain computed tomography and intracranial pressure are positively correlated in adults with hydrocephalus. *Clin Neurol Neurosurg.* (2018) 167:31–35. doi: 10.1016/j.clineuro.2018.02.012
- Bobinski L, Olivecrona M, Koskinen LO. Dynamics of brain tissue changes induced by traumatic brain injury assessed with the Marshall, Morris-Marshall, and the Rotterdam classifications and its impact on outcome in a prostacyclin placebo-controlled study. *Acta Neurochir (Wien).* (2012) 154:1069–79. doi: 10.1007/s00701-012-1345-x
- Chen W, Cockrell CH, Ward K, Najarian K. Predictability of intracranial pressure level in traumatic brain injury: features extraction, statistical analysis and machine learning-based evaluation. *Int J Data Min Bioinform.* (2013) 8:480–94. doi: 10.1504/IJDMB.2013.056617
- Shen Q, Shan Y, Hu Z, Chen W, Yang B, Han J, et al. Quantitative parameters of CT texture analysis as potential markers for early prediction of spontaneous intracranial hemorrhage enlargement. *Eur Radiol.* (2018) 28:4389–96. doi: 10.1007/s00330-018-5364-8
- Avanzo M, Stancanelli J, El Naqa I. Beyond imaging: The promise of radiomics. *Physica Medica.* (2017) 38:122–39. doi: 10.1016/j.ejmp.2017.05.071
- Lubner MG, Smith AD, Sandrasegaran K, Sahani DV, Pickhardt PJ. CT texture analysis: definitions, applications, biologic correlates, and challenges. *Radiographics.* (2017) 37:1483–503. doi: 10.1148/rg.2017170056
- Lambin P, Leijenaar RTH, Deist TM, Peerlings J, de Jong EEC, van Timmeren J, et al. Radiomics: the bridge between medical imaging and personalized medicine. *Nat Rev Clin Oncol.* (2017) 14:749–62. doi: 10.1038/nrclinonc.2017.141
- Guan Y, Wang P, Wang Q, Li P, Zeng J, Qin P, et al. Separability of acute cerebral infarction lesions in CT Based radiomics: toward artificial intelligence-assisted diagnosis. *Biomed Res Int.* (2020) 2020:8864756. doi: 10.1155/2020/8864756
- Nawabi J, Knip H, Elsayed S, Friedrich C, Sporns P, Rusche T, et al. Imaging-based outcome prediction of acute intracerebral hemorrhage. *Transl Stroke Res.* (2021) 12:958–67. doi: 10.1007/s12975-021-00891-8
- Chen S, Zeng L, Hu Z. Progressing haemorrhagic stroke: categories, causes, mechanisms and managements. *J Neurol.* (2014) 261:2061–78. doi: 10.1007/s00415-014-7291-1
- An SJ, Kim TJ, Yoon BW. Epidemiology, risk factors, and clinical features of intracerebral hemorrhage: an update. *J Stroke.* (2017) 19:3–10. doi: 10.5853/jos.2016.00864

Conflict of Interest: The authors declare that the research was conducted in the absence of any commercial or financial relationships that could be construed as a potential conflict of interest.

Publisher's Note: All claims expressed in this article are solely those of the authors and do not necessarily represent those of their affiliated organizations, or those of the publisher, the editors and the reviewers. Any product that may be evaluated in this article, or claim that may be made by its manufacturer, is not guaranteed or endorsed by the publisher.

Copyright © 2022 Shan, Li, Wu, Liu, Zhang, Xue and Gao. This is an open-access article distributed under the terms of the Creative Commons Attribution License (CC BY). The use, distribution or reproduction in other forums is permitted, provided the original author(s) and the copyright owner(s) are credited and that the original publication in this journal is cited, in accordance with accepted academic practice. No use, distribution or reproduction is permitted which does not comply with these terms.



Impaired Glymphatic Transport Kinetics Following Induced Acute Ischemic Brain Edema in a Mouse pMCAO Model

Jiaying Zhang¹, Hongchen Zhao¹, Yang Xue¹, Yiqi Liu¹, Guohang Fan¹, He Wang^{2*}, Qiang Dong^{1,3,4*} and Wenjie Cao^{1*}

¹ Department of Neurology, Huashan Hospital, Fudan University, Shanghai, China, ² The Key Laboratory of Computational Neuroscience and Brain-Inspired Intelligence, Institute of Science and Technology for Brain-Inspired Intelligence, Fudan University, Shanghai, China, ³ State Key Laboratory of Medical Neurobiology, Fudan University, Shanghai, China, ⁴ National Clinical Research Center for Aging and Medicine, Huashan Hospital, Fudan University, Shanghai, China

OPEN ACCESS

Edited by:

Sheng Zhang,
Zhejiang Provincial People's
Hospital, China

Reviewed by:

Xiaoming Rong,
Sun Yat-sen University, China
Mootaz M. Salman,
University of Oxford, United Kingdom

*Correspondence:

He Wang
hewang@fudan.edu.cn
Qiang Dong
dongqiang2222@gmail.com
Wenjie Cao
wenjiecao@fudan.edu.cn

Specialty section:

This article was submitted to
Applied Neuroimaging,
a section of the journal
Frontiers in Neurology

Received: 22 January 2022

Accepted: 18 February 2022

Published: 17 March 2022

Citation:

Zhang J, Zhao H, Xue Y, Liu Y, Fan G,
Wang H, Dong Q and Cao W (2022)
Impaired Glymphatic Transport
Kinetics Following Induced Acute
Ischemic Brain Edema in a Mouse
pMCAO Model.
Front. Neurol. 13:860255.
doi: 10.3389/fneur.2022.860255

Background: Cerebral edema forms immediately after blood flow interruption in ischemic stroke, which largely increased the death and disability. The glymphatic (glial-lymphatic) pathway is a major regulator of the brain liquid dynamics and homeostasis. This study aimed to investigate the transport kinetics of the glymphatic system after the appearance of ischemic edema.

Methods: In this study, a coated filament was attached to the left middle cerebral artery (MCA) of mice to establish a mouse model of permanent middle cerebral artery occlusion with an intact blood-brain barrier (BBB). The glymphatic function was then quantified using contrast-enhanced MRI (11.7T) by employing an injection of gadobenate dimeglumine (BOPTA-Gd) into the cisterna magna of mice. We then evaluated the expression and polarization of aquaporin-4 (AQP4) as a proxy for the physiological state of the glymphatic system.

Results: Our results revealed a positive correlation between the signal intensity in T1-weighted images and the corresponding apparent diffusion coefficient (ADC) values in the cortex, striatum, and periventricular zone, suggesting that impaired glymphatic transport kinetics in these regions is correlated to the cytotoxic edema induced by the occlusion of MCA. Furthermore, the increased depolarization of AQP4 in the parenchyma perivascular space (PVS) was consistent with glymphatic failure following the induced early cerebral ischemic edema.

Conclusions: Glymphatic transport kinetics were suppressed between the onset of cytotoxic edema and the disruption of the BBB, which correlated with the diminishing ADC values that vary based on edema progression, and is associated with depolarization of AQP4 in the parenchyma PVSs.

Keywords: magnetic resonance imaging, glymphatic, aquaporin-4, cerebral ischemic edema, polarization

INTRODUCTION

The severity of cerebral edema following ischemic stroke is predictive of a patient's functional outcome (1). However, current treatment options are often ineffective. Ischemic cerebral edema occurs soon after the cerebral blood flow (CBF) interruption, which can lead to severe stroke-related damage (2). This phenomenon is further exacerbated if the edema is aggravated and can lead to long-term or permanent effects even after the vessels are successfully re-canalized. In patients with early postischemia neurological deterioration, the effect of cerebral edema on the clinical outcome of reperfusion therapy is generally more pronounced (3). Cerebral edema after stroke has mainly been thought to be caused by the destruction of the blood-brain barrier (BBB) (4), which can allow blood components to penetrate this boundary, enter the parenchyma, and damage the tissue. Because of this, previous studies investigating the mechanism of cerebral edema have largely focused on the destruction of the BBB (5). Nevertheless, recent reports showed that cerebral edema develops several hours before significant dysfunction of the BBB (6), which posed a new question regarding other influential factors that arise cerebral ischemia edema. In fact, cytotoxic edema begins within minutes of ischemic destruction and is triggered by spreading depolarizations (SDs). These traveling neurophysiological events form a dysregulated ion homeostasis that often results in cell swelling (7), and are often accompanied by ionic edema and the net entry of water and ions into the brain (8), defined as interstitial edema. Based on this series of evidence, there exists a key time window between the onset of cytotoxic edema and the disruption of the BBB in which the transformation of cytotoxic edema to vasogenic edema occurs.

A previous study verified that an increased glymphatic influx of cerebrospinal fluid (CSF) into the parenchyma perivascular spaces (PVSs) (9) of ischemic brain tissue might be the actual cause of superacute ischemic brain edema (10). CSF influx was observed at (11.4 ± 1.8 s) and (5.24 ± 0.48 min), and was driven by SDs in the cortex following cerebral ischemia and led to edema (10). We then asked in a follow-up study how the kinetics of glymphatic functions were affected after the influx of the CSF. This influx occurred through the glymphatic system which is a brain-wide mass clearance system (11) that functions through fluid transport and has been confirmed in both humans (12) and mice (9, 13). In particular, the PVSs by which the CSF and interstitial fluid (ISF) exchange occurs act as flow channels that ensheath the cerebral vasculature in the mammalian brain (9). Aquaporin-4 (AQP4) is an essential water channel protein that facilitates this process through a complex network of astrocytes (14) that are localized throughout brain tissues facing the PVS (15) and ventricle lining (16). The glymphatic system, therefore, supports convective bulk flow (9, 14) by astrocytic paracellular fluid transport and facilitates the drainage of brain ISF between para-arterial influx and paravenular efflux. We hypothesize this process may facilitate brain swelling by glymphatic malfunctions.

In this study, we aimed to explore the alteration in glymphatic dynamics after the accumulation of fluid in

the brain parenchyma and periventricular zone. We also assessed glymphatic system dysfunction and its correlation with parenchymal and periventricular edema based on the signal intensity (SI) in T1-weighted images (T1WIs) and the corresponding apparent diffusion coefficient (ADC) value and further explored the altered polarization patterns of AQP4 in various affected edema regions in permanent middle cerebral artery occlusion (pMCAO) mice. We quantified the kinetics of glymphatic drainage using 11.7T contrast-enhanced magnetic resonance imaging (CEMRI) with intracisternal injections of BOPTA-Gd (17) after the onset of ischemic edema in a mouse model of pMCAO without BBB disruption (18). The glymphatic functions of sham-operated and pMCAO mice were characterized along both spatial and temporal features to identify glymphatic malfunction in the edema mouse brain induced by occlusion of the MCA.

MATERIALS AND METHODS

The data that support the findings of this study are available from the corresponding author upon reasonable request and are subject to institutional agreements and ethical approvals. All experiments were reported in compliance with the ARRIVE guidelines 2.0 (ARRIVE, Animal Research: Reporting *in Vivo* Experiments) (19).

Animals

All animal procedures were approved by the Huashan Hospital Institutional Review Board. The reason for using only male mice is that estrogen has been shown to significantly affect ischemic stroke (20). Male C57/BL6 mice (bodyweight 25–30 g) aged 10–12 weeks old were used in this study. Animals were housed at constant temperature ($25^{\circ}\text{C} \pm 2^{\circ}\text{C}$) with a 12/12 h light/dark cycle and were provided with *ad libitum* access to food and water. Animals were randomly assigned to two groups using excel-generated random numbers: the sham-operated group or the pMCAO group. The experimenters were blinded to pretreatments and data analysis. This study was carried out per the recommendations of the National Science Council of the Republic of China. All efforts were made to minimize animal suffering and the number of experimental animals used.

pMCAO Model

Previous studies investigating the mechanism of cerebral ischemic edema have mainly focused on the destruction of BBB (5). To do this, most experiments used an animal model of cerebral ischemia/reperfusion. By contrast, the BBB remains intact during permanent MCA occlusion (18), as indicated by continuous isolectin-B4 (IB4) staining (21), which allows for the mechanistic study of ischemic brain edema with an intact BBB. To perform pMCAO, mice were initially anesthetized with 4% isoflurane in 1 l/min oxygen delivered through a nose cone. The isoflurane was then adjusted to between 1.5 and 3% in 1 l/min oxygen to maintain anesthesia and normal breathing throughout the procedure. Animal body temperature was maintained at 37°C with a heating pad throughout the procedure. A laser

Doppler probe was fixed on the skull 5 mm lateral to and 2 mm posterior to Bregma. A coated filament (1622A4, Cinontech Co. Ltd., Beijing, China) was then placed at the left MCA under a stereomicroscope. Concurrent CBF recordings were recorded by laser Doppler to ensure that it was below 25% of baseline. Only the mice presenting with MCAO on a 3D (three-dimensional)-TOF (time-of-flight) MRI performed immediately after surgery were included in subsequent analyses.

Intracisternal Perfusion of Gadolinium-Based Contrast Agents

About 4 μ l of BOPTA-Gd was injected into the cisterna magna with a microsyringe pump (ALC-IP600(H), ALCOTT, Shanghai, China) and a pulled glass micropipette (diameter = \sim 80 μ m) that was connected and sealed to a 50 μ l syringe with hot melt glue (19). This allowed us to perform a single diminutive volume injection of contrast agents without significant injury to the dura mater and, thus, without CSF leakage. The micropipette was left in place for 1 additional minute to allow the wound to close. The intracisternal injection was conducted at a flow rate of 0.6 μ l/min over 6 min. About 28 min after the start of blood occlusion, the function of the glymphatic system and cerebral edema were evaluated by MRI.

MRI Experiments and Imaging Analysis

Following surgery and cisterna magna injection, animals were transferred to an MRI-compatible cradle. About 1.5% isoflurane in oxygen was continuously delivered to the animal through a nose cone. The core body temperature of the mice was maintained at 37°C, and respiratory rate was maintained between 70 and 100 breaths per minute. Each MRI was acquired on an 11.7T Pharmascan MRI system (Bruker, Germany) equipped with surface coils. A baseline scan was acquired before intrathecal infusion of the paramagnetic contrast agent. 3D T1WI was then performed with a fast low angle shot sequence with parameters as follows: magnetic field strength = 11.75123799 Tesla, repetition time/echo time (TR/TE) 50/3.5 ms, field-of-view (FOV) = 16 mm \times 16 mm, matrix = 128 \times 128, slice thickness (ST) = 0.3 mm, flip angle (FA) = 15°. 3D-TOF imaging was performed with the following parameters: TR/TE 12/2.0 ms, field-of-view (FOV) = 16 mm \times 16 mm, matrix = 120 \times 120, ST = 0.13 mm, FA = 20°. T2-weighted (T2W) imaging was performed with the following parameters: TR/TE 2500/30 ms, FOV = 16 mm \times 16 mm, matrix = 256 \times 256, ST = 0.5 mm, FA = 90°. Finally, diffusion-weighted imaging (DWI) was performed with parameters set as follows: TR/TE 3200/23 ms, FOV = 16 mm \times 16 mm, matrix = 180 \times 180, ST = 0.3 mm, FA = 90°. The time course of distribution of the contrast agent throughout the brain was assessed as a measure of glymphatic flow, as demonstrated in a previous study (9, 22). The time-resolved T1W SI in the striatum, cortex, and cerebral ventricles were used to obtain the average hydrodynamic response curves. These time series were also used to illustrate the tissue uptake of BOPTA-Gd tracers over time. The ADC values were calculated automatically by the 11.7T Pharmascan MRI system and were displayed as a parametric map that indicated the degree of water molecule diffusion through different tissues.

Then, ADC measurements were acquired for a given region by drawing regions of interest (ROIs) on the ADC map (23).

Triphenyl Tetrazolium Chloride (TTC) Staining

Animals were anesthetized and perfused with 20 ml of ice-cold saline. After immediate decapitation, the brains were extracted and sliced into six 1.5 mm coronal sections and immersed into 2% 2,3,5-triphenyl tetrazolium chloride (TTC) (Sigma-Aldrich) for 10 min at room temperature. Images were then acquired with a digital camera.

Section Preparation

About 150 min after surgery, the deeply anesthetized pMCAO animals ($n = 4$) and sham-operated animals ($n = 4$) were sacrificed. All animals were then transcardially perfused with ice-cold saline, followed by 4% paraformaldehyde (PFA). Brains were removed, postfixed in PFA overnight at 4°C, dehydrated in the ascending alcohol series, rinsed by xylene, and embedded in paraffin blocks. Coronal sections (bregma +0.38 mm to +1.10 mm) were serially cut at 3 μ m thickness using a paraffin slicing machine (RM2135, Leica Microsystems, Germany).

Immunofluorescence

After deparaffinization and hydration, antigen recovery was performed with ethylene diamine tetraacetic acid antigen retrieval buffer (pH 8.0). Coronal sections were maintained at a subboiling temperature for 8 min to facilitate staining with an AQP4 antibody. Sections were then blocked in phosphate-buffered saline (PBS) with 3% bovine serum albumin (BSA) for 30 min, and stained sequentially with primary mouse antibody AQP4 (1:500, #GB12529, Servicebio) and Alexa Fluor 594 antimouse (1:300, #GB21301, Servicebio), together with the fluorescein isothiocyanate (FITC) conjugate Bandeiraea simplicifolia Isolectin B4 (BSI-B4, 1:50, #L-2895, Sigma). The brain sections were then covered with an antifade medium containing 4',6-diamidino-2-phenylindole (DAPI, #D21490, Invitrogen). For this experimental step, IB4-FITC (2 mg dissolved in 2 ml saline, 0.05 mg per animal) was intravenously administered to the animals to identify the basement membrane. This was an important step as IB4 binds to α -D-galactose residues in the basement membrane secreted by endothelial cells (24). In each group, the circulation period of IB4-FITC was ensured for 180 min before sacrifice.

Immunohistochemistry

After deparaffinization, hydration, and antigen retrieval, sections were washed and incubated with the 3% hydrogen peroxide (H₂O₂) at room temperature for 15 min to block endogenous peroxidase. Then tissues were washed and blocked with 3% BSA at room temperature for 30 min. Tissue sections were incubated with primary mouse antibody AQP4 (1:2,000, #GB12529, Servicebio) at 4°C overnight. Following PBS wash, sections were incubated with secondary antibody goat antimouse IgG (1:200, #GB23303, Servicebio) labeled with horseradish peroxidase, incubate at room temperature for 50 min. Then visualized with diaminobenzidine reagent (#G1211, Servicebio).

Imaging Analysis

Microphotographs for analyzing immunofluorescence were captured by laser scanning confocal microscopy (FV1200, Olympus Microsystems, Japan) to generate 3-channel fluorescence images of the cerebral cortex and striatum. Images were obtained at 100 \times magnification and quantified using the ImageJ software (Bethesda, MD, USA). For immunofluorescent quantification of each antigen, at least three selected visual fields (bregma +0.38 to +1.10 mm) from each animal were imaged. Imaging parameters were constant throughout all imaging sessions. The background fluorescence for each channel was conformably subtracted and the perivascular expression of AQP4 was then measured after that in the soma (“depolarization”) was subtracted.

Microphotographs for analyzing immunohistochemistry were captured by conventional fluorescence microscopy (BX60, Olympus Microsystems, Japan). For the AQP4 examination, at least three high-power fields at 100 \times magnification were randomly selected and imaged for each animal. The ROI on the AQP4 display included the ependymal wall and a small amount of surrounding brain tissue in the bilateral brain of pMCAO animals. The average optical density (AOD) of AQP4 in each field was quantitatively calculated using the ImageJ software. All imaging parameters were constant throughout all imaging sessions.

Quantification of AQP4 Expression and Polarization

To evaluate global and perivascular AQP4 expression levels, the mean AQP4 immunofluorescence intensity was measured within each visual field and the perivascular space. Evaluation of the polarization of AQP4 to perivascular end-feet was performed by measuring the immunofluorescence intensity of AQP4 immunoreactivity across sections of blood vessels labeled by IB4-FITC in each brain region studied. AQP4 polarization was measured by comparing the intensity ratios of AQP4 at perivascular domains vs. those in the parenchymal domains, as evaluated previously (25). The threshold was determined based on immunostained control slices.

Statistical Analysis

Statistical analyses were conducted using Prism (GraphPad Software, V8.3.0, La Jolla, USA). The data are represented as mean \pm SD. Either a repeated measure two-way ANOVA or a regular two-way ANOVA was used for regional comparisons, followed by Tukey’s multiple comparisons test. A one-way ANOVA was used for regional comparisons, and unpaired *t*-tests were used for single comparisons. Pearson correlation analysis was utilized to evaluate the link between edema and glymphatic failure. A *p*-value < 0.05 was considered statistically significant.

RESULTS

Occlusion of Blood Flow in pMCAO Mice

To study the dynamics of glymphatic flow following cerebral edema, we induced pMCAO (Figure 1A) in the left (L)

hemisphere of mice, examined ischemic regions using TTC staining 24 h after pMCAO (Figures 1Bi–iii). We confirmed the occlusion of MCA by multiplanar reconstructions (Figure 1C) and maximum intensity projections (Figure 1D) in 11.7 T MR images. In both images, pMCAO was represented by a unilateral loss of visible vasculature ipsilateral in the site of model induction. By contrast, bilateral vasculature could be observed in the sham-operated animals. The loss of vascular imaging markers was also quantified by calculating the CBF, as recorded by laser Doppler, to ensure that it was below 25% of baseline. pMCAO resulted in an immediate and strong reduction in the relative CBF (rCBF) ($79.6\% \pm 2.1\%$; Figure 1E).

In vivo Evaluation of Glymphatic Flow in Sham-Operated Mice

We then investigated the glymphatic flow in sham-operated mice by *in vivo* CEMRI with BOPTA-Gd injection (BOPTA-Gd+) in the cisterna magna (Figure 2C). Sequential multiplanar reformation or reconstruction images revealed that gadolinium progressively entered the brain parenchyma, as shown in the schematic diagram in Figure 2A. The schematic diagram of the approximate ROIs used for MRI quantification is indicated in Figure 2B. In these images, an increase in SI, representing contrast agent uptake, can be observed as a function of time. Overall, the routes of CSF distribution were consistent with previous reports (Figure 2C) (26). Meanwhile, the contrast agent sequentially flowed from the cisterna magna to the bilateral, third, and fourth cerebral ventricles, as shown in Figure 2C. At 70 min postinjection, the brain ROI were completely perfused with the tracers (Figure 2C). The average time evolution curves illustrate the dynamics of tissue uptake of BOPTA-Gd tracers (Figure 2D). We also detected extracerebral CSF drainage routes at 14 min after BOPTA-Gd injection. Tracers drained from the subarachnoid space alongside the cranial nerves, such as the cochleovestibular and optic nerves (Figure 2E).

Glymphatic Transport Kinetics Malfunction in the Acute Phase of pMCAO Mice

Interestingly, in the MRI we noticed a blockage of the ipsilateral (L) parenchyma and the bilateral ventricle perfusion immediately after pMCAO (Figures 3A,Ci). By contrast, the inflow of contrast agent was observed in the contralateral (R) hemisphere in the pMCAO and the sham-operated animals, further suggesting that glymphatic flow was altered in this pMCAO mouse model. To quantify these effects, we calculated the corresponding SI in the cortex, striatum, and ventricles in the pMCAO and the sham-operated animals (Figures 3Bi,ii,Di,ii). We found that glymphatic perfusion of the ipsilateral cortex/striatum and bilateral cerebral ventricles of the pMCAO mice was reduced compared with sham-operated animals. By contrast, glymphatic perfusion in the contralateral cortex/striatum was increased. These results provide evidence of glymphatic perfusion from the cisterna magna to the cerebral ventricles. However, the volume of the ventricles (Figure 3Cii) was reduced in the ipsilateral pMCAO mice and was accompanied by a delayed influx in the

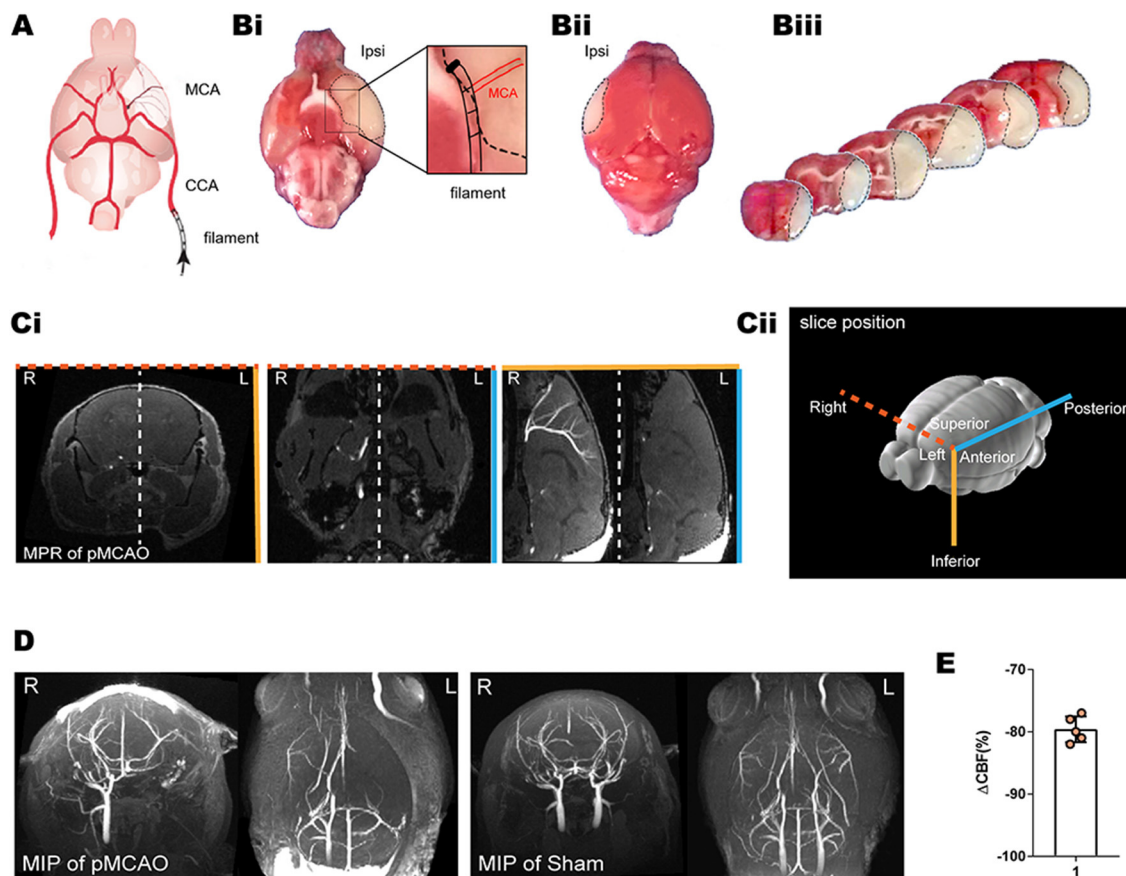


FIGURE 1 | TTC staining, laser Doppler, and MRI of the pMCAO mice model. **(A)** Schematic diagram of the MCA occlusion. Reproduced with permission (10) **(Bi–iii)** Representative TTC staining of cerebral ischemia at 24 h after pMCAO. A lack of TTC staining was defined as infarction, whereas viable brain tissue was stained red. **(Ci,D)** The MCA occlusion displayed in coronal, axial, and sagittal planes of MPR and MIP. Bright signals are associated with the vasculature. L indicates the pMCAO side. **(Cii)** Schematic diagram of the slice positions of the MRI. Color-coded border lines denote the anatomical position of the slice. **(E)** Ipsilateral relative rCBF after MCAO ensured that the CBF decreased to below 25% of baseline as measured by laser Doppler.

bilateral ventricles (**Figure 3D**). The schematic diagram of the anatomical position of ventricles, and the approximate ROIs used for MRI quantification of the lateral ventricle volume are shown in **Figure 3E**.

Analysis of the Link Between Ischemic Edema and Glymphatic Failure

To evaluate cerebral edema, we acquired T1WI, DWI, and ADC brain maps, these sequential scans were performed 28 min after pMCAO with 14 min BOPTA-Gd injections until 178 min (150 + 28 min) ($n = 3$ per group), serial acquisition of MR images was performed using an interval of about 12 min, and confirmed brain infarction by T2W images at ~178 min (**Figure 4A**). Accordingly, we acquired the T1W and ADC value brain maps sequentially in the sham-operation group 14 min after BOPTA-Gd injection. Glymphatic transport kinetics were determined based on the SI in T1WIs, while cytotoxic edema was identified as cases of DWI hyperintensity with reduced diffusion and with ADC dark signal (27). When we measured molecular motion with DWI, only the ADC value was calculated. We observed a

positive correlation between SI in T1WIs and the corresponding ADC value in the cortex, striatum, and periventricular zone, suggesting that the impaired glymphatic transport kinetics in these regions are associated with the progression of pMCAO edema, as indicated by ADC values changes (**Figures 4B–D**).

Immunofluorescent Analysis of AQP4 Expression and Polarization

Representative images of pMCAO and sham-operated animals (**Figures 5A–C**) showed an ischemia-affected ipsilateral (L) cortex and striatum 150 min after surgery. The vascular endothelial surface was delineated by I-B4 staining. At 150 min after pMCAO induction, parenchymal vessels in pMCAO animals exhibited endothelial IB4-FITC signals that did not differ from those of sham-operated animals (**Figure 5B**). This lack of difference indicated that the BBB remained intact (18, 21). In the current work, AQP4 was conjugated with Alexa Fluor 594, and nuclei were visualized with DAPI. AQP4 polarization levels were obtained by comparing the expression ratio of AQP4 at perivascular domains vs. parenchymal domains (25),

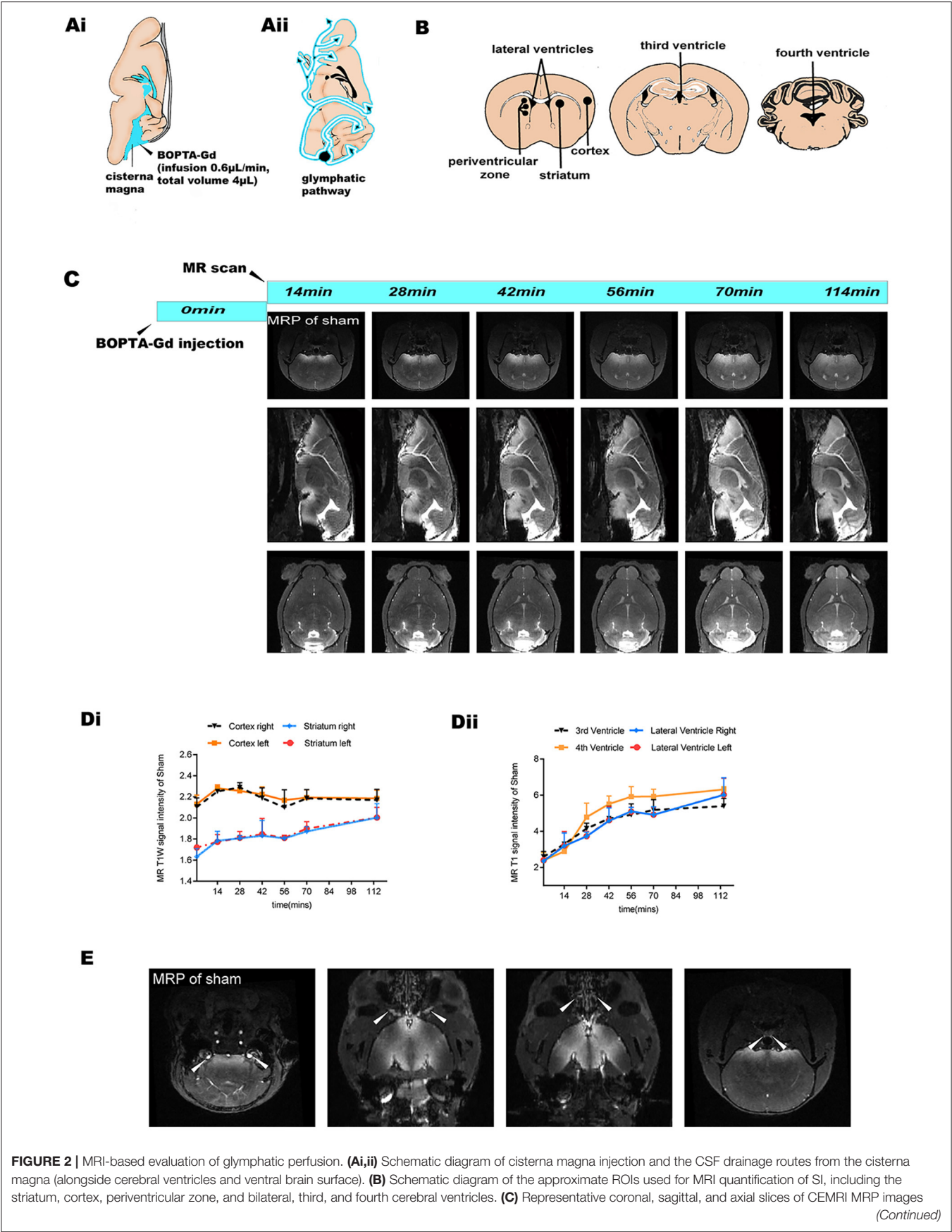


FIGURE 2 | from the sham-operated group (BOPTA-Gd+), showing progressive enhancement of the brain parenchyma and cerebral ventricles. **(Di,ii)** Corresponding quantification of the SI from the sham-operation striatum, cortex, and cerebral ventricles. The average time evolution curves illustrate the dynamic of tissue uptake of BOPTA-Gd tracers ($n = 3$ per group). **(E)** Extracerebral CSF drainage routes revealed by the sham-operated group (BOPTA-Gd+). Arrows indicate cochleovestibular nerves, optic nerves, cribriform plate, and the peritracheal lymph nodes (from left to right, respectively).

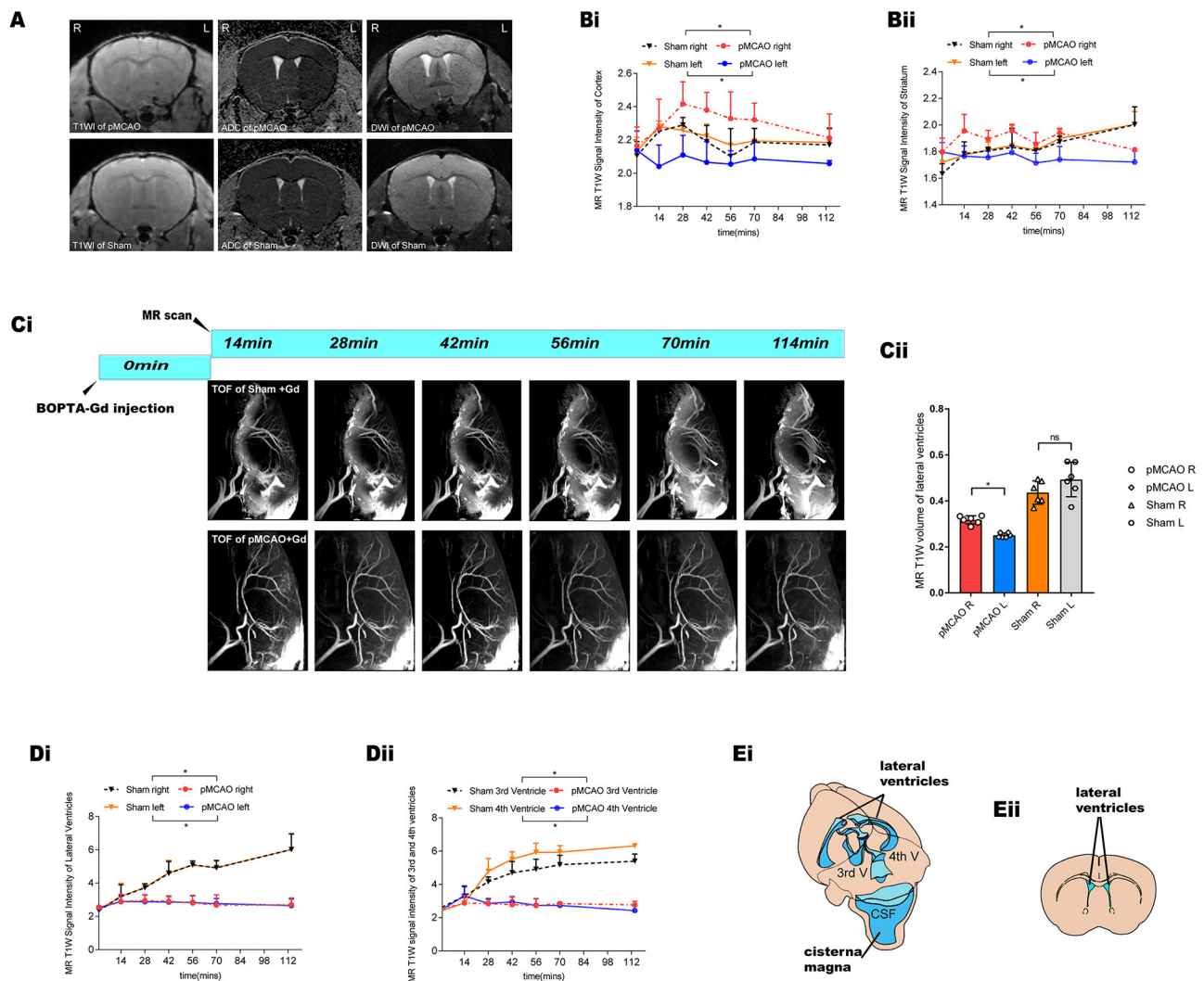
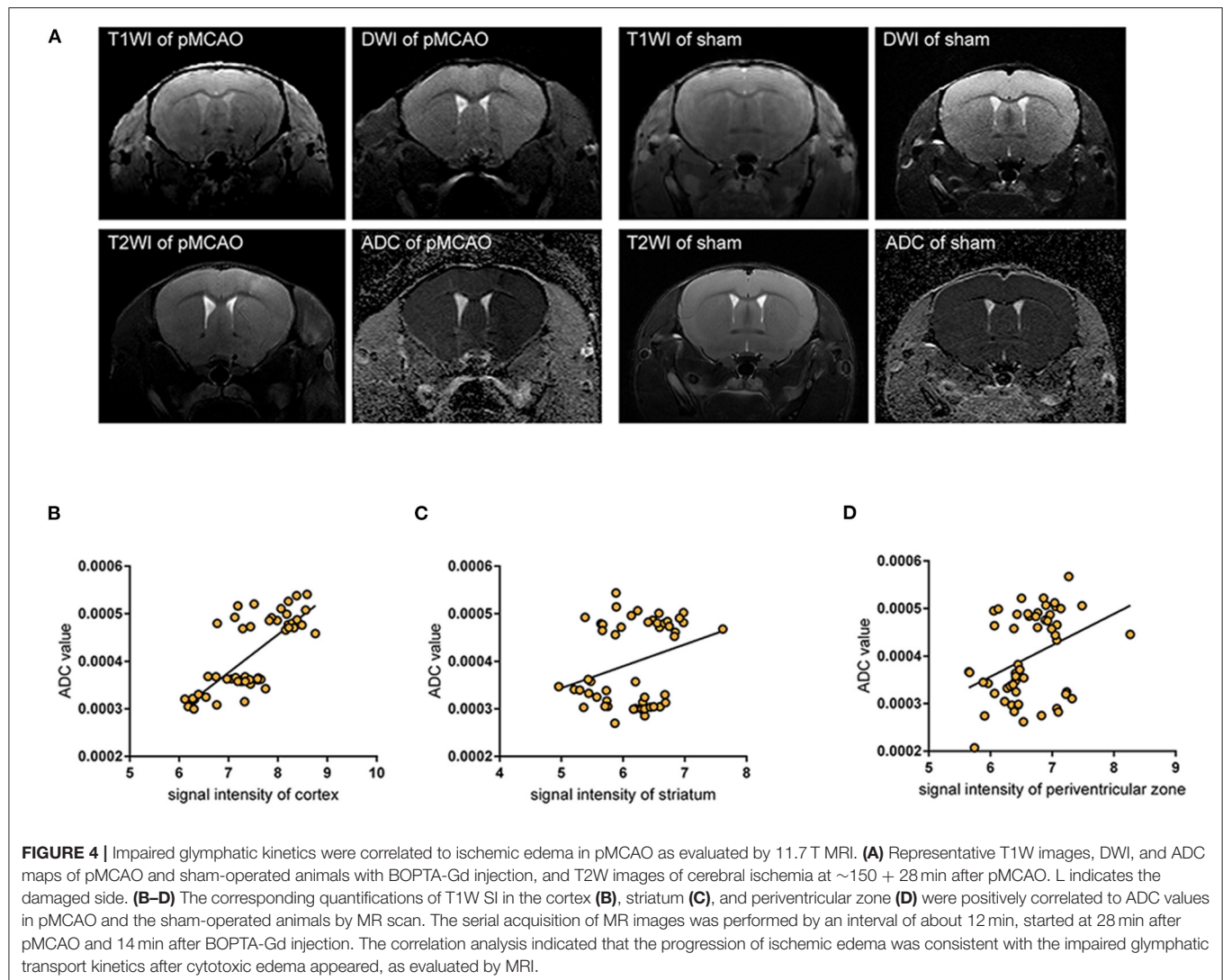


FIGURE 3 | Glymphatic transport kinetics were impaired after the onset of ischemic edema in the pMCAO mice. **(A)** Representative T1W images, DWI, and ADC maps of pMCAO and sham-operated animals with BOPTA-Gd injection. The serial acquisition of MR images was performed at an interval of about 12 min and started at 28 min after pMCAO and 14 min after BOPTA-Gd injection. L indicates the pMCAO side. ROIs used for MRI quantification are as shown in **Figure 2B**. **(B,D)** The corresponding quantification of SI indicated the dynamic of tissue uptaking BOPTA-Gd tracers. Compared to the sham-operated animals, the T1W SI of the pMCAO group was decreased in the ipsilateral cortex/striatum **(Bi,ii)** and the bilateral cerebral ventricles **(Di,ii)** of the pMCAO brain ($n = 3$ per group). Concurrently, the increase in the SI of the contralateral cortex/striatum was detected by the enhancement of contrast agent, as compared to the sham-operated group. **(Ci)** Representative TOF images demonstrate that glymphatic flow was impaired in the bilateral ventricles of mice after the onset of ischemic edema in pMCAO with BOPTA-Gd injection. **(Cii)** Corresponding quantification of ventricular volume changes in the pMCAO and sham-operated animals, for which a decrease in the volume of the ipsilateral ventricles was observed. **(Ei)** Schematic diagram of the anatomical position of ventricles, namely, bilateral (LV), third (3V), and fourth (4V) cerebral ventricles. Reproduced with permission (10) **(Eii)** Blue-dashed areas indicate the approximate ROIs used for MRI quantification of the lateral ventricle volume.

which were analyzed on corresponding images obtained under $100\times$ magnification. Specifically, we compared the contralateral tissue 150 min after surgery in pMCAO and sham-operated animals. Overall, in pMCAO animals, we found no significantly

altered global AQP4 expression (**Figure 5E**). Quantitative analysis showed that perivascular polarity of AQP4 decreased in ipsilateral pMCAO brains, with the most pronounced effects in the cortex and the striatum (**Figure 5D**). The



widespread loss of perivascular AQP4 polarization accompanied the decline in glymphatic dynamics. Representative image of immunofluorescent staining of PVS in the sham-operated group is shown in **Figure 5F**.

Immunohistochemical Analysis of AQP4 Expression in the Ependymal Wall

Representative images showing AQP4 immunohistochemical staining (brown) of coronal brain sections in the lateral ventricle (LV) ependymal barrier (**Figures 6A,B**) revealed that AQP4 expression was decreased in the LV ependymal wall of the ipsilateral pMCAO brain (**Figure 6C**). These images also revealed AOD values with no apparent abnormalities in ependymal architecture. Furthermore, we observed a positive correlation between the corresponding ADC values in the periventricular zone of pMCAO animals at the MR scan acquired after 150 min and the AOD of AQP4 in the immunohistochemical staining of bilateral LV ependymal walls (**Figure 6D**). This result suggests that decreased expression of AQP4 in ependymal

walls was correlated to the diminishing of ADC values in the periventricular zone.

DISCUSSION

Our results demonstrate in a pMCAO model with an intact BBB (18, 21) that the accumulation of edema is not accompanied by the transendothelial extravasation water (28) across the BBB. Of note, at as early as 150 min post-pMCAO, in the period during which the transformation of cytotoxic edema to vasogenic edema occurs, the ischemic edema regions showed a depolarization of AQP4 in the PVSs. The key finding was that there was a positive correlation between T1WI SI and the corresponding ADC values in the cortex, striatum, and periventricular zone. This suggested that glymphatic transport kinetics were impaired after the ischemic edema appeared in pMCAO, were accompanied by depolarization of AQP4, and were correlated to the progression of edema.

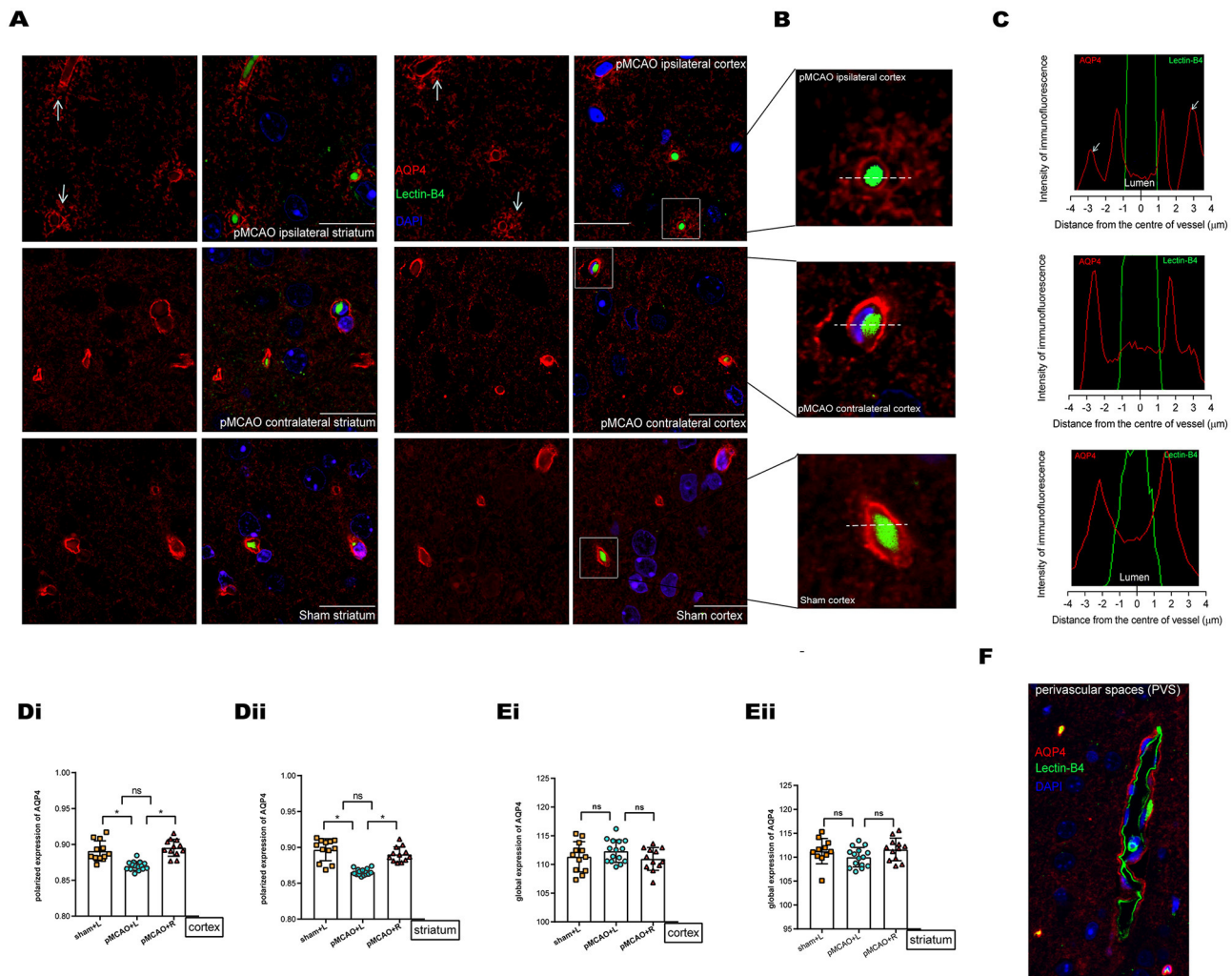


FIGURE 5 | Immunofluorescent staining of AQP4 in the cortex and striatum of sham-operated and 150 min post-pMCAO animals. **(A)** Representative images of immunofluorescent staining of AQP4 in the cortex and striatum in 150 min post-pMCAO and sham-operated animals. The scale bar is 20 μ m. Magnification is 100 \times . **(B)** Three representative magnified images in the boxed areas of **(A)** are shown as a representative expression pattern. **(C)** The axis perpendicular to blood vessels was used to quantify the expression across vessel cross-sections. AQP4 expression surrounding blood vessels in the ipsilateral cortex of pMCAO mice was decreased (depolarization expression pattern). **(D)** Quantification of at least 12 images (a minimum of 3 images per animal, $n = 4$) shows changes in AQP4 polarization. Compared with the sham-operated and contralateral pMCAO, polarized expression of AQP4 immunofluorescence was decreased surrounding blood vessels in the cortex and striatum of the ipsilateral pMCAO brain. **(E)** Quantification of at least 12 images (a minimum of 3 images per animal, $n = 4$) shows changes in global AQP4 expression. Compared with the sham-operated and contralateral pMCAO, global expression of AQP4 immunofluorescence was not significantly altered in the cortex and striatum of the ipsilateral pMCAO brains. **(F)** Representative image of immunofluorescent staining of PVS (red indicates AQP4, green indicates basement membrane, and blue indicates DAPI) in the sham-operated group.

Cerebrospinal fluid (CSF) can provide a predominant source for the initial rise in the brain water content of ischemic tissues. The glymphatic influx of CSF into the PVSs (9) of ischemic brain tissues is the critical cause of acute ischemic brain edema within ~ 5 min (10). Given the possible treatment strategies require the time for the operation to be executed, it is necessary to investigate the specific contribution of the glymphatic dynamics in different stages of acute ischemia edema. As such, we investigated the pattern of glymphatic flow that could account for the liquid drainage in the parenchyma and periventricular zone following induced acute ischemic brain edema as a follow-up study. Uptake

of tracers and extracerebral CSF drainage routes have been observed in sham-operated animals as shown in **Figures 2C,E**. In the pMCAO model, we found that CSF dynamic flow was reduced in the ipsilateral brain parenchyma and accompanied by an increase in flow in the contralateral as indicated in **Figure 3**. These observations suggest that the accumulation of liquid in pMCAO brains may result from an impaired glymphatic system or be responsible for the suppression of the glymphatic dynamics. Glymphatic transport is driven by arterial pulsation (29, 30), and ISF drainage may be increased by vasomotion as a driving force, as observed by two-photon microscopy (31). Therefore, the

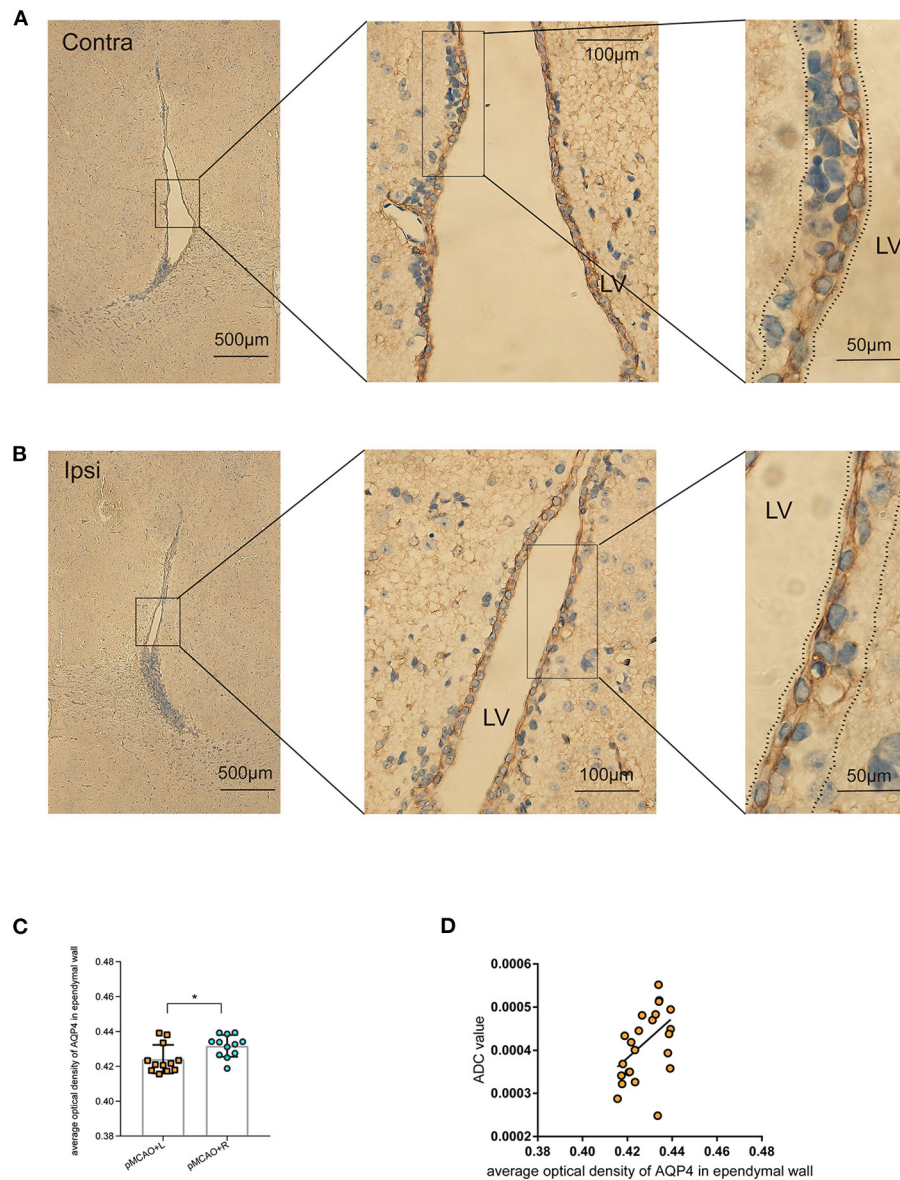


FIGURE 6 | Immunohistochemical staining of AQP4 in the LV ependymal wall of 150 min post-pMCAO animals. **(A,B)** Representative images showing AQP4 immunohistochemical staining (brown) of coronal brain sections in the LV ependymal barrier of the bilateral brain in 150 min post-pMCAO animals. These images revealed comparable morphology of the bilateral ependyma walls outlining LV. Boxed areas are enlarged successively from left to right. The areas between the dotted lines were used to quantify AQP4 expression in the LV ependymal wall. The scale bars are indicated in each box, and the magnification is 4×, 40×, and 100×, respectively. **(C)** Quantification of at least 12 images (a minimum of three images per animal, $n = 4$) revealed changes in AQP4 expression. Compared with the contralateral pMCAO animals, AOD of AQP4 immunohistochemical staining was reduced in the LV ependymal wall of the ipsilateral pMCAO brain. **(D)** The corresponding ADC values in the periventricular zone of pMCAO animals at the 150 min MR scan were positively correlated to the AOD of AQP4 in the immunohistochemical staining of bilateral LV ependymal walls. ROIs used for MRI quantification are as shown in **Figure 2B**.

regional differences in glymphatic flow observed here may be due to discrepancies in a convective flow drive mechanism. However, another study recently provided evidence that the directional movement of CSF in the PVS is not generated by arterial pulsations and can be explained by naturally occurring flow (32). Furthermore, contrast agents were found to rapidly enter the ventricular system in the sham-operated group (**Figure 3**),

suggesting that cistern-labeled CSF could enter the ventricles. Previous data suggest a critical role of the ventricle in brain water drainage (33, 34). PVS pathways were found to connect different parts of the brain to the ventricles. In particular, a connection between the lateral ventricle and ventral brain surface has been identified through PVS pathways surrounding the anterior choroidal artery (33). Thus, there might exist a pathway

that involves the transependymal exchange of CSF, followed by the clearance therefore from the parenchyma *via* a mechanism similar to the glymphatic system.

As a key determinant of the glymphatic system, AQP4 is a transmembrane and bidirectional water channel that is highly expressed on astrocytes, particularly at the sites of fluid transport at the pial surrounding cerebral blood vessels and ependymal surfaces in contact with the CSF in the ventricular system, and acts as a facilitator for water transport both in cells and tissues (16, 35–37). In a recent study, CSF was identified as a major source of water that drives directly AQP4-dependent edema, which acts as a consequence of CSF and brain ISF exchange (10). Other studies suggested a controversial opinion, in that the depletion of astrocytic AQP4 caused water to accumulate in the brain (34) and markedly impaired interstitial solute clearance (38). Moreover, recent studies on AQP4-knockout mice have suggested that the water movement in the paravascular space is mediated through diffusion and convective flow (39, 40), and elucidated the concept that AQP4 plays a vital role in the central nervous system (CNS) water homeostasis. In this sense, AQP4 is thought to facilitate the development or clearance of CNS edema. Previous studies have shown the glymphatic clearance function depends on the highly selective expression of AQP4 in microvascular end-feet of astrocytes in the aging brain, traumatic brain injury, and animal models of cerebral small vessel disease (38, 41, 42). We explored here the loss of polarized AQP4 expression leads to compromised glymphatic activity as soon as edema appeared at 150 min post-pMCAO (**Figure 5**). We also observed a decrease in AQP4 expression in the LV ependymal wall of the ipsilateral pMCAO brain, accompanied by a reduced volume of the ventricles and a delay in CSF uptake from the cisterna magna, as shown in **Figures 3C, 6C**. The participation of AQP4 in structural function, such as the distensibility capacity of the ventricular system, is also related to CSF homeostasis by altering the CSF drainage and the ventricular compliance in AQP4 mutation mice (43). Aquaporins (AQPs) line the periventricular wall. Previous studies have hypothesized that AQP4 participates in the development and integrity of the ependyma, however, the underlying mechanism of this effect has not been identified (44).

Cerebral edema is primarily an intracellular water accumulation process, caused by water influx through AQP4 passively in response to osmotic gradients (16), and usually as a consequence of ischemia-hypoxia. Of all the cell types susceptible to cytotoxic edema in the cerebral nervous system, astrocytes are particularly vulnerable (28). Along these lines, a recently proposed treatment targeting the mechanism of CNS edema is supported by the idea that AQP4 localization is also dynamically regulated at the subcellular level, from intracellular vesicles to the plasma membrane, affecting membrane water permeability (45). Due to the described dynamic subcellular changes of aquaporin abundance (45, 46), and there being highly polarized at the

fluid interface (15), the membrane permeability and either the influx of CSF or ISF dynamics must be selective or suppressed. AQPs have been validated as an important drug target but there is no single drug that has yet been approved to successfully target it, it is hard to target edema and the glymphatic function using one line of therapies (47, 48). The previous studies have shown an increased AQP4 membrane localization in primary human astrocytes which was not accompanied by a change in AQP4 protein expression levels (45, 46). This subcellular mislocalization can be a potential therapeutic target. More studies to investigate the communication between AQPs (mainly AQP4) and other therapeutic targets are required to identify AQP modulators. Targeting the ion channel function and regulation mechanisms of AQP4 subcellular relocalization provides new insights into drug development (49). Currently, chelation of Ca^{2+} or CaM inhibition through egtazic acid acetoxymethyl ester (EGTA-AM) (45) or trifluoperazine (TFP) (50) had been reported to effectively reduce ischemia CNS edema.

In conclusion, glymphatic transport kinetics were suppressed between the onset of cytotoxic edema and the disruption of the BBB. These impaired glymphatic transport kinetics were correlated to the diminishing of ADC values that vary depending on edema progression, as measured by MRI, and that are associated with the depolarization of AQP4 in both the parenchyma PVSs and periventricular zone. As such, targeting the dynamic subcellular relocalization of the water channel protein AQP4, and improving glymphatic dynamics by promoting polarization of AQP4 may alleviate acute ischemic cerebral edema and similar pathologies.

DATA AVAILABILITY STATEMENT

The raw data supporting the conclusions of this article will be made available by the authors, without undue reservation.

ETHICS STATEMENT

The animal study was reviewed and approved by Huashan Hospital Institutional Review Board.

AUTHOR CONTRIBUTIONS

JZ, WC, HW, HZ, YX, and GF performed the experiments, participated in data collection, and revision of this manuscript. WC, HW, and QD designed the study. HZ and YX analyzed the data. JZ drafted this manuscript and prepared figures. All authors contributed to the article and approved the submitted version.

FUNDING

This study was supported by the National Nature Science Foundation of China (Nos. 81870915 and 82071197).

REFERENCES

- Rosenberg GA. Ischemic brain edema. *Prog Cardiovasc Dis.* (1999) 42:209–16. doi: 10.1016/S0033-0620(99)70003-4
- Rocha M, Jovin TG. Fast versus slow progressors of infarct growth in large vessel occlusion stroke: clinical and research implications. *Stroke.* (2017) 48:2621–7. doi: 10.1161/STROKEAHA.117.017673
- Ferro D, Matias M, Neto J, Dias R, Moreira G, Petersen N, et al. Neutrophil-to-lymphocyte ratio predicts cerebral edema and clinical worsening early after reperfusion therapy in stroke. *Stroke.* (2021) 52:859–67. doi: 10.1161/STROKEAHA.120.032130
- Klatzo I. Pathophysiological aspects of brain edema. *Acta Neuropathol.* (1987) 72:236–9. doi: 10.1007/BF00691095
- Li Z, Li M, Shi SX, Yao N, Cheng X, Guo A, et al. Brain transforms natural killer cells that exacerbate brain edema after intracerebral hemorrhage. *J Exp Med.* (2020) 217:e20200213. doi: 10.1084/jem.20200213
- Dreier JP, Lemale CL, Kola V, Friedman A, Schoknecht K. Spreading depolarization is not an epiphenomenon but the principal mechanism of the cytotoxic edema in various gray matter structures of the brain during stroke. *Neuropharmacology.* (2018) 134:189–207. doi: 10.1016/j.neuropharm.2017.09.027
- Young W, Rappaport ZH, Chalif DJ, Flamm ES. Regional brain sodium, potassium, and water changes in the rat middle cerebral artery occlusion model of ischemia. *Stroke.* (1987) 18:751–9. doi: 10.1161/01.STR.18.4.751
- Simard JM, Kent TA, Chen M, Tarasov KV, Gerzanich V. Brain oedema in focal ischaemia: molecular pathophysiology and theoretical implications. *Lancet Neurol.* (2007) 6:258–68. doi: 10.1016/S1474-4422(07)70055-8
- Iliff JJ, Wang M, Liao Y, Plogg BA, Peng W, Gundersen GA, et al. A paravascular pathway facilitates CSF flow through the brain parenchyma and the clearance of interstitial solutes, including amyloid β . *Sci Transl Med.* (2012) 4:147ra111. doi: 10.1126/scitranslmed.3003748
- Mestre H, Du T, Sweeney AC, Liu G, Samson AJ, Peng W, et al. Cerebrospinal fluid influx drives acute ischemic tissue swelling. *Science.* (2020) 367:eaax7171. doi: 10.1126/science.aax7171
- Louveau A, Plog BA, Antila S, Alitalo K, Nedergaard M, Kipnis J. Understanding the functions and relationships of the glymphatic system and meningeal lymphatics. *J Clin Invest.* (2017) 127:3210–9. doi: 10.1172/JCI90603
- Lee S, Yoo RE, Choi SH, Oh SH, Ji S, Lee J, et al. Contrast-enhanced MRI T1 mapping for quantitative evaluation of putative dynamic glymphatic activity in the human brain in sleep-wake states. *Radiology.* (2021) 300:661–8. doi: 10.1148/radiol.2021203784
- Rasmussen MK, Mestre H, Nedergaard M. The glymphatic pathway in neurological disorders. *Lancet Neurol.* (2018) 17:1016–24. doi: 10.1016/S1474-4422(18)30318-1
- Alshuhri MS, Gallagher L, Work LM, Holmes WM. Direct imaging of glymphatic transport using H217O MRI. *JCI Insight.* (2021) 6:e141159. doi: 10.1172/jci.insight.141159
- Nielsen S, Nagelhus EA, Amiry-Moghadam M, Bourque C, Agre P, Ottersen OP. Specialized membrane domains for water transport in glial cells: high-resolution immunogold cytochemistry of aquaporin-4 in rat brain. *J Neurosci.* (1997) 17:171–80. doi: 10.1523/JNEUROSCI.17-01-00171.1997
- Salman MM, Kitchen P, Halsey A, Wang MX, Tornroth-Horsefield S, Conner AC, et al. Emerging roles for dynamic aquaporin-4 subcellular relocalization in CNS water homeostasis. *Brain.* (2021). doi: 10.1093/brain/awab311
- Gaberel T, Gakuba C, Goulay R, Martinez De Lizarrondo S, Hanouz JL, Emery E, et al. Impaired glymphatic perfusion after strokes revealed by contrast-enhanced MRI: a new target for fibrinolysis? *Stroke.* (2014) 45:3092–6. doi: 10.1161/STROKEAHA.114.006617
- O'Donnell ME, Chen YJ, Lam TI, Taylor KC, Walton JH, Anderson SE. Intravenous HOE-642 reduces brain edema and Na uptake in the rat permanent middle cerebral artery occlusion model of stroke: evidence for participation of the blood-brain barrier Na/H exchanger. *J Cereb Blood Flow Metab.* (2013) 33:225–34. doi: 10.1038/jcbfm.2012.160
- Percie du Sert N, Hurst V, Ahluwalia A, Alam S, Avey MT, Baker M, et al. The ARRIVE guidelines 2.0: Updated guidelines for reporting animal research. *J Cereb Blood Flow Metab.* (2020) 40:1769–77. doi: 10.1177/0271678X20943823
- Engler-Chiurazzi EB, Brown CM, Povroznik JM, Simpkins JW. Estrogens as neuroprotectants: Estrogenic actions in the context of cognitive aging and brain injury. *Prog Neurobiol.* (2017) 157:188–211. doi: 10.1016/j.pneurobio.2015.12.008
- Krueger M, Mages B, Hobusch C, Michalski D. Endothelial edema precedes blood-brain barrier breakdown in early time points after experimental focal cerebral ischemia. *Acta Neuropathol Commun.* (2019) 7:17. doi: 10.1186/s40478-019-0671-0
- Iliff JJ, Lee H, Yu M, Feng T, Logan J, Nedergaard M, et al. Brain-wide pathway for waste clearance captured by contrast-enhanced MRI. *J Clin Invest.* (2013) 123:1299–309. doi: 10.1172/JCI67677
- El Kady RM, Choudhary AK, Tappouni R. Accuracy of apparent diffusion coefficient value measurement on PACS workstation: a comparative analysis. *AJR Am J Roentgenol.* (2011) 196:W280–284. doi: 10.2214/AJR.10.4706
- Peters BP, Goldstein IJ. The use of fluorescein-conjugated Bandeiraea simplicifolia B4-isolectin as a histochemical reagent for the detection of alpha-D-galactopyranosyl groups. Their occurrence in basement membranes. *Exp Cell Res.* (1979) 120:321–34. doi: 10.1016/0014-4827(79)90392-6
- Wang M, Iliff JJ, Liao Y, Chen MJ, Shinseki MS, Venkataraman A, et al. Cognitive deficits and delayed neuronal loss in a mouse model of multiple microinfarcts. *J Neurosci.* (2012) 32:17948–60. doi: 10.1523/JNEUROSCI.1860-12.2012
- Ramos M, Burdon Bechet N, Battistella R, Pavan C, Xavier ALR, Nedergaard M, et al. Cisterna magna injection in rats to study glymphatic function. *Methods Mol Biol.* (2019) 1938:97–104. doi: 10.1007/978-1-4939-9068-9_7
- Gaddamanugu S, Shafaat O, Sotoudeh H, Sarraimi AH, Rezaei A, Saadatpour Z, et al. Clinical applications of diffusion-weighted sequence in brain imaging: beyond stroke. *Neuroradiology.* (2022) 64:15–30. doi: 10.1007/s00234-021-02819-3
- Stokum JA, Gerzanich V, Simard JM. Molecular pathophysiology of cerebral edema. *J Cereb Blood Flow Metab.* (2016) 36:513–38. doi: 10.1177/0271678X15617172
- Iliff JJ, Wang M, Zeppenfeld DM, Venkataraman A, Plog BA, Liao Y, et al. Cerebral arterial pulsation drives paravascular CSF-interstitial fluid exchange in the murine brain. *J Neurosci.* (2013) 33:18190–9. doi: 10.1523/JNEUROSCI.1592-13.2013
- Mestre H, Tithof J, Du T, Song W, Peng W, Sweeney AM, et al. Flow of cerebrospinal fluid is driven by arterial pulsations and is reduced in hypertension. *Nat Commun.* (2018) 9:4878. doi: 10.1038/s41467-018-07318-3
- van Veluw SJ, Hou SS, Calvo-Rodriguez M, Arbel-Ornath M, Snyder AC, Frosch MP, et al. Vasomotion as a driving force for paravascular clearance in the awake mouse brain. *Neuron.* (2020) 105:549–61.e545. doi: 10.1016/j.neuron.2019.10.033
- Kedarasetti RT, Drew PJ, Costanzo F. Arterial pulsations drive oscillatory flow of CSF but not directional pumping. *Sci Rep.* (2020) 10:10102. doi: 10.1038/s41598-020-66887-w
- Magdoo KN, Brown A, Rey J, Mareci TH, King MA, Sarntinoranont M. MRI of whole rat brain perivascular network reveals role for ventricles in brain waste clearance. *Sci Rep.* (2019) 9:11480. doi: 10.1038/s41598-019-44938-1
- Vindedal GE, Thoren AE, Jensen V, Klungland A, Zhang Y, Holtzman MJ, et al. Removal of aquaporin-4 from glial and ependymal membranes causes brain water accumulation. *Mol Cell Neurosci.* (2016) 77:47–52. doi: 10.1016/j.mcn.2016.10.004
- Mestre H, Hablitz LM, Xavier AL, Feng W, Zou W, Pu T, et al. Aquaporin-4-dependent glymphatic solute transport in the rodent brain. *Elife.* (2018) 7. doi: 10.7554/eLife.40070.022
- Mamtilahun M, Tang G, Zhang Z, Wang Y, Tang Y, Yang GY. Targeting water in the brain: role of aquaporin-4 in ischemic brain edema. *Curr Drug Targets.* (2019) 20:748–55. doi: 10.2174/1389450120666190214115309
- Buffoli B. Aquaporin biology and nervous system. *Curr Neuropharmacol.* (2010) 8:97–104. doi: 10.2174/157015910791233204
- Kress BT, Iliff JJ, Xia M, Wang M, Wei HS, Zeppenfeld D, et al. Impairment of paravascular clearance pathways in the aging brain. *Ann Neurol.* (2014) 76:845–61. doi: 10.1002/ana.24271

39. Smith AJ, Yao X, Dix JA, Jin BJ, Verkman AS. Test of the 'glymphatic' hypothesis demonstrates diffusive and aquaporin-4-independent solute transport in rodent brain parenchyma. *Elife*. (2017) 6. doi: 10.7554/eLife.27679.019
40. Ray L, Iliff JJ, Heys JJ. Analysis of convective and diffusive transport in the brain interstitium. *Fluids Barriers CNS*. (2019) 16:6. doi: 10.1186/s12987-019-0126-9
41. Ren Z, Iliff JJ, Yang L, Yang J, Chen X, Chen MJ, et al. 'Hit & Run' model of closed-skull traumatic brain injury (TBI) reveals complex patterns of post-traumatic AQP4 dysregulation. *J Cereb Blood Flow Metab*. (2013) 33:834–45. doi: 10.1038/jcbfm.2013.30
42. Xue Y, Liu N, Zhang M, Ren X, Tang J, Fu J. Concomitant enlargement of perivascular spaces and decrease in glymphatic transport in an animal model of cerebral small vessel disease. *Brain Res Bull*. (2020) 161:78–83. doi: 10.1016/j.brainresbull.2020.04.008
43. Trillo-Contreras JL, Toledo-Aral JJ, Echevarría M, Villadiego J. AQP1 and AQP4 Contribution to Cerebrospinal Fluid Homeostasis. *Cells*. (2019) 8:197. doi: 10.3390/cells8020197
44. Li X, Kong H, Wu W, Xiao M, Sun X, Hu G. Aquaporin-4 maintains ependymal integrity in adult mice. *Neuroscience*. (2009) 162:67–77. doi: 10.1016/j.neuroscience.2009.04.044
45. Kitchen P, Salman MM, Halsey AM, Clarke-Bland C, MacDonald JA, Ishida H, et al. Targeting aquaporin-4 subcellular localization to treat central nervous system edema. *Cell*. (2020) 181:784–99. doi: 10.1016/j.cell.2020.03.037
46. Salman MM, Kitchen P, Woodroffe MN, Brown JE, Bill RM, Conner AC, et al. Hypothermia increases aquaporin 4 (AQP4) plasma membrane abundance in human primary cortical astrocytes via a calcium/transient receptor potential vanilloid 4 (TRPV4)- and calmodulin-mediated mechanism. *Eur J Neurosci*. (2017) 46:2542–7. doi: 10.1111/ejn.13723
47. Verkman AS, Anderson MO, Papadopoulos MC. Aquaporins: important but elusive drug targets. *Nat Rev Drug Discov*. (2014) 13:259–77. doi: 10.1038/nrd4226
48. Abir-Awan M, Kitchen P, Salman MM, Conner MT, Conner AC, Bill RM. Inhibitors of Mammalian Aquaporin Water Channels. *Int J Mol Sci*. (2019) 20:1589. doi: 10.3390/ijms20071589
49. Salman MM, Kitchen P, Yool AJ, Bill RM. Recent breakthroughs and future directions in drugging aquaporins. *Trends Pharmacol Sci*. (2022) 43:30–42. doi: 10.1016/j.tips.2021.10.009
50. Sylvain NJ, Salman MM, Pushie MJ, Hou H, Meher V, Herlo R, et al. The effects of trifluoperazine on brain edema, aquaporin-4 expression and metabolic markers during the acute phase of stroke using photothrombotic mouse model. *Biochim Biophys Acta Biomembr*. (2021) 1863:183573. doi: 10.1016/j.bbame.2021.183573

Conflict of Interest: The authors declare that the research was conducted in the absence of any commercial or financial relationships that could be construed as a potential conflict of interest.

Publisher's Note: All claims expressed in this article are solely those of the authors and do not necessarily represent those of their affiliated organizations, or those of the publisher, the editors and the reviewers. Any product that may be evaluated in this article, or claim that may be made by its manufacturer, is not guaranteed or endorsed by the publisher.

Copyright © 2022 Zhang, Zhao, Xue, Liu, Fan, Wang, Dong and Cao. This is an open-access article distributed under the terms of the Creative Commons Attribution License (CC BY). The use, distribution or reproduction in other forums is permitted, provided the original author(s) and the copyright owner(s) are credited and that the original publication in this journal is cited, in accordance with accepted academic practice. No use, distribution or reproduction is permitted which does not comply with these terms.



Early Edema Within the Ischemic Core Is Time-Dependent and Associated With Functional Outcomes of Acute Ischemic Stroke Patients

Qing Han^{1†}, Jianhong Yang^{1†}, Xiang Gao², Jichuan Li¹, Yuefei Wu¹, Yao Xu¹, Qing Shang¹, Mark W. Parsons^{3*} and Longting Lin^{1,3*}

¹ Department of Neurology, Ningbo First Hospital, Ningbo, China, ² Department of Neurosurgery, Ningbo First Hospital, Ningbo, China, ³ Sydney Brain Center, University of New South Wales, Sydney, NSW, Australia

OPEN ACCESS

Edited by:

Peiyu Huang,
Zhejiang University, China

Reviewed by:

Yang-Kun Chen,
Southern Medical University, China
Tobias Djamsched Faizy,
University Medical Center
Hamburg-Eppendorf, Germany

*Correspondence:

Longting Lin
longting.lin@unsw.edu.au
Mark W. Parsons
Mark.Parsons@unsw.edu.au

[†]These authors have contributed
equally to this work

Specialty section:

This article was submitted to
Applied Neuroimaging,
a section of the journal
Frontiers in Neurology

Received: 24 January 2022

Accepted: 08 March 2022

Published: 07 April 2022

Citation:

Han Q, Yang J, Gao X, Li J, Wu Y,
Xu Y, Shang Q, Parsons MW and Lin L
(2022) Early Edema Within the
Ischemic Core Is Time-Dependent
and Associated With Functional
Outcomes of Acute Ischemic Stroke
Patients. *Front. Neurol.* 13:861289.
doi: 10.3389/fneur.2022.861289

Objective: To investigate the difference in early edema, quantified by net water uptake (NWU) based on computed tomography (CT) between ischemic core and penumbra and to explore predictors of NWU and test its predictive power for clinical outcome.

Methods: Retrospective analysis was conducted on patients admitted to Ningbo First Hospital with anterior circulation stroke and multi-modal CT. In 154 included patients, NWU of the ischemic core and penumbra were calculated and compared by Mann–Whitney *U* test. Correlations between NWU and variables including age, infarct time (time from symptom onset to imaging), volume of ischemic core, collateral status, and National Institutes of Health Stroke Scale (NIHSS) scores were investigated by Spearman's correlation analyses. Clinical outcome was defined using the modified Rankin Scale (mRS) at 90 days. Logistic regression and receiver operating characteristic analyses were performed to test the predictive value of NWU. Summary statistics are presented as median (interquartile range), mean (standard deviation) or estimates (95% confidence interval).

Results: The NWU within the ischemic core [6.1% (2.9–9.2%)] was significantly higher than that of the penumbra [1.8% (–0.8–4.0%)]. The only significant predictor of NWU within the ischemic core was infarct time ($p = 0.004$). The NWU within the ischemic core [odds ratio = 1.23 (1.10–1.39)], the volume of ischemic core [1.04, (1.02–1.06)], age [1.09 (1.01–1.17)], and admission NIHSS score [1.05 (1.01–1.09)] were associated with the outcome of patients adjusted for sex and treatment. The predictive power for the outcome of the model was significantly higher when NWU was included (area under the curve 0.875 vs. 0.813, $p < 0.05$ by DeLong test).

Conclusions: Early edema quantified by NWU is relatively limited in the ischemic core and develops in a time-dependent manner. NWU estimates within the ischemic core may help to predict clinical outcomes of patients with acute ischemic stroke.

Keywords: edema, net water uptake, multimodal CT, acute ischemic stroke, ischemic core, penumbra, functional outcome

INTRODUCTION

Cerebral edema is defined as a pathological increase in the water mass contained in the brain interstitial space (1). The disruption of water homeostasis can occur in the hyperacute stage after brain ischemia (2) and plays an important role in the pathophysiology of ischemic stroke. Early cerebral edema is a sign of damage to the blood–brain barrier (BBB) and disruption of neuronal ion channels, which contribute to poor clinical outcomes (3–5). However, it is difficult to quantify early cerebral edema after acute stroke.

Computed tomography (CT)-based net water uptake (NWU) is an emerging tool for the quantitative assessment of tissue edema (6, 7). NWU within early infarct was reported as a reliable biomarker identifying patients within the time window of thrombolysis (7, 8) and predicting malignant edema or poor outcome after large vessel occlusion (9–11).

Cerebral edema, quantified by NWU, may provide essential information on the assessment of patients with acute ischemic stroke; however, the relationship between NWU and other important predictors (12–15) such as age, the volume of infarct lesion, National Institutes of Health Stroke Scale (NIHSS) scores, and collateral status need further exploration. In addition, previous studies testing the correlations between NWU and clinical prognosis were limited to patients with large vessel occlusion. It is, therefore, not known whether NWU in the ischemic lesion is predictive of outcome in patients with small-vessel occlusion.

Previous studies have also focused primarily on infarct core (tissue that has already infarcted); however, the occurrence and predictive role of edema in the penumbra (hypoperfused tissue that is at risk of infarction but potentially salvageable) (16) remains unknown.

Therefore, this study was designed to investigate the difference in edema between ischemic core and penumbra, explore the relevant predictors of NWU within early infarct, and test whether it is a reliable predictor of poor outcomes in acute ischemic stroke.

METHODS

Patients

All patients with acute ischemic stroke who received multi-modal CT imaging on admission between July 2017 and September 2019 at Ningbo First Hospital, China were retrospectively screened for inclusion.

Inclusion criteria for this study were as follows: (1) ischemic core and penumbra in anterior circulation territory confirmed by CT perfusion (CTP) and dynamic CT angiography (CTA), including either large vessel or small vessel occlusion; (2) assessment by NIHSS score on admission; (3) documented infarct time (from symptom onset to admission imaging) except for patients with wake-up strokes. The exclusion criteria included preexisting infarctions, hemorrhage, and any other abnormal alteration of density on admission non-contrast CT (NCCT). Baseline demographic data and clinical characteristics were extracted from the medical records. The modified Rankin Scale

(mRS) score after 90 days was extracted from the follow-up database.

The study had institutional ethical approval, and written informed consent was obtained for each patient for their collected data.

Image Acquisitions

Patients received multi-modal CT on admission, including NCCT, CT angiography (CTA), and CTP on a 320-slice scanner (Toshiba Aquilion ONE, Toshiba Medical Imaging, Tokyo, Japan). The CTP was performed with the following protocol: temporally, 19 time points were obtained, with the acquisition commencing 4 s after non-ionic iodinated contrast injection into an antecubital vein (50 ml, 5 ml/s; Bayer HealthCare, Berlin, Germany). Spatially, 320 axial sections with a thickness of 0.5 mm were obtained, which covered the whole brain (160 mm total coverage). CTP data were processed by using commercial software (Mistar, Apollo Medical Imaging Technology, Melbourne, VIC, Australia). The mathematical model of delay-corrected singular value decomposition was chosen to generate perfusion parameters, including cerebral blood volume (CBV), cerebral blood flow (CBF), mean transit time (MTT), and delay time (DT) (17). The volumes of ischemic lesion, ischemic core, and penumbra were then quantified by appropriate thresholds reported elsewhere (18): DT <3 s for total ischemic lesion, CBF <30% for acute ischemic core, and penumbra measured by the total ischemic lesion volume minus ischemic core volume. CTA data were post-processed on a Vitrea workstation (Vitrea version 1.0, Vital Images, Minnetonka, MN, United States).

Image Analysis

All imaging measurements were performed using commercial software Mistar (Apollo Medical Imaging Technology, Melbourne, VIC, Australia). NWU was defined as increased volume of water after stroke (ΔV_{water}) per unit volume of the ischemic lesion (V_{ischemic}). A standardized procedure was performed to quantify NWU within early ischemic core based on multi-modal CT. Briefly, regions of interest (ROIs) for ischemic core and penumbra were firstly drawn according to CTP and then automatically mirrored contralateral ROIs were defined as normal tissue. These ROIs were placed on NCCT and were sampled between 20 and 80 Hounsfield units (HU) to exclude voxels including CSF or calcification (Figure 1). All densitometric CT measurements (D_{normal} , D_{ischemic} including D_{core} and D_{penumbra}) were then used to calculate NWU according to the following equations (6, 7).

$$\begin{aligned} NWU &= \frac{\Delta V_{\text{water}}}{V_{\text{ischemic}}} = \frac{V_{\text{ischemic}} - V_{\text{normal}}}{V_{\text{ischemic}}} \\ &= \left(1 - \frac{D_{\text{ischemic}}}{D_{\text{normal}}}\right) \times 100\% \end{aligned}$$

Statistical Analysis

According to the results of Kolmogorov–Smirnov test, all numerical variables were described as mean [standard deviation (SD)], or median [interquartile range (IQR)]. Categorical

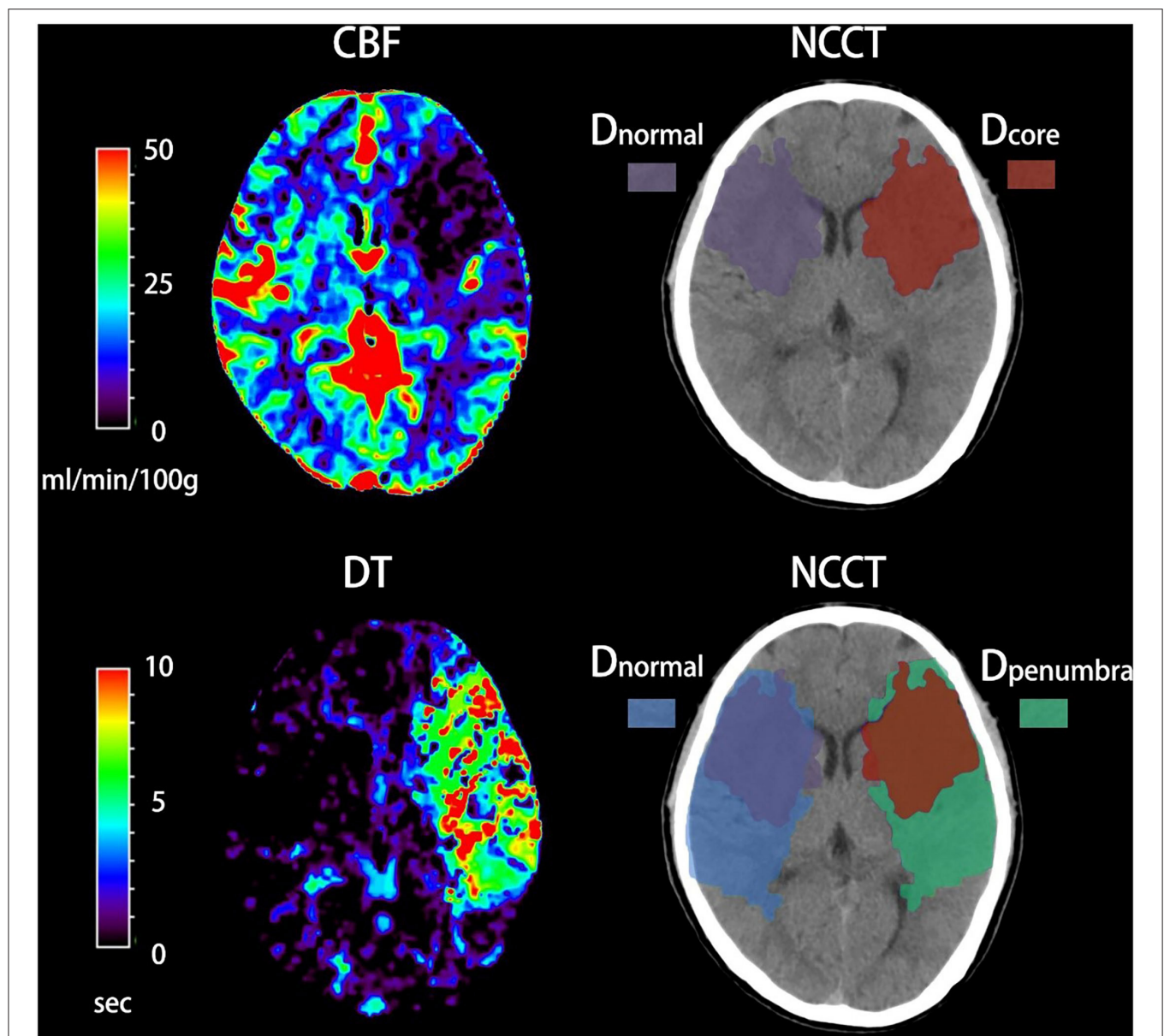


FIGURE 1 | Quantification of net water uptake (NWU) per volume of early infarct in admission non-contrast computed tomography (NCCT). The ischemic core and penumbra were identified by cerebral blood volume (CBV) and delay time (DT) maps based on computed tomography perfusion (CTP). The mean density of early infarct (D_{core} and $D_{penumbra}$) and the normal tissue (D_{normal}) derived from a mirrored contralateral region of interest were then calculated.

data were expressed as numbers (percentages). The NWU within ischemic core and penumbra were calculated and then compared by Student's *t*-test or Mann-Whitney *U* test as appropriate. The relationship between NWU within the ischemic core and other baseline variables including infarct time (time from symptom onset to imaging), age, NNHSS score, the volume of ischemic core, and collateral status were assessed using Pearson's correlation analysis or Spearman's correlation analysis as appropriate. Collateral status was classified by a modified version of the ASITN/SIR (American Society of Interventional and Therapeutic Neuroradiology/Society of

Interventional Radiology) collateral scale on dynamic CTA (19, 20), and it was further dichotomized into good collateral (ASITN/SIR score 3–4) and poor collateral (ASITN/SIR score 0–2) status. The relationship between NWU within the ischemic core and collateral status (good vs. poor collateral) was further tested on Mann-Whitney *U* test.

We defined poor functional outcome (functional dependence or death) as a modified Rankin Scale (mRS) of ≥ 3 at 90 days. Baseline data were compared after dichotomization into mRS score 0–2 and mRS score 3–6 using the Mann-Whitney *U* Test for metric variables and Chi-square test for categorical variables.

To investigate the predictive value of ischemic core NWU and other variables for the likelihood of the poor functional outcome, we performed binary logistic regression analyses presenting odds ratio (OR) estimates along with 95% confidence intervals (CI). The diagnostic power of variables and predictive models were assessed by univariate receiver operating characteristic (ROC) curve analysis. The ROC comparisons between different predicting models were performed using the DeLong test.

A two-tailed $p < 0.05$ was considered statistically significant. All Statistical analyses were performed using SPSS Statistics for Windows, Version 22.0 (IBM Corp., Armonk, NY, USA) and MedCalc (version 9.2.1; Mariakerke, Belgium).

RESULTS

Of the 248 screened patients, 154 fulfilled the inclusion criteria of which 127 had documented the time of symptom onset and 27 had wake-up strokes. In all 154 included patients, NWU within the ischemic core, penumbra, and contralateral healthy tissue were calculated and then compared using the Mann-Whitney U test. The density of ischemic core on admission NCCT was significantly lower than that of contralateral normal tissue [median 31.8 HU (30.3–33.2) vs. median 33.9 HU (32.4–35.4), $p < 0.001$, **Figure 2A**]. The density of penumbra was also lower than that of contralateral normal tissue but this difference was not statistically significant [median 34.8 HU (33.3–36.1) vs. median 35.0 HU (33.5–36.6), $p = 0.158$, **Figure 2B**]. The NWU within the ischemic core was significantly higher than that of the penumbra [median 6.1% (2.9–9.2%) vs. 1.8% (–0.8 to 4.0%), $p < 0.001$, **Table 1** and **Figure 2C**].

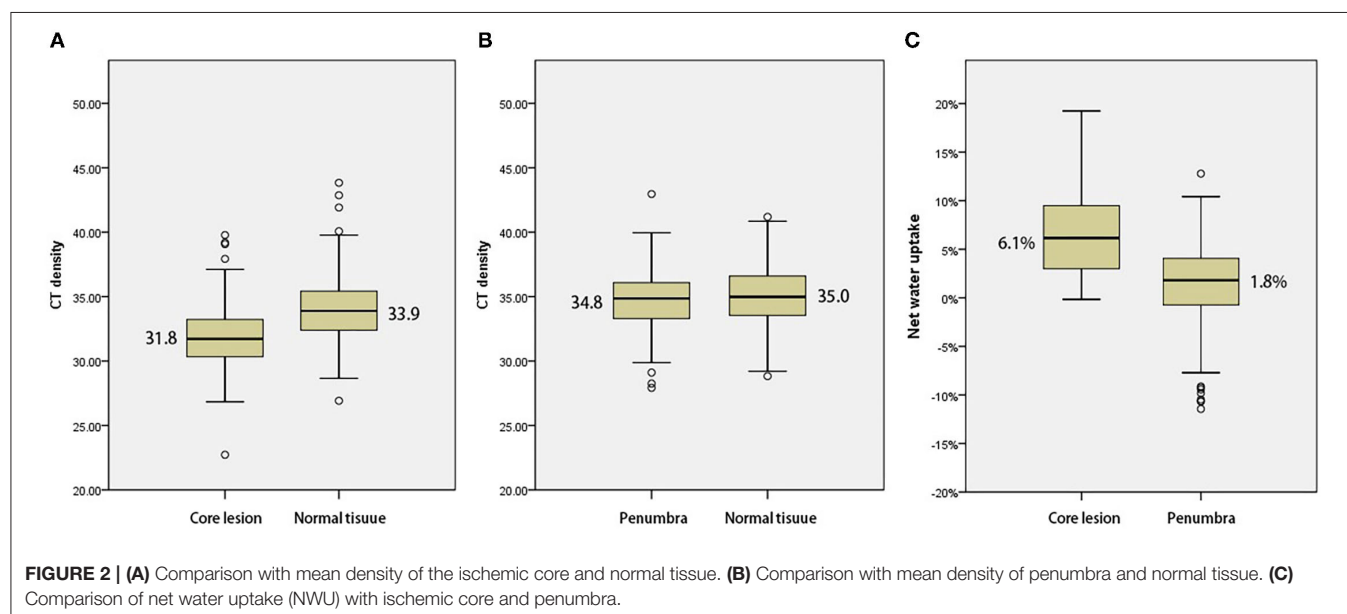
A Spearman test was performed to investigate correlations between NWU within ischemic core and age, admission NHISS score, and volume of ischemic core in 154 patients. The correlation between NWU and infarct time was analyzed in

those 127 patients with a documented time of onset. There was a significant correlation between NWU and infarct time ($p = 0.004$, **Figure 3A**). However, the NWU within the ischemic core was not correlated with age ($p = 0.954$), admission NHISS score ($p = 0.821$), ASITN/SIR score ($p = 0.287$), the volume of the ischemic core ($p = 0.094$, **Figure 3B**). There was no significant difference of NWU between the good collateral group (ASITN/SIR score 3–4) and poor collateral group (ASITN/SIR score 0–2) on Mann-Whitney U test ($p = 0.137$), although patients with good collateral showed a tendency of lower NWU

TABLE 1 | Net water uptake in different categories of lesion, infarct time, core volume, and collateral status.

Category	Net water uptake % median (IQR)
Region	
Ischemic core	6.1 (2.9–9.2)
Penumbra	1.8 (–0.8–4.0)
Time from onset to CT	
0–3 h, $n = 32$	3.4 (0.9–7.3)
3–6 h, $n = 74$	6.2 (3.3–9.0)
6–24 h, $n = 21$	9.2 (4.2–13.3)
Volume of ischemic core	
0–30 ml, $n = 76$	4.5 (1.9–7.6)
30–50 ml, $n = 35$	7.5 (3.6–11.4)
50–70 ml, $n = 18$	5.9 (2.0–7.9)
>70 ml, $n = 25$	6.8 (4.0–9.3)
Collateral status	
ASITN/SIR 0–2, $n = 105$	6.4 (3.2–9.3)
ASITN/SIR 3–4, $n = 49$	4.4 (1.8–9.2)

IQR, interquartile range; CT, computed tomography; ASITN/SIR, modified version of American Society of Interventional and Therapeutic Neuroradiology/Society of Interventional Radiology collateral scale on dynamic CT angiography.



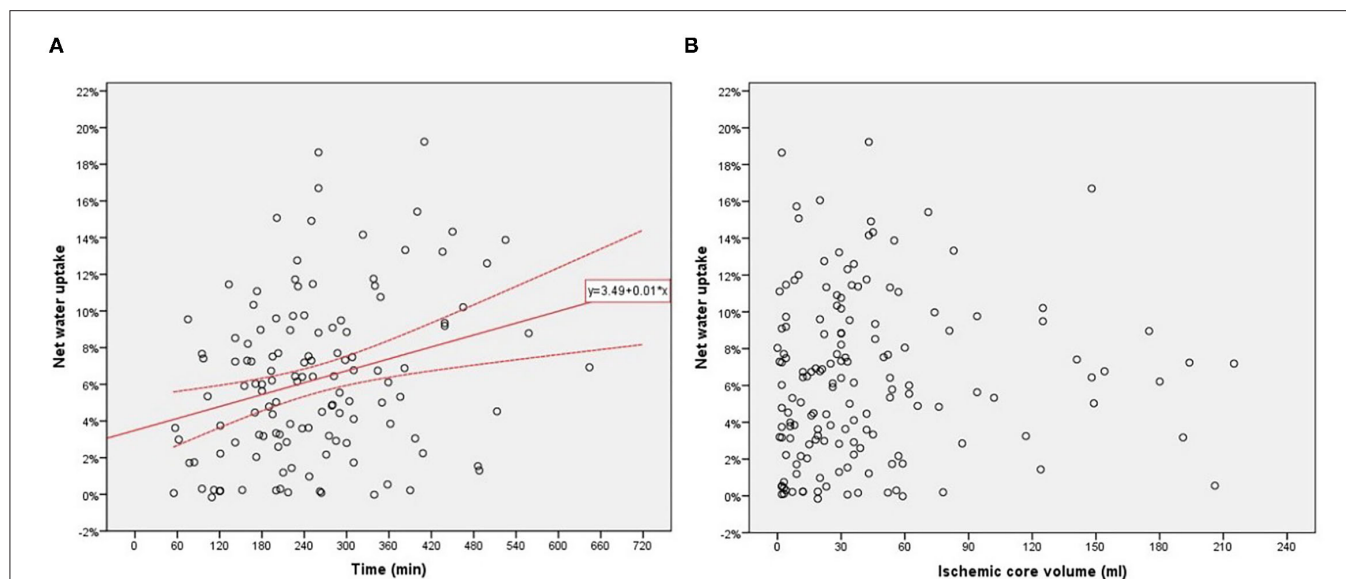


FIGURE 3 | (A) Relationship between net water uptake (NWU) within the ischemic core and infarct time from onset to imaging. **(B)** Relationship between NWU within ischemic core and core volume.

(4.4 vs. 6.4, **Supplementary Figure 1**). The value of NWU in different categories of infarct time, core volume, and collateral status are summarized in **Table 1**.

Of the 154 patients, 128 were followed up at 90 days; these 128 patients were divided into good outcome (mRS score 0–2, $n = 53$) and poor outcome groups (mRS score 3–6, $n = 75$). The main characteristics of the two groups are summarized in **Table 2**. The NWU within the ischemic core in patients with good outcomes was significantly lower compared to patients with poor outcomes. Patients with the good outcome also tended to be younger, have a smaller volume of the ischemic core and lower NIHSS score at baseline, and were less likely to be female than those with poor outcome. The infarct time and treatment of the two groups did not significantly differ.

We performed multivariate logistic regression analysis to determine the effects of NWU within the ischemic core, age, sex, ischemic core volume, admission NIHSS score, and treatment on likelihood of poor functional outcome. The result showed the NWU within ischemic core [odds ratio = 1.23 (95% CI 1.10–1.39)], volume of ischemic core [odds ratio = 1.04 (95% CI 1.02–1.06)], age [odds ratio = 1.09 (95% CI 1.01–1.17)] and admission NIHSS score [odds ratio = 1.05 (95% CI 1.01, 1.09)] were independently and significantly associated with poor functional outcome while sex and treatment were not (**Table 3**).

We tested the power of NWU within the ischemic core to predict the poor functional outcome by the area under the curve (AUC) after receiver operating characteristic curve (ROC) analysis. The AUC of the model including NWU (NWU within ischemic core, volume of ischemic core, age, and NIHSS score) was 0.875 while the AUC of the model without NWU was 0.813 (**Table 3** and **Figure 4**). The power of the model including NWU to predict poor functional outcomes was significantly higher

than that of the model without NWU according to the DeLong test ($p = 0.021$).

DISCUSSION

This study confirmed an important role for acute lesion edema, quantified by NWU, in predicting stroke outcomes. One of the main findings of this study was that edema was affected by the severity of ischemia, with limited NWU detected in the ischemic penumbra but significantly higher NWU detected in the ischemic core. Moreover, the severity of edema was not predicted by core volume, but rather by infarct time. This study indicates that the more late a patient with stroke is presented, the more severe is the edema within the ischemic core.

A novel finding of this study was the lack of significant edema in the penumbra region. Previous studies measured NWU either in the whole hypoperfused region (combining both core and penumbra into a single measurement) or ischemic core only. The lack of edema detected in the penumbra may relate to the slower progression of pathophysiological pathways compared to the core. Processes such as ATP depletion, reactive oxygen species generation, oxidative membrane injury, ionic imbalance, and tissue edema develop in the penumbra over several hours or days (21, 22). Previous ultrastructural studies also demonstrated that the degree of edema, degeneration of neurons, glia, and capillaries decreased gradually from ischemic core to penumbra (23, 24). Although this study confirmed previous findings of significantly increased NWU within the ischemic core, the NWU detected was lower compared to previous studies (7, 9, 25, 26). This is probably a result of different thresholds of ischemic core on CTP measurements. Most previous studies used a more severe threshold of CBV $\leq 6/100$ ml while we defined ischemic core using CBF $< 30\%$. As NWU gradually decreased based on the

TABLE 2 | Characteristics of patients with anterior circulation infarct stratified by prognosis.

Characteristics	Good prognosis (mRS at 90 days 0–2)	Poor prognosis (mRS at 90 days 3–6)	p-value ^a
Subjects, <i>n</i> (%)	53 (41.4)	75 (58.6)	
Female sex, <i>n</i> (%)	18 (34.0)	40 (53.3)	0.033*
Age in years, median (IQR)	68 (56–76)	74 (66–81)	0.009*
Admission NIHSS, median (IQR)	15 (9–18)	20 (14–25)	<0.001*
Time from onset to CT, median h (IQR) ^b	4.2 (2.8–4.9), <i>n</i> = 45	3.8 (2.9–5.7), <i>n</i> = 62	0.464
Volume of ischemic core, median ml (IQR)	12 (4–30)	42 (22–62)	<0.001*
Treatment			0.162
Mechanical thrombectomy, <i>n</i> (%)	19 (35.8)	40 (53.3)	
DPT, median min (IQR)	93 (80–127)	97 (81–132)	
Intravenous lysis, <i>n</i> (%)	18 (34.0)	22 (29.3)	
DNT, median min (IQR)	49 (36–61)	52 (32–64)	
Both, <i>n</i> (%)	12 (22.6)	8 (10.7)	
None, <i>n</i> (%)	4 (7.5)	5 (6.7)	
Net water uptake, median % (IQR)	4.1 (1.2–7.4)	7.2 (4.4–10.9)	<0.001*
Net water uptake/time, median %/h (IQR) ^b	1.1 (0.3–2.1), <i>n</i> = 45	1.5 (1.0–2.2), <i>n</i> = 62	0.059

^a Difference between good and poor prognosis groups.

^b Twenty-one patients with wake-up strokes were excluded due to unknown time from onset.

*Statistical difference between two groups.

mRS, modified Rankin scale; CT, computed tomography; IQR, interquartile range; NIHSS, National Institutes of Health Stroke Scale; DPT, door-to-puncture time; DNT, door-to-needle time.

degree of perfusion, we can also assume that the early tissue edema would depend on the severity of ischemia within the infarct core.

This study emphasizes the importance of treating stroke patients early. When treated early, further development of edema in the ischemic tissue could be prevented. Another novelty of this study was the discovery of the positive relationship between early edema and infarct time. With prolonged time to treatment, early edema developed, as demonstrated by increased NWU value within the ischemic core. Infarction and edema are dynamic processes with time-dependent development, and this study demonstrated that the severity of edema increased with increased time from onset to reperfusion. It was demonstrated that early edema within the ischemic core could help predict the functional outcome of patients. The high value of NWU within the ischemic core indicated the severity of ionic edema and vasogenic edema, which in turn is related to early damage to the BBB, ion channel disturbance, and other complex mechanisms (3–5), which all may contribute to the poor outcome of patients. All of these findings emphasize the importance of early treatment in patients with acute stroke.

Besides the infarct time, other factors may relate to early edema. The collateral status reflects the cerebral microperfusion

status of patients with acute ischemic stroke, which is linked to edema formation and core growth (27). A previous study showed an association between favorable venous flow profiles and ischemic lesion NWU growth (28). Favorable tissue-level collaterals were also reported predicting less ischemic lesion NWU after performing thrombectomy in patients with large vessel occlusion (29). We did not find a statistically significant relation between modified ASITN/SIR score on dynamic CT and NWU, but there was the tendency of different NWU between good collateral and poor collateral groups. More included cases and appropriate assessments on tissue-level collaterals together with venous outflow (27) may strongly approve the relation between NWU and collateral status of patients with ischemic stroke. Another factor is ischemic core volume, which is recognized as the most essential variable influencing prognosis. In the current study, no significant relation was found between core volume and NWU. This might indicate that NWU within the ischemic core, besides core volume, is a relatively independent factor associated with the functional outcome of patients with ischemic stroke. Finally, factors not assessed in the study, such as admission blood glucose (30, 31), may also affect early edema of ischemic tissues.

The clinical applications of this study include the following two aspects. First, measuring NWU in addition to ischemic core volume for acute stroke management was valuable. Ischemic core volume measured in CTP is not the only imaging biomarker predicting clinical outcomes. Ischemic core volume combined with NWU provides better prognostic value after acute stroke. In addition to admission of NWU, quantitative measures of NWU 24–48 h after treatment and NWU growth (difference between NWU after treatment and on admission) seem to have a significant impact on clinical outcomes as well (29). Secondly, it is important to combine NCCT and CTP when evaluating patients with hyperacute stroke. NCCT has additional value as our study has indicated early edema, quantified by NWU on NCCT, is a potential biomarker to improve the delineation between ischemic core and penumbra.

Our study has several limitations. First, we retrospectively screened patients from a single center. Not every patient with acute ischemic stroke received multi-modal CT imaging. Moreover, patients with mild symptoms and low admission NIHSS scores intended to refuse CTP and were therefore not included in the study. This bias may influence the reliability or generalizability of our findings. Secondly, some potential variables related to prognosis after stroke such as hyperglycemia (30, 31) were not included in our logistic regression analyses due to the lack of admission data. Prospective validation is needed to confirm the predictive power of NWU for functional outcomes. Thirdly, CT density measurements of normal tissue relied on automatically mirrored contralateral ROI. This process might result in inaccuracies as the NCCT images were not absolutely symmetrical. However, this method of CT density measurements had been proved reliable previously (6). Finally, the estimates based on the CTP map in this study might be distinct from studies using other CTP processing software packages.

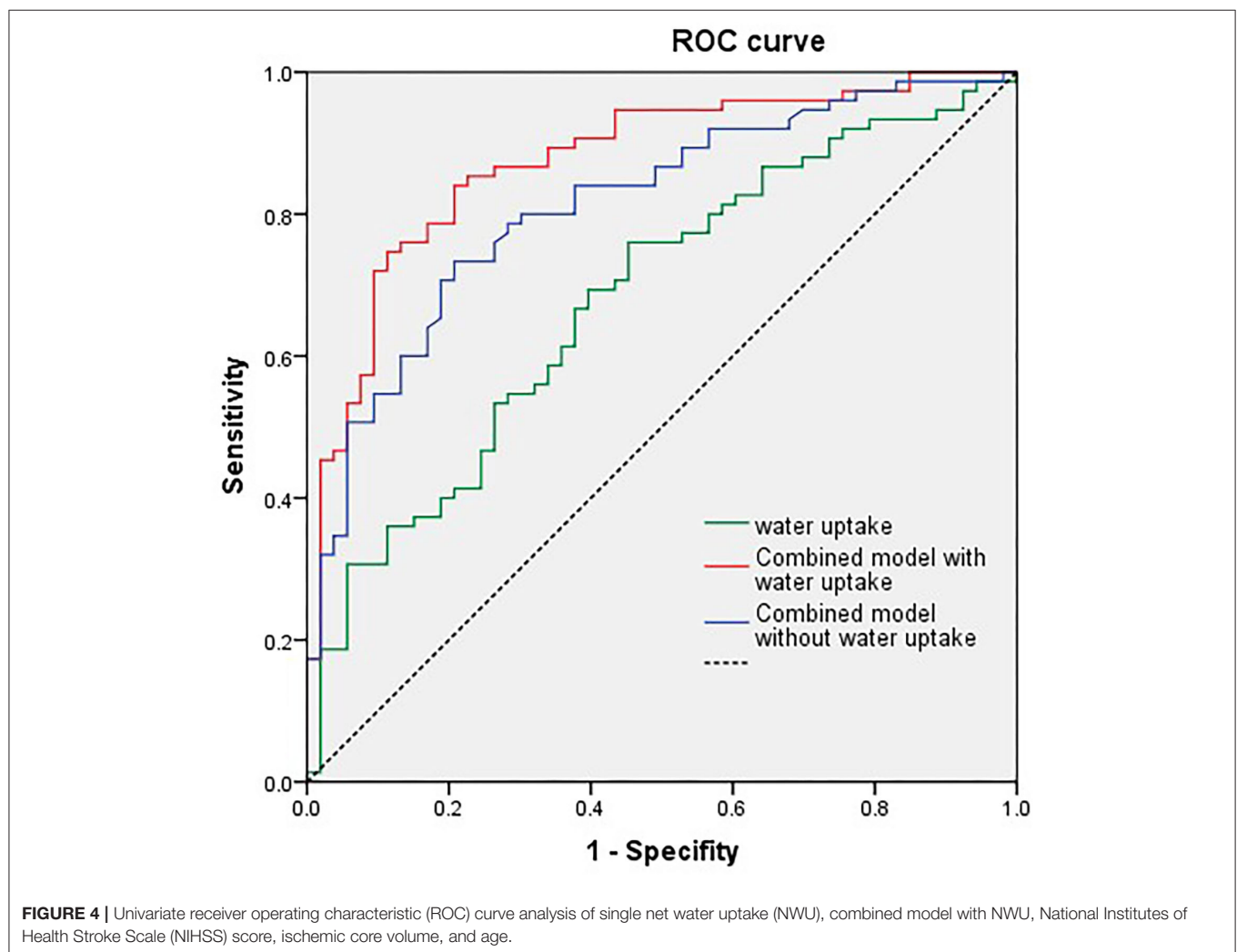
TABLE 3 | Binary logistic regression and ROC curve analysis to probability of prognosis after anterior circulation infarct.

	OR (95%CI)	P-value ^a	AUC (SE)	Sensitivity	Specificity
Variable^b					
Net water uptake	1.23 (1.10–1.39)	<0.001	0.681 (0.047)	69.3%	60.4%
Ischemic core volume	1.04 (1.02–1.06)	<0.001	0.778 (0.041)	61.3%	83.0%
Admission NIHSS	1.09 (1.01–1.17)	0.024	0.716 (0.046)	57.3%	77.4%
Age	1.05 (1.01–1.09)	0.021	0.636 (0.049)	66.7%	56.6%
Combined model					
Net water uptake, Ischemic core volume, Admission NIHSS, Age			0.875 (0.031)	74.7%	88.7%
Ischemic core volume, Admission NIHSS, Age			0.813 (0.038)	73.3%	79.2%

^aSignificance of association with poor prognosis (defined as a score on the modified Rankin scale at 90 days of 3–6) by binary logistic regression.

^bThe gender and treatment included in binary logistic regression were not significant so not listed in the table.

ROC, Receiver operating characteristic; OR, Odds ratio; AUC, Area under curve; SE, Standard error; NIHSS, National Institutes of Health Stroke Scale.



CONCLUSION

The early edema after acute stroke quantified by NWU was relatively limited in the ischemic core region and develop in a time-dependent manner. The quantified edema within the

ischemic core could help predict functional outcomes. These findings emphasize the importance of timely and early treatment of patients with stroke, thereby indicating that early edema quantification using ischemic lesion NWU may be a valuable imaging biomarker based on multimodal CT.

DATA AVAILABILITY STATEMENT

The raw data supporting the conclusions of this article will be made available by the authors, without undue reservation.

ETHICS STATEMENT

The studies involving human participants were reviewed and approved by the Ethics Committee of Ningbo First Hospital. The patients/participants provided their written informed consent to participate in this study.

AUTHOR CONTRIBUTIONS

QH and JY: research project conception, study design, organization, execution, statistical analysis, and writing of the manuscript draft. XG: organization, execution, and study design. JL, YW, YX, and QS: patients' enrolment and follow up and acquisition of data. LL and MP:

research project conception, study design, statistical analysis, review and critique, and manuscript revision of the draft.

FUNDING

This work was supported by the Medicine and Health Science and Technology Projects of Zhejiang Province (2022KY1098), Clinical Research Fund Project of Zhejiang Medical Association (2021ZYC-A10), and Ningbo Health Branding Subject Fund (PPXK2018-04).

SUPPLEMENTARY MATERIAL

The Supplementary Material for this article can be found online at: <https://www.frontiersin.org/articles/10.3389/fneur.2022.861289/full#supplementary-material>

Supplementary Figure 1 | Comparison of net water uptake (NWU) with poor collateral and good collateral patients.

REFERENCES

- Stokum JA, Gerzanich V, Simard MJ. Molecular pathophysiology of cerebral edema. *J Cereb Blood Flow Metab.* (2016) 36:513–38. doi: 10.1177/0271678X15617172
- Todd NV, Picozzi P, Crookard A, Russell WR. Duration of ischemia influences the development and resolution of ischemic brain edema. *Stroke.* (1986) 17:466–71. doi: 10.1161/01.STR.17.3.466
- Bell BA, Symon L, Branstetter MN. CBF and time thresholds for the formation of ischemic cerebral edema, and effect of reperfusion in baboons. *J Neurosurg.* (1985) 62:31–41. doi: 10.3171/jns.1985.62.1.0031
- Yang C, Hawkins KE, Doré S, Candelario-Jalil E. Neuroinflammatory mechanisms of blood-brain barrier damage in ischemic stroke. *Am J Physiol Cell Physiol.* (2019) 316:C135–53. doi: 10.1152/ajpcell.00136.2018
- Nilius B, Droogmans G. Ion channels and their functional role in vascular endothelium. *Physiol Rev.* (2001) 81:1415–59. doi: 10.1152/physrev.2001.81.4.1415
- Broocks G, Flottmann F, Ernst M, Faizy TD, Minnerup J, Siemonsen S, et al. Computed tomography-based quantification of lesion water uptake in ischemic brain: relationship between density and direct volumetry. *Invest Radiol.* (2018) 53:207–13. doi: 10.1097/RLI.0000000000000430
- Minnerup J, Broocks G, Kalkoffen J, Langner S, Knauth M, Psychogios MN, et al. Computed tomography-based quantification of lesion water uptake identifies patients within 4.5 hours of stroke onset: a multicenter observational study. *Ann Neurol.* (2016) 80:924–34. doi: 10.1002/ana.24818
- Broocks G, Leischner H, Hanning U, Flottmann F, Faizy TD, Schön G, et al. Lesion age imaging in acute stroke: water uptake in CT versus DWI-FLAIR mismatch. *Ann Neurol.* (2020) 88:1144–52. doi: 10.1002/ana.25903
- Broocks G, Flottmann F, Scheibel A, Aigner A, Faizy TD, Hanning U, et al. Quantitative lesion water uptake in acute stroke computed tomography is a predictor of malignant infarction. *Stroke.* (2018) 49:1906–12. doi: 10.1161/STROKEAHA.118.020507
- Nawabi J, Flottmann F, Kemmling A, Knip H, Leischner H, Sporns P, et al. Elevated early lesion water uptake in acute stroke predicts poor outcome despite successful recanalization - when “tissue clock” and “time clock” are desynchronized. *Int J Stroke.* (2019) 16:863–72. doi: 10.1177/1747493019884522
- Faizy TD, Kabiri R, Christensen S, Mlynash M, Kuraitis G, Broocks G, et al. Perfusion imaging-based tissue-level collaterals predict ischemic lesion net water uptake in patients with acute ischemic stroke and large vessel occlusion. *J Cereb Blood Flow Metab.* (2021) 41:2067–75. doi: 10.1177/0271678X21992200
- Sajobi TT, Menon BK, Wang M, Lawal O, Shuaib A, Williams D, et al. Early trajectory of stroke severity predicts long-term functional outcomes in ischemic stroke subjects: results from the ESCAPE trial (endovascular treatment for small core and anterior circulation proximal occlusion with emphasis on minimizing CT to recanalization times). *Stroke.* (2017) 48:105–10. doi: 10.1161/STROKEAHA.116.014456
- Thomalla G, Hartmann F, Juettler E, Singer OC, Lehnhardt FG, Köhrmann M, et al. Prediction of malignant middle cerebral artery infarction by magnetic resonance imaging within 6 hours of symptom onset: a prospective multicenter observational study. *Ann Neurol.* (2010) 68:435–45. doi: 10.1002/ana.22125
- Veerbeek JM, Kwakkel G, van Wegen EE, Ket JC, Heymans WM. Early prediction of outcome of activities of daily living after stroke: a systematic review. *Stroke.* (2011) 42:1482–8. doi: 10.1161/STROKEAHA.110.604090
- Wu S, Yuan R, Wang Y, Wei C, Zhang S, Yang X, et al. Early prediction of malignant brain edema after ischemic stroke. *Stroke.* (2018) 49:2918–27. doi: 10.1161/STROKEAHA.118.022001
- Ramos-Cabrera P, Campos F, Sobrino T, Castillo J. Targeting the ischemic penumbra. *Stroke.* (2011) 42(1 Suppl.):S7–11. doi: 10.1161/STROKEAHA.110.596684
- Lin L, Bivard A, Kleinig T, Spratt NJ, Levi CR, Yang Q, et al. Correction for delay and dispersion results in more accurate cerebral blood flow ischemic core measurement in acute stroke. *Stroke.* (2018) 49:924–30. doi: 10.1161/STROKEAHA.117.019562
- Lin L, Bivard A, Krishnamurthy V, Levi CR, Parsons WM. Whole-brain CT perfusion to quantify acute ischemic penumbra and core. *Radiology.* (2016) 279:876–87. doi: 10.1148/radiol.2015150319
- Higashida RT, Furlan AJ, Roberts H, Tomsick T, Connors B, Barr J, et al. Trial design and reporting standards for intra-arterial cerebral thrombolysis for acute ischemic stroke. *Stroke.* (2003) 34:e109–37. doi: 10.1161/01.STR.0000082721.62796.09
- Tian H, Chen C, Garcia-Esperon C, Parsons MW, Lin L, Levi CR, et al. Dynamic CT but not optimized multiphase CT angiography accurately identifies CT perfusion target mismatch ischemic stroke patients. *Front Neurol.* (2019) 10:1130. doi: 10.3389/fneur.2019.01130
- Moskowitz MA. Brain protection: maybe yes, maybe no. *Stroke.* (2010) 41(10 Suppl.):S85–6. doi: 10.1161/STROKEAHA.110.598458
- Iadecola C, Anrather J. Stroke research at a crossroad: asking the brain for directions. *Nat Neurosci.* (2011) 14:1363–8. doi: 10.1038/nn.2953
- Uzdensky A, Demyanenko S, Fedorenko G, Lapteva T, Fedorenko A. Protein profile and morphological alterations in penumbra after focal

- photothrombotic infarction in the rat cerebral cortex. *Mol Neurobiol.* (2017) 54:4172–88. doi: 10.1007/s12035-016-9964-5
24. Jiang W, Gu W, Hossmann KA, Mies G, Wester P. Establishing a photothrombotic 'ring' stroke model in adult mice with late spontaneous reperfusion: quantitative measurements of cerebral blood flow and cerebral protein synthesis. *J Cereb Blood Flow Metab.* (2006) 26:927–36. doi: 10.1038/sj.jcbfm.9600245
 25. Broocks G, Hanning U, Faizy TD, Scheibel A, Nawabi J, Schön G, et al. Ischemic lesion growth in acute stroke: water uptake quantification distinguishes between edema and tissue infarct. *J Cereb Blood Flow Metab.* (2020) 40:823–32. doi: 10.1177/0271678X19848505
 26. Broocks G, Kniep H, Kemmling A, Flottmann F, Nawabi J, Elsayed S, et al. Effect of intravenous alteplase on ischaemic lesion water homeostasis. *Eur J Neurol.* (2020) 27:376–83. doi: 10.1111/ene.14088
 27. Faizy TD, Kabiri R, Christensen S, Mlynash M, Kuraitis GM, Broocks G, et al. Favorable venous outflow profiles correlate with favorable tissue-level collaterals and clinical outcome. *Stroke.* (2021) 52:1761–7. doi: 10.1161/STROKEAHA.120.032242
 28. van Horn N, Heit JJ, Kabiri R, Broocks G, Christensen S, Mlynash M, et al. Venous outflow profiles are associated with early edema progression in ischemic stroke. *Int J Stroke.* (2022) 17474930211065635. doi: 10.1177/17474930211065635.[Epub ahead of print].
 29. Faizy TD, Kabiri R, Christensen S, Mlynash M, Kuraitis G, Meyer L, et al. Venous outflow profiles are linked to cerebral edema formation at noncontrast head CT after treatment in acute ischemic stroke regardless of collateral vessel status at CT angiography. *Radiology.* (2021) 299:682–90. doi: 10.1148/radiol.2021203651
 30. Li WA, Moore-Langston S, Chakraborty T, Rafols JA, Conti AC, Ding Y. Hyperglycemia in stroke and possible treatments. *Neurol Res.* (2013) 35:479–91. doi: 10.1179/1743132813Y.0000000209
 31. Garg R, Chaudhuri A, Munschauer F, Dandona P. Hyperglycemia, insulin, and acute ischemic stroke: a mechanistic justification for a trial of insulin infusion therapy. *Stroke.* (2006) 37:267–73. doi: 10.1161/01.STR.0000195175.29487.30

Conflict of Interest: The authors declare that the research was conducted in the absence of any commercial or financial relationships that could be construed as a potential conflict of interest.

Publisher's Note: All claims expressed in this article are solely those of the authors and do not necessarily represent those of their affiliated organizations, or those of the publisher, the editors and the reviewers. Any product that may be evaluated in this article, or claim that may be made by its manufacturer, is not guaranteed or endorsed by the publisher.

Copyright © 2022 Han, Yang, Gao, Li, Wu, Xu, Shang, Parsons and Lin. This is an open-access article distributed under the terms of the Creative Commons Attribution License (CC BY). The use, distribution or reproduction in other forums is permitted, provided the original author(s) and the copyright owner(s) are credited and that the original publication in this journal is cited, in accordance with accepted academic practice. No use, distribution or reproduction is permitted which does not comply with these terms.



Filling Defect of Ipsilateral Transverse Sinus in Acute Large Artery Occlusion

Yi Chen^{1†}, Sheng Zhang^{2†}, Shenqiang Yan¹, Meixia Zhang³, Ruiting Zhang⁴, Feina Shi¹, David S. Liebeskind⁵, Mark Parsons⁶ and Min Lou^{1*}

¹ Department of Neurology, The Second Affiliated Hospital of Zhejiang University, Hangzhou, China, ² Department of Neurology, Zhejiang Provincial People's Hospital, People's Hospital of Hangzhou Medical College, Hangzhou, China, ³ Department of Neurology, Jinhua Municipal Central Hospital, Jinhua Hospital of Zhejiang University, Jinhua, China, ⁴ Department of Radiology, The Second Affiliated Hospital of Zhejiang University, Hangzhou, China, ⁵ UCLA Stroke Center, University of California, Los Angeles, Los Angeles, CA, United States, ⁶ Department of Neurology, John Hunter Hospital, University of Newcastle, New Lambton Heights, NSW, Australia

OPEN ACCESS

Edited by:

Robin Lemmens,
University Hospitals Leuven, Belgium

Reviewed by:

Adrien Guenego,
Stanford Healthcare, United States
Zhen-Ni Guo,
First Affiliated Hospital of Jilin
University, China

*Correspondence:

Min Lou
loumingxc@vip.sina.com;
lm99@zju.edu.cn

[†]These authors have contributed
equally to this work and share first
authorship

Specialty section:

This article was submitted to
Stroke,
a section of the journal
Frontiers in Neurology

Received: 27 January 2022

Accepted: 21 March 2022

Published: 10 May 2022

Citation:

Chen Y, Zhang S, Yan S, Zhang M,
Zhang R, Shi F, Liebeskind DS,
Parsons M and Lou M (2022) Filling
Defect of Ipsilateral Transverse Sinus
in Acute Large Artery Occlusion.
Front. Neurol. 13:863460.
doi: 10.3389/fneur.2022.863460

Background and Purpose: Cerebral venous systems play a key role in regulating stroke outcomes. We aimed to elucidate the effect of the transverse sinus (TS) filling patterns on edema expansion and neurological outcomes in patients with acute large artery occlusion (LAO).

Materials and Methods: We recruited consecutive patients with acute M1 middle cerebral artery and/or internal carotid artery occlusion who underwent pretreatment computed tomographic perfusion (CTP). On the reconstructed 4-dimensional computed tomographic angiography derived from CTP, the filling defect of the ipsilateral transverse sinus (FDITS) was defined as the length of contrast filling defect occupying at least half of the ipsilateral TS. An unfavorable outcome was defined as having a modified Rankin Scale (mRS) score of 3–6 at 3 months.

Results: A total of 318 patients were enrolled in the final analysis and 70 (22.0%) patients had baseline FDITS. The presence of FDITS was associated with the baseline NIHSS (odds ratio [OR] 1.119; 95% CI, 1.051–1.192; $p < 0.001$) and poor arterial collaterals (OR 3.665; 95% CI 1.730–7.766; $p = 0.001$). In addition, FDITS was associated with 24-h brain edema expansion (OR 7.188; 95% CI, 3.095–16.696; $p < 0.001$) and 3-month unfavorable outcome (OR 8.143; 95% CI 2.547–26.041; $p < 0.001$) independent of arterial collateral status. In the subgroup analysis of patients with FDITS who received reperfusion therapy, no significant difference was found in the rate of edema expansion and unfavorable outcome between non-reperfusion and reperfusion subgroups (both $p > 0.05$).

Conclusion: Filling defect of the ipsilateral transverse sinus was associated with edema expansion and an unfavorable outcome irrespective of the baseline arterial collateral status in patients with acute LAO, indicating that FDITS may be an important stroke-related prognostic imaging marker.

Keywords: large artery occlusion in anterior circulation, transverse sinus, computer tomography, brain edema, reperfusion therapy

INTRODUCTION

Despite the development of reperfusion therapy, the rate of severe disability and mortality in patients with acute large artery occlusion (LAO) remains high (1). Previous studies on acute ischemic stroke (AIS) have focused on arterial pathophysiology; however, it was recently discovered that cerebral venous systems also have a role in determining the prognosis of AIS after reperfusion therapy (2–4).

Cerebral veins have been used to predict stroke outcomes, though the exact mechanisms are still unclear (2, 3, 5–7). Cortical and deep veins were both suggested to be good venous markers for stroke outcomes (2, 3, 5–7). Nevertheless, in terms of patients with LAO, these veins may not reflect the entire venous drainage abnormalities in the corresponding regions supplied by cerebral arteries. Additionally, there were difficulties in recognizing the cortical and deep veins due to the broad variation of cerebral venous across different centers (8).

The transverse sinus (TS), functioning as a pool gathering cortical and deep veins, is superficial and easier to identify than cerebral veins (8). Additionally, the vein of Labbé collects the blood flow of the lateral temporal area supplied by the middle cerebral artery (MCA), joining into ipsilateral TS directly (9). Therefore, TS might be an appropriate target to reflect the abnormality of hemispheric venous drainage, especially in patients with acute LAO of the anterior circulation.

We thus evaluated the drainage pattern of TS on the reconstructed four-dimensional CT angiography (4D-CTA) derived from CT perfusion (CTP) in AIS patients with anterior circulation LAO and investigated whether the drainage abnormality of ipsilateral TS would influence their clinical outcomes.

SUBJECTS AND METHODS

Ethics Statement

Each subject or an appropriate family member had given written informed consent prior to the study, and the protocols had been approved by the local ethics committee. All clinical investigations were conducted according to the principles expressed in the Declaration of Helsinki.

Study Subjects

We retrospectively reviewed our prospectively collected database, namely, Comparison Influence to Prognosis of CTP and MRP in AIS Patients (CIPPIS, <http://www.clinicaltrials.gov>, Unique identifier: NCT03367286), of patients with consecutive AIS who were admitted within 9 h of stroke onset or with an unknown time of onset and underwent CTP before the treatment between January 2014 and January 2019. Reperfusion therapy, including intravenous thrombolysis and/or endovascular therapy, was given to eligible patients with informed consent according to the guidelines of the time. We enrolled patients who had middle cerebral artery M1 segment and/or intracranial internal carotid artery (ICA) occlusion on pretreatment 4D-CTA reconstructed from CTP. We excluded patients who (1) had pre-stroke a modified Rankin Scale score (mRS) >2; (2) had bilateral acute ischemic lesions; (3) had poor image quality due to severe head motion artifact on the image; and (4) could not tolerate follow-up CT/MRI or were lost to follow-up within 3 months.

Patients' demographic, clinical, laboratory, and radiological data, including age, sex, comorbid conditions, such as the history of stroke/transient ischemic attacks (TIA), hypertension, diabetes mellitus, coronary artery disease, and atrial fibrillation, were retrieved. Baseline neurologic severity was assessed by the

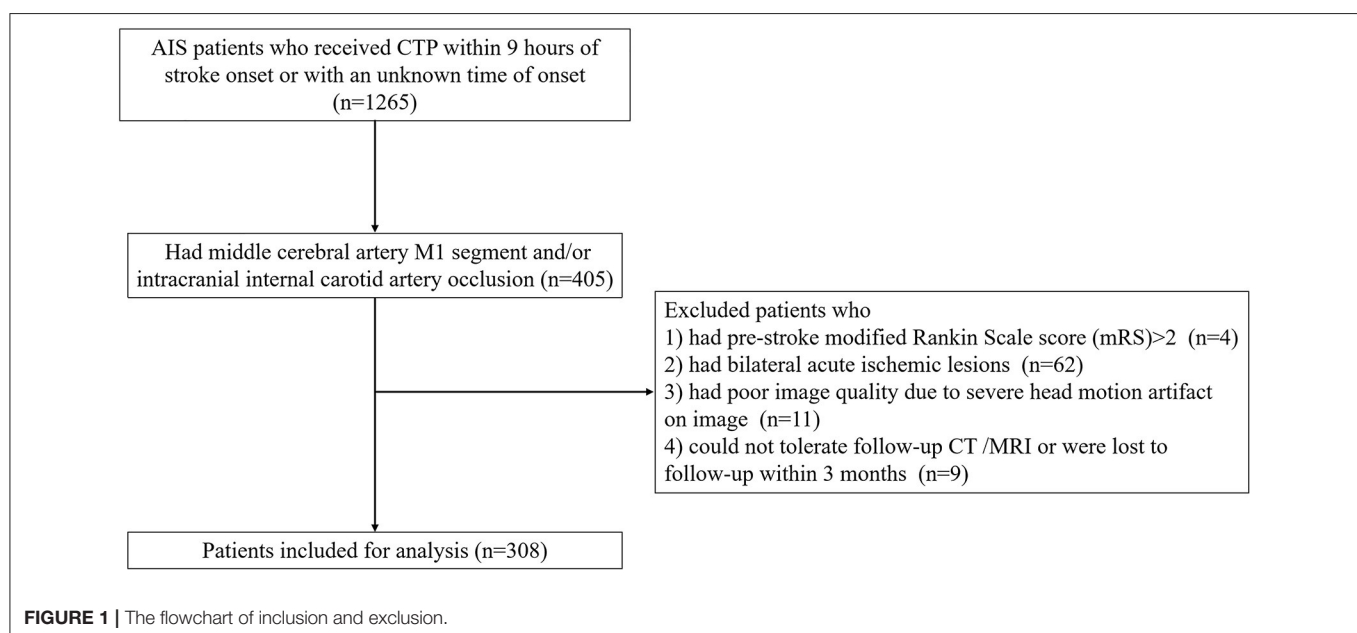


TABLE 1 | Baseline characteristics and outcomes dichotomized by the presence of FDITS.

	FDITS (<i>n</i> = 70)	Non-FDITS (<i>n</i> = 248)	<i>P</i> -value
Demographics and clinical features			
Age, year	71 ± 14	70 ± 13	0.684
Male, <i>n</i> (%)	43 (61.4)	154 (62.1)	0.999
Baseline NIHSS, median (IQR)	18 (14–20)	13 (9–16)	<0.001*
Onset to door time, min ^a , median (IQR)	194 (120–318)	174 (86–260)	0.167*
Onset to needle time, min ^b , median (IQR)	259 (168–337)	208 (135–296)	0.061*
Baseline systolic BP, mmHg	155 ± 25	150 ± 23	0.167
Baseline diastolic BP, mmHg	84 ± 15	83 ± 14	0.444
Baseline blood glucose, mmol/L	7.31 ± 2.45	7.65 ± 2.40	0.310
INR, median (IQR)	1.04 (0.98–1.11)	1.02 (0.98–1.10)	0.246*
History of atrial fibrillation, <i>n</i> (%)	36 (52.2)	123 (50.4)	0.892
History of hypertension, <i>n</i> (%)	50 (72.5)	154 (63.1)	0.156
History of diabetes mellitus, <i>n</i> (%)	9 (13.0)	46 (18.9)	0.289
History of coronary artery disease, <i>n</i> (%)	8 (11.6)	33 (13.5)	0.840
History of stroke/ TIA, <i>n</i> (%)	13 (18.8)	55 (22.5)	0.620
Baseline imaging data			
Baseline hypoperfusion volume, ml, median (IQR)	154 (97–213)	124 (74–168)	0.005*
Baseline ischemic core volume, ml, median (IQR)	80 (41–140)	48 (25–84)	<0.001*
Poor collaterals, <i>n</i> (%)	57 (83.8)	111 (46.6)	<0.001
Baseline edema score, median (IQR)	0 (0–1)	0 (0–0)	0.021*
Outcomes			
PH, <i>n</i> (%)	12 (17.1)	25 (10.1)	0.137
slCH, <i>n</i> (%)	6 (8.6)	16 (6.5)	0.594
Edema score at 24-h, median (IQR)	3 (2–4)	1 (0–2)	<0.001*
Brain edema expansion, <i>n</i> (%)	62 (88.6)	93 (37.5)	<0.001
Reperfusion, <i>n</i> (%) ^c	21 (48.8)	111 (58.7)	0.306
Unfavorable outcome, <i>n</i> (%)	65 (92.9)	132 (53.2)	<0.001

*Mann–Whitney *U*-test.^a Estimated as the midpoint of sleep (i.e., the time between going to sleep and waking up with symptoms) among patients with wake-up stroke.^b Evaluated in patients who received intravenous thrombolysis (*n* = 243, FDITS vs. non-FDITS = 50 vs. 193).^c Evaluated in patients who had both baseline and 24-h perfusion images (*n* = 232, FDITS vs. non-FDITS = 43 vs. 189).

FDITS, filling defect of the ipsilateral transverse sinus; NIHSS, National Institutes of Health Stroke Scale; BP, blood pressure; INR, International normalized ratio; TIA, Transient ischemic attack; PH, parenchymal hemorrhage; slCH, symptomatic intracranial hemorrhage.

National Institutes of Health Stroke Scale (NIHSS). Favorable outcome and unfavorable outcome were defined as mRS scores of 0–2 and 3–6 at 3 months, respectively (10).

Imaging Protocols

All patients underwent baseline CTP, including non-contrast CT (NCCT) and volume perfusion CT (VPCT), and follow-up CTP or magnetic resonance perfusion or NCCT at 24-h after admission in accordance with our routine stroke

TABLE 2 | Binary logistic regression analysis for unfavorable outcome.

	OR	95% CI	<i>P</i> -value
Age, year	1.030	1.004–1.056	0.021
Male	0.464	0.235–0.918	0.027
History of hypertension	1.573	0.821–3.013	0.172
Onset to door time, per minute	1.003	1.001–1.005	0.012
Baseline NIHSS	1.068	1.001–1.140	0.045
Baseline ischemic core, per ml	1.011	1.002–1.020	0.018
FDITS	8.143	2.547–26.041	<0.001
Poor collaterals	3.115	1.575–6.162	0.001
Application of endovascular therapy	0.390	0.202–0.754	0.005

FDITS, filling defect of the ipsilateral transverse sinus; NIHSS, National Institutes of Health Stroke Scale; OR, odds ratio; CI, confidence interval.

imaging protocol (11). The detailed parameters are listed in the **Supplementary Material**. VPCT images were reconstructed to obtain time to maximum (Tmax) maps and 4D-CTA images were presented in axial, coronal, and sagittal planes with 20-mm-thick maximum intensity projections by commercial software (MISAR; Apollo Medical Imaging Technology, Melbourne, Australia).

Defining the Filling Defect of The Ipsilateral Transverse Sinus (FDITS)

The contrast filling of TS of each hemisphere was evaluated on a coronal view of temporally fused maximum intensity projections (tMIPs) reconstructed from 4D-CTA images. According to the contrast filling pattern of the ipsilateral TS, the presence of a filling defect of the ipsilateral transverse sinus (FDITS) was confirmed by two steps: (1) contrast filling defect was defined as the width of the contrast filling in ipsilateral TS being ≤50% width of the contralateral TS (12); and (2) the length of contrast filling defect occupied at least half of the ipsilateral TS. Hypoplasia and aplasia of TS of the ischemic side were also identified as FDITS. A similar definition was used for the filling defect of contralateral TS (FDCTS) and all others were defined as symmetric TS. Both FDCTS and symmetric TS were set as non-FDITS.

Assessment of Arterial Collaterals on 4D-CTA

Arterial collaterals were evaluated on peak arterial opacification (peak phase) and tMIPs were reconstructed from 4D-CTA images, and the regional leptomeningeal collateral (rLMC) score was graded on peak phase (rLMC-P) and tMIP (rLMC-M), respectively. The integrated collateral grading scale (CGS) was used to assess the arterial collateral status: poor collaterals (score 0: rLMC-P ≤11 and rLMC-M ≤16), intermediate collaterals (score 1: rLMC-P ≤11 and rLMC-M >16, or rLMC-P >11 and rLMC-M ≤16), and good collaterals (score 2: rLMC-P >11 and rLMC-M >16) (13).

Defining Hypoperfusion and Ischemic Core

A threshold of Tmax > 6 s was used for the volumetric measurement of baseline and 24-h hypoperfusion areas (14).

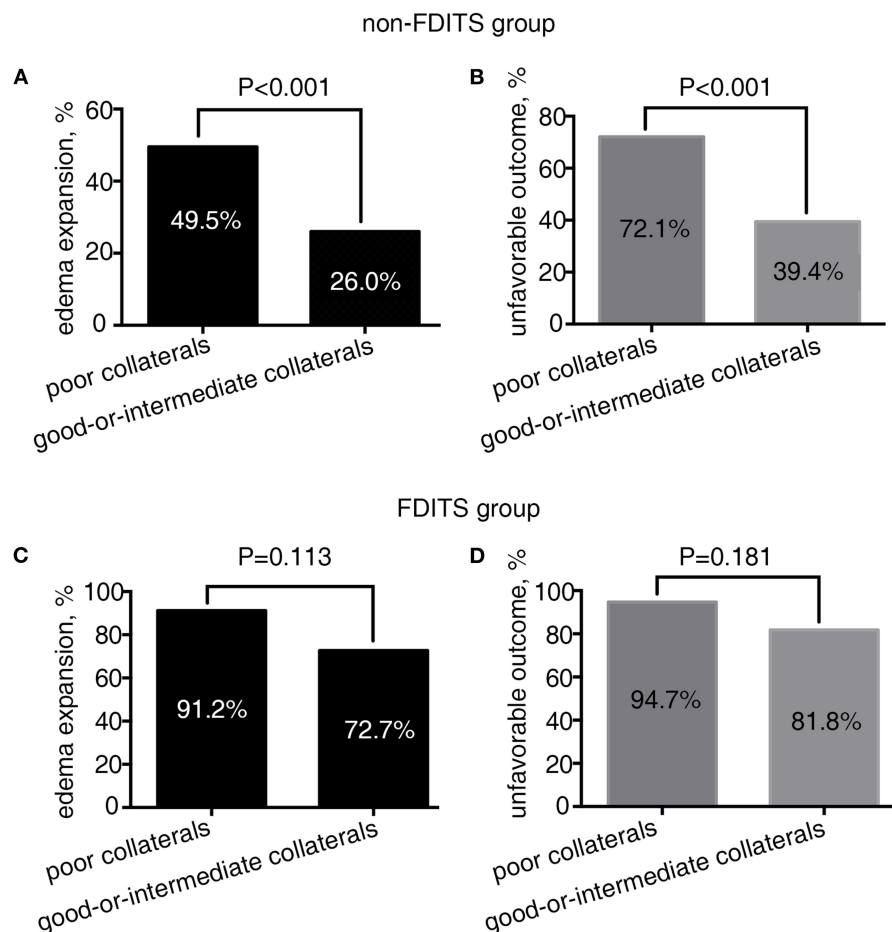


FIGURE 2 | The relationship between collateral status and outcome in the filling defect of ipsilateral transverse sinus (FDITS) and non-FDITS groups. The poor collaterals subgroup was more likely to undergo edema expansion (A) and an unfavorable outcome (B) than those with good-or-intermediate collaterals in patients with non-FDITS. While in the FDITS group, no significant difference was found in the rate of edema expansion (C) or an unfavorable outcome (D) between patients with poor and good-or-intermediate collaterals.

Baseline relative cerebral blood flow (rCBF) $< 30\%$ was used for calculating the ischemic core volume (15). At 24 h, Diffusion Weighted Imaging (DWI) or NCCT was used to calculate the final infarct volume (13).

Reperfusion, Hemorrhagic Transformation, and Brain Edema

Reperfusion ratio (RR) = (baseline hypoperfusion volume – 24-h hypoperfusion volume)/baseline hypoperfusion volume. Based on RR, we defined reperfusion as $RR \geq 80\%$ and non-reperfusion as $RR < 80\%$ (16).

Hemorrhagic transformation, including parenchymal hemorrhage (PH), was classified according to the European Cooperative Acute Stroke Study criteria. Symptomatic intracranial hemorrhage (sICH) was defined as any intracranial hemorrhage associated with an increase of ≥ 4 points on NIHSS or leading to death (17).

Brain edema was assessed with a 7-point scale at baseline NCCT and 24-h NCCT or DWI (18, 19). To minimize the grading error, 24-h brain edema expansion was defined as

an increase of ≥ 2 in grade from baseline imaging to 24-h imaging (19).

Reproducible Parameters

Two evaluators (Y.C. and S.Z.) who jointly evaluated the TS were blinded to the patients' 24-h imaging and clinical data. A single trained observer (Y.C.) measured the TS of all patients two times, at an interval of 3 months apart. Another observer (S.Z.) independently made the same evaluation. Similarly, rLMC, brain edema, and PH were assessed by two neurologists independently (Y.C. and S.Z.), respectively. The Kappa statistic was used to test the inter- and intra-rater reliability for detecting the presence of FDITS and PH, and the weighted Kappa statistic was used to test the inter- and intra-rater reliability for rLMC and brain edema score.

There was a good level of inter- and intra-observer agreement in the evaluation of arterial collaterals status (weighted $\kappa = 0.80$ and 0.86), FDITS ($\kappa = 0.81$ and 0.92), and an excellent level of agreement for brain edema (weighted $\kappa = 0.86$ and 0.90), hemorrhagic transformation ($\kappa = 0.86$ and 0.99).

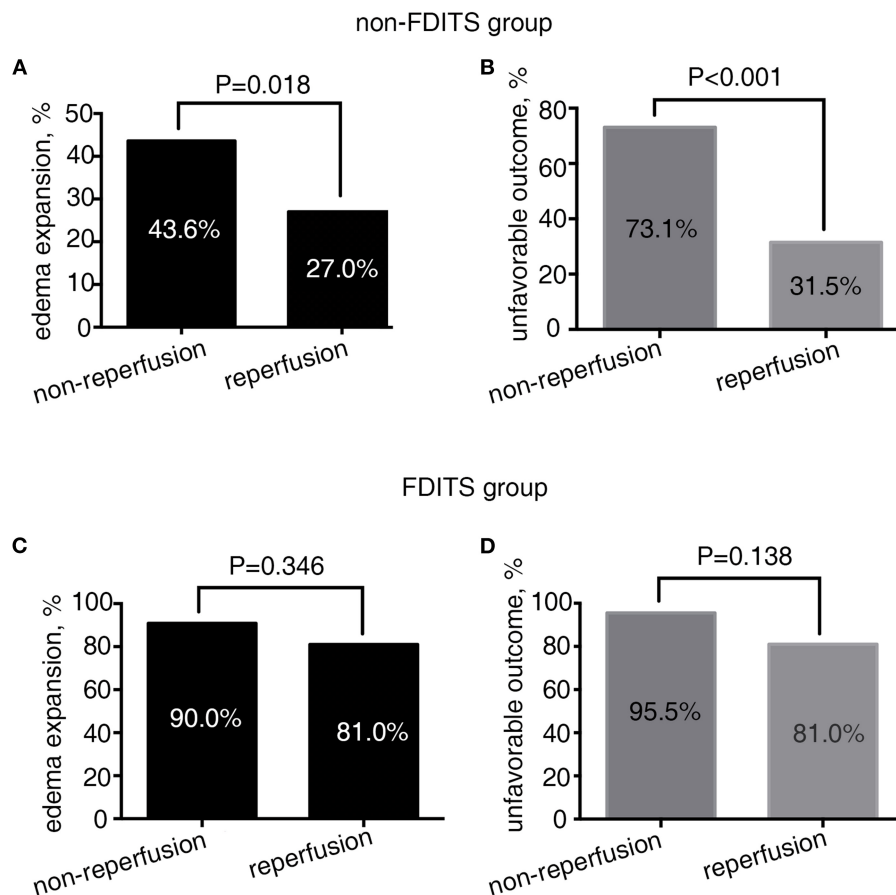


FIGURE 3 | The relationship between reperfusion status and outcome in the FDITS and non-FDITS groups. A non-reperfusion subgroup was more likely to undergo edema expansion (A) and unfavorable outcome (B) than reperfusion subgroup in patients with non-FDITS. While in the FDITS group, no significant difference was found in the rate of edema expansion (C) or unfavorable outcome (D) between two subgroups.

Statistical Analysis

All numeric variables were expressed as mean \pm SD and median (interquartile range, IQR). Categorical variables were presented as frequency (percentage). Fisher's exact test was used to compare the dichotomous variables between groups, while Mann-Whitney *U*-test was used for ordered categorical variables, and independent samples 2-tailed *t*-test or Mann-Whitney *U*-test was used for continuous variables, depending on the normality of the distribution. Variables identified by univariate analysis ($p < 0.05$) were included in the binary logistic regression model except for potential linearly correlated ones. Independent factors for the presence of FDITS, edema expansion, and unfavorable outcomes were evaluated using the binary logistic regression analysis, respectively. Then, the subgroup analysis was made for the effects of FDITS on edema expansion and unfavorable outcomes under the condition of different collateral status and reperfusion status, separately. All analyses were performed blinded to the participant identifying information. Statistical significance was set as a probability value of <0.05 . The statistical analysis was performed using SPSS 18 (SPSS Inc., Chicago, IL, USA).

RESULTS

Overall Characteristics

A total of 318 patients were enrolled in the final analysis (Figure 1). The average age was 70 ± 13 years and 197 (61.9%) patients were men. The median baseline NIHSS was 14 (IQR 10–18). Among them, 287 (90.3%) patients received reperfusion therapy, including endovascular treatment ($n = 142$). FDITS occurred in 70 (22.0%) patients. Non-FDITS was identified in 248 (78.0%) patients, including 82 FDCTS and 166 symmetric TS. Baseline poor arterial collaterals (score 0) were found in 168 (54.9%) patients. At 24 h, 155 (48.7%) patients underwent brain edema expansion. At 3 months, 197 (61.9%) patients suffered unfavorable outcomes.

Association Between FDITS and Baseline Characteristics

Table 1 shows the baseline characteristics and outcomes dichotomized by the presence of FDITS. Compared with the non-FDITS group, patients with FDITS had higher baseline NIHSS,

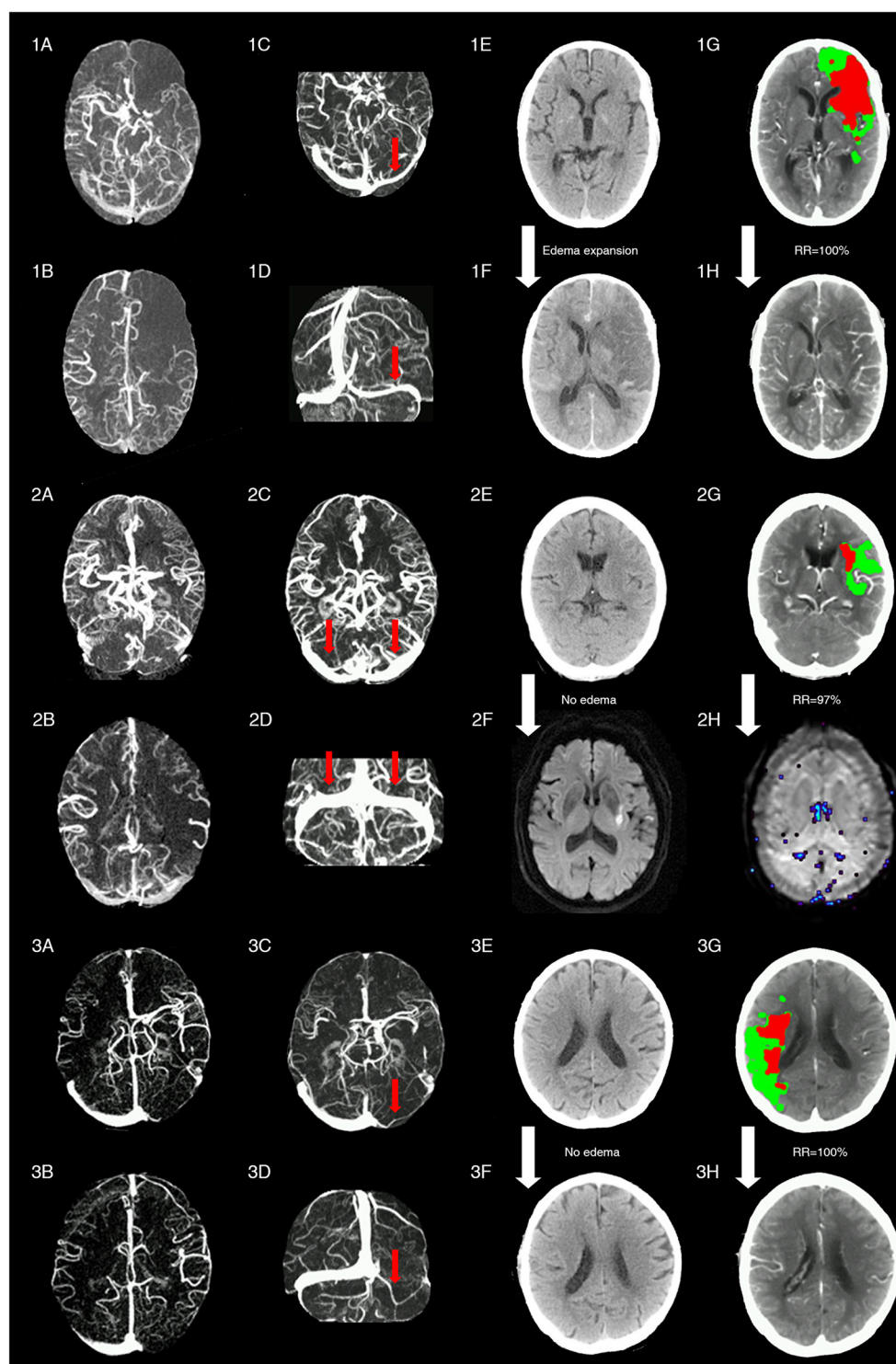


FIGURE 4 | Representative images of patients with different status of ipsilateral transverse sinus and collaterals. Patient 1 with acute left middle cerebral artery occlusion (MCAO) (baseline NIHSS = 14) presented with poor collaterals [integrated collateral grading scale (CGS) = 0] (1A,1B) and FDITS (the red arrow in 1C,1D) on 4-dimensional computed tomographic angiography (4D-CTA). The patient received intravenous thrombolysis bridging with endovascular therapy at 2.5 h from stroke onset. At 24 h after reperfusion therapy, this patient developed brain edema expansion on non-contrast CT (NCCT) from baseline score 0 (1E) to 2 (1F), although reperfusion rate was 100% with hypoperfusion (red plus green area) volume changing from 220 ml (1G) to 0 ml (1H) on lesion map. The modified Rankin scale (mRS) score was 4 at 3 months. Patient 2 with acute left MCAO (baseline NIHSS = 13), presented with good collaterals (CGS = 2) (2A,2B) and symmetric bilateral transverse sinuses (non-FDITS) (two red arrows in 2C,2D) on 4D-CTA. The patient received intravenous thrombolysis at 4 h from stroke onset. At 24 h after

(Continued)

FIGURE 4 | reperfusion therapy, this patient developed no brain edema with edema score keeping 0 from baseline NCCT (2E) to 24-h diffusing weighted imaging (DWI) (2F), and reperfusion rate was 97% with hypoperfusion (red plus green area) volume changing from 29 ml (2G) to 1 ml (2H) on lesion map. The mRS score was 0 at 3 months. Patient 3 with acute right MCAO (baseline NIHSS = 11), presented with good collaterals (CGS = 2) (3A,3B) and filling defect of contralateral transverse sinus (FDCTS) (the red arrow in 3C,3D) on 4D-CTA. The patient received intravenous thrombolysis bridging with endovascular therapy at 2 h from stroke onset. After reperfusion therapy, this patient developed no brain edema with edema score keeping 0 on NCCT from baseline (3E) to 24 h (3F), and reperfusion rate was 100% with hypoperfusion (red plus green area) volume changing from 137 ml (3G) to 0 ml (3H) on lesion map. The mRS score was 0 at 3 months.

larger baseline hypoperfusion volume and ischemic core volume, and a higher rate of poor arterial collaterals.

Binary logistic regression analysis revealed that the presence of FDITS was independently associated with baseline NIHSS (odds ratio [OR] 1.119; 95% CI 1.051–1.192; $p < 0.001$) and poor arterial collaterals (OR 3.665; 95% CI 1.730–7.766; $p = 0.001$) after adjusting for ischemic core volume (OR 1.002; 95% CI 0.997–1.007; $p = 0.372$).

The Associations of FDITS With Edema Expansion and Unfavorable Outcome

The patients with FDITS showed a higher rate of brain edema expansion and unfavorable outcomes (Table 1). The univariate analysis for the association between factors and edema expansion and outcome is separately shown in Supplementary Tables 1, 2. The binary logistic regression analysis showed that the presence of FDITS was independently associated with unfavorable outcomes (92.9 vs. 53.2%, OR 8.143; 95% CI 2.547–26.041; $p < 0.001$) (Table 2). In addition, we found that the presence of FDITS was associated with edema expansion (88.6 vs. 37.5%, OR 7.188; 95% CI 3.095–16.696; $p < 0.001$) (Supplementary Table 3). Baseline hypoperfusion volume remarkably correlated linearly with the baseline ischemic volume ($r_s = 0.778$, $p < 0.001$) and thus was not included in the binary logistic regression.

Subgroup Study in Patients With FDITS and Non-FDITS

As Figure 2 shows, in patients with FDITS, the rate of edema expansion (91.2 vs. 72.7%, $p = 0.113$) and unfavorable outcome (94.7 vs. 81.8%, $p = 0.181$) was comparable between the poor collaterals subgroup and the good-or-intermediate subgroup. However, among patients with non-FDITS, the poor collaterals subgroup was likely to have a higher rate of edema expansion (49.5 vs. 26.0%, $p < 0.001$) and unfavorable outcome (72.1 vs. 39.4%, $p < 0.001$) than the good-or-intermediate collaterals subgroup.

As Figure 3 shows, in patients with FDITS, no significant difference was found in the rate of edema expansion (90.9 vs. 81.0%, $p = 0.346$) or unfavorable outcome (95.5 vs. 81.0%, $p = 0.138$) between the non-reperfusion subgroup and the reperfusion subgroup. However, patients with non-FDITS were likely to develop a higher rate of edema expansion (43.6 vs. 27.0%, $p = 0.018$) and unfavorable outcome (73.1 vs. 31.5%, $p < 0.001$) when reperfusion was not achieved.

Figure 4 shows three cases with representative images.

DISCUSSION

In our study, we found that FDITS had a close relationship with baseline arterial collateral status, and FDITS was associated with 24-h edema expansion and subsequently 3-month unfavorable outcome independent of the baseline arterial collateral status.

The venous drainage system is a major blood reservoir. A prior study revealed that the ipsilateral absent filling of the superficial middle cerebral vein (SMCV) was influenced by the severity of reduction in upstream arterial flow among patients with stroke (2). Considering the high rate of congenital hypoplastic TS, it is difficult to clarify whether the asymmetry of TS was congenital or a result of ischemia in patients with stroke in our study since we had no pre-stroke imaging of the same patient for comparison. However, we infer that stroke itself may influence TS symmetry because the rate of symmetric TS was actually changed in patients with stroke. In a healthy population, 50–60% of patients had right dominant TS and 10–20% had left dominant TS, leaving the occurrence rate of symmetric TS as low as 30% (20, 21), whereas in other two stroke studies, 57% of patients had symmetric TS and 21–30% had “hypoplasia” or “occlusion” of ipsilateral TS (22, 23). Similarly, in our study, 52.2% of patients presented symmetric TS and 22% presented FDITS, indicating that TS morphology may be modulated by ischemic stroke and might be a stroke-related imaging feature.

In addition, our findings on the relationship between disturbed drainage of TS and poor arterial collaterals suggest that venous outflow is influenced by the severity of low arterial flow. This finding is consistent with a previous study which demonstrated that the patients with asymmetrical clearance of TS were more likely to have incomplete arterial collateral filling on dynamic magnetic resonance angiography ($p = 0.015$) (24). A similar phenomenon was reported in the MCA occlusion model of the African green monkey, showing that the poor collateral circulation was related to a back and forth blood pooling with no venous return into cortical veins, leading to no flow into the venous sinus (25).

Previous studies described the independent impact of venous drainage patterns on outcomes in patients with AIS (2, 3), which supported the view that cerebral veins played a vital role in the maintenance of CBF and brain function after ischemia. In the current study, we first identified that FDITS was also independently associated with unfavorable outcomes in the acute LAO of anterior circulation. Importantly, we found that although FDITS and poor collaterals were both independently associated with 24-h brain edema expansion, their prognostic values were different. When FDITS was absent, about 50% of patients who had poor collaterals suffered severe brain edema. However, if baseline FDITS was present, the possibility of an obvious edema

expansion within 24 h was as high as about 90% regardless of the arterial collateral status. Decreased cerebral venous outflow in ipsilateral TS would greatly change the venous pressure, which was previously suggested as the primary driving force in the development of brain edema. When venous pressure is increased beyond the tissue pressure, the pressure difference might interfere with venous reflux and lead to parenchymal edema and subsequent unfavorable clinical outcome (2, 26, 27). Actually, ischemic brain edema is a crucial cause of death for stroke survivors (28), as malignant cerebral infarct, usually related to poor collaterals, leads to a poor outcome. It is thus worth exploring in future studies whether the early identification of FDITS at admission in patients with acute LAO would help to guide appropriate treatment to prevent or alleviate edema expansion by all means, for example, the widely announced early decompressive hemicraniectomy (28), or intravenous glyburide as a promising intervention (29), in addition to reperfusion effort (30).

However, the subgroup analysis result is surprising because patients with FDITS still had edema expansion at 24 h and an unfavorable outcome at 3 months even though they were treated with reperfusion therapy and even if reperfusion was obtained. This is different from the previous result, which revealed no significant difference in outcome between patients with or without ipsilateral SMCV if reperfusion was successfully achieved (2). It is believed that cerebral veins have sufficient anastomosis and the drainage area of TS is obviously much larger than that of cortical veins. Thus, it might be assumed that the occurrence of FDITS indicates the possibility of venous collateral failure to severe arterial ischemia, which would not be compensated even after successful reperfusion, leading to a synergistic influence on the tissue outcome (8). Although we could not jump to doubt whether reperfusion therapy might be of limited significance in patients with initial FDITS according to the current small sample subgroup results, our study emphasizes the need for ancillary judgment of venous drainage to guide reperfusion therapy, and future large prospective studies are needed to clarify this issue.

Our study has limitations attributed to its retrospective collection of data in a single center with a moderate sample size, which may pose a potential risk of selection bias. Second, the edema evaluation scale may not well differentiate vasogenic edema from infarction. To minimize the impact of this error, we focused on 24-h edema change to reflect relatively actual edema development. Third, due to the lack of a gold standard, such as DSA, the accuracy of 4D-CTA in identifying the filling defect of transverse sinus needs to be further validated. Fourth, we

could not differentiate the asymmetry of TS as nature or nurture from baseline 4D-CTA due to its recognition ability of jugular foramen dominance. Fifth, 4D-CTA derived from CTP would not necessarily be performed on patients with LAO who arrive early at some large centers, which would further limit utility. In addition, we did not analyze the drainage pattern changes of TS after reperfusion therapy due to the lack of enough follow-up image data. Further studies are still needed to prove our findings and investigate the possible mechanisms.

CONCLUSION

The filling defect of the ipsilateral transverse sinus was strongly associated with the level of arterial collateral flow. It was associated with edema expansion and an unfavorable outcome, irrespective of baseline arterial collaterals. FDITS might be identified as a potential imaging marker for neurological outcomes in acute LAO of the anterior circulation, and prevention of edema expansion might be an important ultra-early target once FDITS is identified.

DATA AVAILABILITY STATEMENT

The raw data supporting the conclusions of this article will be made available by the authors, without undue reservation.

ETHICS STATEMENT

The studies involving human participants were reviewed and approved by the Ethics Committee of SAHZU. The patients/participants provided their written informed consent to participate in this study.

AUTHOR CONTRIBUTIONS

YC, SZ, and ML contributed to the conception and design of the study. YC, SZ, SY, MZ, FS, and MP contributed to the acquisition and analysis of the data. YC, SZ, DL, and ML contributed to drafting the text. YC, SZ, and RZ prepared the figures. ML is responsible for the overall content as guarantor. All authors contributed to the article and approved the submitted version.

SUPPLEMENTARY MATERIAL

The Supplementary Material for this article can be found online at: <https://www.frontiersin.org/articles/10.3389/fneur.2022.863460/full#supplementary-material>

REFERENCES

- Goyal M, Menon B, van Zwam W, Dippel D, Mitchell P, Demchuk A, et al. Endovascular thrombectomy after large-vessel ischaemic stroke: a meta-analysis of individual patient data from five randomised trials. *Lancet*. (2016) 387:1723–31. doi: 10.1016/S0140-6736(16)00163-X
- Zhang S, Lai Y, Ding X, Parsons M, Zhang JH, Lou M. Absent filling of ipsilateral superficial middle cerebral vein is associated with poor outcome after reperfusion therapy. *Stroke*. (2017) 48:907–14. doi: 10.1161/STROKEAHA.116.016174
- Zhang X, Zhang S, Chen Q, Ding W, Campbell B, Lou M. Ipsilateral prominent thalamostriate vein on susceptibility-weighted imaging predicts poor outcome after intravenous thrombolysis in acute ischemic stroke. *AJNR Am J Neuroradiol*. (2017) 38:875–81. doi: 10.3174/ajnr.A5135
- Jansen IGH, van Vuuren AB, van Zwam WH, van den Wijngaard IR, Berkhemer OA, Lingsma HF, et al. Absence of cortical vein opacification

- is associated with lack of intra-arterial therapy benefit in stroke. *Radiology*. (2018) 286:731. doi: 10.1148/radiol.2017174043
5. Bhaskar S, Bivard A, Stanwell P, Attia J, Parsons M, Nilsson M, et al. Association of cortical vein filling with clot location and clinical outcomes in acute ischaemic stroke patients. *Sci Rep*. (2016) 6:38525. doi: 10.1038/srep38525
 6. Sharma VK, Yeo LL, Teoh HL, Shen L, Chan BP, Seet RC, et al. Internal cerebral vein asymmetry on follow-up brain computed tomography after intravenous thrombolysis in acute anterior circulation ischemic stroke is associated with poor outcome. *J Stroke Cerebrovasc Dis: Off J National Stroke Assoc*. (2014) 23:e39–45. doi: 10.1016/j.jstrokecerebrovasdis.2013.08.007
 7. Terasawa Y, Yamamoto N, Morigaki R, Fujita K, Izumi Y, Satomi J, et al. Brush sign on 3-T T2*-weighted MRI as a potential predictor of hemorrhagic transformation after tissue plasminogen activator therapy. *Stroke*. (2014) 45:274–6. doi: 10.1161/STROKEAHA.113.002640
 8. Tong LS, Guo ZN, Ou YB, Yu YN, Zhang XC, Tang J, et al. Cerebral venous collaterals: a new fort for fighting ischemic stroke? *Prog Neurobiol*. (2018) 163:172–93. doi: 10.1016/j.pneurobio.2017.11.001
 9. Munuera J, Blasco G, Hernandez-Perez M, Daunis IEP, Davalos A, Liebeskind DS, et al. Venous imaging-based biomarkers in acute ischaemic stroke. *J Neurol Neurosurg Psychiatry*. (2017) 88:62–9. doi: 10.1136/jnnp-2016-314814
 10. Hacke W, Kaste M, Bluhmki E, Brozman M, Davalos A, Guidetti D, et al. Thrombolysis with alteplase 3 to 45 hours after acute ischemic stroke. *N Eng J Med*. (2008) 359:1317–29. doi: 10.1056/NEJMoa0804656
 11. Yu Y, Han Q, Ding X, Chen Q, Ye K, Zhang S, et al. Defining core and penumbra in ischemic stroke: a voxel- and volume-based analysis of whole brain CT perfusion. *Sci Rep*. (2016) 6:20932. doi: 10.1038/srep20932
 12. Fofi L, Giugni E, Vadala R, Vanacore N, Aurilia C, Egeo G, et al. Cerebral transverse sinus morphology as detected by MR venography in patients with chronic migraine. *Headache*. (2012) 52:1254–61. doi: 10.1111/j.1526-4610.2012.02154.x
 13. Zhang S, Chen W, Tang H, Han Q, Yan S, Zhang X, et al. The prognostic value of a four-dimensional ct angiography-based collateral grading scale for reperfusion therapy in acute ischemic stroke patients. *PLoS ONE*. (2016) 11:e0160502. doi: 10.1371/journal.pone.0160502
 14. Lin L, Bivard A, Levi C, Parsons M. Comparison of computed tomographic and magnetic resonance perfusion measurements in acute ischemic stroke: back-to-back quantitative analysis. *Stroke*. (2014) 45:1727–32. doi: 10.1161/STROKEAHA.114.005419
 15. Campbell B, Christensen S, Levi C, Desmond P, Donnan G, Davis S, et al. Cerebral blood flow is the optimal CT perfusion parameter for assessing infarct core. *Stroke*. (2011) 42:3435–40. doi: 10.1161/STROKEAHA.111.618355
 16. Miteff F, Levi C, Bateman G, Spratt N, McElduff P, Parsons M. The independent predictive utility of computed tomography angiographic collateral status in acute ischaemic stroke. *Brain*. (2009) 132(Pt 8):2231–8. doi: 10.1093/brain/awp155
 17. Larrue V, von Kummer RR, Müller A, Bluhmki E. Risk factors for severe hemorrhagic transformation in ischemic stroke patients treated with recombinant tissue plasminogen activator: a secondary analysis of the European-Australasian acute stroke study (ECASS II). *Stroke*. (2001) 32:438–41. doi: 10.1161/01.str.32.2.438
 18. Wardlaw J, Sellar R. A simple practical classification of cerebral infarcts on CT and its interobserver reliability. *AJNR Am J Neuroradiol*. (1994) 15:1933–9.
 19. Rowat AM, Wardlaw JM, Dennis MS. Abnormal breathing patterns in stroke: relationship with location of acute stroke lesion and prior cerebrovascular disease. *J Neurol Neurosurg Psychiatry*. (2007) 78:277–9. doi: 10.1136/jnnp.2006.102228
 20. Alper F, Kantarci M, Dane S, Gumustekin K, Onbas O, Durur I. Importance of anatomical asymmetries of transverse sinuses: an MR venographic study. *Cerebrovascular Dis*. (2004) 18:236–9. doi: 10.1159/000079960
 21. Bono F, Lupo MR, Lavano A, Mangone L, Fera F, Pardatscher K, et al. Cerebral MR venography of transverse sinuses in subjects with normal CSF pressure. *Neurology*. (2003) 61:1267–70. doi: 10.1212/01.wnl.0000092021.88299.b4
 22. Yu W, Rives J, Welch B, White J, Stehel E, Samson D. Hypoplasia or occlusion of the ipsilateral cranial venous drainage is associated with early fatal edema of middle cerebral artery infarction. *Stroke*. (2009) 40:3736–9. doi: 10.1161/STROKEAHA.109.563080
 23. Volny O, Cimflova P, Mikulik R. Ipsilateral sinus hypoplasia and poor leptomeningeal collaterals as midline shift predictors. *J Stroke Cerebrovasc Dis*. (2016) 25:1792–6. doi: 10.1016/j.jstrokecerebrovasdis.2016.04.004
 24. Hernández-Pérez M, Puig J, Blasco G, Pérez de la Ossa N, Dorado L, Dávalos A, et al. Dynamic magnetic resonance angiography provides collateral circulation and hemodynamic information in acute ischemic stroke. *Stroke*. (2016) 47:531–4. doi: 10.1161/strokeaha.115.010748
 25. Sasaki M, Honmou O, Radtke C, Kocsis J. Development of a middle cerebral artery occlusion model in the non-human primate and a safety study of iv infusion of human mesenchymal stem cells. *PLoS ONE*. (2011) 6:e26577. doi: 10.1371/journal.pone.0026577
 26. Pranevicius O, Pranevicius M, Liebeskind DS. Partial aortic occlusion and cerebral venous steal: venous effects of arterial manipulation in acute stroke. *Stroke*. (2011) 42:1478–81. doi: 10.1161/STROKEAHA.110.603852
 27. Kasner SE, Demchuk AM, Berrouschot J, Schmutzhard E, Harms L, Verro P, et al. Predictors of fatal brain edema in massive hemispheric ischemic stroke. *Stroke*. (2001) 32:2117–23. doi: 10.1161/hs0901.095719
 28. Wijndicks E, Sheth K, Carter B, Greer D, Kasner S, Kimberly W, et al. Recommendations for the management of cerebral and cerebellar infarction with swelling: a statement for healthcare professionals from the American heart association/American stroke association. *Stroke*. (2014) 45:1222–38. doi: 10.1161/01.str.0000441965.15164.d6
 29. Sheth KN, Petersen NH, Cheung K, Elm JJ, Hinson HE, Molyneux BJ, et al. Long-term outcomes in patients aged ≤ 70 years with intravenous glyburide from the phase II games-RP study of large hemispheric infarction: an exploratory analysis. *Stroke*. (2018) 49:1457–63. doi: 10.1161/STROKEAHA.117.020365
 30. Kimberly WT, Dutra BG, Boers AMM, Kasner SE, Kimberly WT, Schwab S, et al. Association of reperfusion with brain edema in patients with acute ischemic stroke: a secondary analysis of the MR clean trial. *JAMA Neurol*. (2018) 75:453–61. doi: 10.1001/jamaneurol.2017.5162

Conflict of Interest: The authors declare that the research was conducted in the absence of any commercial or financial relationships that could be construed as a potential conflict of interest.

Publisher's Note: All claims expressed in this article are solely those of the authors and do not necessarily represent those of their affiliated organizations, or those of the publisher, the editors and the reviewers. Any product that may be evaluated in this article, or claim that may be made by its manufacturer, is not guaranteed or endorsed by the publisher.

Copyright © 2022 Chen, Zhang, Yan, Zhang, Zhang, Shi, Liebeskind, Parsons and Lou. This is an open-access article distributed under the terms of the Creative Commons Attribution License (CC BY). The use, distribution or reproduction in other forums is permitted, provided the original author(s) and the copyright owner(s) are credited and that the original publication in this journal is cited, in accordance with accepted academic practice. No use, distribution or reproduction is permitted which does not comply with these terms.



The Recipient Vessel Hemodynamic Features Affect the Occurrence of Cerebral Edema in Moyamoya Disease After Surgical Revascularization: A Single-Center Retrospective Study

Liang Xu[†], Yin Li[†], Yun Tong, Jun-wen Hu, Xu-chao He, Xiong-jie Fu, Guo-Yang Zhou, Yang Cao, Xiao-bo Yu, Hang Zhou, Chao-ran Xu and Lin Wang*

OPEN ACCESS

Edited by:

Chengcheng Zhu,
University of Washington,
United States

Reviewed by:

Jiaqi Liu,
Shanghai General Hospital, China
Tsuyoshi Izumo,
Nagasaki University, Japan

*Correspondence:

Lin Wang
dr_wang@zju.edu.cn

[†]These authors have contributed
equally to this work

Specialty section:

This article was submitted to
Stroke,
a section of the journal
Frontiers in Neurology

Received: 05 March 2022

Accepted: 01 April 2022

Published: 16 May 2022

Citation:

Xu L, Li Y, Tong Y, Hu J-w, He X-c,
Fu X-j, Zhou G-Y, Cao Y, Yu X-b,
Zhou H, Xu C-r and Wang L (2022)
The Recipient Vessel Hemodynamic
Features Affect the Occurrence of
Cerebral Edema in Moyamoya
Disease After Surgical
Revascularization: A Single-Center
Retrospective Study.
Front. Neurol. 13:890126.
doi: 10.3389/fneur.2022.890126

Department of Neurosurgery, School of Medicine, The Second Affiliated Hospital, Zhejiang University, Hangzhou, China

Objective: In moyamoya disease (MMD) with direct or combined revascularization, the initially hemodynamic recipient features are likely one of the main causes of acute hemodynamic disruption. Previous studies have explored the relationship between recipient diameter or flow velocity and postoperative complications, but there are still no optimal selection criteria with multiple potential recipient vessels. Cerebral edema is one of the most common radiological manifestations in the acute postoperative period. This study assessed the hemodynamic characteristics of cortex vessels related to postoperative cerebral edema.

Methods: All patients who had undergone direct or combined revascularization with preoperative digital subtraction angiography (DSA) between 2019 and 2021 were eligible for inclusion in this study. The application of DSA was performed and regular radiological examinations were employed after surgery. DSA was analyzed with the hemodynamic features within chosen recipient vessels. Cerebral edema was identified as a low-density image on CT or high signaling in the MRI T2 phase. The recipient hemodynamic characteristics and demographic presentation, as well as clinical data, were retrospectively analyzed in this study.

Results: A total of 103 patients underwent direct or combined revascularization with preoperative DSA. The mean age of this enrolled cohort was 44.31 ± 10.386 years, in which bilaterally involved MMD accounted for the main part. The preliminary correlation analysis found preoperative disease period ($p = 0.078$), recipients observed in angiography ($p = 0.002$), and surgery on the left ($p = 0.097$) may be associated with cerebral edema. The following regression analysis confirmed low occurrence of cerebral edema was accompanied by recipients observed in angiography ($p = 0.003$). After subdividing by flow direction and hemodynamic sources, the incidence rate of anterograde direction, anterior sources, and posterior sources were significantly lower than undetected recipients.

Conclusions: Cerebral edema is a common radiological manifestation in MMDs after surgery. In this study, the observation in angiography reliably identifies a variety of physiological or pathological recipient detection, flow direction, and hemodynamic sources in patients with MMD after revascularization, which indicates the selection strategy of potential recipients and highlights the importance of recipient observability in DSA. Meanwhile, vascular conditions determined by recipient hemodynamics mediate the occurrence of postoperative cerebral edema.

Keywords: moyamoya disease (MMD), cerebral edema, recipient vessels, digital subtraction angiography (DSA), flow direction, stroke

INTRODUCTION

Moyamoya disease (MMD) is a chronic cerebrovascular disease that is characterized by progressive steno-occlusive in bilateral internal carotid arteries and their proximal branches (1). Surgical revascularization has been recognized as an effective treatment to improve the impaired cerebral hemodynamics and decreased the risk of recurrent stroke (2). However, a previous study found about 16% of MMDs suffered a postoperative stroke with permanent deficits (3) and the watershed-shift phenomenon was as high as 10.9% after surgery (4). Surgical revascularization changed the distribution of the recipient's vessels and the sharp hemodynamic shift caused by vascular anastomosis may boost postoperative neurological morbidity. Recent research demonstrated that blood flow changes before and after vascular anastomosis were evident in MMDs with postoperative complications (5). Recipients with an initially retrograde flow direction presented great potential for flow increase after surgery (6) and arteries with the earliest intraoperative fluorescence emission were prone to occur symptomatic complications (7). In addition, hemodynamic sources of recipient arteries were concerned with postoperative hyperperfusion (8).

The radiologic incidence of stroke was higher than symptomatic stroke, in which 33.3% of MMDs were reported with postoperative diffusion-weighted imaging (DWI)-detected lesions (9). Cerebral edema is a common imaging performance related to hemodynamic compromise after surgical revascularization and may be warning sign that focal parenchymal tissues fail to adapt to hemodynamics disruption. Thus, this study aimed to analyze the effects of recipient hemodynamic features on postoperative cerebral edema in MMDs.

MATERIALS AND METHODS

Patients Selection

This study included 103 MMDs with surgical revascularization at our hospital between November 2019 and February 2021 after 15 patients were excluded (Figure 1). The diagnosis of MMD was confirmed based on the guidelines for MMD diagnosis

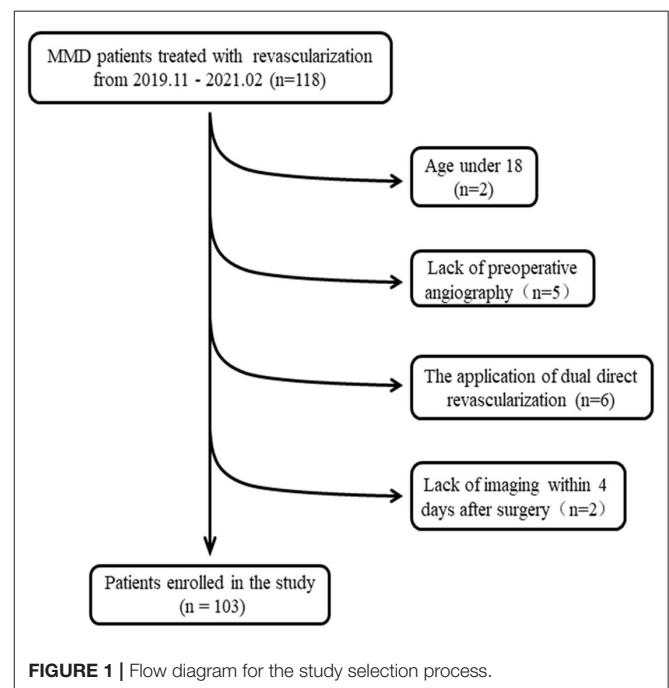


FIGURE 1 | Flow diagram for the study selection process.

and treatment published by the Research Committee on the Pathology and Treatment of Spontaneous Occlusion of the Circle of Willis (10). Besides, the inclusion criteria of this study were as follows:

- (1) Age ≥ 18 years;
- (2) Definite diagnosis of MMD confirmed by DSA;
- (3) The application of direct or combined revascularization;
- (4) Radiological examinations, including computed tomography (CT) or magnetic resonance imaging (MRI), were performed within 4 days after surgery.

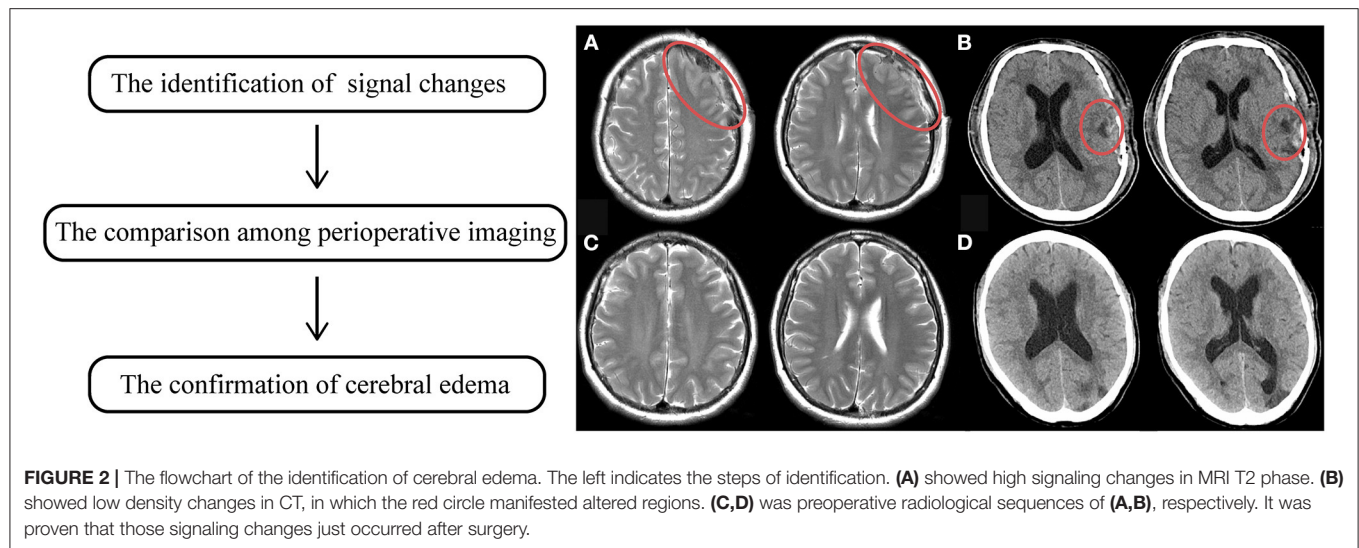
The exclusion criteria were as follows:

- (1) The employment of dual direct revascularization;
- (2) Lack of preoperative angiography in our hospital.

Surgical Procedures

Direct revascularization indicates superficial temporal artery (STA)—middle cerebral artery (MCA) bypass (11). Combined

Abbreviations: ACA, Anterior cerebral artery; CT, Computed Tomography; DSA, Digital Subtraction Angiography; MCA, Middle cerebral artery; MMD, Moyamoya disease; STA, Superficial temporal artery.



revascularization has been described previously (12) and consists of direct and indirect revascularization (encephalo-duro-myosynangiosis, EDMS). Meanwhile, intraoperative indocyanine green was immediately injected to confirm the patency of anastomotic sites.

The Evaluation of Recipient Hemodynamic Features and Postoperative Cerebral Edema

The hemodynamic characteristics of the recipient's were assessed through preoperative DSA by two experienced neurosurgeons. Of note, the flow direction of the recipient's vessels was categorized as follows:

- (1) Anterograde direction: blood flow from M3 segment to M4 segment;
- (2) Retrograde direction: blood flow from M4 segment to M3 segment;
- (3) Undetected direction: no or little flow direction was detected in angiography.

The hemodynamic sources of the recipient's vessels were categorized as follows:

- (1) Anterior sources: blood supply was from an anterior cerebral artery (ACA) or MCA;
- (2) Posterior sources: blood supply was from a posterior cerebral artery (PCA) or vertebrobasilar artery;
- (3) Undetected sources: no or few hemodynamic sources were detected in angiography.

The evaluation of cerebral edema was relatively fussy. The first step is to identify signal changes around the anastomotic area of postoperative radiological examinations, which presented as either slightly low-density on CT or high-signaling in the MRI T2 phase. Subsequently, the comparison among perioperative imaging was applied to confirm whether the changes were recent, which means occurring or not. The occurrence of cerebral edema

was confirmed by two experienced neurosurgeons independently and the results were reached after consensus, as shown in Figure 2.

Data Analysis

The SPSS 24.0 (SPSS, Inc., Chicago, IL, USA) was used for statistical analysis. A descriptive summary is presented as mean \pm standard deviation (SD), median (interquartile range), frequency, or percentage, as appropriate. For comparison between the non-postoperative cerebral edema group and postoperative cerebral edema group, an independent-sample *t*-test, Pearson's chi-squared, or Fisher's exact test correlation analysis was performed. Afterward, the logistic regression analysis was conducted for significant factors achieving $P < 0.10$ in the univariate analysis. All tests were two-tailed. $P < 0.05$ was considered to be statistically significant.

RESULTS

Demographics and Clinical Presentation

Of the 118 consecutive patients with MMD, who underwent surgical revascularization from November 2019 to February 2021, we identified 103 MMDs who met the inclusion and exclusion criteria of this research (Figure 1). The mean age of MMDs was 44.31 ± 10.386 years. The female ratio was 69.9% in this study. Eighty-three out of 103 (80.6%) patients presented with bilateral MMD. Thirty-four percent of patients presented with postoperative cerebral edema. The other clinical characteristics of total MMDs are summarized in Table 1.

Effects of Recipient Vessel Characteristics on Cerebral Edema

Initially, we analyzed basic features between the non-postoperative (non-postop) edema group and the postoperative (postop) edema group. As shown in Table 2, the demographics of the two groups were similar and had no statistical significance.

TABLE 1 | The baseline characteristics of enrolled MMD patients.

	Patients (n = 103)
Age, yrs	44.31 ± 10.386
Female (%)	73 (69.9)
Comorbidity (%)	
Smoking	19 (18.4)
Alcohol consumption	20 (19.4)
Dyslipidemia	24 (23.3)
Hypertension	33 (32.0)
Diabetes	10 (9.7)
MMD characteristics (%)	
Bilateral involved	83 (80.6)
Onset manifestation	
Ischemic	58 (56.3)
Hemorrhagic	39 (37.9)
Others	6 (5.8)
Preop disease period, mos*	5.00 (10)
Suzuki stage	
1	13 (12.6)
2	18 (17.5)
3	52 (50.5)
4	18 (17.5)
5	2 (1.9)
Surgical information (%)	
Surgical type	
Direct revascularization	7 (6.8)
Combined revascularization	96 (93.2)
The left side of operation	53 (51.5)
Postop cerebral edema (%)	35 (34.0)
mRS on admission*	0.00 (0)

MMD, moyamoya disease; Preop, preoperative; Postop, postoperative.

*Indicates that values are presented as median (interquartile range).

And the comorbidities apart from MMD in groups presented no significant differences. Besides, disease-related aspects were consistent between the two groups. However, the preoperative disease period was inclined to be shorter in the postop edema group than the non-postop edema group ($p = 0.078$). Remarkably, the proportion of recipient's vessels observed in preoperative angiography was less in the postop edema group significantly, compared with the non-postop edema group ($p = 0.002$), which presented as 54.3 vs. 82.4%. Meanwhile, the duration of the postop edema group was prone to be longer than the non-postop edema group statistically (17.94 ± 7.840 vs. 14.66 ± 3.896 , $p = 0.024$). Also, the time of postoperative imaging was irrelevant to cerebral edema ($p = 0.181$). After possible factors were included in logistic regression, we found recipient vessels observed in preoperative angiography were an independent factor associated with postoperative cerebral edema (OR = 3.930, 95% CI: 1.579–9.778, $p = 0.003$).

Afterward, we further investigated the flow direction and hemodynamic sources of recipient vessels on the occurrence of cerebral edema. The two different features had obvious

statistical differences in the two groups ($p = 0.012$; $p = 0.002$, **Table 3**). Of note, the interrater reliability between the evaluation of two independent surgeons in the flow direction, hemodynamic sources, and cerebral edema is a significantly almost perfect agreement ($K = 0.906$; $K = 0.903$; $K = 0.916$, **Table 4**). On the one hand, the occurrence rate of cerebral edema in the undetected direction was higher than antegrade direction ($p = 0.004$, **Figure 3**), but no significant differences were shown between the retrograde direction and the undetected direction. On the other hand, undetected sources were vulnerable to cerebral edema statistically, compared with anterior sources and posterior sources ($p = 0.008$; $p = 0.005$; **Figure 4**).

DISCUSSION

In this study, 103 patients accepted surgical revascularization and ischemia was the major onset manifestation in enrolled MMDs. Disease severity was classified by the angiography-based Suzuki classification and stage 3 accounted for the bulk of all patients. No severe neurological deficits were observed on admission. Thirty-five cases were caught in cerebral edema. The anastomosis to undetected recipient vessels in angiography was inclined to cause postoperative edema. After further subdivision of recipient hemodynamic features, the antegrade direction was less prone to develop edema. Meanwhile, the incidence of edema in anterior and posterior hemodynamic sources was lower than that in recipient vessels with undetected sources, respectively.

Surgical revascularization has been applied in the treatment and effectively improves the long-term outcome of MMD (13, 14). Direct revascularization immediately improves impaired hemodynamic status after surgery, but ischemic parenchymal tissues are possibly unadaptable to dramatic hemodynamic changes. There were 16–20% of patients involved with complications after direct or combined revascularization (2, 3), which was higher than other craniotomy surgery. The radiological signal changes are before the onset of neurological symptoms. A previous study reported that 27.5% MMDs after STA-MCA bypass experienced cerebral hyperperfusion syndrome (15). Radiological hyperperfusion syndrome is defined as a great increase in recipient cerebral blood flow (16), which requires specific sequences measuring hemodynamic differences. As a postoperative common radiological appearance, the discrimination of cerebral edema requires simple image examinations. Surgical techniques caused little disturbance and limited edema on the cerebral cortex, while the hemodynamic compromise occurred in the blood flow competition between the donor and recipient arteries (17). As the watershed shift, reversed flow direction may contribute to the hypoperfusion of the distal MCA field (18), followed with the appearance and progression of cerebral edema. Consequently, edema after bypass probably implied the inadequate adaptation of focal brain tissues in early postoperative hemodynamic variation.

TABLE 2 | The factors related with postoperative cerebral edema in adults with moyamoya.

	Univariate analysis			Multivariate analysis		
	Non-postop edema (n = 68)	Postop edema (n = 35)	p-value	OR	95% CI	p-value
Age, yrs	43.66 ± 10.633	45.57 ± 9.915	0.379 ^a			
Female (%)	49 (72.1)	23 (65.7)	0.506 ^b			
Smoking (%)	12 (17.6)	7 (20.0)	0.771 ^b			
Bilateral disease (%)	52 (76.5)	31 (88.6)	0.141 ^b			
Onset manifestation (%)			0.407 ^b			
Ischemic	37 (54.4)	21 (60.0)				
Hemorrhagic	24 (35.3)	13 (37.1)				
Others	7 (10.3)	1 (2.9)				
Preop disease period, mos	10.61 ± 16.137	6.71 ± 5.800	0.078 ^a			
Suzuki stage (%)			0.905 ^c			
1	8 (11.8)	5 (14.3)				
2	11 (16.2)	7 (20.0)				
3	35 (51.5)	17 (48.6)				
4	13 (19.1)	5 (14.3)				
5	1 (1.5)	1 (2.9)				
Recipient vessels observed in preop angiography (%)	56 (82.4)	19 (54.3)	0.002 ^b	3.930	1.579–9.778	0.003
Surgery on the left (%)	31 (45.6)	22 (62.9)	0.097 ^b			
Time of postop imaging, days	2.37 ± 0.976	2.66 ± 1.136	0.181 ^a			
Duration, days	14.66 ± 3.896	17.94 ± 7.840	0.024 ^a			

Preop, preoperative; postop, postoperative.

^aIndependent-samples t-test.

^bPearson chi-square.

^cFisher's exact test.

TABLE 3 | The hemodynamic features of recipient vessels involved with postoperative cerebral edema.

Preop recipient vessels characteristics (%)	Non-postop edema (n = 68)	Postop edema (n = 35)	p-value
Observed in angiography	56 (82.4)	19 (54.3)	0.002
Flow direction (Ref = undetected)			0.012 ^a
Anterograde	40 (58.8)	13 (37.1)	0.004 ^b
Retrograde	16 (23.5)	6 (17.1)	
Undetected	12 (17.6)	16 (45.7)	
Hemodynamic sources (Ref = Undetected sources)			0.002 ^a
Anterior	48 (70.6)	19 (54.3)	0.008 ^b
Posterior	8 (11.8)	0 (0.0)	0.005 ^a
Undetected sources	12 (17.6)	16 (45.7)	

Preop, preoperative; postop, postoperative.

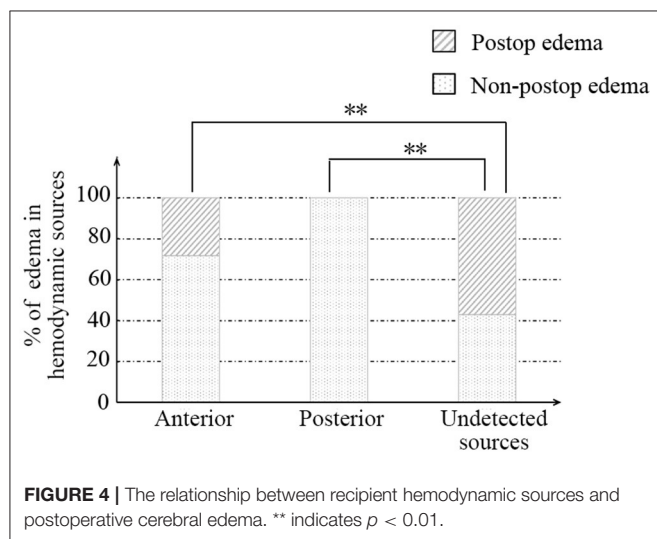
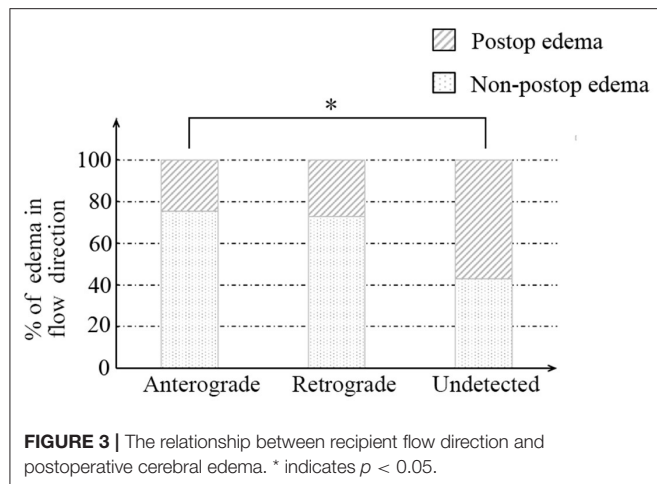
^aFisher's exact test.

^bPearson chi-square.

TABLE 4 | The interrater reliability involved in the estimation of recipient hemodynamic features and postoperative cerebral edema.

	Surgeon 1	Surgeon 2	p-value	Kappa (95% CI)
Flow direction (%)			<0.001	0.906 (0.833, 0.979)
Anterograde	51 (49.5)	55 (53.4)		
Retrograde	24 (23.3)	20 (19.4)		
Undetected	28 (27.2)	28 (27.2)		
Hemodynamic sources (%)			<0.001	0.903 (0.821, 0.985)
Anterior	65 (63.1)	68 (66.0)		
Posterior	28 (27.2)	28 (27.2)		
Undetected sources	10 (9.7)	7 (6.8)		
Cerebral edema (%)			<0.001	0.916 (0.836, 0.996)
Edema	36 (35.0)	38 (36.9)		
Non-edema	67 (65.0)	65 (63.1)		

anastomotic process and draw high compensatory outflow as a primary determinant of direct revascularization function (20). However, the matched calibers between STA and MCA are sufficient to avoid anastomotic failure (19). Also, hemodynamic features of recipient's vessels are heavily associated with postoperative complications.



Multiple applications have focused on recipient vessel selection to reduce acute complications *via* intraoperative indocyanine green video angiography, which indicated the earliest emission was prone to occur symptomatic hyperperfusion, and the latest was related to white thrombus of anastomotic sites (5, 7, 21).

Recipient vessels with preoperative detection in DSA are at a significantly lower risk of cerebral edema, as shown in **Table 2**. The angiographic appearance of recipient's vessels manifests the strong communication between cortex vessels and large intracranial arteries, which also indicates the potential adaptation of neighboring parenchymal tissues. In contrast, the missing angiographic recipients presented high rates of edema. Undetected angiographic vessels were accompanied by high vascular resistance or severe proximal perfusion deficit. After the subsequent blood flow shock from donor arteries, cortical vessels showed maladaptive manifestations, of which the most familiar is cerebral edema.

Furthermore, an initially anterograde blood flow direction, anterior and posterior hemodynamic sources within possible recipients, was less likely to occur in cerebral edema than undetected flow direction, shown in **Figures 3, 4** and **Table 3**. We believe that these characteristics indicate great accommodated capacity with little vascular resistance because failure to show in DSA is caused by arterial steal and loss of vascular autoregulation. In general, the primary prerequisite of initially regular flow orientations requires integrated vascular networks. Besides, the disposition of extracranial strike recruits local strong vascular autoregulation. Similarly, anterior or posterior hemodynamic sources within potential cortex vessels could indicate the integrality of the vascular bed. Intriguingly, the combination of heel and toe recipient orientations occasionally appeared in the anterior or posterior hemodynamic sources. In effect, the blood supply from anterior or posterior cerebral arteries reverses through distal cortical vessels and into the recipient encephalic region, in a certain area which run in forward directions at times, shown in **Figure 5**. The two different categories seem to be arguable in position-specific flow orientations, but there are exactly two diverse directions in particular arteries. With these mentioned discoveries, we have ample reason to believe cortex vessels with anterior directions from anterior or posterior hemodynamic sources could achieve less cerebral edema. Meanwhile, the specious contradiction may also support the hypothesis that the distribution dynamics of preceding DSA through intracranial branches and into the recipient bed serve as an indicator of vascular conditions. After all, complementary flow from the fish-mouthed graft to promote the filling of the recipients requires sufficient vascular spaces for shock absorption in the acute postoperative period (22). It is not a question of which direction or source of recipient's vessels are, but rather how much of recipients could be detected in angiography. Thus, the recipient observation in DSA indicates vascular conditions and serves as a mediator in cerebral edema. Of note, the medical strategy in enrolled MMDs after surgery reduced changes in blood flow requiring receptor vascular adaptation. The unstable blood pressure possibly caused sharp changes in extra-intracranial arterial pressure difference. The strict control of blood pressure between 120 and 140 mmHg was beneficial to narrow down hemodynamic fluctuations and avoid other fatal complications, such as anastomotic rupture or bleeding.

Several potential limitations of this study should be noted. First, it was a retrospective analysis with small sample size. The operative indications and surgical procedures were based on individual characteristics and institutional experience. Second, cerebral edema was simply recognized by daily CT or MRI examinations, and there were still patients with mild cerebral edema missing in this study. Third, further multicenter studies with a larger cohort of MMD and focused on the type of edema and risk factors should be conducted.

CONCLUSIONS

Cerebral edema is a common radiological manifestation in patients with MMD after surgery. In this study, the

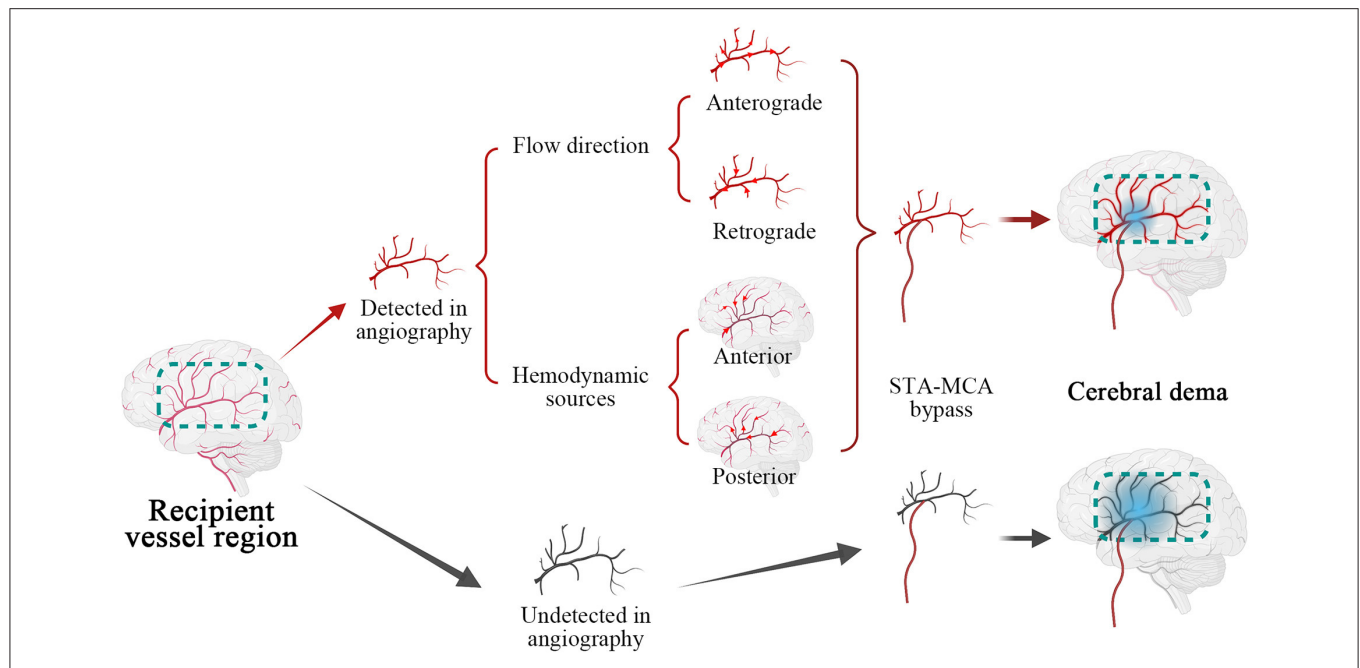


FIGURE 5 | Illustrations of recipient hemodynamic features on the cerebral edema. Marked by the dotted box in green, recipient vessel region was categorized as angiographic detected in red and undetected in black. The cortex vessels were applied with superficial temporal artery (STA)- middle cerebral artery (MCA) bypass, after subdivided by flow direction and hemodynamic sources, in which red arrows indicated specific directions of blood flow. Subsequently, the recipients with different hemodynamic characteristics developed cerebral edema implied by gradient blue circle and undetected recipients were prone to postoperative cerebral edema.

observation in angiography reliably identifies a variety of physiological or pathological recipient detection, flow direction, and hemodynamic sources in patients with MMD after revascularization, which indicates the selection strategy of potential recipients and highlights the importance of recipient observability in DSA. Meanwhile, vascular conditions determined by recipient hemodynamics mediate the occurrence of postoperative cerebral edema.

DATA AVAILABILITY STATEMENT

The raw data supporting the conclusions of this article will be made available by the authors, without undue reservation.

ETHICS STATEMENT

The studies involving human participants were reviewed and approved by the Local Ethics Committee of The Second Affiliated Hospital of School of Medicine, Zhejiang University. The patients/participants provided their written informed consent to participate in this study.

REFERENCES

1. Zeng H, Guo Y, Li Y, Yu X, Yan F, Tan X, et al. Comparison of operative and conservative treatment for asymptomatic moyamoya disease: preliminary experience in small retrospective series. *World Neurosurg.* (2021) 146:e955–60. doi: 10.1016/j.wneu.2020.11.045

AUTHOR CONTRIBUTIONS

Material preparation, data collection, and analysis were performed by LX and YL. The first draft of the manuscript was written by LX and all authors commented on previous versions of the manuscript. All authors contributed to the study conception, design, read and approved the final manuscript.

FUNDING

This work was supported by the National Science Foundation of China (Nos. 81870910 and 82171271) and Zhejiang Provincial Natural Science Foundation of China (LQ19H160039).

ACKNOWLEDGMENTS

We thank Qian Yu and Zi-hang Chen for participating in our discussion and providing us with additional information for the article. We wish to thank patients for participating in this study. Also, **Figure 4** was created with <https://www.BioRender.com>.

2. Cho WS, Kim JE, Kim CH, Ban SP, Kang HS, Son YJ, et al. Long-term outcomes after combined revascularization surgery in adult moyamoya disease. *Stroke.* (2014) 45:3025–31. doi: 10.1161/STROKEAHA.114.005624
3. Mesiwala AH, Sviri G, Fatemi N, Britz GW, Newell DW. Long-term outcome of superficial temporal artery-middle cerebral artery bypass for

- patients with moyamoya disease in the US. *Neurosurg Focus*. (2008) 24:E15. doi: 10.3171/FOC/2008/24/2/E15
4. Tashiro R, Fujimura M, Kameyama M, Mugikura S, Endo H, Takeuchi Y, et al. Incidence and risk factors of the watershed shift phenomenon after superficial temporal artery-middle cerebral artery anastomosis for adult moyamoya disease. *Cerebrovasc Dis*. (2019) 47:178–87. doi: 10.1159/000500802
 5. Uda K, Araki Y, Muraoka S, Ota S, Wada K, Yokoyama K, et al. Intraoperative evaluation of local cerebral hemodynamic change by indocyanine green videoangiography: prediction of incidence and duration of postoperative transient neurological events in patients with moyamoya disease. *J Neurosurg*. (2018) 1:1–9. doi: 10.3171/2017.10.JNS171523
 6. Goldberg J, Vajkoczy P, Hecht N. Indocyanine green videoangiography for recipient vessel stratification in superficial temporal artery-middle cerebral artery bypass surgery. *J Neurosurg*. (2020) 28:1–9. doi: 10.3171/2020.5.JNS20642
 7. Kanamori F, Araki Y, Yokoyama K, Uda K, Mamiya T, Nishihori M, et al. Editors' choice indocyanine green emission timing of the recipient artery in revascularization surgery for moyamoya disease. *Nagoya J Med Sci*. (2021) 83:523–34. doi: 10.18999/nagjms.83.3.523
 8. Zhang J, Li S, Fujimura M, Lau TY, Wu X, Hu M, et al. Hemodynamic analysis of the recipient parasylvian cortical arteries for predicting postoperative hyperperfusion during STA-MCA bypass in adult patients with moyamoya disease. *J Neurosurg*. (2019) 134:17–24. doi: 10.3171/2019.10.JNS191207
 9. Funaki T, Takahashi JC, Takagi Y, Kikuchi T, Yoshida K, Mitsuhara T, et al. Unstable moyamoya disease: clinical features and impact on perioperative ischemic complications. *J Neurosurg*. (2015) 122:400–7. doi: 10.3171/2014.10.JNS14231
 10. Research Committee on the P, Treatment of Spontaneous Occlusion of the Circle of W, Health Labour Sciences Research Grant for Research on Measures for Infractable D. Guidelines for diagnosis and treatment of moyamoya disease (spontaneous occlusion of the circle of Willis). *Neurol Med Chir*. (2012) 52:245–66. doi: 10.2176/nmc.52.245
 11. Acker G, Fekonja L, Vajkoczy P. Surgical management of moyamoya disease. *Stroke*. (2018) 49:476–82. doi: 10.1161/STROKEAHA.117.018563
 12. Zhao J, Liu H, Zou Y, Zhang W, He S. Clinical and angiographic outcomes after combined direct and indirect bypass in adult patients with moyamoya disease: a retrospective study of 76 procedures. *Exp Ther Med*. (2018) 15:3570–6. doi: 10.3892/etm.2018.5850
 13. Miyamoto S, Yoshimoto T, Hashimoto N, Okada Y, Tsuji I, Tominaga T, et al. Effects of extracranial-intracranial bypass for patients with hemorrhagic moyamoya disease: results of the Japan adult moyamoya trial. *Stroke*. (2014) 45:1415–21. doi: 10.1161/STROKEAHA.113.004386
 14. Yu S, Zhang N, Liu J, Li C, Qian S, Xu Y, et al. Surgical revascularization vs. conservative treatment for adult hemorrhagic moyamoya disease: analysis of rebleeding in 322 consecutive patients. *Neurosurg Rev*. (2021) 45:1709–20. doi: 10.1007/s10143-021-01689-w
 15. Fujimura M, Mugikura S, Kaneta T, Shimizu H, Tominaga T. Incidence and risk factors for symptomatic cerebral hyperperfusion after superficial temporal artery-middle cerebral artery anastomosis in patients with moyamoya disease. *Surg Neurol*. (2009) 71:442–7. doi: 10.1016/j.surneu.2008.02.031
 16. Dobashi K, Kubo Y, Kimura K, Katakura Y, Chida K, Kobayashi M, et al. *De novo* cerebral microbleeds and cognitive decline in cerebral hyperperfusion after direct revascularization for adult moyamoya disease. *J Stroke Cerebrovasc Dis*. (2022) 31:106166. doi: 10.1016/j.jstrokecerebrovasdis.2021.106166
 17. Ishii D, Okazaki T, Matsushige T, Shinagawa K, Ichinose N, Sakamoto S, et al. Postoperative dilatation of superficial temporal artery associated with transient neurologic symptoms after direct bypass surgery for moyamoya angiopathy. *World Neurosurg*. (2017) 106:435–41. doi: 10.1016/j.wneu.2017.07.037
 18. Hayashi T, Shirane R, Fujimura M, Tominaga T. Postoperative neurological deterioration in pediatric moyamoya disease: watershed shift and hyperperfusion. *J Neurosurg Pediatr*. (2010) 6:73–81. doi: 10.3171/2010.4.PEDS09478
 19. Woitzik J, Horn P, Vajkoczy P, Schmiedek P. Intraoperative control of extracranial-intracranial bypass patency by near-infrared indocyanine green videoangiography. *J Neurosurg*. (2005) 102:692–8. doi: 10.3171/jns.2005.102.4.0692
 20. Amin-Hanjani S, Du X, Mlinarevich N, Meglio G, Zhao M, Charbel FT. The cut flow index: an intraoperative predictor of the success of extracranial-intracranial bypass for occlusive cerebrovascular disease. *Neurosurgery*. (2005) 56 (1 Suppl.):75–85. doi: 10.1227/01.NEU.0000143032.35416.41
 21. Zhang X, Ni W, Feng R, Li Y, Lei Y, Xia D, et al. Evaluation of hemodynamic change by indocyanine green-FLOW 800 videoangiography mapping: prediction of hyperperfusion syndrome in patients with moyamoya disease. *Oxid Med Cell Longev*. (2020) 2020:8561609. doi: 10.1155/2020/8561609
 22. Januszewski J, Beecher JS, Chalif DJ, Dehdashti AR. Flow-based evaluation of cerebral revascularization using near-infrared indocyanine green videoangiography. *Neurosurg Focus*. (2014) 36:E14. doi: 10.3171/2013.12.FOCUS13473

Conflict of Interest: The authors declare that the research was conducted in the absence of any commercial or financial relationships that could be construed as a potential conflict of interest.

Publisher's Note: All claims expressed in this article are solely those of the authors and do not necessarily represent those of their affiliated organizations, or those of the publisher, the editors and the reviewers. Any product that may be evaluated in this article, or claim that may be made by its manufacturer, is not guaranteed or endorsed by the publisher.

Copyright © 2022 Xu, Li, Tong, Hu, He, Fu, Zhou, Cao, Yu, Zhou, Xu and Wang. This is an open-access article distributed under the terms of the Creative Commons Attribution License (CC BY). The use, distribution or reproduction in other forums is permitted, provided the original author(s) and the copyright owner(s) are credited and that the original publication in this journal is cited, in accordance with accepted academic practice. No use, distribution or reproduction is permitted which does not comply with these terms.



Automated Measurement of Net Water Uptake From Baseline and Follow-Up CTs in Patients With Large Vessel Occlusion Stroke

Atul Kumar¹, Yasheng Chen¹, Aaron Corbin², Ali Hamzehloo¹, Amin Abedini³, Zeynep Vardar⁴, Grace Carey¹, Kunal Bhatia¹, Laura Heitsch⁵, Jamal J. Derakhshan³, Jin-Moo Lee¹ and Rajat Dhar^{1*}

¹ Department of Neurology, Washington University in St. Louis School of Medicine, Saint Louis, MO, United States, ² Saint Louis University School of Medicine, Saint Louis, MO, United States, ³ Department of Radiology, Washington University in St. Louis School of Medicine, Saint Louis, MO, United States, ⁴ Department of Radiology, University of Massachusetts Medical School, Worcester, MA, United States, ⁵ Department of Emergency Medicine, Washington University in St. Louis School of Medicine, Saint Louis, MO, United States

OPEN ACCESS

Edited by:

Peiyu Huang,
Zhejiang University, China

Reviewed by:

Carole Frindel,
Université de Lyon, France
Dong-Seok Gwak,
Dongguk University Ilsan Hospital,
South Korea

*Correspondence:

Rajat Dhar
dharr@wustl.edu

Specialty section:

This article was submitted to
Stroke,
a section of the journal
Frontiers in Neurology

Received: 17 March 2022

Accepted: 06 June 2022

Published: 27 June 2022

Citation:

Kumar A, Chen Y, Corbin A, Hamzehloo A, Abedini A, Vardar Z, Carey G, Bhatia K, Heitsch L, Derakhshan JJ, Lee J-M and Dhar R (2022) Automated Measurement of Net Water Uptake From Baseline and Follow-Up CTs in Patients With Large Vessel Occlusion Stroke. *Front. Neurol.* 13:898728. doi: 10.3389/fneur.2022.898728

Quantifying the extent and evolution of cerebral edema developing after stroke is an important but challenging goal. Lesional net water uptake (NWU) is a promising CT-based biomarker of edema, but its measurement requires manually delineating infarcted tissue and mirrored regions in the contralateral hemisphere. We implement an imaging pipeline capable of automatically segmenting the infarct region and calculating NWU from both baseline and follow-up CTs of large-vessel occlusion (LVO) patients. Infarct core is extracted from CT perfusion images using a deconvolution algorithm while infarcts on follow-up CTs were segmented from non-contrast CT (NCCT) using a deep-learning algorithm. These infarct masks were flipped along the brain midline to generate mirrored regions in the contralateral hemisphere of NCCT; NWU was calculated as one minus the ratio of densities between regions, removing voxels segmented as CSF and with HU outside thresholds of 20–80 (normal hemisphere and baseline CT) and 0–40 (infarct region on follow-up). Automated results were compared with those obtained using manually-drawn infarcts and an ASPECTS region-of-interest based method that samples densities within the infarct and normal hemisphere, using intraclass correlation coefficient (ρ). This was tested on serial CTs from 55 patients with anterior circulation LVO (including 66 follow-up CTs). Baseline NWU using automated core was 4.3% (IQR 2.6–7.3) and correlated with manual measurement ($\rho = 0.80$, $p < 0.0001$) and ASPECTS ($r = -0.60$, $p = 0.0001$). Automatically segmented infarct volumes (median 110-ml) correlated to manually-drawn volumes ($\rho = 0.96$, $p < 0.0001$) with median Dice similarity coefficient of 0.83 (IQR 0.72–0.90). Automated NWU was 24.6% (IQR 20–27) and highly correlated to NWU from manually-drawn infarcts ($\rho = 0.98$) and the sampling-based method ($\rho = 0.68$, both $p < 0.0001$). We conclude that this automated imaging pipeline is able to accurately quantify region of infarction and NWU from serial CTs and could be leveraged to study the evolution and impact of edema in large cohorts of stroke patients.

Keywords: stroke, cerebral edema area, computed tomography, machine learning, image segmentation

INTRODUCTION

A major consequence of brain ischemia is the development of cerebral edema. This water accumulation within and around the injured tissue leads to brain swelling, raising compartmental pressure and eventually leading to midline shift and herniation. The development of malignant cerebral edema represents the greatest source of mortality in the acute period after ischemic stroke, especially for strokes due to large vessel occlusion (LVO) (1). As key mediators remain incompletely understood, few interventions currently exist to mitigate cerebral edema (2). One of the major limitations in studying edema is the need for an accurate means of quantifying its formation in the early stages after stroke (3, 4). Midline shift is a crude measure that does not adequately capture edema as it develops over the first 24–48 h after stroke, but only captures its delayed and decompensated phenotype. Furthermore, labeling edema only when it leads to deterioration (i.e., malignant edema) obscures a continuum of injury severity that is seen across almost all LVO stroke patients (5).

One of the hallmarks of evolving brain edema is tissue hypoattenuation (6). This can be captured by the progressively decreasing density (measured in Hounsfield Units, HU) of infarcted tissue on non-contrast computed tomography (NCCT) imaging. NCCT is readily available and routinely performed in almost all stroke patients, both acutely on presentation and frequently at follow-up. It affords an accessible means of serially assessing edema as it develops in the days after stroke. However, measurement of the total lesional hypodensity volume encompasses both infarcted tissue and associated edema, with relative proportions varying across patients (5, 7). A recent imaging method has been proposed to disentangle the contribution of edema to subacute lesion volume and quantify the progression edema after stroke (8). *Net water uptake* (NWU) evaluates the relative density of the ischemic tissue compared to a contralateral homologous region; increasing NWU on admission NCCT has been associated with longer time from stroke onset to imaging and poor collateral status (9, 10). NWU has also exhibited promise in quantifying edema progression, rising more in those with malignant outcomes and in those without successful recanalization (11, 12). Therefore, it has emerged as one of the most promising biomarkers of edema after stroke, with a wide array of potential applications across LVO cohorts (13).

However, implementation of NWU measurement from serial CTs in large stroke cohorts faces several challenges. The principal challenge is that its assessment is dependent on identification and delineation of the area of early infarction on acute and subacute CTs. As this region is not usually clearly visible on baseline NCCT within a few hours of stroke onset, most studies measuring early NWU have relied on CT perfusion (CTP) images to visually guide manual delineation of core infarct. In some studies where CTP was not available, NWU was estimated by measuring density within regions-of-interest (ROIs) placed within ASPECTS regions exhibiting early hypoattenuation and matched regions in the contralateral hemisphere (14). Measurement of NWU on follow-up NCCT requires manually outlining the visible region of infarction and

flipping this manual ROI to create a homologous normal region for density assessment. This approach is time-consuming, subject to variability, and makes studying edema in large cohorts with NWU, although attractive in theory, challenging to perform in practice. Our objective was to develop an accurate means of automatically extracting infarct regions and measuring NWU from both baseline and follow-up CTs of LVO stroke patients. This imaging algorithm could then be leveraged to accelerate research into edema using larger cohorts of stroke patients (15).

METHODS

Study Participants

We evaluated patients undergoing stroke assessment at a single institution between May 2018 and November 2019 who underwent multimodal CT (NCCT with CT angiography and CTP) on presentation. We selected those who had evidence of LVO in the anterior circulation, affecting either the internal carotid artery (ICA) or proximal segment of the middle cerebral artery (MCA). We limited our analysis to those with measurable infarct core on baseline CTP (as assessed using the RAPID software package, iSchemaView, Redwood City, California). Approval from the institutional review board was obtained for a waiver of participant consent given the retrospective, de-identified nature of this research.

Imaging Analysis

We collected all NCCT and CTP images performed at baseline as well as all follow-up NCCTs performed within 1 week of stroke onset. The CTP images were processed using an in-house algorithm that automatically extracts high-resolution image maps of perfusion parameters, including cerebral blood flow (CBF) and time to maximum (Tmax), as described in the **Supplementary Methods** and outlined in **Supplementary Figure 1**. Core infarct regions were defined by tissue with CBF below 30% of normal, where normal brain was defined as tissue with Tmax below 4 s (16). To assess consistency of core extraction, the volume of this core region was compared to the volume extracted by the RAPID software.

All NCCTs at baseline and follow-up were processed using an automated analysis workflow that is fully described in the **Supplementary Methods**. Key steps include: (i) registration of an atlas template with midline delineated on all slices to the target NCCT (17); (ii) segmentation of cerebrospinal fluid (CSF) regions using our well-established deep learning model (18, 19); and (iii) segmentation of visible acute infarct regions using a novel deep learning-based algorithm. This algorithm employed a deep learning model based on the U-Net architecture and previously trained for CSF segmentation (full details of this fully convolutional neural network provided in **Supplementary Methods**) (20). This network was further trained on 335 manually outlined infarct regions defined on NCCTs from a prior three institution stroke cohort as ground-truth labels. This training set was divided into ~90% (304 infarcts) for training and the remainder (21) for internal validation. The infarct region proposed by this algorithm was further refined by identifying the largest connected region in three dimensions as the likely

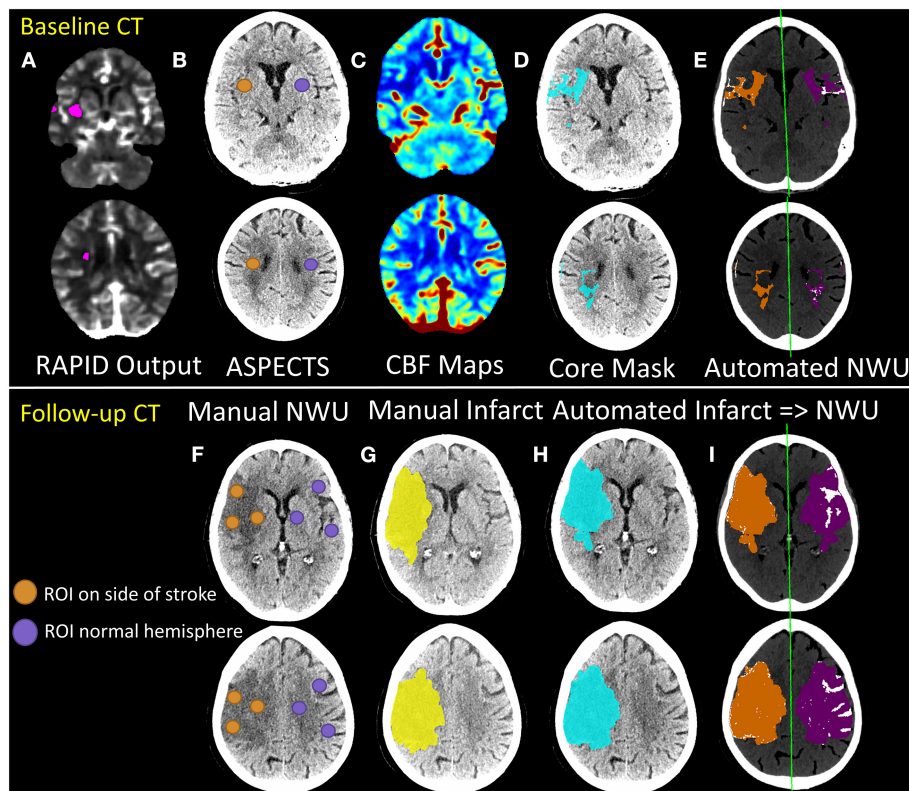


FIGURE 1 | Outline of manual vs. automated techniques for estimation of net water uptake from baseline (top panels) and follow-up (bottom panel) CT scans of stroke patients. The RAPID core output (**A**) from CTP processing is used to determine the ASPECTS regions to be used for manual estimation of NWU from baseline NCCT (**B**). Regions-of-interest (ROIs) are placed in these regions within the affected hemisphere (orange) and matched ROIs are placed in the contralateral hemisphere (purple). Manual NWU is calculated as one minus the ratio of mean densities of the two sets of ROIs. For automated measurement of NWU on baseline CTs, CBF maps (**C**) are generated from raw CTP data (as fully detailed in the **Supplementary Methods** and shown in **Supplementary Figure 1**). The core mask (defined by thresholding at CBF < 30% of normal) is then registered and overlaid onto the NCCT (blue region in **D**). This infarct region is then flipped across the midline (purple region; method fully outlined in the **Supplementary Methods** and shown in **Supplementary Figure 2**) to create a matching mirror region (**E**). Automated NWU is calculated as one minus the mean densities of these two regions, after removing voxels of CSF (from separate CSF segmentation) or with HU density below 20 or above 80 from both regions (removed voxels shown in white). Lower panels show similar workflow for follow-up CTs (or baseline CTs with visible hypodensity). ROIs are placed within ASPECTS regions within the visible infarct and matching ROIs are placed in the contralateral hemisphere to calculate manual ROI-based NWU (**F**). The infarct region is also manually segmented (yellow, **G**). A deep learning-algorithm is applied to automatically segment regions of hypodensity and generate an infarct mask (blue, **H**). Infarct regions are then flipped to create matching mirror ROIs (purple, **I**). Regions of CSF are then removed, as are voxels outside the thresholds (HU 0–40 for infarct, 20–80 for normal brain). Automated NWU is then calculated. In this example, manual NWU on baseline CT was 16.0 and automated NWU was 12.3. For follow-up CT, the manual infarct volume was 135 ml and the automated volume was 143 ml. The manual NWU was 29.8 using ASPECTS ROI-method, 25.4 using the whole manual infarct, compared with 25.0 for the fully automated NWU.

primary infarct territory and excluding smaller disconnected voxels. The algorithm was then applied to all NCCTs in this cohort, including a test cohort of 28 subjects where the infarct region was manually segmented on all slices. The Dice Similarity Coefficient (DSC), a stringent metric of spatial overlap of voxels between the automated infarct region and the manually outlined ground-truth was calculated as twice the union of the two regions divided by the sum of their volumes.

This infarct region was utilized as the infarct mask for evaluating NWU on follow-up NCCTs, as well as for any baseline NCCTs on which infarct was already clearly visible. For the remainder of baseline CTs, the core regions from CTP analysis were utilized in place of infarct masks. These CTP-defined core masks were registered to

the NCCT using FLIRT from FSL (FMRIB, Oxford, UK) (22). The brain was divided into hemispheres, using the registered midline, as previously applied to measure the hemispheric CSF ratio (23). The infarct region was then flipped along the brain midline to generate a homologous region in the contralateral hemisphere (as shown in **Supplementary Figure 2**).

For baseline CTs, we also instituted an automated patch-based approach for estimating NWU (that does not require CTP), similar to one recently proposed, to allow comparison with our full-infarct method (24). For this approach, square standard patches were placed on four separate axial slices within each MCA territory of a CT atlas and then this atlas was registered to each patient's baseline NCCT, allowing estimation of NWU from

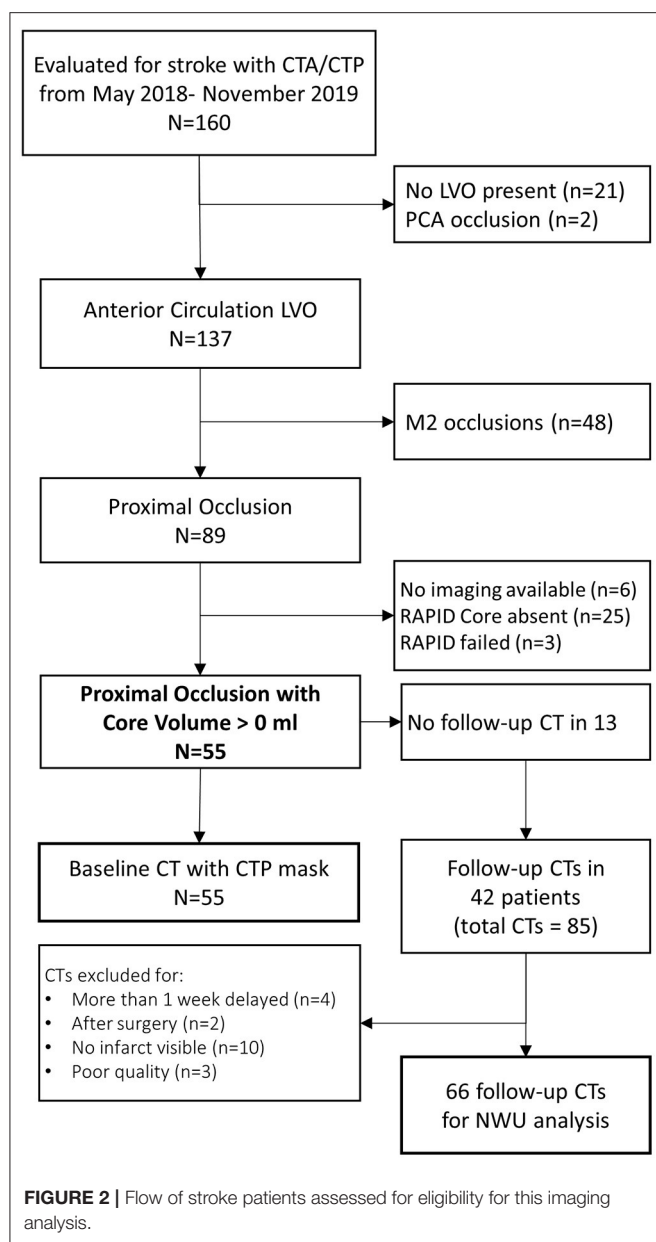


TABLE 1 | Characteristics of study cohort of 55 patients with large vessel occlusion stroke.

Age, years	74 (65–84)
Sex, female	27 (48%)
Race/ethnicity: white, non-Hispanic	45 (82%)
Hispanic	1 (2%)
African-American	9 (16%)
History of atrial fibrillation	24 (44%)
History of diabetes mellitus	14 (25%)
NIHSS, baseline	17 ± 6
NIHSS, 24-h	16 ± 10
Glucose (mg/dl)	121 (106–154)
Onset to baseline CT, hours	5 (2–10)
ASPECTS < 7	15 (27%)
Treated with tPA	23 (42%)
Treated with Thrombectomy	35 (64%)
Reperfusion outcome: mTICI 0	3
mTICI 2a	4
mTICI 2b/2c	12
mTICI 3	15
Core volume (RAPID), ml	31 (14–65)
Penumbra volume (RAPID), ml	133 (94–175)
Midline shift	19 (35%)

transformation often extended above 40 HU; this is supported studies of HU within intracerebral hematomas and should also exclude regions of contrast staining within evolving infarcts, specifically defined by HU > 40 (26, 27). Therefore, removing voxels with density above 40 HU from within the infarct would avoid contamination of NWU calculations by regions of HT and contrast staining, both issues that has confounded prior studies of NWU (28). The standard 20–80 threshold was used for the normal brain region and for the CTP core mask at baseline where significant low density or hemorrhagic regions would not be expected; the 0–40 threshold for applied only for region of visible infarction segmented by the deep learning algorithm. The mean HU density (D) of all voxels (after CSF and threshold-based exclusions) within each region (ischemic vs. normal) was calculated and NWU was defined as:

$$NWU = 1 - \frac{D_{\text{ischemic}}}{D_{\text{normal}}} \quad (1)$$

We also calculated NWU using the standard 20–80 threshold for the infarct region and compared results to those obtained using our modified approach. The code for the manipulation of the infarct region and calculation of NWU is publicly available at: https://github.com/dharlabwustl/csf_ratio_nwu.

Automated NWU results were compared to a sampling based method that places circular regions of ~10-mm diameter within the infarct in up to 13 territories across two axial brain slices, corresponding to the ASPECTS regions as well as three more subcortical regions (selecting regions with visible infarct, while avoiding those with hemorrhage or CSF, as outlined in a prior paper for manual NWU measurement) (14). These same

the density within the ischemic MCA territory compared with the contralateral side (**Supplementary Figure 3**).

All regions of CSF were removed from both infarct and mirror regions and thresholding was applied to remove voxels with HU outside an established range, initially set at 20–80, per prior protocols for NWU measurement (12). However, on review of the distribution of densities within regions of infarction on follow-up CTs [both from the literature (25) and our own data], we determined that expanding the lower limit to 0 HU would better capture lower density voxels that would otherwise be excluded if using a threshold of 20 (leading to an underestimation of NWU). We also chose to restrict the upper limit of infarct regions to 40 HU rather than 80; we found that most voxels within bland infarcts had densities below 40 HU while regions of hemorrhagic

regions were then mirrored to the normal hemisphere and mean density of each set of ROIs were obtained and from this the manual NWU was calculated. For baseline NCCTs where clear infarction was not visible, the RAPID core images were used to guide manual ROI placement within ischemic tissue. If no acute infarction was visible on follow-up CTs based on the consensus of two independent raters, then NWU could not be obtained manually (and hence this scan was excluded). Manual NWU measurements were performed by two independent raters for all follow-up CTs and for a subset of the baseline CTs. The manual NWU used for comparison was the mean of the raters' measurements. In addition, for those 28 subjects with manual infarct segmentations performed, comparisons of manual volumes with automated infarct volumes as well as NWU values obtained using these manual vs. automated infarct masks were performed. **Figure 1** outlines the major steps in obtaining manual vs. automated NWU measurements on baseline and follow-up CTs. **Supplementary Figure 2** provides a more detailed, step-by-step outline of the automated image analysis workflow.

Statistical Analysis

All analyses were performed in R (version 4.0.3, Foundation for Statistical Computing, Vienna, Austria). All measurements were first assessed for normality using inspection of their distributions and with Shapiro-Wilk's tests. We present means (with standard deviations) for normally distributed and medians (with interquartile ranges) for all non-normally distributed variables. We compared automated to manual measurements of NWU and infarct volume using intraclass correlation coefficients (ρ) with a two-way random effects model evaluating absolute agreement of raters, with the manual NWU as the ground-truth (ICC 2,1), using the package *psych* (29, 30). We constructed Bland-Altman plots of the difference between the two measures using the package *BlomAltmanLeh*. This allowed us to calculate the bias (mean difference) and limits of agreement (range within which 95% of differences in measurement lie).

RESULTS

We evaluated 160 patients who underwent acute stroke evaluation at our institution during the study period for eligibility. Of these 89 had LVO affecting the ICA or M1 segments and 55 had infarct core present on baseline imaging (see **Figure 2**). A description of this cohort is provided in **Table 1**. Mean NIHSS on presentation was 17 and 35 (64%) underwent thrombectomy (27 achieving mTICI 2b/3 reperfusion). Median time to baseline CT was 5 h (IQR 2–10). Median ASPECTS was 8 (IQR 6–10). Over one-third developed cerebral edema with midline shift (median of 3.7 mm, IQR 2.8–5.7) (time to scans).

NWU on Baseline CTs

Baseline CTP images (median time from stroke onset of 4.3 h, IQR 2–10) were analyzed for core volume. Median core volume provided by RAPID software was 31 ml (IQR 14–65). Automated CTP processing allowed core masks to be extracted in 49 (89%) cases with a median volume of 36 ml (IQR 23–77).

There was a strong intraclass correlation between the RAPID core volumes and our algorithm's volumes ($\rho = 0.81$, **Table 2**; **Supplementary Figure 4**). One case (with RAPID core of 4-ml) had no identifiable core on our processing and so no mask could be extracted. Two NCCTs had too much artifact to allow calculation of either manual or automated NWU. Baseline NWU using the manual ASPECTS ROI method was a median of 6.9 (IQR 4.2–10.0). The agreement of two manual raters for baseline NWU, tested in 22 cases, was good ($\rho = 0.73$, $p = 1 \times 10^{-10}$). In five cases with visible infarct on baseline CT, we used the automated infarct mask to define the infarct region; the automated CTP core masks were used to measure NWU in the remainder. There was strong agreement between manual and automated baseline NWU measurements ($\rho = 0.80$, $p = 1 \times 10^{-16}$) with minimal bias (**Table 2**; **Figures 3A,B**). The patch-based approach for NWU estimation exhibited modest concordance with manual methods ($\rho = 0.63$, $p = 2 \times 10^{-8}$) but with wider limits of agreement (−9.0 to 12.8, see **Supplementary Figure 5**).

The automated NWU on baseline CT was negatively correlated with ASPECTS score ($r = -0.60$, $p < 0.0001$, **Supplementary Figure 6**), comparable with that observed for manual NWU ($r = -0.59$) but higher than for the patch-based NWU ($r = -0.45$). Automated NWU was higher in those who subsequently developed edema with midline shift (median 6.1 vs. 3.6, $p < 0.0001$). The automated NWU increased with longer time from stroke onset (beta = 0.12 per h, $p = 0.0003$), but the slope was significantly higher in those who subsequently developed edema with midline shift ($p = 0.017$ for interaction of edema with time, **Supplementary Figure 7**).

NWU on Follow-Up CTs

There were a total of 85 follow-up CTs performed in 42 subjects. Of these, two were performed after hemicraniectomy and four scans were from more than 1 week after stroke. Of the remaining 79 scans, 69 exhibited visible regions of infarction. Three were too poor quality for NWU estimation, leaving 66 CTs for evaluation of NWU. Median time to follow-up CT was 60 h (IQR 35–116) with 27 (41%) being within 48 h of stroke onset. Hemorrhagic transformation was present in 48, including HI-1 in 18, HI-2 in 22, and PH-1 hematomas in 9 scans. The automated infarct segmentation algorithm correctly identified the region of infarction in all but two cases (97%). Manual delineation of infarct regions was performed in 28 scans with excellent correlation to the automated volumes ($\rho = 0.96$, see **Supplementary Figure 8**). The DSC for overlap of infarct segmentation (automated vs. manual) was a median of 0.83 (IQR 0.72–0.90) with a median automated infarct volume of 110-ml (IQR 39–194). There was no significant correlation between infarct volume and DSC ($r = 0.26$, $p = 0.18$) or time to scan and DSC ($r = 0.32$, $p = 0.10$).

NWU was manually estimated on these 66 scans by two raters, using the ASPECTS ROI-based approach, with strong intraclass correlation between raters ($\rho = 0.88$, $p = 3 \times 10^{-54}$). Fully automated NWU was obtained by applying the automated infarct segmentation in 63 cases (two excluded for failure of infarct segmentation, one due to lack of voxel information in file header).

TABLE 2 | Comparison of manual and automated measures of core/infarct volume and net water uptake (NWU).

Comparison	Manual value Median (IQR)	Automated value Median (IQR)	Mean difference Limits of agreement	Intraclass correlation (95% CI)
Core volume: RAPID vs. automated CTP	31 (14–65) N = 55	36 (23–77) N = 49	–2.0 (–61.7 to 57.7)	0.81 (0.71–0.87)
Baseline NWU ASPECTS ROI vs. automated [†]	6.9 (4.2–9.9) N = 53	4.3 (2.6–7.3) N = 49	2.3 (–5.0 to 9.7)	0.80 (0.61–0.89)
Baseline NWU ASPECTS ROI vs. automated patch	7.0 (4.0–8.6) N = 50	5.5 (2.5–8.0) N = 50	1.9 (–9.0 to 12.8)	0.63 (0.47–0.75)
Follow-up infarct volume Manual vs. automated [†]	105 (39–140) N = 28	110 (39–194) N = 63	–12.1 (–60.9 to 36.7)	0.96 (0.92–0.97)
Follow-up NWU: Manual mask vs. automated [†]	25.3 (19.7–27.8) N = 28	24.6 (19.8–26.9) N = 63	0.6 (–2.4 to 3.6)	0.98 (0.96–0.98)
Follow-up NWU ASPECTS ROI vs. automated [†]	27.1 (21.9–31.7) N = 66	24.6 (19.8–26.9) N = 63	2.7 (–9.2 to 14.6)	0.68 (0.52–0.79)
All NWU values ASPECTS ROI vs. automated [†]	19.0 (7.3–28.1) N = 126	17.5 (5.5–25.3) N = 117	2.4 (–8.1 to 12.7)	0.88 (0.81–0.92)

[†] Automated measurement using full-infarct mask (i.e., automated infarct segmentation or automated CTP core).

The automated NWU (median 24.6, IQR 19.8–26.9) exhibited excellent agreement with NWU obtained from the manually drawn infarct masks ($\rho = 0.98$, **Supplementary Figure 9**). These values also correlated well with the manual ROI-based method ($\rho = 0.68$, **Figure 3C**). There was minimal bias (mean difference of 2.7) in NWU measurement, with no greater discrepancy in those with increasing severities of hemorrhagic transformation (**Figure 3D**). For example, in one case with focal hematoma, the manual NWU was 21.0 and the automated value was 21.6 (**Figure 4**).

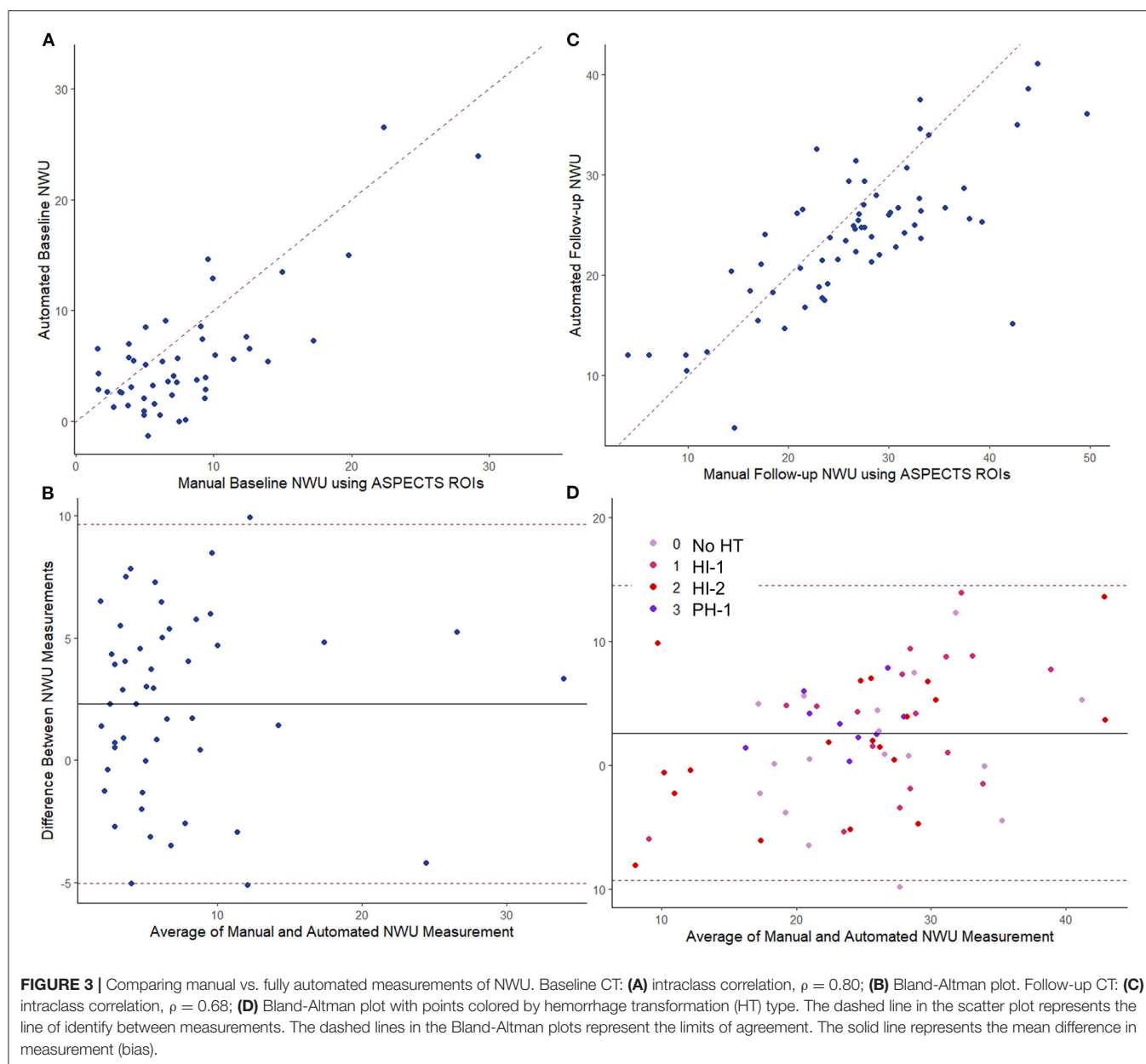
NWU results using our modified thresholding (0–40 for the infarct region) were compared with the standard thresholding of 20–80. NWU was significantly lower with the original method (median 16 vs. 24.6) and underestimated the manually ascertained NWU (median 25.3). This was due to higher mean HU measured within the infarct region as a result of both exclusion of infarct voxels with density below 20 HU (i.e., regions of more severe edema) and inclusion of regions of hemorrhagic transformation within the infarct region. A review of voxels densities within infarct regions is shown in **Supplementary Figure 10**, highlighting the fact that 14% had densities below 20 HU and would have been excluded using the 20–80 thresholds. A comparison of the two thresholding methods for one representative example is shown in **Supplementary Figure 1**, where the modified approach yielded NWU of 24.7 while the standard threshold of 20–80 provided an estimate of 13.7 for NWU. The manual ROI-based method calculated by two raters was an average of 27.2. The overall correlation with manual NWU was lower ($\rho = 0.43$) compared with that obtained using the modified 0–40 approach ($\rho = 0.66$). Furthermore, the automated 20–80 method under-estimated the manual measurement (mean difference

of –11.3), with wider limits of agreement, ranging from +3 to –26.

We then combined all automated NWU measurements together (total of 117 baseline and follow-up measurements): there was a strong correlation of automated to manual NWU across time points ($\rho = 0.88$, $p < 0.0001$) with minimal bias (**Supplementary Figure 11**). There was no difference in the accuracy of NWU (automated vs. manual discrepancy) based on time to scan, infarct volume, or degree of hemorrhagic transformation.

DISCUSSION

Quantifying the evolution and severity of cerebral edema, using routine CT imaging, presents the promise of accelerating research into clinical and biologic factors mediating this critical source of secondary injury (21). The application of NWU in small LVO cohorts has already led to several interesting observations: for example, those with worse collateral scores exhibited greater early edema progression (9). Hyperglycemia was also associated with enhanced edema formation (31). Estimation of NWU, which represents the proportion of stroke lesion that constituted of excess water, allows the separation of primary infarct from secondary edema within an infarct-related hypodensity on subacute CT (32). Not only does this allow delineation of edema severity but this adjusted infarct volume correlates well with final infarct volume, an important stroke outcome measure. Furthermore, it is likely that the product of infarct volume and NWU provides a meaningful volumetric measure of water accumulation, termed total edema volume (33). However, despite this promise, measurement of NWU in these previous studies was



performed manually and hence was time-consuming, requiring investigators to outline the region of infarction across multiple CT slices, mirror this region to the normal hemisphere, and then measure the density in both, applying pixel-based intensity thresholds to try to exclude CSF regions that might contaminate the measurement.

We now present a substantial advance to facilitate scalable NWU measurement: that is, an automated approach that accurately quantifies NWU from both baseline and follow-up CTs. This was built upon two new algorithms to extract regions of infarction: one a deep learning model that was able to segment the region of infarct-related hypodensity from follow-up CTs and a second that extracted CBF-based core masks from baseline CTP images. While the latter is qualitatively similar to the automated

processing of core volumes provided by several commercial software packages (34), it is performed at native resolution and provides voxel-by-voxel maps for research applications. In comparison, output from RAPID software is not provided in native resolution and cannot be easily incorporated on a voxel-by-voxel level for analysis.

Segmentation of infarct regions from follow-up CTs in the first days after stroke is not a trivial task, as early hypodensity can be subtle and challenging to delineate even for experienced human raters. Simple thresholding of CT images for infarct is not accurate as infarcts overlap in density with CSF and other brain structures. An approach utilized in the MR CLEAN cohort applied an intensity-based region-growing approach that begins with a manual seed and also excludes neighboring ventricular

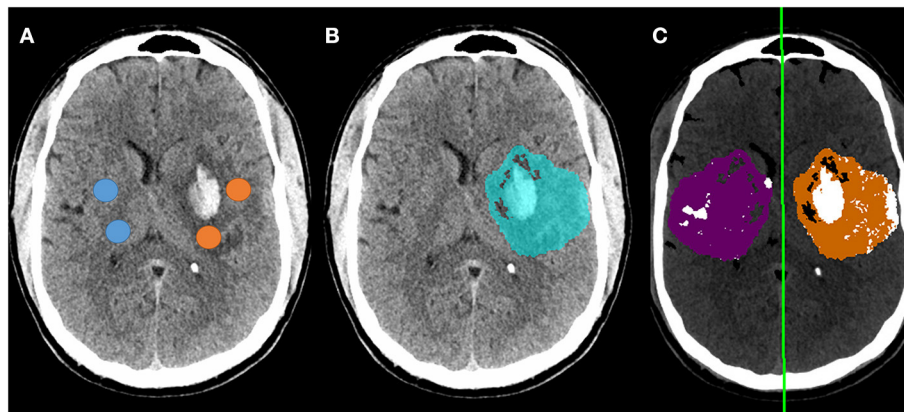


FIGURE 4 | Example of follow-up CT in a patient who developed a focal parenchymal hematoma within the region of infarction. **(A)** Original non-contrast CT with regions-of-interest manually placed within the infarct (avoiding hemorrhage) and in contralateral matching regions (avoiding CSF); **(B)** Blue region indicates automated segmentation of infarct lesion; **(C)** Processing of follow-up CT to measure NWU using automated infarct mask, with removal of voxels representing CSF (white regions within purple normal mask) and voxels outside the range of 0–40 HU (removing most regions of hemorrhage). The manual NWU was 21.0 and the fully automated NWU was 21.6.

CSF regions that would be misinterpreted as infarction. This multi-stage process exhibited similar accuracy to that achieved with our algorithm (i.e., both had correlation of automated to manual infarct volumes of 0.98) (35). Two recent deep learning-based approaches have been proposed for this task: one employed a combination of three patch-based convolutional neural networks to identify infarct regions from follow-up scans in the HERMES collaborative (25). This method (trained on 630 scans, tested on 396) resulted in a lower DSC for infarct segmentation (0.57 vs. 0.83) and lower ICC (0.88 vs. 0.96) for infarct volumes measurement than seen with our algorithm, although we cannot directly compare without head-to-head testing on a single cohort, given differences in infarct types (for example, the median infarct volume in our series was 110 vs. 48-ml in the other study). The performance for larger, more hypodense infarcts was higher, with DSC of 0.78 and ICC of 0.98, comparable to our findings. The second study employed a generative adversarial network (GAN) to enhance the U-Net architecture (36). This was trained on 60 scans and tested on 60 others, with DSC of 0.71 and correlation to manual volumes of 0.93. The advantage of this automated method is that it does not require human input and so can segment large numbers of scans within the context of the broader automated NWU algorithm. Given a few outliers where segmentation failed (<5% of cases), we still recommend manual review of the infarct/NWU results. However, there is likely some leeway as long as the segmented infarct region overlaps broadly with the infarct for estimation of the mean infarct density.

These advances allowed us to measure NWU on both baseline and follow-up CTs, while most studies have focused on a single time point. We applied these infarct masks, along with technical developments to flip the region along the registered midline, to obtain the ratio of densities between these two regions (i.e., NWU). In doing so, we modified the prior thresholds used for NWU calculation. As in prior studies (25), we noted that a

significant portion of infarcted tissue had HU below 20 and so excluding voxels with $HU < 20$ would lead to under-estimation of the actual infarct density and therefore NWU (as shown in comparing the results obtained from the two thresholds) (25). One reason for thresholding at 20 HU is to avoid contamination of the regions by low-density CSF, an issue in prior studies; we applied our well-established CSF segmentation algorithm to subtract these non-brain regions and avoid such contamination.

Presence of hemorrhagic transformation within the infarct has also confounded measurements of NWU, as voxels with hemorrhage would have high HU and would lead to significant underestimation of the actual difference in densities between infarct and normal brain. This bias has often led to those scans with significant HT being excluded from NWU studies. This is a major drawback, as HT occurs in 20–40% of LVO patients (37), limiting the number of patients who can be analyzed and generalizability of findings. A recent study of edema measurement after thrombectomy found that presence of hemorrhage and/or contrast staining often contaminated measurement of NWU, leading to under-estimation and even some negative NWU values; this issue compromised the value of NWU in comparison to volumetric edema biomarkers (28). We did not exclude those with HT but applied an upper threshold of 40 H; this removed regions of significant HT (as shown in **Figure 4**) and allowed us to measure NWU from all scans (including those with variable degrees of hemorrhage) without any noticeable increase in error. However, our cohort did not include any patients with very large PH-2 hemorrhages; in such cases where the hemorrhage encompasses the entire region of infarction, NWU could not be calculated by any method. We demonstrate that the NWU obtained from our automated algorithm accurately reflected those obtained using manually-drawn infarct regions and those using an established ASPECTS ROI-based method for both baseline and follow-up CTs (14). There was only a small bias, with automated

NWU providing lower values (by $\sim 2\%$) than manual NWU; this might actually be because the manual method involves sampling select regions within the infarct (or core) and thereby focuses on more obvious hypodense regions where NWU is higher (compared with our full-infarct method, which measures edema using the full range of densities within the infarct) (8).

There have been other recent attempts to operationalize and simplify measurement of NWU. Notably, all have focused on estimation of NWU from baseline CTs only and most require manual region selection or other input/review. One approach applied an automated core region (similar to our CTP-based method) but derived from commercial software (38); it was unclear how this region was transferred to the NCCT as alignment of CTP source images with NCCT is not trivial, but likely involved manual inspection and alignment. Another study manually placed a standard large ROI within the MCA territory (on a single slice) to estimate where ischemia might be seen and avoid the need to use CTP to locate the exact core region (39). Baseline NWU was estimated from the density of this region vs. a manually translated contralateral mirror region, but was not compared to a gold-standard measurement. Only one automated method has been proposed: using commercial software (syngo.via from Siemens) to measure the density within affected ASPECTS regions on baseline CT (40). This technique approximates our manual ASPECTS-based sampling method but has the advantage of not requiring CTP for NWU measurement and being relatively automated (manual inspection of regions was required to check accuracy). We were not able to compare our automated method to this automated ASPECTS-NWU approach as we did not have access to the commercial software, but did use a comparable manual ASPECTS approach as our ground-truth for NWU.

Finally, a fourth study applied standardized regions (patches) within the MCA territory to obtain relative density and estimate NWU without requiring CTP to generate core masks (41). However, these regions had to be manually selected to avoid regions of CSF and old infarcts and would tend to underestimate NWU as it inevitably includes non-ischemic regions. In that study, this patch-based method was compared to a full-infarct approach (based on region of infarction on follow-up CT, manually outlined) and found limits of agreement from -9 to $+10$, similar to what we found (-5 to $+9.7$). For comparison within our own dataset, we implemented a fully automated version of this patch-based sampling method to measure NWU from the baseline CTs and showed that it exhibited moderate agreement with manual ASPECTS region-based measurements and with our automated approach. This is likely because this method places regions within the MCA territory, presuming that these will capture the ischemic tissue with early edema. As might be expected from a sampling method that estimates early edema, this approach exhibited wider limits of agreement compared to our full-infarct/core based method. Nonetheless, it is an attractive complementary or back-up option if CTP is not available to define core and the infarct is not visible.

These studies also confirmed, as we did, that baseline NWU was higher in those who subsequently developed midline shift and/or malignant edema. However, none of these studies incorporated automated assessment of NWU from follow-up CTs. Our method is therefore more comprehensive in allowing measurement of NWU from serial CTs at various time points in a fully automated manner (without manual inspection, flipping of masks, etc.). We believe that this approach will empower large cohort studies and clinical trials that seek to understand the dynamic evolution of edema after stroke (14).

There remains limitations to applying NWU to study edema, regardless of measurement approach. As stated above, NWU cannot be used to estimate edema in the presence of extensive parenchymal hematoma. In these cases, water accumulation is unlikely the main contributor to midline shift and deterioration (37). Instead, efforts at measuring hematoma volume may allow quantification of secondary injury better than NWU (42). Concomitant CTP with measurable core volume is generally required to facilitate measurement of NWU from baseline CTs unless infarct is clearly visible (as it was in only five of our 55 cases); this limits its applicability to studies of early edema. Application of ASPECTS-based approaches may obviate the need for CTP but rely on presence of early ischemic changes and would not be possible in those with “normal” appearing baseline CTs (i.e., ASPECTS = 10). Similarly, NWU cannot be assessed from early follow-up CTs before infarct hypodensity is clearly visible. There were several CTs in our cohort where either no infarct was visible or it was too subtle for segmentation. We have recently demonstrated how volumetric CSF-based biomarkers of evolving edema can be measured and reflect edema formation within the first 12–24 h after stroke (23). It is possible that these two biomarkers capture different aspects of edema formation, one densitometric and other volumetric. The current study provides technical validation of our approach but was performed in a pilot cohort too small to analyze clinical outcomes. It also requires external validation in an independent cohort to ensure generalizability. We now plan on evaluating both density and volume ratios (i.e., NWU and CSF ratio) in larger cohorts using these automated algorithms so that we can understand the relation of these biomarkers to one another and to relevant edema outcomes.

DATA AVAILABILITY STATEMENT

The raw data supporting the conclusions of this article will be made available by the authors, without undue reservation.

ETHICS STATEMENT

The studies involving human participants were reviewed and approved by Human Research Protection Office, Washington University in St. Louis. Written informed consent for participation was not required for this study

in accordance with the national legislation and the institutional requirements.

AUTHOR CONTRIBUTIONS

RD contributed to the conception and design of the study, performed statistical analyses, and wrote the original draft. AK, YC, AA, ZV, and JD contributed to the technical development and analyses and as well as contributing and/or editing key sections of the manuscript. AC, AH, GC, KB, and LH contributed to the acquisition of data for the study. J-ML contributed to the conception of the study and provided critical revisions to the manuscript. All authors contributed to the manuscript revision and have read and approved the submitted version.

REFERENCES

- Hacke W, Schwab S, Horn M, Spranger M, De Georgia M, von Kummer R. 'Malignant' middle cerebral artery territory infarction: clinical course and prognostic signs. *Arch Neurol.* (1996) 53:309–15. doi: 10.1001/archneur.1996.00550040037012
- Kirsch E, Szejko N, Falcone GJ. Genetic underpinnings of cerebral edema in acute brain injury: an opportunity for pathway discovery. *Neurosci Lett.* (2020) 730:135046. doi: 10.1016/j.neulet.2020.135046
- Kimberly WT, Battey TW, Wu O, Singhal AB, Campbell BC, Davis SM, et al. Novel imaging markers of ischemic cerebral edema and its association with neurological outcome. *Acta Neurochir Suppl.* (2016) 121:223–6. doi: 10.1007/978-3-319-18497-5_40
- Yoo AJ, Sheth KN, Kimberly WT, Chaudhry Z, Elm JJ, Jacobson S, et al. Validating imaging biomarkers of cerebral edema in patients with severe ischemic stroke. *J Stroke Cerebrovasc Dis.* (2013) 22:742–9. doi: 10.1016/j.jstrokecerebrovasdis.2012.01.002
- Battey TW, Karki M, Singhal AB, Wu O, Sadaghiani S, Campbell BC, et al. Brain edema predicts outcome after nonlacunar ischemic stroke. *Stroke.* (2014) 45:3643–8. doi: 10.1161/STROKEAHA.114.006884
- Watanabe O, West CR, Bremer A. Experimental regional cerebral ischemia in the middle cerebral artery territory in primates. Part 2: effects on brain water and electrolytes in the early phase of Mca stroke. *Stroke.* (1977) 8:71–6. doi: 10.1161/01.STR.8.1.71
- Broocks G, Faizy TD, Flottmann F, Schon G, Langner S, Fiehler J, et al. Subacute infarct volume with edema correction in computed tomography is equivalent to final infarct volume after ischemic stroke: improving the comparability of infarct imaging endpoints in clinical trials. *Invest Radiol.* (2018) 53:472–6. doi: 10.1097/RLI.0000000000000475
- Broocks G, Flottmann F, Ernst M, Faizy TD, Minnerup J, Siemonsen S, et al. Computed tomography-based imaging of voxel-wise lesion water uptake in ischemic brain: relationship between density and direct volumetry. *Invest Radiol.* (2018) 53:207–13. doi: 10.1097/RLI.0000000000000430
- Broocks G, Kemmling A, Meyer L, Nawabi J, Schon G, Fiehler J, et al. Computed tomography angiography collateral profile is directly linked to early edema progression rate in acute ischemic stroke. *Stroke.* (2019) 50:3424–30. doi: 10.1161/STROKEAHA.119.027062
- Minnerup J, Broocks G, Kalkoffen J, Langner S, Knauth M, Psychogios MN, et al. Computed tomography-based quantification of lesion water uptake identifies patients within 45 hours of stroke onset: a multicenter observational study. *Ann Neurol.* (2016) 80:924–34. doi: 10.1002/ana.24818
- Broocks G, Flottmann F, Hanning U, Schon G, Sporns P, Minnerup J, et al. Impact of endovascular recanalization on quantitative lesion water uptake in ischemic anterior circulation strokes. *J Cereb Blood Flow Metab.* (2019) 40:437–445. doi: 10.1177/0271678X18823601
- Broocks G, Flottmann F, Scheibel A, Aigner A, Faizy TD, Hanning U, et al. Quantitative lesion water uptake in acute stroke computed

FUNDING

J-ML received funding from NIH (R01NS085419 and U24NS107230), RD received funding from NIH (K23NS099440), LH received funding from NIH (K23NS099487), and JD was supported by the 2018–2020 ASNR/RSNA Scholar Award (RR1817) and Mallinckrodt Institute of Radiology.

SUPPLEMENTARY MATERIAL

The Supplementary Material for this article can be found online at: <https://www.frontiersin.org/articles/10.3389/fneur.2022.898728/full#supplementary-material>

- tomography is a predictor of malignant infarction. *Stroke.* (2018) 49:1906–12. doi: 10.1161/STROKEAHA.118.020507
- Cheng X, Shi J, Wu H, Zhu W, Lu G. Review of net water uptake in the management of acute ischemic stroke. *Eur Radiol.* (2022). doi: 10.1007/s00330-022-08658-x (accessed March 2012).
- Vorasayan P, Bevers MB, Beslow LA, Sze G, Molyneaux BJ, Hinson HE, et al. Intravenous glibenclamide reduces lesional water uptake in large hemispheric infarction. *Stroke.* (2019) 50:3021–7. doi: 10.1161/STROKEAHA.119.026036
- Dhar R, Chen Y, An H, Lee JM. Application of machine learning to automated analysis of cerebral edema in large cohorts of ischemic stroke patients. *Front Neurol.* (2018) 9:687. doi: 10.3389/fneur.2018.00687
- Demeestere J, Wouters A, Christensen S, Lemmens R, Lansberg MG. Review of perfusion imaging in acute ischemic stroke: from time to tissue. *Stroke.* (2020) 51:1017–24. doi: 10.1161/STROKEAHA.119.028337
- Rorden C, Bonilha L, Fridriksson J, Bender B, Karnath HO. Age-specific Ct and Mri templates for spatial normalization. *Neuroimage.* (2012) 61:957–65. doi: 10.1016/j.neuroimage.2012.03.020
- Chen Y, Dhar R, Heitsch L, Ford A, Fernandez-Cadenas I, Carrera C, et al. Automated quantification of cerebral edema following hemispheric infarction: application of a machine-learning algorithm to evaluate Csf shifts on serial head Cts. *Neuroimage Clin.* (2016) 12:673–80. doi: 10.1016/j.nicl.2016.09.018
- Dhar R, Chen Y, Hamzehloo A, Kumar A, Heitsch L, He J, et al. Reduction in cerebrospinal fluid volume as an early quantitative biomarker of cerebral edema after ischemic stroke. *Stroke.* (2020) 51:462–7. doi: 10.1161/STROKEAHA.119.027895
- Ronneberger O, Fisher P, Brox T. U-Net: convolutional neural networks for biomedical image segmentation. In: Navab N, Hornegger J, Wells W, Frangi A, editors. *Medical Image Computing and Computer-Assisted Intervention - Miccai 2015 Lecture Notes in Computer Science*, Vol. 9351. Munich: Springer (2015).
- Dhar R. Automated quantitative assessment of cerebral edema after ischemic stroke using Csf volumetrics. *Neurosci Lett.* (2020) 724:134879. doi: 10.1016/j.neulet.2020.134879
- Jenkinson M, Bannister P, Brady M, Smith S. Improved optimization for the robust and accurate linear registration and motion correction of brain images. *Neuroimage.* (2002) 17:825–41. doi: 10.1006/nimg.2002.1132
- Dhar R, Hamzehloo A, Kumar A, Chen Y, He J, Heitsch L, et al. Hemispheric Csf volume ratio quantifies progression and severity of cerebral edema after acute hemispheric stroke. *J Cereb Blood Flow Metab.* (2021) 41:2907–15. doi: 10.1177/0271678X211018210
- Fu B, Qi S, Tao L, Xu H, Kang Y, Yao Y, et al. Image patch-based net water uptake and radiomics models predict malignant cerebral edema after ischemic stroke. *Front Neurol.* (2020) 11:609747. doi: 10.3389/fneur.2020.609747
- Sales Barros R, Tolhuisen ML, Boers AM, Jansen I, Ponomareva E, Dippel DWJ, et al. Automatic segmentation of cerebral infarcts in follow-up computed tomography images with convolutional neural networks. *J Neurointerv Surg.* (2020) 12:848–52. doi: 10.1136/neurintsurg-2019-015471

26. Jeong HG, Bang JS, Kim BJ, Bae HJ, Han MK. Hematoma hounsfield units and expansion of intracerebral hemorrhage: a potential marker of hemostatic clot contraction. *Int J Stroke*. (2021) 16:163–71. doi: 10.1177/1747493019895703
27. Amans MR, Cooke DL, Vella M, Dowd CF, Halbach VV, Higashida RT, et al. Contrast staining on Ct after Dsa in ischemic stroke patients progresses to infarction and rarely hemorrhages. *Interv Neuroradiol*. (2014) 20:106–15. doi: 10.15274/INR-2014-10016
28. Ng FC, Yassi N, Sharma G, Brown SB, Goyal M, Majoie C, et al. Correlation between computed tomography-based tissue net water uptake and volumetric measures of cerebral edema after reperfusion therapy. *Stroke*. (2022) 101161STROKEAHA121037073. doi: 10.1161/STROKEAHA.121.037073 (accessed April 2022).
29. Shrout PE, Fleiss JL. Intraclass correlations: uses in assessing rater reliability. *Psychol Bull*. (1979) 86:420–8. doi: 10.1037/0033-2909.86.2.420
30. Koo TK, Li MY. A guideline of selecting and reporting intraclass correlation coefficients for reliability research. *J Chiropr Med*. (2016) 15:155–63. doi: 10.1016/j.jcm.2016.02.012
31. Broocks G, Kemmling A, Aberle J, Kniep H, Bechstein M, Flottmann F, et al. Ischemic lesion water uptake in acute stroke: is blood glucose related to cause and effect? *J Stroke*. (2019) 21:347–9. doi: 10.5853/jos.2019.01935
32. Broocks G, Hanning U, Faizy TD, Scheibel A, Nawabi J, Schon G, et al. Ischemic lesion growth in acute stroke: water uptake quantification distinguishes between edema and tissue infarct. *J Cereb Blood Flow Metab*. (2020). doi: 10.1177/0271678X19848505
33. Nawabi J, Flottmann F, Hanning U, Bechstein M, Schon G, Kemmling A, et al. Futile recanalization with poor clinical outcome is associated with increased edema volume after ischemic stroke. *Invest Radiol*. (2019) 54:282–7. doi: 10.1097/RLI.0000000000000539
34. Vagal A, Wintermark M, Nael K, Bivard A, Parsons M, Grossman AW, et al. Automated Ct perfusion imaging for acute ischemic stroke: pearls and pitfalls for real-world use. *Neurology*. (2019) 93:888–98. doi: 10.1212/WNL.0000000000008481
35. Boers AM, Marquering HA, Jochem JJ, Besselink NJ, Berkhemer OA, van der Lugt A, et al. Automated cerebral infarct volume measurement in follow-up noncontrast Ct scans of patients with acute ischemic stroke. *AJNR Am J Neuroradiol*. (2013) 34:1522–7. doi: 10.3174/ajnr.A3463
36. Kuang H, Menon BK, Qiu W. Automated stroke lesion segmentation in non-contrast Ct scans using dense multi-path contextual generative adversarial network. *Phys Med Biol*. (2020) 65:215013. doi: 10.1088/1361-6560/aba166
37. van Kranendonk KR, Treurniet KM, Boers AMM, Berkhemer OA, van den Berg LA, Chalos V, et al. Hemorrhagic transformation is associated with poor functional outcome in patients with acute ischemic stroke due to a large vessel occlusion. *J Neurointerv Surg*. (2019) 11:464–8. doi: 10.1136/neurintsurg-2018-014141
38. Xia H, Sun H, He S, Zhao M, Huang W, Zhang Z, et al. Absent cortical venous filling is associated with aggravated brain edema in acute ischemic stroke. *AJNR Am J Neuroradiol*. (2021) 42:1023–9. doi: 10.3174/ajnr.A7039
39. Xu HB, Sun YF, Luo N, Wang JQ, Chang GC, Tao L, et al. Net water uptake calculated in standardized and blindly outlined regions of the middle cerebral artery territory predicts the development of malignant edema in patients with acute large hemispheric infarction. *Front Neurol*. (2021) 12:645590. doi: 10.3389/fneur.2021.645590
40. Cheng X, Wu H, Shi J, Dong Z, Liu J, Zhou C, et al. Aspects-based net water uptake as an imaging biomarker for lesion age in acute ischemic stroke. *J Neurol*. (2021). doi: 10.1007/s00415-021-10584-9
41. Dhar R, Falcone GJ, Chen Y, Hamzehloo A, Kirsch EP, Noche RB, et al. Deep learning for automated measurement of hemorrhage and perihematomal edema in supratentorial intracerebral hemorrhage. *Stroke*. (2020) 51:648–51. doi: 10.1161/STROKEAHA.119.027657
42. van Kranendonk KR, Treurniet KM, Boers AMM, Berkhemer OA, Coutinho JM, Lingsma HF, et al. Added prognostic value of hemorrhagic transformation quantification in patients with acute ischemic stroke. *Front Neurol*. (2020) 11:582767. doi: 10.3389/fneur.2020.582767

Conflict of Interest: The authors declare that the research was conducted in the absence of any commercial or financial relationships that could be construed as a potential conflict of interest.

Publisher's Note: All claims expressed in this article are solely those of the authors and do not necessarily represent those of their affiliated organizations, or those of the publisher, the editors and the reviewers. Any product that may be evaluated in this article, or claim that may be made by its manufacturer, is not guaranteed or endorsed by the publisher.

Copyright © 2022 Kumar, Chen, Corbin, Hamzehloo, Abedini, Vardar, Carey, Bhatia, Heitsch, Derakhshan, Lee and Dhar. This is an open-access article distributed under the terms of the Creative Commons Attribution License (CC BY). The use, distribution or reproduction in other forums is permitted, provided the original author(s) and the copyright owner(s) are credited and that the original publication in this journal is cited, in accordance with accepted academic practice. No use, distribution or reproduction is permitted which does not comply with these terms.



Association Between Post-procedure Cerebral Blood Flow Velocity and Severity of Brain Edema in Acute Ischemic Stroke With Early Endovascular Therapy

Jie Pan^{1,2†}, Huadong Wu^{2†}, Tingting Wu², Yu Geng^{1,2*} and Ruozhen Yuan^{2*}

¹ Suzhou Medical College of Soochow University, Suzhou, China, ² Center for Rehabilitation Medicine, Department of Neurology, Zhejiang Provincial People's Hospital (Affiliated People's Hospital, Hangzhou Medical College), Hangzhou, China

OPEN ACCESS

Edited by:

Peiyu Huang,
Zhejiang University, China

Reviewed by:

Haihui Jiang,
Peking University Third Hospital, China
Tu Wei,
Second Affiliated Hospital of
Nanchang University, China

*Correspondence:

Ruozhen Yuan
yuanrz822@sina.com
Yu Geng
gengy2004@126.com

[†]These authors have contributed
equally to this work

Specialty section:

This article was submitted to
Applied Neuroimaging,
a section of the journal
Frontiers in Neurology

Received: 28 March 2022

Accepted: 17 June 2022

Published: 18 July 2022

Citation:

Pan J, Wu H, Wu T, Geng Y and
Yuan R (2022) Association Between
Post-procedure Cerebral Blood Flow
Velocity and Severity of Brain Edema
in Acute Ischemic Stroke With Early
Endovascular Therapy.
Front. Neurol. 13:906377.
doi: 10.3389/fneur.2022.906377

Objectives: We aimed to investigate the association between post-procedure cerebral blood flow velocity (CBFV) and severity of brain edema in patients with acute ischemic stroke (AIS) who received early endovascular therapy (EVT).

Methods: We retrospectively included patients with AIS who received EVT within 24 h of onset between February 2016 and November 2021. Post-procedure CBFV of the middle cerebral artery was measured in the affected and the contralateral hemispheres using transcranial Doppler ultrasound. The severity of brain edema was measured using the three-level cerebral edema grading from the Safe Implementation of Thrombolysis in Stroke-Monitoring Study, with grades 2–3 indicating severe brain edema. The Association between CBFV parameters and severity of brain edema was analyzed.

Results: A total of 101 patients (mean age 64.2 years, 65.3% male) were included, of whom 56.3% (57/101) suffered brain edema [grade 1, 23 (22.8%); grade 2, 10 (9.9%); and grade 3, 24 (23.8%)]. Compared to patients with non-severe brain edema, patients with severe brain edema had lower affected/contralateral ratios of systolic CBFV (median 1 vs. 1.2, $P = 0.020$) and mean CBFV (median 0.9 vs. 1.3, $P = 0.029$). Multivariate logistic regression showed that severe brain edema was independently associated with affected/contralateral ratios of systolic CBFV [odds ratio (OR) = 0.289, 95% confidence interval (CI): 0.069–0.861, $P = 0.028$] and mean CBFV (OR = 0.278, 95% CI: 0.084–0.914, $P = 0.035$) after adjusting for potential confounders.

Conclusion: Post-procedure affected/contralateral ratio of CBFV may be a promising predictor of brain edema severity in patients with AIS who received early EVT.

Keywords: ischemic stroke, endovascular therapy, edema, cerebral blood flow velocity, transcranial Doppler

INTRODUCTION

Brain edema is one of the most devastating complications after acute ischemic stroke (AIS) (1). Malignant brain edema (MBE) is the most severe type of brain edema, and it usually occurs following the occlusion of the internal carotid artery (ICA) or the middle cerebral artery (MCA) (2). MBE is characterized by a disastrous clinical course, with a mortality rate reaching 80% in

conservatively treated patients (3). Since effective treatment options are limited once MBE occurs, early prediction and identification of patients at risk of severe brain edema is essential to improve prognosis (4).

Endovascular therapy (EVT) is the most effective treatment for patients with large vessel occlusion (5). Recent studies showed that revascularization was associated with a reduced risk of MBE (4) and that EVT was inversely associated with the use of decompressive craniectomy for patients with AIS (6). However, about 20% of patients with large vessel occlusion still developed MBE despite successful recanalization (7, 8). Whether post-procedure factors could guide the early prediction of brain edema severity is still unknown for patients receiving EVT.

Transcranial Doppler (TCD) as a non-invasive approach for measuring cerebral blood flow velocity (CBFV) and estimating increased intracranial pressure at the bedside is widely used in neurocritical care (9, 10). CBFV reflects real-time cerebral hemodynamics in patients with AIS; however, the value of CBFV in predicting brain edema has been poorly studied (11). Therefore, in this study, we aimed to investigate the value of post-procedure CBFV in predicting the severity of brain edema in patients with AIS who received early EVT.

MATERIALS AND METHODS

Patient Selection

Patients with AIS who were admitted to Zhejiang Provincial People's Hospital (Hangzhou, China) from February 2016 to November 2021 and received early EVT were prospectively included in our study. Stroke was diagnosed according to the World Health Organization criteria, and ischemic stroke was confirmed by brain computed tomography (CT) or magnetic resonance imaging (MRI). We included patients who received EVT for occlusion of the MCA or ICA within 24 h of stroke onset. We excluded patients who had more than one EVT within 1 week of stroke onset, who had no imaging scan or TCD examination within 1 week of EVT, or who underwent post-procedure TCD after the last CT scan.

This study was approved by the Ethics Committee of Zhejiang Provincial People's Hospital. Informed consent was obtained from patients or their relatives.

Clinical Management and Data Collection

Upon admission, a brain non-contrast CT scan was performed for every patient with AIS. Patients who were suspected of large vessel occlusion were further evaluated by CT angiography and CT perfusion scanning (Aquilion/ONE TSX-301A, Toshiba, Tokyo, Japan). We conformed to the latest guidelines for the selection of candidates for early EVT (5, 12). The final decision to perform EVT was made after discussing it with the patient's families. In our center, EVT includes mechanical thrombectomy with a stent retriever, direct aspiration, and angioplasty/stenting. Which procedure to perform is determined by the neuro-interventionalist in charge.

From all patients, we collected demographic information, time of onset, past medical history, and stroke severity on admission. Stroke severity was measured using the National Institutes

of Health Stroke Scale (NIHSS) (13) and Glasgow Coma Scale (GCS) (14). The state of post-procedure recanalization was evaluated using the modified Treatment in Cerebral Ischemia (mTICI) score (15). Hemorrhagic transformation was determined using the European Cooperative Acute Stroke Study (ECASS) criteria (16), which comprised hemorrhagic infarction and parenchymal hemorrhage.

Post-procedure CBFV of the MCA was measured using TCD (EMS-9PB, Delica, Shenzhen, China) within seven days of stroke onset. We used a 2-MHz probe to obtain the CBFV of bilateral MCAs through the temporal bone window, with a depth of 45–60 mm (9). Systolic, diastolic, and mean CBFVs were recorded. We performed a brain CT scan immediately after EVT. We strictly maintained post-procedure blood pressure under 140/90 mmHg in all patients receiving EVT. If angioplasty or stenting was performed during EVT, blood pressure was further controlled around 110–120/70–80 mmHg. If the patient met indications for decompressive craniectomy, neurosurgeons were consulted.

Osmotic therapy was prescribed when the radiological sign of space-occupying brain edema was observed. Mannitol and/or glycerol infusion was the most used regimen. The dosage of osmotic therapy was determined by the neurologist in charge. Follow-up brain CT/MRI was scheduled on the first, third, and seventh days after EVT, or in case of neurological worsening.

Outcome Measures

Brain edema was defined as effacement of cortical sulci or the ventricular system due to compression of adjacent brain tissue (17). The severity of brain edema was further assessed using the cerebral edema (CED) grading from the Safe Implementation of Thrombolysis in Stroke-Monitoring Study (SITS-MOST) (18), a three-level scale that classifies brain edema into CED-1 (focal brain edema up to one-third of the hemisphere), CED-2 (brain edema greater than one-third of the hemisphere), and CED-3 (brain edema with midline shift, MLS). Typical imaging observations of different severity grades of brain edema are shown in **Figure 1**.

The primary outcome of this study was severe brain edema (SBE), defined as brain edema of grades CED-2 or CED-3. The secondary outcome was MBE, defined as clinical deterioration (decrease in NIHSS ≥ 4 points or decrease in NIHSS item 1a of ≥ 1 point), together with radiological signs of space-occupying edema (MLS ≥ 5 mm) within seven days of onset (4). MLS was defined as the distance of septum pellucidum displacement at the level of the Foramen of Monro (19).

Statistical Analyses

All statistical analyses were performed using SPSS version 23.0 (IBM, Armonk, NY, USA). We reported the mean \pm standard deviation (SD) or median with interquartile range (IQR) for reporting continuous variables, and number with percentage for categorical variables. All ratios presented throughout the article indicate the proportion of the parameter in the affected hemisphere compared with the contralateral hemisphere.

Baseline variables were compared between groups with different severity of brain edema (SBE vs. non-SBE, MBE

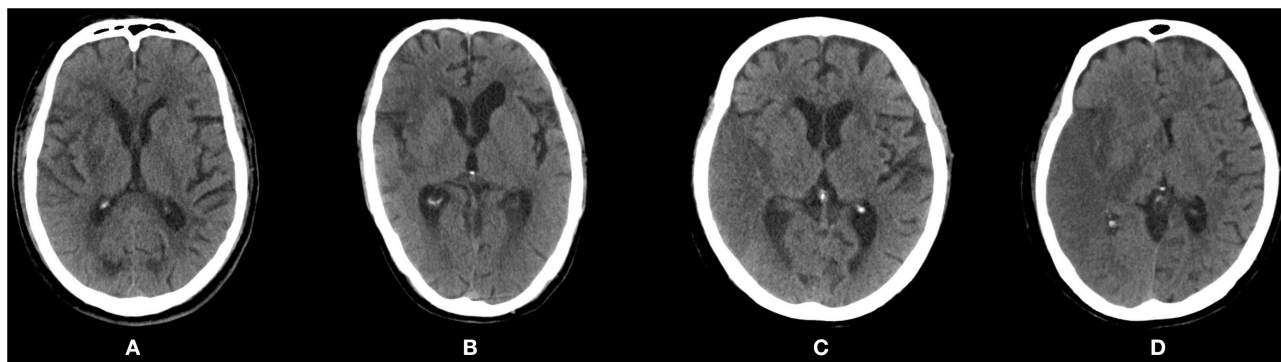
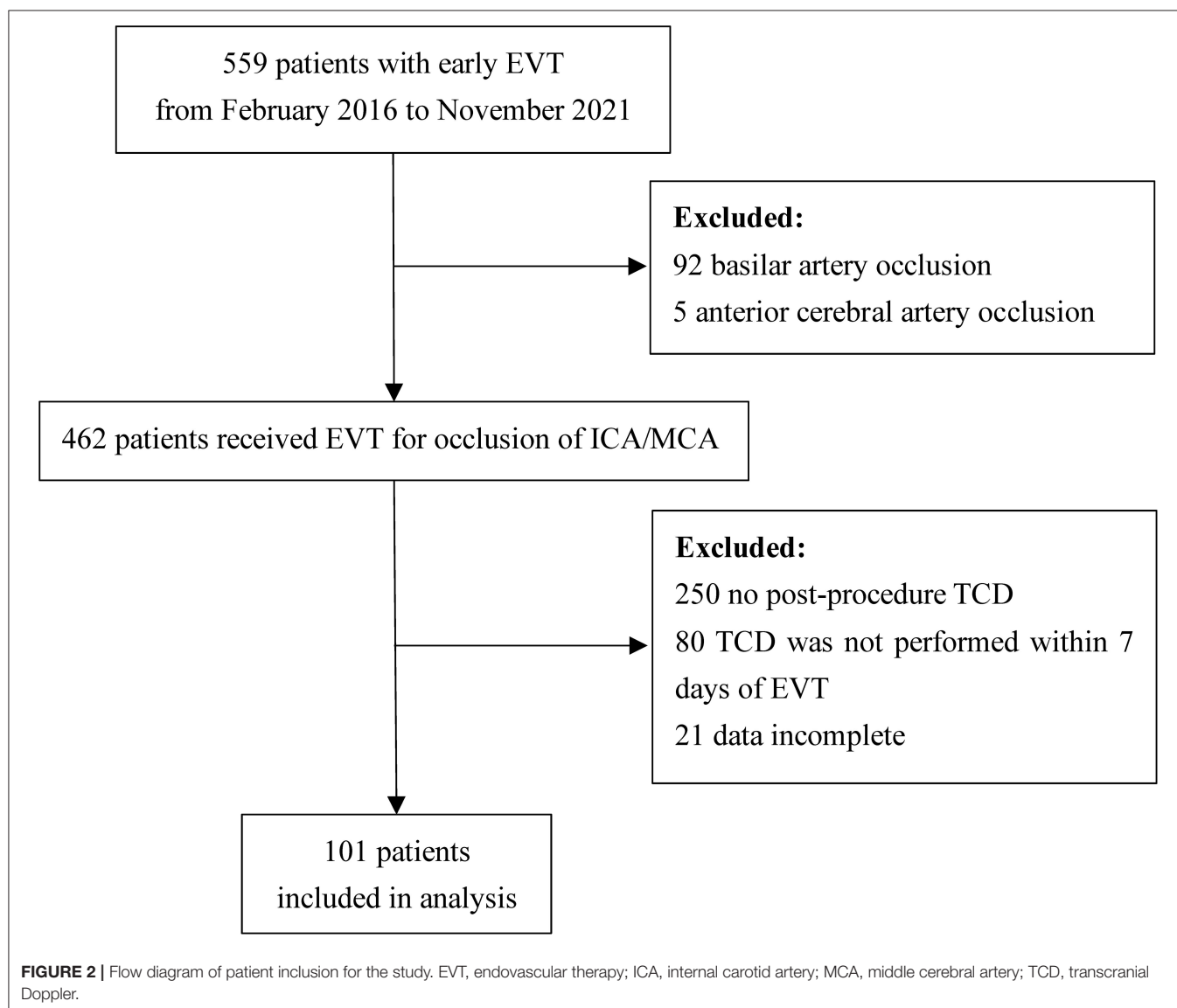


FIGURE 1 | Post-procedure computed tomography scans showing different severity of brain edema according to the Safe Implementation of Thrombolysis in Stroke-Monitoring Study (SITS-MOST). **(A)** CED-0: no edema. **(B)** CED-1: focal brain edema up to one-third of the hemisphere. **(C)** CED-2: brain edema greater than one-third of the hemisphere. **(D)** CED-3: brain edema with midline shift. CED, cerebral edema.



vs. non-MBE). Analysis of variance (ANOVA) or Mann-Whitney U test were used to compare continuous variables, and χ^2 or Fisher's exact test were used to compare categorical variables as appropriate. Multivariate logistic regression was applied to examine the association between CBFV and severity of brain edema after adjustment for potential confounders. Multivariate analysis was conducted using variables that were associated with $P < 0.10$ in the univariate analysis, as well as variables previously linked to brain edema (4, 20, 21). Consequently, we selected age, NIHSS score, and atrial fibrillation as potential confounders. Correlations between TCD parameters and severity of MLS were assessed using Spearman's correlation coefficients. A two-sided $P < 0.05$ was considered statistically significant.

RESULTS

Patients' Demographic and Clinical Characteristics

Details of patient inclusion are shown in **Figure 2**. Five hundred and fifty-nine patients received early EVT from February 2016 to November 2021 in our center. We excluded 92 patients for basilar artery occlusion, 5 patients for anterior cerebral artery occlusion, 250 patients for no post-procedure TCD, 80 patients for no TCD examination within 1 week of EVT, and 21 patients for incomplete data. Finally, a total of 101 patients were included in the analysis; 65.3% (66/101) were male and the mean age was 64.2 years.

The occluded artery of the index stroke was the ICA in 31.7% (32/101) of patients, the M1 segment of MCA in 47.5% (48/101), and the M2 segment of MCA in 20.8% (21/101). The median time from onset to TCD examination was 5 days (IQR: 3–6 days). Median systolic CBFV was 87 cm/s, median diastolic CBFV was 32 cm/s, and mean CBFV of the MCA on the affected side was 49.7 cm/s. The hemorrhagic transformation occurred in 42.6% (43/101) of patients within seven days of onset. Hemorrhagic infarction grade 1 affected 4% (4/101); hemorrhagic infarction grade 2, 19.8% (20/101); parenchymal hemorrhage grade 1, 14.9% (15/101); and parenchymal hemorrhage grade 2, 4% (4/101). Other baseline characteristics are shown in **Table 1**.

Brain edema was present on follow-up imaging in 56.3% (57/101) of included patients. CED-1 was present in 23 (22.8%) of included patients; CED-2, 10 (9.9%); and CED-3, 24 (23.8%). For patients with CED-3, the median value of MLS was 4 mm (IQR: 3–7 mm). Six patients developed MBE within seven days of stroke onset.

Comparison of CBFV Between Patients Who Are Non-SBE and Patients With SBE

Compared to patients who are non-SBE (CED 0–1), patients with SBE (CED 2–3) had lower ratio of systolic CBFV (median: 1 vs. 1.2, $P = 0.020$), and lower ratio of mean CBFV (median: 0.9 vs. 1.3, $P = 0.029$). Similar trends were observed for the ratio of diastolic CBFV, but the intergroup difference did not reach statistical significance. Other baseline characteristics were comparable between the two groups (**Table 2**).

TABLE 1 | Baseline characteristics and outcomes of included patients.

Characteristic	Value
Age, mean \pm SD	64.2 \pm 15.0
Male, n (%)	66 (65.3)
Hypertension, n (%)	62 (61.4)
Diabetes mellitus, n (%)	17 (16.8)
Atrial fibrillation, n (%)	49 (48.5)
Coronary heart disease, n (%)	7 (6.9)
Stroke history, n (%)	13 (12.9)
NIHSS on admission, median (IQR)	16 (13–20)
GCS on admission, median (IQR)	13 (12–14)
Duration from onset to TCD, days, median (IQR)	5.0 (3.0–6.0)
Intravenous thrombolysis, n (%)	42 (41.6)
Etiology, n (%)	
Large-artery atherosclerosis	31 (30.7)
Cardioembolism	55 (54.5)
Others	8 (7.9%)
Undetermined	7 (6.9)
Left hemisphere affected, n (%)	53 (52.5)
Occlusion site, n (%)	
ICA	32 (31.7)
M1	48 (47.5)
M2	21 (20.8)
Postoperative mTICI, n (%)	
<2b	3 (3.0)
2b	25 (24.8)
3	73 (72.3)
Affected MCA	
Systolic CBFV, cm/s, median (IQR)	87.0 (62.0–114.5)
Diastolic CBFV, cm/s, median (IQR)	32.0 (22.0–44.4)
Mean CBFV, cm/s, median (IQR)	49.7 (35.5–67.3)
PI, mean \pm SD	1.1 \pm 0.2
RI, mean \pm SD	0.6 \pm 0.1
Contralateral MCA	
Systolic CBFV, cm/s, median (IQR)	79.0 (67.5–97.5)
Diastolic CBFV, cm/s, median (IQR)	31.0 (23.0–38.1)
Systolic CBFV, cm/s, median (IQR)	47.0 (37.7–58.3)
PI, mean \pm SD	1.1 \pm 0.2
RI, mean \pm SD	0.6 \pm 0.1
Systolic CBFV ratio, median (IQR)	1.1 (0.9–1.4)
Diastolic CBFV ratio, median (IQR)	1.1 (0.8–1.5)
Mean CBFV ratio, median (IQR)	1.1 (0.8–1.4)
PI ratio, median (IQR)	1.0 (0.8–1.1)
RI ratio, median (IQR)	1.0 (0.9–1.1)
Malignant brain edema, n (%)	6 (5.9)
Severity of brain edema, n (%)	
No edema	44 (43.6)
CED-1	23 (22.8)
CED-2	10 (9.9)
CED-3	24 (23.8)

All ratios indicate the proportion between affected/contralateral hemispheres.

CBFV, cerebral blood flow velocity; CED, cerebral edema; GCS, Glasgow Coma Scale; ICA, internal carotid artery; IQR, interquartile range; M1, horizontal segment of middle cerebral artery; M2, insular segment of middle cerebral artery; MCA, middle cerebral artery; mTICI, modified Treatment in Cerebral Ischemia; NIHSS, National Institutes of Health Stroke Scale; PI, pulsatility index; RI, resistance index; SD, standard deviation; TCD, transcranial Doppler.

TABLE 2 | Comparison of baseline characteristics between patients with or without severe brain edema (SBE).

Characteristic	SBE (n = 34)	Non-SBE (n = 67)	P
Age, mean \pm SD	65.0 \pm 14.4	63.9 \pm 15.4	0.722
Male, n (%)	20 (58.8)	46 (68.7)	0.326
Hypertension, n (%)	21 (61.8)	41 (61.2)	0.956
Diabetes mellitus, n (%)	6 (17.6)	11 (16.4)	0.876
Atrial fibrillation, n (%)	20 (58.8)	29 (43.3)	0.140
Coronary heart disease, n (%)	1 (2.9)	6 (9.0)	0.418
Stroke history, n (%)	6 (17.6)	7 (10.4)	0.353
NIHSS at admission, median (IQR)	17 (15–19)	15 (12–20)	0.048
GCS at admission, median (IQR)	13 (12–14)	13 (12–14)	0.527
Duration from onset to TCD, days, median (IQR)	5 (3–6)	5 (3–6)	0.870
Intravenous thrombolysis, n (%)	15 (44.1)	27 (40.3)	0.713
Etiology, n (%)			0.529
Large-artery atherosclerosis	10 (29.4)	21 (31.3)	
Cardioembolism	21 (61.8)	34 (50.7)	
Others	1 (2.9)	7 (10.4)	
Undetermined	2 (5.9)	5 (7.5)	
Left hemisphere affected, n (%)	16 (47.1)	37 (55.2)	0.437
Occlusion site, n (%)			0.725
ICA	10 (29.4)	22 (32.8)	
M1	18 (52.9)	30 (44.8)	
M2	6 (17.6)	15 (22.4)	
Postoperative mTICI, n (%)			0.740
<2b	1 (2.9)	2 (3.0)	
2b	10 (29.4)	15 (22.4)	
3	23 (67.6)	50 (74.6)	
Systolic CBFV of affected MCA, cm/s, median (IQR)	84.0 (60.0–104.5)	88.0 (62.0–123.0)	0.327
Diastolic CBFV of affected MCA, cm/s, median (IQR)	31.5 (20.8–38.8)	33.0 (24.0–47.0)	0.394
Mean CBFV of affected MCA, cm/s, median (IQR)	47.7 (34.3–60.6)	51.0 (36.7–72.3)	0.304
PI of affected MCA, median (IQR)	1.0 (1.0–1.2)	1.0 (0.9–1.2)	0.752
RI of affected MCA, median (IQR)	0.6 (0.6–0.7)	0.6 (0.6–0.7)	0.752
Systolic CBFV of contralateral MCA, cm/s, median (IQR)	85.0 (71.5–107.3)	78.0 (66.0–94.0)	0.197
Diastolic CBFV of contralateral MCA, cm/s, median (IQR)	31.5 (22.0–42.0)	31.0 (23.0–38.0)	0.479
Mean CBFV of contralateral MCA, cm/s, median (IQR)	49.1 (41.3–62.3)	46.7 (37.3–55.7)	0.273
PI of contralateral MCA, median (IQR)	1.1 (0.9–1.3)	1.0 (0.9–1.2)	0.782
RI of contralateral MCA, median (IQR)	0.6 (0.6–0.7)	0.6 (0.6–0.7)	0.782
Systolic CBFV ratio, median (IQR)	1.0 (0.8–1.3)	1.2 (0.9–1.4)	0.020
Diastolic CBFV ratio, median (IQR)	1.0 (0.8–1.3)	1.3 (0.9–1.6)	0.050
Mean CBFV ratio, median (IQR)	0.9 (0.8–1.3)	1.3 (0.9–1.5)	0.029
PI ratio, median (IQR)	1.0 (0.9–1.1)	1.0 (0.8–1.2)	0.994
RI ratio, median (IQR)	1.0 (0.9–1.1)	1.0 (0.9–1.1)	0.903

All ratios indicate the proportion between affected/contralateral hemisphere. CBFV, cerebral blood flow velocity; GCS, Glasgow Coma Scale; ICA, internal carotid artery; IQR, interquartile range; M1, horizontal segment of middle cerebral artery; M2, insular segment of middle cerebral artery; MCA, middle cerebral artery; mTICI, modified Treatment in Cerebral Ischemia; NIHSS, National Institutes of Health Stroke Scale; PI, pulsatility index; RI, resistance index; SBE, severe brain edema; SD, standard deviation; TCD, transcranial Doppler. P-values in bold indicate statistically significant.

TABLE 3 | Multivariate analysis of the association between the ratio of cerebral blood flow velocity and severe brain edema.

Multivariate regression model	OR	95% CI	P
Model 1			
Age	0.994	0.962–1.027	0.733
NIHSS score	1.083	0.993–1.181	0.072
Atrial fibrillation	1.709	0.666–4.385	0.265
Systolic CBFV ratio	0.289	0.069–0.861	0.028
Model 2			
Age	0.994	0.962–1.026	0.700
NIHSS score	1.078	0.990–1.173	0.084
Atrial fibrillation	1.677	0.657–4.279	0.280
Diastolic CBFV ratio	0.428	0.161–1.139	0.089
Model 3			
Age	0.994	0.962–1.027	0.717
NIHSS score	1.082	0.993–1.180	0.073
Atrial fibrillation	1.667	0.651–4.271	0.287
Mean CBFV ratio	0.278	0.084–0.914	0.035

All ratios indicate the proportion between affected/contralateral hemispheres.

P-values in bold indicate statistically significant.

CBFV, cerebral blood flow velocity; CI, confidence interval; NIHSS, National Institutes of Health Stroke Scale; OR, odds ratio.

TABLE 4 | Correlation between transcranial Doppler parameters and severity of midline shift in patients with CED-3 (n = 24).

Transcranial Doppler parameter	r	P
Affected MCA		
Systolic CBFV	−0.467	0.021
Diastolic CBFV	−0.465	0.022
Mean CBFV	−0.481	0.018
PI	0.164	0.444
RI	0.164	0.444
Contralateral MCA		
Systolic CBFV	−0.206	0.334
Diastolic CBFV	−0.075	0.728
Mean CBFV	−0.141	0.512
PI	−0.142	0.507
RI	−0.142	0.507
Systolic CBFV ratio	−0.300	0.155
Diastolic CBFV ratio	−0.436	0.033
Mean CBFV ratio	−0.372	0.073
PI ratio	0.255	0.229
RI ratio	0.259	0.223

All ratios indicate the proportion between affected/contralateral hemispheres.

P-values in bold indicate statistically significant.

CBFV, cerebral blood flow velocity; CED, cerebral edema; MCA, middle cerebral artery; PI, pulsatility index; RI, resistance index.

After adjusting for potential confounders, including age, admission NIHSS score, and atrial fibrillation, we found increased risk of SBE to be independently associated with lower ratio of systolic CBFV (OR = 0.289, 95% CI: 0.069–0.861, $P = 0.028$) and lower ratio of mean CBFV (OR = 0.278, 95% CI: 0.084–0.914, $P = 0.035$) (Table 3). Among patients with MLS

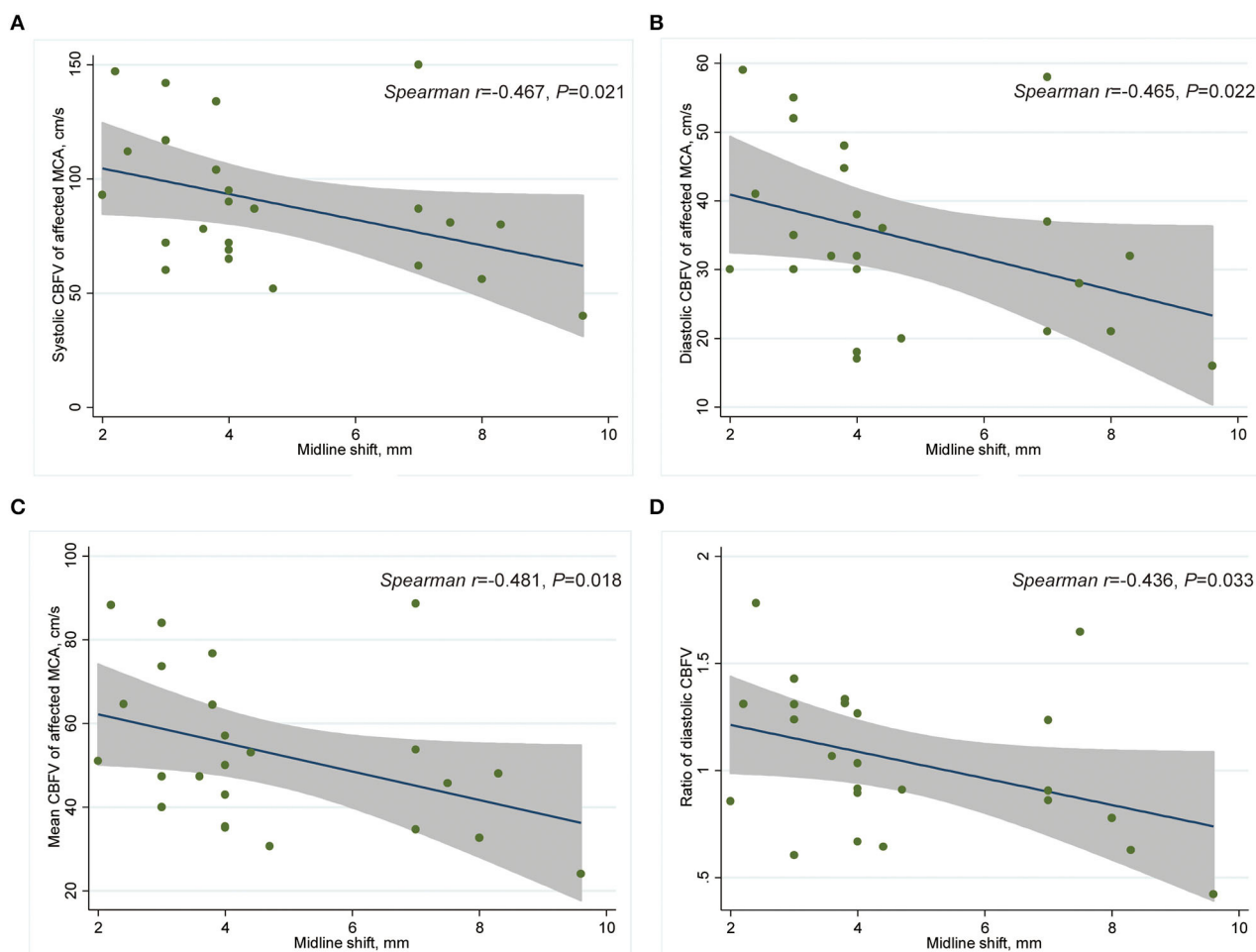


FIGURE 3 | Scatter plot showing correlation between CBFV and MLS in patients with CED-3 ($n = 24$). **(A)** Systolic CBFV of the affected MCA and MLS; **(B)** diastolic CBFV of the affected MCA and MLS; **(C)** mean CBFV of the affected MCA and MLS; **(D)** and affected/contralateral ratio of diastolic CBFV and MLS. CBFV, cerebral blood flow velocity; CED, cerebral edema; MCA, middle cerebral artery; MLS, midline shift.

(CED-3), severity of MLS correlated with CBFV (systolic: $r = -0.467$, $P = 0.021$; diastolic: $r = -0.465$, $P = 0.022$; mean: $r = -0.481$, $P = 0.018$) in the affected MCA and ratio of diastolic CBFV ($r = -0.436$, $P = 0.033$) (Table 4; Figure 3).

Comparison of CBFV Between Patients Who Are Non-MBE and Patients With MBE

Compared to patients with non-MBE, patients with MBE had a lower ratio of systolic CBFV (0.8 vs. 1.1, $P = 0.049$) and a lower ratio of mean CBFV (0.8 vs. 1.1, $P = 0.041$) (Table 5). The multivariate analysis could not be performed due to the small number of patients in the MBE group.

Comparison of CBFV Between Hemorrhagic Transformation Subgroups

Compared to patients with hemorrhagic infarction, patients with parenchymal hemorrhage had a higher ratio of diastolic CBFV

(1.3 vs. 0.9, $P = 0.043$), while values of CBFV were similar between patients with or without hemorrhagic transformation.

DISCUSSION

Patients with AIS with large vessel occlusion are at high risk of developing MBE even after EVT. However, reliable markers for the prediction of post-EVT brain edema severity are lacking. Thus, here, we aimed to investigate the association between post-procedure CBFV measured by TCD and the severity of brain edema to evaluate the prognostic capacity of CBFV. In a Chinese cohort of patients, we found that a lower ratio of affected/contralateral CBFV was independently associated with an increased risk of severe brain edema.

In AIS research, TCD has traditionally been used as a real-time screening tool for recanalization, perfusion state, and microemboli during EVT (22, 23), but studies on the association between TCD parameters and brain edema are limited. One study

TABLE 5 | Comparison of baseline characteristics between patients with or without malignant brain edema (MBE).

Characteristic	MBE (n = 6)	Non-MBE (n = 95)	P
Age, median (IQR)	80.5 (59.8–83.3)	65.0 (55.0–74.0)	0.131
Male, n (%)	4 (66.7)	62 (65.3)	>0.999
Hypertension, n (%)	4 (66.7)	58 (61.1)	>0.999
Diabetes mellitus, n (%)	3 (50.0)	14 (14.7)	0.058
Atrial fibrillation, n (%)	6 (100.0)	43 (45.3)	0.011
Coronary heart disease, n (%)	0 (0)	7 (7.4)	>0.999
Stroke history, n (%)	1 (16.7)	12 (12.6)	0.572
NIHSS at admission, median (IQR)	18 (17–22)	16 (12–20)	0.091
GCS at admission, median (IQR)	13 (10–13)	13 (12–14)	0.167
Duration from onset to TCD, days, median (IQR)	3 (2–5)	5 (3–6)	0.142
Intravenous thrombolysis, n (%)	3 (50.0)	39 (41.1)	0.691
Etiology, n (%)			0.149
Large-artery atherosclerosis	0 (0)	31 (32.6)	
Cardioembolism	6 (100.0)	49 (51.6)	
Others	0 (0)	8 (8.4)	
Undetermined	0 (0)	7 (7.4)	
Left hemisphere affected, n (%)	3 (50.0)	50 (52.6)	>0.999
Occlusion site, n (%)			0.684
ICA	2 (33.3)	30 (31.6)	
M1	2 (33.3)	46 (48.4)	
M2	2 (33.3)	19 (20.0)	
Postoperative mTICI, n (%)			0.097
<2b	1 (16.7)	2 (2.1)	
2b	2 (33.3)	23 (24.2)	
3	3 (50.0)	70 (73.7)	
Systolic CBFV of affected MCA, cm/s, median (IQR)	80.5 (52.0–102.8)	88.0 (62.0–117.0)	0.417
Diastolic CBFV of affected MCA, cm/s, median (IQR)	30.0 (19.8–41.5)	32.0 (23.0–44.7)	0.610
Mean CBFV of affected MCA, cm/s, median (IQR)	46.8 (30.5–61.9)	50.0 (35.7–68.3)	0.490
PI of affected MCA, median (IQR)	1.0 (1.0–1.1)	1.0 (0.9–1.2)	0.966
RI of affected MCA, median (IQR)	0.6 (0.6–0.6)	0.6 (0.6–0.7)	0.966
Systolic CBFV of contralateral MCA, cm/s, median (IQR)	104.0 (61.3–136.3)	79.0 (68.0–96.0)	0.214
Diastolic CBFV of contralateral MCA, cm/s, median (IQR)	44.5 (24.5–58.0)	31.0 (23.0–38.0)	0.117
Mean CBFV of contralateral MCA, cm/s, median (IQR)	66.0 (36.3–81.6)	46.7 (37.7–56.3)	0.145
PI of contralateral MCA, median (IQR)	1.0 (0.8–1.2)	1.1 (0.9–1.2)	0.429
RI of contralateral MCA, median (IQR)	0.6 (0.5–0.7)	0.6 (0.6–0.7)	0.429
Systolic CBFV ratio, median (IQR)	0.8 (0.6–1.0)	1.1 (0.9–1.4)	0.049
Diastolic CBFV ratio, median (IQR)	0.7 (0.6–1.1)	1.2 (0.9–1.5)	0.056
Mean CBFV ratio, median (IQR)	0.8 (0.6–1.0)	1.1 (0.9–1.4)	0.041
PI ratio, median (IQR)	1.0 (0.9–1.3)	1.0 (0.8–1.1)	0.566
RI ratio, median (IQR)	1.0 (0.9–1.2)	1.0 (0.9–1.1)	0.481

All ratios indicate the proportion between affected/contralateral hemispheres.

P-values in bold indicate statistically significant.

CBFV, cerebral blood flow velocity; GCS, Glasgow Coma Scale; ICA, internal carotid artery; IQR, interquartile range; M1, horizontal segment of middle cerebral artery; M2, insular segment of middle cerebral artery; MBE, malignant brain edema; MCA, middle cerebral artery; mTICI, modified Treatment in Cerebral Ischemia; NIHSS, National Institutes of Health Stroke Scale; PI, pulsatility index; RI, resistance index; TCD, transcranial Doppler.

(24) assessed cerebral autoregulation using CBFV and arterial blood pressure in 46 patients with MCA infarction and found that impaired cerebral autoregulation was associated with brain edema on admission and 24 h after admission. In contrast, in this study, we assessed direct TCD parameters, which are more widely used in clinical practice than analysis of cerebral autoregulation.

In our study, a lower ratio of CBFV in the affected MCA relative to the contralateral MCA was associated with a higher risk of SBE. On the contrary, one study (25) included 185 patients with large vessel occlusion who received EVT, and found that a pathologically high ratio of peak systolic velocity (in the recanalized/contralateral MCA) was associated with 3-month poor outcomes, although the incidence of brain edema was not reported. Notably, the mean peak systolic velocity ratio was highest immediately after EVT and decreased with time in this study (25).

The detrimental effects of high CBFV could be explained by secondary injury due to cerebral hyperperfusion syndrome (26), while hypoperfusion itself is a strong risk factor for ischemia damage (27). Consistent with this, a study on traumatic brain injury showed that deviation of optimal cerebral perfusion pressure in either direction was associated with poor outcomes (28). Besides, contradictory results were observed when CBFV was measured at different times after EVT, suggesting that differences in when TCD was evaluated may be another reason for the observed disparity among studies. In a study of 123 patients with AIS receiving early EVT (29), the elevation of mean blood flow index (recanalized/contralateral MCA) within 24 h of EVT (mean time: 6.6 h) was associated with a higher risk of hemorrhagic transformation and unfavorable outcomes. While another study of 31 patients with AIS receiving EVT (30) reported that acceleration of CBFV within seven days (mean: 3.4 days) of mechanical thrombectomy was not associated with clinical deterioration.

Among TCD parameters, pulsatility index (PI) has been correlated with intracranial pressure in patients with traumatic brain injury (31). One study (32) investigated the association between PI generated from the contralateral MCA and MLS in patients with large MCA infarction. Researchers found that baseline PI values and their increase correlated with MLS on day 3, suggesting that higher PI was an indicator of increased intracranial pressure in AIS (32). In our study, however, PI values were similar between the SBE and non-SBE groups, which indicated that the relative decrease of CBFV in the affected hemisphere was not caused by the edema itself. We speculate that ischemia and mechanical injury to the vascular endothelium may cause dysfunction of cerebral autoregulation, which further aggravates ischemic damage and leads to brain edema (24, 33, 34).

Notably, although 33.7% of included patients in our study had SBE, only six of them developed MBE, which has a more profound influence on clinical outcomes (2). In our previous systematic review, the median time for detection of MBE in existing studies was 6 days (4). Here, the median time from onset to MBE was 5 days (2.8–5.3 days) and the median time from onset to TCD was 2.5 days (1.5–4.8 days) for patients with MBE. In an early post-mortem study (35), the extent of MLS reached its peak about 4 days

after onset. A sonographic study detected a gradual increase in MLS during the first 4 days after hemispheric infarction (36). Therefore, CBFV measured by TCD early after EVT may offer valuable information for predicting space-occupying brain edema and subsequent MBE. However, this hypothesis could not be confirmed in the current study due to the small number of MBE cases.

Our study presents several limitations. First, the retrospective design might cause a selection bias, which may mean that some patients with severe edema did not undergo TCD because of their unstable condition. Second, the timing of TCD evaluations was not standardized. On the other hand, these two limitations may mean that our results better reflect actual clinical practice. Measuring CBFV immediately after EVT, and then, dynamically thereafter could help illuminate the natural course of brain edema following EVT and offer more information for clinical decisions. Prospective, multi-center studies with larger samples and quantitative analysis of brain edema are needed (37). A nomogram or grading scale derived from multivariate models is also needed to evaluate the reliability and strength of CBFV in predicting brain edema.

CONCLUSION

A lower affected/contralateral ratio of CBFV in MCA within seven days of EVT may be associated with an increased risk of severe brain edema in patients with AIS. Post-procedure CBFV measured by TCD may be a predictor of severe brain edema.

REFERENCES

- Balami JS, Chen RL, Grunwald IQ, Buchan AM. Neurological complications of acute ischaemic stroke. *Lancet Neurol.* (2011) 10:357–71. doi: 10.1016/S1474-4422(10)70313-6
- Huttner HB, Schwab S. Malignant middle cerebral artery infarction: clinical characteristics, treatment strategies, and future perspectives. *Lancet Neurol.* (2009) 8:949–58. doi: 10.1016/S1474-4422(09)70224-8
- Berrouschot J, Sterker M, Bettin S, Koster J, Schneider D. Mortality of space-occupying ('malignant') middle cerebral artery infarction under conservative intensive care. *Intensive Care Med.* (1998) 24:620–3. doi: 10.1007/s001340050625
- Wu S, Yuan R, Wang Y, Wei C, Zhang S, Yang X, et al. Early prediction of malignant brain edema after ischemic stroke. *Stroke.* (2018) 49:2918–27. doi: 10.1161/STROKEAHA.118.022001
- Powers WJ, Rabinstein AA, Ackerson T, Adeoye OM, Bambakidis NC, Becker K, et al. Guidelines for the Early Management of Patients With Acute Ischemic Stroke: 2019 Update to the 2018 Guidelines for the Early Management of Acute Ischemic Stroke: A Guideline for Healthcare Professionals From the American Heart Association/American Stroke Association. *Stroke.* (2019) 50:e344–418. doi: 10.1161/STR.0000000000000211
- Khattar NK, Ugiliweneza B, Fortuny EM, Adams SW, Meyer KS, Sharma M, et al. Inverse national trends in decompressive craniectomy versus endovascular thrombectomy for stroke. *World Neurosurg.* (2020) 138:e642–51. doi: 10.1016/j.wneu.2020.03.022
- Wang C, Zhu Q, Cui T, Wang L, Yang T, Hao Z, et al. Early prediction of malignant edema after successful recanalization in patients with acute ischemic stroke. *Neurocrit Care.* (2021) 36:822–30. doi: 10.1007/s12028-021-01380-4
- Broocks G, Hanning U, Flottmann F, Schönfeld M, Faizy TD, Sporns P, et al. Clinical benefit of thrombectomy in stroke patients with low

DATA AVAILABILITY STATEMENT

The raw data supporting the conclusions of this article will be made available by the authors, without undue reservation.

ETHICS STATEMENT

The studies involving human participants were reviewed and approved by Medical Ethics Committee of Zhejiang Provincial People's Hospital. The patients/participants provided their written informed consent to participate in this study.

AUTHOR CONTRIBUTIONS

HW, JP, and RY carried out the studies, participated in collecting data, and drafted the manuscript. YG and RY performed the statistical analysis and participated in its design. TW participated in the acquisition, analysis, or interpretation of data and drafted the manuscript. All authors read and approved the final manuscript.

FUNDING

This work was supported by Projects of Medical and Health Science and Technology in Zhejiang Province of China (2019RC099, 2019KY010, 2021KY509, and 2022KY573) and the Scientific Research Fund of Zhejiang Provincial Education Department (Y201942650).

- ASPECTS is mediated by oedema reduction. *Brain.* (2019) 142:1399–407. doi: 10.1093/brain/awz057
- D'Andrea A, Conte M, Cavallaro M, Scarafie R, Riegler L, Cocchia R, et al. Transcranial doppler ultrasonography: from methodology to major clinical applications. *World J Cardiol.* (2016) 8:383–400. doi: 10.4330/wjc.v8.i7.383
- Robba C, Cardim D, Sekhon M, Budohoski K, Czosnyka M. Transcranial Doppler: a stethoscope for the brain-neurocritical care use. *J Neurosci Res.* (2018) 96:720–30. doi: 10.1002/jnr.24148
- Zhang Z, Pu Y, Mi D, Liu L. Cerebral hemodynamic evaluation after cerebral recanalization therapy for acute ischemic stroke. *Front Neurol.* (2019) 10:719. doi: 10.3389/fneur.2019.00719
- Powers WJ, Derdeyn CP, Biller J, Coffey CS, Hoh BL, Jauch EC, et al. 2015 American Heart Association/American Stroke Association Focused Update of the 2013 Guidelines for the Early Management of Patients With Acute Ischemic Stroke Regarding Endovascular Treatment: A Guideline for Healthcare Professionals From the American Heart Association/American Stroke Association. *Stroke.* (2015) 46:3020–35. doi: 10.1161/STR.0000000000000074
- Brott T, Adams HP, Olinger CP, Marler JR, Barsan WG, Biller J, et al. Measurements of acute cerebral infarction - a clinical examination scale. *Stroke.* (1989) 20:864–70. doi: 10.1161/01.STR.20.7.864
- Teasdale G, Jennett B. Assessment of coma and impaired consciousness - practical scale. *Lancet.* (1974) 2:81–4. doi: 10.1016/S0140-6736(74)91639-0
- Wintermark M, Albers GW, Broderick JP, Demchuk AM, Fiebach JB, Fiehler J, et al. Acute stroke imaging research roadmap II. *Stroke.* (2013) 44:2628–39. doi: 10.1161/STROKEAHA.113.002015
- Hacke W, Kaste M, Fieschi C, Toni D, Lesaffre E, von Kummer R, et al. Intravenous thrombolysis with recombinant tissue plasminogen activator for acute hemispheric stroke. The European Cooperative Acute Stroke Study (ECASS). *JAMA.* (1995) 274:1017–25. doi: 10.1001/jama.274.13.1017

17. Barber PA, Demchuk AM, Zhang J, Buchan AM. Validity and reliability of a quantitative computed tomography score in predicting outcome of hyperacute stroke before thrombolytic therapy. ASPECTS Study Group Alberta Stroke Programme Early CT Score. *Lancet*. (2000) 355:1670–4. doi: 10.1016/S0140-6736(00)02237-6
18. Thorén M, Azevedo E, Dawson J, Egido JA, Falcou A, Ford GA, et al. Predictors for cerebral edema in acute ischemic stroke treated with intravenous thrombolysis. *Stroke*. (2017) 48:2464–71. doi: 10.1161/STROKEAHA.117.018223
19. Liao CC, Chen YF, Xiao F. Brain midline shift measurement and its automation: a review of techniques and algorithms. *Int J Biomed Imaging*. (2018) 2018:4303161. doi: 10.1155/2018/4303161
20. Sun W, Li G, Song Y, Zhu Z, Yang Z, Chen Y, et al. A web based dynamic MANA Nomogram for predicting the malignant cerebral edema in patients with large hemispheric infarction. *BMC Neurol*. (2020) 20:360. doi: 10.1186/s12883-020-01935-6
21. Greenland S. Modeling and variable selection in epidemiologic analysis. *Am J Public Health*. (1989) 79:340–9. doi: 10.2105/AJPH.79.3.340
22. Tsivgoulis G, Ribo M, Rubiera M, Vasdekis SN, Barlinn K, Athanasiadis D, et al. Real-time validation of transcranial Doppler criteria in assessing recanalization during intra-arterial procedures for acute ischemic stroke: an international, multicenter study. *Stroke*. (2013) 44:394–400. doi: 10.1161/STROKEAHA.112.675074
23. Rubiera M, Cava L, Tsivgoulis G, Patterson DE, Zhao L, Zhang Y, et al. Diagnostic criteria and yield of real-time transcranial Doppler monitoring of intra-arterial reperfusion procedures. *Stroke*. (2010) 41:695–9. doi: 10.1161/STROKEAHA.109.565762
24. Castro P, Azevedo E, Serrador J, Rocha I, Sorond F. Hemorrhagic transformation and cerebral edema in acute ischemic stroke: Link to cerebral autoregulation. *J Neurol Sci*. (2017) 372:256–61. doi: 10.1016/j.jns.2016.11.065
25. Baracchini C, Farina F, Palmieri A, Kulyk C, Pieroni A, Viaro F, et al. Early hemodynamic predictors of good outcome and reperfusion injury after endovascular treatment. *Neurology*. (2019) 92:e2774–83. doi: 10.1212/WNL.00000000000007646
26. van Mook WN, Rennenberg RJ, Schurink GW, van Oostenbrugge RJ, Mess WH, Hofman PA, et al. Cerebral hyperperfusion syndrome. *Lancet Neurol*. (2005) 4:877–88. doi: 10.1016/S1474-4422(05)70251-9
27. Caplan LR, Hennerici M. Impaired clearance of emboli (washout) is an important link between hypoperfusion, embolism, and ischemic stroke. *Arch Neurol*. (1998) 55:1475–82. doi: 10.1001/archneur.55.11.1475
28. Aries MJ, Czosnyka M, Budohoski KP, Steiner LA, Lavinio A, Kolias AG, et al. Continuous determination of optimal cerebral perfusion pressure in traumatic brain injury. *Crit Care Med*. (2012) 40:2456–63. doi: 10.1097/CCM.0b013e3182514eb6
29. Kneihl M, Niederkorn K, Deutschmann H, Enzinger C, Poltrum B, Fischer R, et al. Increased middle cerebral artery mean blood flow velocity index after stroke thrombectomy indicates increased risk for intracranial hemorrhage. *J Neurointerv Surg*. (2018) 10:882–7. doi: 10.1136/neurintsurg-2017-013617
30. Perren F, Kargiotis O, Pignat JM, Pereira VM. Hemodynamic changes may indicate vessel wall injury after stent retrieval thrombectomy for acute stroke. *J Neuroimaging*. (2018) 28:412–5. doi: 10.1111/jon.12513
31. Moreno JA, Mesalles E, Gener J, Tomasa A, Ley A, Roca J, et al. Evaluating the outcome of severe head injury with transcranial Doppler ultrasonography. *Neurosurg Focus*. (2000) 8:e8. doi: 10.3171/foc.2000.8.1.1702
32. Asil T, Uzunca I, Utku U, Berberoglu U. Monitoring of increased intracranial pressure resulting from cerebral edema with transcranial Doppler sonography in patients with middle cerebral artery infarction. *J Ultrasound Med*. (2003) 22:1049–53. doi: 10.7863/jum.2003.22.10.1049
33. Guo ZN, Shao A, Tong LS, Sun W, Liu J, Yang Y, et al. The role of nitric oxide and sympathetic control in cerebral autoregulation in the setting of subarachnoid hemorrhage and traumatic brain injury. *Mol Neurobiol*. (2016) 53:3606–15. doi: 10.1007/s12035-015-9308-x
34. Dohmen C, Bosche B, Graf R, Reithmeier T, Ernestus RI, Brinker G, et al. Identification and clinical impact of impaired cerebrovascular autoregulation in patients with malignant middle cerebral artery infarction. *Stroke*. (2007) 38:56–61. doi: 10.1161/01.STR.0000251642.18522.b6
35. Shaw CM, Alvord EC, Berry RG. Swelling of the brain following ischemic infarction with arterial occlusion. *Arch Neurol*. (1959) 1:161–77. doi: 10.1001/archneur.1959.03840020035006
36. Gerriets T, Stolz E, Modrau B, Fiss I, Seidel G, Kaps M, et al. Sonographic monitoring of midline shift in hemispheric infarctions. *Neurology*. (1999) 52:45–9. doi: 10.1212/WNL.52.1.45
37. Dhar R. Automated quantitative assessment of cerebral edema after ischemic stroke using CSF volumetrics. *Neurosci Lett*. (2020) 724:134879. doi: 10.1016/j.neulet.2020.134879

Conflict of Interest: The authors declare that the research was conducted in the absence of any commercial or financial relationships that could be construed as a potential conflict of interest.

Publisher's Note: All claims expressed in this article are solely those of the authors and do not necessarily represent those of their affiliated organizations, or those of the publisher, the editors and the reviewers. Any product that may be evaluated in this article, or claim that may be made by its manufacturer, is not guaranteed or endorsed by the publisher.

Copyright © 2022 Pan, Wu, Wu, Geng and Yuan. This is an open-access article distributed under the terms of the Creative Commons Attribution License (CC BY). The use, distribution or reproduction in other forums is permitted, provided the original author(s) and the copyright owner(s) are credited and that the original publication in this journal is cited, in accordance with accepted academic practice. No use, distribution or reproduction is permitted which does not comply with these terms.



OPEN ACCESS

EDITED BY

Peiyu Huang,
Zhejiang University, China

REVIEWED BY

Vasu Saini,
University of Miami Health System,
United States
Jawed Nawabi,
University Medical Center
Hamburg-Eppendorf, Germany

*CORRESPONDENCE

Longting Lin
longting.lin@unsw.edu.au
Mark W. Parsons
Mark.Parsons@unsw.edu.au

†These authors have contributed
equally to this work

SPECIALTY SECTION

This article was submitted to
Applied Neuroimaging,
a section of the journal
Frontiers in Neurology

RECEIVED 24 March 2022

ACCEPTED 27 June 2022

PUBLISHED 27 July 2022

CITATION

Xu T, Yang J, Han Q, Wu Y, Gao X,
Xu Y, Huang Y, Wang A, Parsons MW
and Lin L (2022) Net water uptake, a
neuroimaging marker of early brain
edema, as a predictor of symptomatic
intracranial hemorrhage after acute
ischemic stroke.
Front. Neurol. 13:903263.
doi: 10.3389/fneur.2022.903263

COPYRIGHT

© 2022 Xu, Yang, Han, Wu, Gao, Xu,
Huang, Wang, Parsons and Lin. This is
an open-access article distributed
under the terms of the [Creative
Commons Attribution License \(CC BY\)](#).
The use, distribution or reproduction
in other forums is permitted, provided
the original author(s) and the copyright
owner(s) are credited and that the
original publication in this journal is
cited, in accordance with accepted
academic practice. No use, distribution
or reproduction is permitted which
does not comply with these terms.

Net water uptake, a neuroimaging marker of early brain edema, as a predictor of symptomatic intracranial hemorrhage after acute ischemic stroke

Tianqi Xu^{1†}, Jianhong Yang^{1†}, Qing Han^{1†}, Yuefei Wu¹,
Xiang Gao², Yao Xu¹, Yi Huang^{2,3}, Aiju Wang⁴,
Mark W. Parsons^{5,6*} and Longting Lin^{1,5*}

¹Department of Neurology, Ningbo First Hospital, Ningbo Hospital of Zhejiang University, Ningbo, China, ²Department of Neurosurgery, Ningbo First Hospital, Ningbo Hospital of Zhejiang University, Ningbo, China, ³Key Laboratory of Precision Medicine for Atherosclerotic Diseases of Zhejiang Province, Ningbo, China, ⁴Department of Neurology, Ningbo Fourth Hospital, Ningbo, China, ⁵Sydney Brain Center, University of New South Wales, Sydney, NSW, Australia, ⁶Department of Neurology, Liverpool Hospital, Sydney, NSW, Australia

Objective: We hypothesized that quantitative net water uptake (NWU), a novel neuroimaging marker of early brain edema, can predict symptomatic intracranial hemorrhage (sICH) after acute ischemic stroke (AIS).

Methods: We enrolled patients with AIS who completed admission multimodal computed tomography (CT) within 24 h after stroke onset. NWU within the ischemic core and penumbra was calculated based on admission CT, namely NWU-core and NWU-penumbra. sICH was defined as the presence of ICH in the infarct area within 7 days after stroke onset, accompanied by clinical deterioration. The predictive value of NWU-core and NWU-penumbra on sICH was evaluated by logistic regression analyses and the receiver operating characteristic (ROC) curve. A pure neuroimaging prediction model was built considering imaging markers, which has the potential to be automatically quantified with an artificial algorithm on image workstation.

Results: 154 patients were included, of which 93 underwent mechanical thrombectomy (MT). The median time from symptom onset to admission CT was 262 min (interquartile range, 198–368). In patients with MT, NWU-penumbra (OR = 1.442; 95% CI = 1.177–1.766; $P < 0.001$) and NWU-core (OR = 1.155; 95% CI = 1.027–1.299; $P = 0.016$) were independently associated with sICH with adjustments for age, sex, time from symptom onset to CT, hypertension, lesion volume, and admission National Institutes of Health Stroke Scale (NIHSS) score. ROC curve showed that NWU-penumbra had better predictive performance than NWU-core on sICH [area under the curve (AUC): 0.773 vs. 0.673]. The diagnostic efficiency of the predictive model was improved with the containing of NWU-penumbra (AUC: 0.853 vs. 0.760). A pure imaging model also presented stable predictive power (AUC = 0.812). In patients without MT, however, only admission NIHSS score (OR = 1.440; 95% CI = 1.055–1.965; $P = 0.022$) showed significance in predicting sICH in multivariate analyses.

Conclusions: NWU-penumbra may have better predictive performance than NWU-core on sICH after MT. A pure imaging model showed potential value to automatically screen patients with sICH risk by image recognition, which may optimize treatment strategy.

KEYWORDS

brain edema, multimodal CT, net water uptake, symptomatic intracranial hemorrhage (sICH), acute ischemic stroke (AIS), mechanical thrombectomy (MT)

Introduction

Brain edema is an important pathophysiological process after acute ischemic stroke (AIS). The pathophysiological mechanisms are primarily cytotoxic edema, angiogenic edema, and cerebrospinal fluid influx (1, 2). Progressive edema will lead to irreversible tissue injury, secondary neurological deterioration, and poor outcome (3). Current assessments of brain edema degree are mainly based on follow-up non-contrast computed tomography (NCCT), as brain edema peaks around 3 days after stroke onset (4). Imaging characteristics such as shrunken sulci, low density around infarct core, midline shift, and even brain hernia suggest brain edema indirectly (5). However, there are few neuroimaging markers able to detect brain edema early, directly, and quantitatively, and none of these neuroimaging markers were available in CT until recently (6).

Quantitative net water uptake (NWU) is a relatively novel neuroimaging marker of early brain edema after AIS, first described in 2016 based on admission multimodal CT (7). Researchers subsequently reported that NWU within the ischemic core can identify patients within the thrombolysis time window and predict poor outcomes at 90 days, and those with malignant edema (8–10). In the hyperacute stage of AIS, cytotoxic edema will lead to endothelial cell swelling, further blood-brain barrier (BBB) breakdown, increased permeability, and ultimately may contribute to hemorrhagic transformation (HT). Previous research reported that NWU within the ischemic core was a predictor of HT in patients with successful reperfusion (11). In this study, NWU within the ischemic core and the ischemic penumbra were calculated separately. The predictive values of NWU-core and NWU-penumbra on symptomatic intracranial hemorrhages (sICH) after AIS were further investigated.

Methods

Patients

This is a single-institute retrospective study. The clinical and imaging data were obtained from an established database, which contains data from all patients with AIS admitted to the

Emergency Department at Ningbo First Hospital (Advanced Stroke Center) between July 2017 and September 2019. Inclusion criteria: (1) acute anterior circulation infarction; (2) admission multimodal CT including NCCT, CT angiography (CTA), and CT perfusion (CTP) were completed within 24 h after symptom onset. In patients with wake-up stroke, we estimated the time of stroke onset by taking the midpoint between sleep time and wake time (12); (3) follow-up CT scans performed at 24 h and 1 week after stroke onset or immediately in case of clinical deterioration; (4) the absence of intracranial hemorrhage, brain tumor, or preexisting infarctions in admission NCCT. The thrombolysis in cerebral infarction (TICI) grading scale is used to define endpoints of successful revascularization (13).

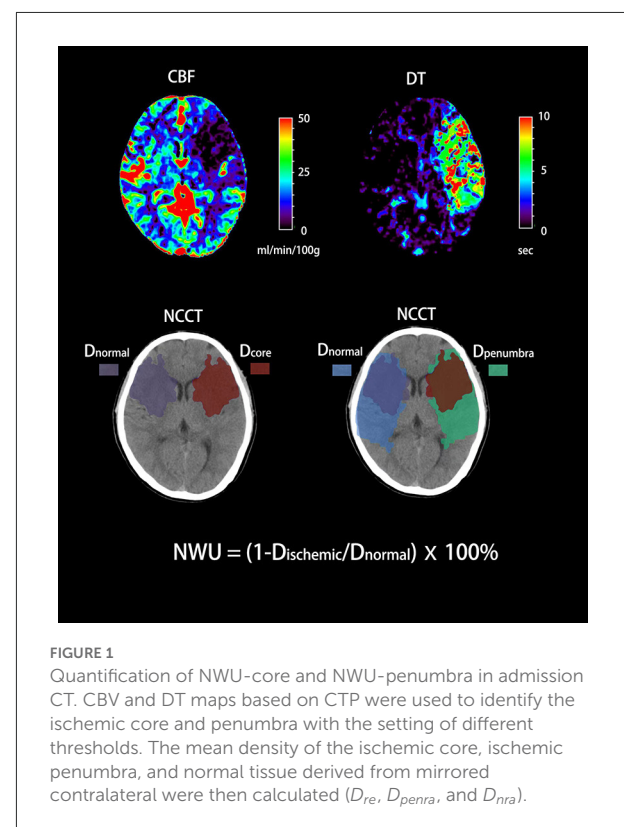


TABLE 1 Baseline characteristics of enrolled patients.

	Non-sICH (<i>n</i> = 126)	sICH* (<i>n</i> = 28)	<i>P</i> -value
Demographics			
Age, mean ± SD	69 ± 13	70 ± 11	0.353
Sex, male (%)	74 (58.7)	13 (46.4)	0.293
Comorbidities			
Hypertension, <i>n</i> (%)	73 (57.9)	22 (78.6)	0.053
Diabetes mellitus, <i>n</i> (%)	11 (8.7)	6 (21.4)	0.088
Atrial fibrillation, <i>n</i> (%)	75 (59.5)	19 (67.9)	0.522
Coronary heart disease, <i>n</i> (%)	15 (12.0)	4 (14.3)	0.753
Stroke etiology			
Atherothrombotic, <i>n</i> (%)	27 (21.4)	4 (14.3)	
Cardioembolic, <i>n</i> (%)	72 (57.1)	18 (64.3)	
Others, <i>n</i> (%)	27 (21.4)	6 (21.4)	
NIHSS score, median (IQR)	17 (12–21)	21 (15–28)	0.008
Time from symptom onset to CT, min, median (IQR)	253 (194–366)	310 (242–398)	0.100
Imaging biomarkers			
Ischemic core volume, ml, median (IQR)	24 (9–45)	48 (32–62)	<0.001
Ischemic penumbra volume, ml, median (IQR)	66 (33–102)	87 (57–136)	0.060
NWU-core, %, median (IQR)	5.3 (2.7–8.9)	8.2 (5.8–10.9)	0.015
NWU-penumbra, %, median (IQR)	0.9 (–1.5 to 3.5)	3.6 (2.1–5.1)	<0.001
Treatment			
Mechanical thrombectomy, <i>n</i> (%)	51 (40.5)	18 (64.3)	
Intravenous thrombolysis, <i>n</i> (%)	44 (34.9)	4 (14.1)	
Bridging therapy, <i>n</i> (%)	19 (15.1)	5 (17.9)	
Antiplatelet agents, <i>n</i> (%)	12 (9.5)	1 (3.6)	0.069

sICH, symptomatic intracranial hemorrhage; NIHSS, National Institutes of Health Stroke Scale; NWU-core, net water uptake within ischemic core; NWU-penumbra, net water uptake within ischemic penumbra.

For continuous variables that follow a normal distribution, data were expressed as mean ± SD, the *t*-test was used for group comparison. For non-normal continuous variables, data were presented in the form of the medians (interquartile ranges), and the Mann-Whitney *U*-test was applied. Categorical variables were expressed as frequencies (percentages), using the χ^2 test or Fisher's test as appropriate.

*sICH was defined in reference to ECASSii criterion as hemorrhagic hyperintense in the infarction area scanned by CT within 1 week from symptom onset, accompanied by an increase of at least 4 points in the NIHSS score from baseline. The bold values means *p* < 0.1.

Definition of sICH

According to the European Cooperative Acute Stroke Study (ECASS) II criteria, hemorrhagic transformation (HT) of infarcted brain tissue can be divided into four types, including HI1 (scattered small petechiae, no mass effect), HI2 (confluent petechiae, no mass effect), PH1 (hematoma within infarcted tissue, occupying < 30%, no substantive mass effect), and PH2 (hematoma occupying 30% or more of the infarcted tissue, with obvious mass effect). sICH was defined as the presence of hemorrhagic hyperdensity in the infarction area on follow-up CT scans within 7 days, accompanied by clinical deterioration (an NIHSS score increase ≥ 4 from baseline) (14, 15) with no explanation for the clinical deterioration other than secondary intracerebral hemorrhage.

Imaging analysis

Admission multimodal CT was conducted by a 320-slice scanner (Toshiba Aquilion ONE, Canon Medical Imaging, Tokyo, Japan) with 320 axial sections and 0.5 mm thickness. All imaging data were processed by commercial software (Mistar, Apollo Medical Imaging Technology, Melbourne, VIC, Australia). CTP was used to identify the ischemic core and ischemic penumbra. The threshold of ischemic core was delay time (DT) > 3 s and cerebral blood flow (CBF) < 30%. The threshold of ischemic penumbra was DT > 3 s and CBF > 30% (16). Regions of interest (ROIs) corresponding to the ischemic core and penumbra according to these thresholds were drawn manually, and mirrored contralateral ROIs were generated automatically and defined as normal tissue. These

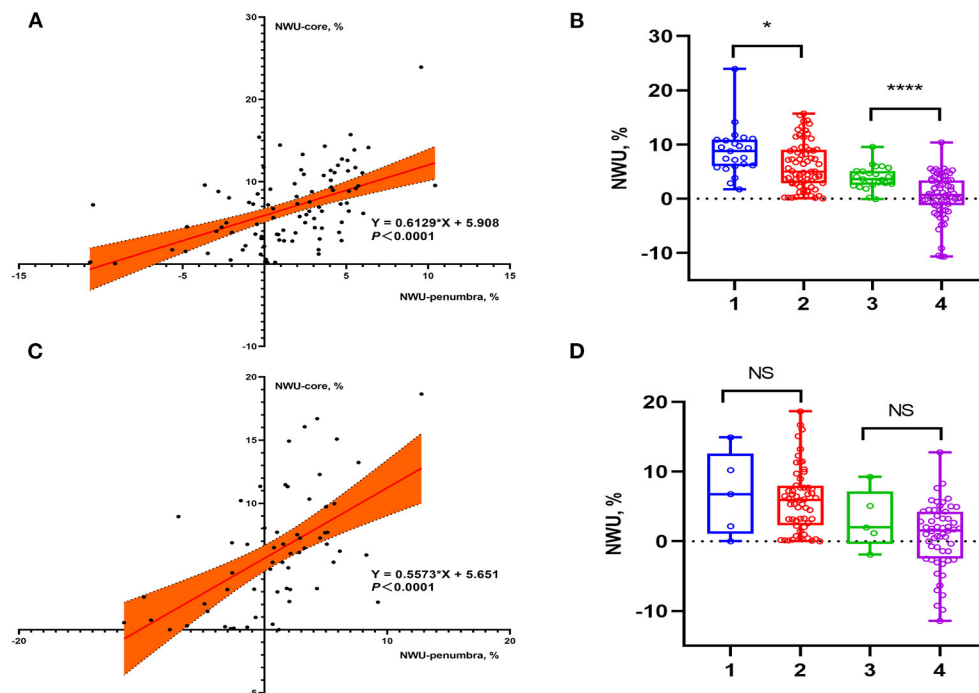


FIGURE 2

Data distributions of NWU-core and NWU-penumbra in patients stratified by reperfusion therapies. (A) Scatter plot showed the relationship between NWU-core and NWU-penumbra in patients with MT. (B) Group 1: NWU-core of sICH patients, group 2: NWU-core of non-sICH patients, group 3: NWU-penumbra of sICH patients, group 4: NWU-penumbra of non-sICH patients. Box plot showed that in patients with MT, sICH group had higher NWU-core [8.8 (6.0–10.9) vs. 5.0 (2.8–9.0), $P = 0.013$] and NWU-penumbra [2.6 (3.6–5.1) vs. 0.7 (–1.2 to 3.4), $P < 0.001$] than those without sICH. (C) Scatter plot showed the relationship between NWU-core and NWU-penumbra in patients without MT. (D) Group 1: NWU-core of sICH patients, group 2: NWU-core of non-sICH patients, group 3: NWU-penumbra of sICH patients, group 4: NWU-penumbra of non-sICH patients. Box plot showed that in patients without MT, there was no statistical difference in NWU-core [6.8 (1.1–12.6) vs. 6.0 (2.3–8.0), $P = 0.885$] and NWU-penumbra [2.0 (–0.4 to 7.2) vs. 1.5 (–2.8 to 4.1), $P = 0.318$] between sICH and non-sICH group. * $p < 0.05$; ** $p < 0.01$; *** $p < 0.001$; **** $p < 0.0001$.

ROIs were then superimposed on NCCT to measure CT density (D_{re} , D_{penra} , and D_{nra}) with Hounsfield units (HU) between 20 and 80 (Figure 1). NWU-core was defined as an elevated volume of water (Δ_{ater}) per unit volume of ischemic core ($core$). Similarly, NWU-penumbra was defined as Δ_{ater} per unit volume of ischemic penumbra ($penumbra$), according to the following equations (6, 7):

$$NWU_{core} = \frac{V_{water}}{V_{core}} = \left(1 - \frac{D_{core}}{D_{normal}}\right) \times 100\%$$

$$NWU_{penumbra} = \frac{V_{water}}{V_{penumbra}} = \left(1 - \frac{D_{penumbra}}{D_{normal}}\right) \times 100\%$$

Statistical methods

We performed the statistical analyses under the supervision of professional statisticians. SPSS version 22.0 (SPSS Inc, Chicago, IL, USA), MedCalc version 20.027 (MedCalc Software Ltd, Ostend, Belgium), and GraphPad Prism version 8.0 (GraphPad Software, San Diego, CA, USA) were used in

these analyses. Baseline characteristics were compared between patients with and without sICH. For continuous variables that followed a normal distribution, data were expressed as mean \pm SD, and the t -test was used for group comparison. For non-normal continuous variables, data were presented in the form of the medians (interquartile ranges), and the Mann-Whitney U test was applied. Categorical variables were expressed as frequencies (%) using the χ^2 test or Fisher's test as appropriate. Univariate logistic regression analyses were used to explore the associations between sICH, NWU-core, and NWU-penumbra. Backward stepwise multivariate logistic regression analyses were then performed. We used age, sex, admission NIHSS score, time from symptom onset to CT, lesion volume, and variables with $P < 0.10$ in the univariate analyses as covariates. The variance inflation factor (VIF) was calculated to examine multicollinearity among variables included in regression models. Predictive models containing NWU-core and NWU-penumbra were further built. The predictive power of NWU-core, NWU-penumbra, and regression models were measured by receiver operating characteristic (ROC) curve analysis.

TABLE 2 Univariate logistic regression analysis for risk of sICH in patients stratified by reperfusion therapies.

	With MT (<i>n</i> = 93)		Without MT (<i>n</i> = 61)	
	OR (95% CI)	<i>P</i> -value	OR (95% CI)	<i>P</i> -value
Clinical characteristics				
Age	1.020 (0.981–1.060)	0.322	0.996 (0.919–1.079)	0.926
Male	0.818 (0.318–2.100)	0.676	0.342 (0.053–2.227)	0.262
Hypertension	3.812 (1.274–11.406)	0.017	1.744 (0.181–16.778)	0.630
Diabetes mellitus	1.042 (0.388–2.797)	0.935	11.778 (1.394–99.511)	0.024
Atrial fibrillation	1.632 (0.442–6.021)	0.462	3.467 (0.364–33.001)	0.280
Coronary heart disease	1.605 (0.435–5.926)	0.478	NA	0.999
Stroke etiology	1.018 (0.634–1.636)	0.940	1.221 (0.523–2.850)	0.644
NIHSS score	1.054 (0.980–1.134)	0.157	1.237 (1.066–1.434)	0.005
Time from symptom onset to CT	1.001 (0.998–1.003)	0.657	1.003 (0.996–1.009)	0.412
Imaging biomarkers				
Ischemic core volume	1.014 (1.001–1.027)	0.034	1.009 (0.996–1.022)	0.194
Ischemic penumbra volume	1.003 (0.994–1.011)	0.542	0.995 (0.974–1.016)	0.617
NWU-core	1.143 (1.024–1.277)	0.018	1.035 (0.858–1.250)	0.717
NWU-penumbra	1.431 (1.159–1.766)	0.001	1.131 (0.911–1.405)	0.265

sICH, symptomatic intracranial hemorrhage; MT, mechanical thrombectomy; NIHSS, National Institutes of Health Stroke Scale; NWU-core, net water uptake within ischemic core; NWU-penumbra, net water uptake within ischemic penumbra. The bold values means $p < 0.1$.

Results

Baseline characteristics of enrolled patients

A total of 154 patients with acute anterior circulation ischemic stroke were included in the study. There were 58 cases of HT (37.7%), including 8 cases of HI1 (5.2%), 24 cases of HI2 (15.6%), 12 cases of PH1 (7.8%), and 14 cases of PH2 (9.1%). sICH occurred in 28 patients (18.2%). Table 1 shows the baseline characteristics of patients. The median time from symptom onset to multimodal CT was 262 min (interquartile range, 198–368). Compared with non-sICH patients, patients with sICH have higher median admission NIHSS score [21 (15–28) vs. 17 (12–21), $P = 0.008$], higher median ischemic core volume [48 (32–62) vs. 24 (9–45), $P < 0.001$], higher median NWU-core [8.2 (5.8–10.9) vs. 5.3 (2.7–7.9), $P = 0.015$] and higher median NWU-penumbra [3.6 (2.1–5.1) vs. 0.9 (–1.5 to 3.5), $P < 0.001$].

Univariate logistic regression analysis for risks of sICH in patients stratified by reperfusion therapies

Among the 154 enrolled patients, 93 underwent MT, of which 73 patients (78.5%) received successful reperfusion according to the TICI grading scale. Of the 61 patients who did not receive MT, 48 underwent intravenous thrombolysis

and 13 received antiplatelet agents only. Supplementary Table 1 shows patient's demographics of group MT vs. non-MT and indicates that 23 (82.1%) of the 28 patients with sICH underwent MT. Figure 2 shows the data distributions of NWU-core and NWU-penumbra. In the MT group, patients with sICH had higher NWU-core [8.8 (6.0–10.9) vs. 5.0 (2.8–9.0), $P = 0.013$] and higher NWU-penumbra [2.6 (3.6–5.1) vs. 0.7 (–1.2 to 3.4), $P < 0.001$]. Univariate analysis showed that hypertension (OR = 3.812; 95% CI = 1.274–11.406; $P = 0.017$), ischemic core volume (OR = 1.014; 95% CI = 1.001–1.027; $P = 0.034$), NWU-core (OR = 1.143; 95% CI = 1.024–1.277; $P = 0.018$), and NWU-penumbra (OR = 1.431; 95% CI = 1.159–1.766; $P = 0.001$) were associated with sICH after MT. However, in patients without MT, none of the imaging biomarkers showed significance, only admission NIHSS score (OR = 1.237; 95% CI = 1.066–1.434; $P = 0.005$) and diabetes mellitus (OR = 11.778; 95% CI = 1.394–99.511; $P = 0.024$) were significantly correlated with sICH (Table 2). The associations between NWU-core and NWU-penumbra with different types of HT are shown in Supplementary Table 2.

Multivariate logistic regression analysis for predictive models of sICH in patients stratified by reperfusion therapies

Table 3 shows four different predictive models of sICH in patients with MT. Model 1 was built without NWU for

TABLE 3 Multivariable logistic regression analysis for predictive models of sICH in patients with MT.

	OR (95% CI)	P-value
Model 1: without NWU		
Hypertension	3.663 (1.199–11.186)	0.023
Ischemic core volume	1.013 (0.999–1.026)	0.067
Model 2: containing NWU-core		
NWU-core	1.155 (1.027–1.299)	0.016
Hypertension	4.338 (1.330–14.150)	0.015
Ischemic core volume	1.012 (0.998–1.026)	0.091
Model 3: containing NWU-penumbra		
NWU-penumbra	1.442 (1.177–1.766)	<0.001
Hypertension	5.209 (1.466–18.508)	0.011
Ischemic core volume	1.017 (1.000–1.034)	0.052
Model 4: pure imaging biomarkers		
NWU-penumbra	1.412 (1.150–1.735)	0.001
Ischemic core volume	1.017 (1.001–1.033)	0.034

sICH, symptomatic intracranial hemorrhage; MT, mechanical thrombectomy; NWU-core, net water uptake within ischemic core; NWU-penumbra, net water uptake within ischemic penumbra.

Model 1 was built without NWU for subsequent comparison. Model 2 containing NWU-core was adjusted by age, sex, baseline NIHSS score, time from symptom onset to CT. Model 3 containing NWU-penumbra was adjusted by age, sex, baseline NIHSS score, time from symptom onset to CT. Model 4 was a pure imaging predictive model without the adjustment of clinical characteristics. The bold values means $p < 0.1$.

subsequent comparison. Models 2 and 3 included NWU-core and NWU-penumbra separately as they were correlated (Spearman correlation coefficient = 0.555; $P < 0.001$). Model 4 contained only imaging markers. We found that NWU-penumbra (OR = 1.442; 95% CI = 1.177–1.766; $P < 0.001$) and NWU-core (OR = 1.155; 95% CI = 1.027–1.299; $P = 0.016$) were independently associated with sICH after adjustment for age, sex, admission NIHSS score, time from symptom onset to CT, lesion volume, and hypertension. The imaging-only model contained ischemic core volume (OR = 1.017; 95% CI = 1.001–1.033; $P = 0.034$) and NWU-penumbra (OR = 1.412; 95% CI = 1.150–1.735; $P = 0.001$). In patients without MT, only admission NIHSS score (OR = 1.440; 95% CI = 1.055–1.965; $P = 0.022$) was independently associated with sICH.

ROC curve analyses of sICH in patients with MT

With multivariate regression analysis, we discovered that NWU-penumbra and NWU-core were independently associated with sICH in the MT group and built four different predictive models. ROC curve analyses were conducted to test the predictive power of individual variables for models predicting sICH. Figure 3 shows that the area under the curve (AUC) of NWU-penumbra was higher than that of NWU-core

(0.773 vs. 0.673). The diagnostic efficiency of the predictive model was improved with the inclusion of NWU-penumbra (AUC of model 3 vs. model 1 = 0.853 vs. 0.760). The pure imaging predictive model also demonstrated a stable predictive effect (AUC of model 4 = 0.812). It is also noteworthy that NWU-penumbra demonstrated high sensitivity (91.30; 95% CI = 72.0–98.9) in predicting sICH with an optimal cut point of 1.7%. Supplementary Figure 1 shows the illustrative cases for high NWU with sICH vs. low NWU without sICH.

Discussion

In this research, quantitative NWU was used to assess the degree of early post-stroke brain edema within the ischemic core and penumbra separately. We found that NWU-penumbra may have a better value than NWU-core for predicting sICH after MT, and a pure imaging model containing NWU-penumbra and ischemic core volume showed a potential value for predicting sICH after MT independent of clinical variables.

Quantitative NWU, based on admission multimodal CT, has been described as a novel neuroimaging marker of early brain edema (6, 7). The NWU began immediately after AIS with the extravasation of fluid into ischemic tissue through the BBB, which may allow the detection of ionic edema earlier and more sensitively than previous methods (17). Previous studies reported that NWU within the ischemic core was an independent predictor for patients with AIS developing malignant edema (9, 18, 19) and poor neurological outcomes (8, 10). The cerebral ischemic lesion consists of a central irreversible necrotic zone and reversible peripheral ischemic penumbra. One of the main findings in our study was that NWU-penumbra demonstrates better predictive performance than NWU-core on sICH after MT. The most likely mechanisms for this water uptake involve disruption of the BBB caused by cytotoxic edema and angiogenic edema (20, 21). Although speculative, the presence and elevation of early brain edema within the penumbra may indicate a more serious tissue injury and damage expansion. Timely reperfusion can salvage ischemic penumbra but may also aggravate BBB destruction due to reperfusion injury. Tissue edema may compress the small blood vessels, leading to the impairment of microcirculation, which may contribute to vascular endothelial injury and secondary hemorrhage (22). Previous studies indicated that NWU-core was associated with HT within 36 h after successful endovascular treatment (11, 23). In this study, we focused on sICH within 7 days after stroke onset, which was defined as the presence of HT accompanied by clinical deterioration (the NIHSS score increased by more than 4 points from baseline). From a clinical perspective, sICH is strongly related to patient outcomes and often leads to longer hospital stays and more attention from neurologists to optimize treatment strategies, such as reducing intraoperative heparin dosage, avoiding dual antiplatelet, and

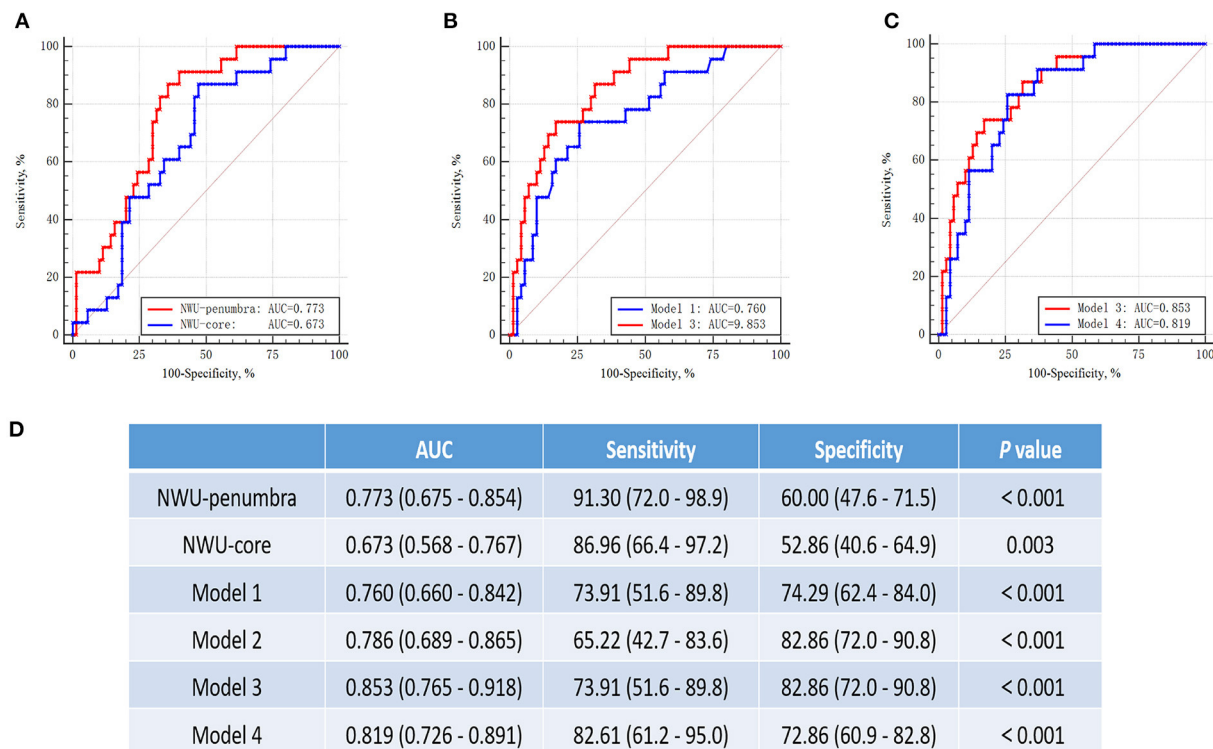


FIGURE 3 ROC curves for prediction of sICH in patients with mechanical thrombectomy. **(A)** The ROC curves of NWU-penumbra vs. NWU-core (AUC: 0.773 vs. 0.673). **(B)** The ROC curves of model 1 vs. model 3 (AUC: 0.760 vs. 0.853). **(C)** The curves of model 3 vs. model 4 (AUC: 0.853 vs. 0.812). **(D)** Table showed the data of ROC curve analysis.

appropriate blood pressure management. This study showed that in patients with AIS without MT, the predictive value of NWU on sICH might be overwhelmed by the admission NIHSS score. This result may be explained by an insufficient number of patients and a comparably low incidence of sICH among patients without MT. Patients who received MT tended to have larger vessel occlusions and had a higher recanalization probability, which may result in more severe reperfusion injury and BBB disruption. The surgery itself can also cause damage to blood vessels.

In this study, we examined several different models for predicting sICH after MT and found that the inclusion of NWU-penumbra significantly improved the predictive power of such models. Importantly, the pure imaging model containing NWU-penumbra and ischemic core volume also showed a stable predictive value for sICH after MT. In most hospitals, CT at admission is the standard care for patients with AIS, with the advantages of being widely and rapidly available and intrinsically quantitative (24). Therefore, compared with other predictors for sICH, such as serum occludin level, interleukin-33, and platelet-to-lymphocyte ratio (25–27), imaging makers would be comparatively simple and practical. A pure imaging model that does not include clinical characteristics may have the potential

to be calculated automatically on the image workstation through deep neural networks (28). In future studies, the imaging model may be served as part of the computer-aided diagnosis systems to screen patients at sICH risk before treatment.

Our study has some limitations. Foremost, is the fact that it was a retrospective and single-center study. Further external validation trials in larger cohorts are required before clinical implementation. Secondly, the incidence of sICH was relatively low in the non-MT group, which may result in insufficient statistical power.

In conclusion, we found that NWU-penumbra had better predictive performance than NWU-core on sICH after MT. The pure imaging model based on admission CT may automatically flag patients with elevated sICH risk. It helps further hypothesis generation to better identify patients at risk of reperfusion injury or parenchymal hemorrhagic transformation in patients undergoing endovascular thrombectomy.

Data availability statement

The raw data supporting the conclusions of this article will be made available by the authors, without undue reservation.

Ethics statement

The studies involving human participants were reviewed and approved by Ningbo First Hospital, Ningbo Hospital of Zhejiang University. The patients/participants provided their written informed consent to participate in this study.

Author contributions

TX: conceptualization, methodology, formal analysis, and writing-original draft. JY: project administration. QH: data curation. YW, YX, and AW: resources. XG, YH, and YX: funding acquisition. MP and LL: validation and writing-review and editing. All authors contributed to the article and approved the submitted version.

Funding

This study was supported by Ningbo Health Branding Subject Fund (PPXK2018-04) and Medicine and Health Science and Technology Projects of Zhejiang Province (2022KY305, 2022KY322, 2019KY162).

Conflict of interest

The authors declare that the research was conducted in the absence of any commercial or financial relationships that could be construed as a potential conflict of interest.

References

- Stokum JA, Gerzanich V, Simard JM. Molecular pathophysiology of cerebral edema. *J Cereb Blood Flow Metab.* (2016) 36:513–38. doi: 10.1177/0271678X15617172
- Mestre H, Du T, Sweeney AM, Liu G, Samson AJ, Peng W, et al. Cerebrospinal fluid influx drives acute ischemic tissue swelling. *Science.* (2020) 367:eaax7171. doi: 10.1126/science.aax7171
- Batley TW, Karki M, Singhal AB, Wu O, Sadaghiani S, Campbell BC, et al. Brain edema predicts outcome after nonlacunar ischemic stroke. *Stroke.* (2014) 45:3643–8. doi: 10.1161/STROKEAHA.114.006884
- Gotoh O, Asano T, Koide T, Takakura K. Ischemic brain edema following occlusion of the middle cerebral artery in the rat. I: the time courses of the brain water, sodium and potassium contents and blood-brain barrier permeability to 125I-albumin. *Stroke.* (1985) 16:101–9. doi: 10.1161/01.STR.16.1.101
- Walberer M, Blaes F, Stolz E, Muller C, Schoenburger M, Tschernatsch M, et al. Midline-shift corresponds to the amount of brain edema early after hemispheric stroke—an MRI study in rats. *J Neurosurg Anesthesiol.* (2007) 19:105–10. doi: 10.1097/ANA.0b013e31802c7e33
- Broocks G, Flottmann F, Ernst M, Faizy TD, Minnerup J, Siemonsen S, et al. Computed tomography-based imaging of voxel-wise lesion water uptake in ischemic brain. *Invest Radiol.* (2018) 53:207–13. doi: 10.1097/RLL.0000000000000430
- Minnerup J, Broocks G, Kalkoffen J, Langner S, Knauth M, Psychogios MN, et al. Computed tomography-based quantification of lesion water uptake identifies

Publisher's note

All claims expressed in this article are solely those of the authors and do not necessarily represent those of their affiliated organizations, or those of the publisher, the editors and the reviewers. Any product that may be evaluated in this article, or claim that may be made by its manufacturer, is not guaranteed or endorsed by the publisher.

Supplementary material

The Supplementary Material for this article can be found online at: <https://www.frontiersin.org/articles/10.3389/fneur.2022.903263/full#supplementary-material>

SUPPLEMENTARY FIGURE 1

Illustrative cases for high NWU with sICH vs. low NWU without sICH. Case 1 (A–C), (A) lesion map, green region represents ischemic penumbra and red represents ischemic core. (B) NCCT with hand-drawn ROI, NWU-core = 4.8%, NWU-penumbra = –0.5%. (C) Follow-up CT didn't indicate ICH. Case 2 (D–F), (D) lesion map, green region represents ischemic penumbra and red represents ischemic core. (E) NCCT with hand-drawn ROI, NWU-core = 11.3%, NWU-penumbra = 5.1%. (F) Follow-up CT indicates parenchymatous hematoma in the basal ganglia.

SUPPLEMENTARY TABLE 1

Patient's demographics of group MT vs. non-MT.

SUPPLEMENTARY TABLE 2

Univariate logistic regression analysis for risks of NWU-core and NWU-penumbra on different types of HT.

patients within 4.5 hours of stroke onset: a multicenter observational study. *Ann Neurol.* (2016) 80:924–34. doi: 10.1002/ana.24818

8. Broocks G, Kemmling A, Tessarek S, McDonough R, Meyer L, Faizy TD, et al. Quantitative lesion water uptake as stroke imaging biomarker: a tool for treatment selection in the extended time window? *Stroke.* (2022) 53:201–9. doi: 10.1161/STROKEAHA.120.033025

9. Broocks G, Flottmann F, Scheibel A, Aigner A, Faizy TD, Hanning U, et al. Quantitative lesion water uptake in acute stroke computed tomography is a predictor of malignant infarction. *Stroke.* (2018) 49:1906–12. doi: 10.1161/STROKEAHA.118.020507

10. Nawabi J, Flottmann F, Kemmling A, Knip H, Leischner H, Sporns P, et al. Elevated early lesion water uptake in acute stroke predicts poor outcome despite successful recanalization – when “tissue clock” and “time clock” are desynchronized. *Int J Stroke.* (2021) 16:863–72. doi: 10.1177/1747493019884522

11. Nawabi J, Knip H, Schön G, Flottmann F, Leischner H, Kabiri R, et al. Hemorrhage after endovascular recanalization in acute stroke: lesion extent, collaterals and degree of ischemic water uptake mediate tissue vulnerability. *Front Neurol.* (2019) 10:569. doi: 10.3389/fneur.2019.00569

12. Henry M, Bruce C, Mark P, Leonid C, Christopher L, Chung H, et al. Thrombolysis guided by perfusion imaging up to 9 hours after onset of stroke. *N Engl J Med.* (2019) 380:1795–803. doi: 10.1056/NEJMoa1813046

13. Fugate JE, Klunder AM, Kallmes DF. What is meant by “tici”? *AJNR Am J Neuroradiol.* (2013) 34:1792–7. doi: 10.3174/ajnr.A3496

14. Hacke W, Kaste M, Fieschi C, von Kummer R, Davalos A, Meier D, et al. Randomised double-blind placebo-controlled trial of thrombolytic therapy with intravenous alteplase in acute ischaemic stroke (ecass ii). Second european-australasian acute stroke study investigators. *Lancet*. (1998) 352:1245–51. doi: 10.1016/S0140-6736(98)08020-9
15. Berger C, Fiorelli M, Steiner T, Schabitz WR, Bozzao L, Bluhmki E, et al. Hemorrhagic transformation of ischemic brain tissue: asymptomatic or symptomatic? *Stroke*. (2001) 32:1330–5. doi: 10.1161/01.STR.32.6.1330
16. Lin L, Bivard A, Krishnamurthy V, Levi CR, Parsons MW. Whole-brain ct perfusion to quantify acute ischemic penumbra and core. *Radiology*. (2016) 279:876–87. doi: 10.1148/radiol.2015150319
17. Simard JM, Kent TA, Chen M, Tarasov KV, Gerzanich V. Brain oedema in focal ischaemia: molecular pathophysiology and theoretical implications. *Lancet Neurol*. (2007) 6:258–68. doi: 10.1016/S1474-4422(07)70055-8
18. Shi J, Wu H, Dong Z, Liang X, Liu Q, Zhu W, et al. Automated quantitative lesion water uptake in acute stroke is a predictor of malignant cerebral edema. *Eur Radiol*. (2022) 32:2771–80. doi: 10.1007/s00330-021-08443-2
19. Gabriel B, Sarah E, Helge K, Andre K, Fabian F, Matthias B, et al. Early prediction of malignant cerebellar edema in posterior circulation stroke using quantitative lesion water uptake. *Neurosurgery*. (2021) 88:531–37. doi: 10.1093/neuros/nyaa438
20. Okada T, Suzuki H, Travis ZD, Zhang JH. The stroke-induced blood-brain barrier disruption: current progress of inspection technique, mechanism, and therapeutic target. *Curr Neuropharmacol*. (2020) 18:1187–212. doi: 10.2174/1570159X18666200528143301
21. Bernardo-Castro S, Sousa JA, Bras A, Cecilia C, Rodrigues B, Almendra L, et al. Pathophysiology of blood-brain barrier permeability throughout the different stages of ischemic stroke and its implication on hemorrhagic transformation and recovery. *Front Neurol*. (2020) 11:594672. doi: 10.3389/fneur.2020.594672
22. Ng FC, Churilov L, Yassi N, Kleinig TJ, Thijs V, Wu TY, et al. Microvascular dysfunction in blood-brain barrier disruption and hypoperfusion within the infarct posttreatment are associated with cerebral edema. *Stroke*. (2021) 53:1597–605. doi: 10.1161/STROKEAHA.121.036104
23. Nawabi J, Elsayed S, Scholz H, Kemmling A, Meyer L, Knierp H, et al. Interaction effect of baseline serum glucose and early ischemic water uptake on the risk of secondary hemorrhage after ischemic stroke. *Front Neurol*. (2021) 12:690193. doi: 10.3389/fneur.2021.690193
24. Watanabe O, West CR, Bremer A. Experimental regional cerebral ischemia in the middle cerebral artery territory in primates. Part 2: effects on brain water and electrolytes in the early phase of mca stroke. *Stroke*. (1977) 8:71–6. doi: 10.1161/01.STR.8.1.71
25. Yuan S, Li W, Hou C, Kang H, Ma Q, Ji X, et al. Serum occludin level combined with nihss score predicts hemorrhage transformation in ischemic stroke patients with reperfusion. *Front Cell Neurosci*. (2021) 15:714171. doi: 10.3389/fncel.2021.714171
26. Yang Y, Xie D, Zhang Y. Increased platelet-to-lymphocyte ratio is an independent predictor of hemorrhagic transformation and in-hospital mortality among acute ischemic stroke with large-artery atherosclerosis patients. *Int J Gen Med*. (2021) 14:7545–55. doi: 10.2147/IJGM.S329398
27. Chen Z, Hu Q, Huo Y, Zhang R, Fu Q, Qin X. Serum interleukin-33 is a novel predictive biomarker of hemorrhage transformation and outcome in acute ischemic stroke. *J Stroke Cerebrovasc Dis*. (2021) 30:105506. doi: 10.1016/j.jstrokecerebrovasdis.2020.105506
28. Nowinski WL, Gupta V, Qian G, He J, Poh LE, Ambrosius W, et al. Automatic detection, localization, and volume estimation of ischemic infarcts in noncontrast computed tomographic scans: method and preliminary results. *Invest Radiol*. (2013) 48:661–70. doi: 10.1097/RLI.0b013e31828d8403



OPEN ACCESS

EDITED BY

Sheng Zhang,
Zhejiang Provincial People's
Hospital, China

REVIEWED BY

Xiaofeng Deng,
Capital Medical University, China
Yizheng Yao,
Harvard Medical School, United States

*CORRESPONDENCE

Guoyi Gao
gao3@sina.com

SPECIALTY SECTION

This article was submitted to
Applied Neuroimaging,
a section of the journal
Frontiers in Neurology

RECEIVED 27 March 2022

ACCEPTED 18 July 2022

PUBLISHED 25 August 2022

CITATION

Liu J, Shan Y and Gao G (2022) The
application value of CT radiomics
features in predicting pressure
amplitude correlation index in patients
with severe traumatic brain injury.
Front. Neurol. 13:905655.
doi: 10.3389/fneur.2022.905655

COPYRIGHT

© 2022 Liu, Shan and Gao. This is an
open-access article distributed under
the terms of the [Creative Commons
Attribution License \(CC BY\)](https://creativecommons.org/licenses/by/4.0/). The use,
distribution or reproduction in other
forums is permitted, provided the
original author(s) and the copyright
owner(s) are credited and that the
original publication in this journal is
cited, in accordance with accepted
academic practice. No use, distribution
or reproduction is permitted which
does not comply with these terms.

The application value of CT radiomics features in predicting pressure amplitude correlation index in patients with severe traumatic brain injury

Jiaqi Liu², Yingchi Shan¹ and Guoyi Gao^{1*}

¹Department of Neurosurgery, Shanghai General Hospital, Shanghai Jiao Tong University School of Medicine, Shanghai, China, ²Department of Plastic and Reconstructive Surgery, Shanghai 9th People's Hospital, Shanghai Jiao Tong University School of Medicine, Shanghai, China

Purpose: To explore the application value of a machine learning model based on CT radiomics features in predicting the pressure amplitude correlation index (RAP) in patients with severe traumatic brain injury (sTBI).

Methods: Retrospectively analyzed the clinical and imaging data in 36 patients with sTBI. All patients underwent surgical treatment, continuous ICP monitoring, and invasive arterial pressure monitoring. The pressure amplitude correlation index (RAP) was collected within 1 h after surgery. Three volume of interest (VOI) was selected from the craniocerebral CT images of patients 1 h after surgery, and a total of 93 radiomics features were extracted from each VOI. Three models were established to be used to evaluate the patients' RAP levels. The accuracy, precision, recall rate, F1 score, receiver operating characteristic (ROC) curve, and area under the curve (AUC) were used to evaluate the predictive performance of each model.

Results: The optimal number of features for three predicting models of RAP was five, respectively. The accuracy of predicting the model of the hippocampus was 77.78%, precision was 88.24%, recall rate was 60%, the F1 score was 0.6, and AUC was 0.88. The accuracy of predicting the model of the brainstem was 63.64%, precision was 58.33%, the recall rate was 60%, the F1 score was 0.54, and AUC was 0.82. The accuracy of predicting the model of the thalamus was 81.82%, precision was 88.89%, recall rate was 75%, the F1 score was 0.77, and AUC was 0.96.

Conclusions: CT radiomics can predict RAP levels in patients with sTBI, which has the potential to establish a method of non-invasive intracranial pressure (NI-ICP) monitoring.

KEYWORDS

traumatic brain injuries, intracranial pressure, computed tomography, non-invasive evaluation, texture features

Introduction

Traumatic brain injuries (TBI) are a type of trauma with high morbidity, disability, and mortality rates (1). Currently, the treatment of patients with TBI is based on surgery combined with neurological intensive care (2, 3). Intensive care treatment is a very important part of the patient's treatment process, in which intracranial pressure (ICP) monitoring is necessary for neurocritical care treatment (3). In clinical work, ICP monitoring alone does not provide comprehensive information about the patient's intracranial pressure, and its derived parameters such as the relationship of amplitude and pressure (RAP) can more comprehensively and objectively reflect the patient's ICP level (4, 5). The RAP can reflect the changes in the ICP level of patients more comprehensively and objectively, which can assist physicians to make decisions and adjustments in patient treatment and to implement individualized medical treatment precisely (6).

The implementation of ICP monitoring relies on the surgical placement of an intracranial pressure monitoring probe, which is not yet in line with modern neurosurgery's pursuit of speed, accuracy, and efficiency. CT scanning is one of the most popular imaging techniques used in neurosurgery, and is fast, non-invasive, and efficient, thus playing a key role in neurosurgical care. In the past, clinicians used CT images to interpret the degree of displacement of intracranial structures to assess the ICP level of patients, but this method lacks theoretical support. The essence of this study is to obtain high-throughput, quantitative imaging features from CT images, filter the features, and build a reasonable prediction model through machine learning. The aim of this study is to explore the relationship between CT imaging histological features and RAP in patients with TBI, so as to reveal whether building a machine learning model based on CT imaging histological features can objectively and in real-time reflect ICP-related parameters of patients, and to explore the clinical application value of this machine learning model for realizing non-invasive ICP monitoring.

Materials and methods

Study design and setting

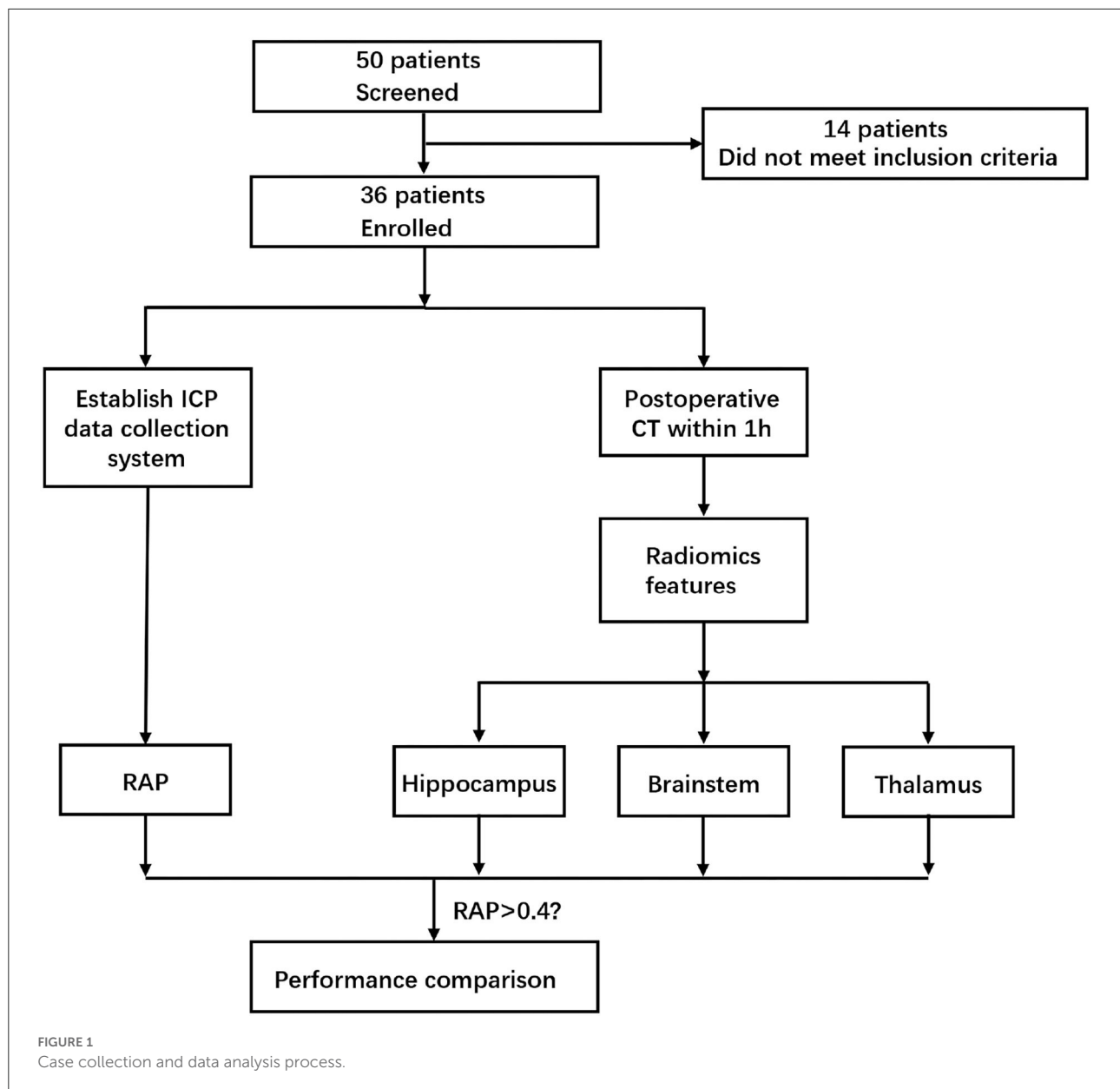
Clinical data of patients with sTBI admitted to the Department of Neurosurgery, Shanghai General Hospital from January 2019 to December 2020 were collected and analyzed. Inclusion criteria were as follows: (1) emergency admission due to closed craniocerebral injury with a clear history of trauma; (2) older than 18 years of age, younger than 65 years of age, regardless of gender; (3) received invasive ICP monitoring; (4) cranial CT was reviewed within 1 h after surgery. Exclusion criteria were as follows: (1) patients with a history of traumatic brain injury, cerebral infarction, brain tumor, or

other neurological diseases or cranial surgical interventions that might result in an abnormal anatomical structure; (2) with previous coagulopathy and blood system related diseases. The study protocol conformed to the ethical guidelines of the Declaration of Helsinki, and this study was approved by the Ethics Committee of Shanghai General Hospital, Shanghai Jiao Tong University School of Medicine. Participants' right to know was fully guaranteed and indicated in the ethical approval document.

Data sources and measurements

In addition to the baseline characteristics, we mainly collected and analyzed the cranial CT after the surgery and the RAP value recorded by a Neumatic data collector (a machine that could analyze the waveform of intracranial pressure). The CT-related features were acquired from the Digital Imaging and Communications in Medicine (DICOM) file of the last cranial CT before ICP monitoring using a 64-slice spiral CT machine (General Electric Medical Systems, USA). As per the routine protocol of a CT scan, the CT slices were parallel to the orbitomeatal plane from the foramen magnum to the vertex. The scanning slice thickness was 1 mm. Patients were returned to ICU after surgery. Radial artery puncture was performed in all patients, the arterial indwelling needle was connected to the baroreceptor, and the baroreceptor was connected to the bedside monitor, for continuous invasive arterial pressure monitoring. Finally, the Neumatic data collector was connected to the bedside monitor through a network cable port to collect real-time intracranial pressure-related parameters. All RAP data collected within 1 h after the start of monitoring (monitoring sampling frequency is 3 s, a total of 1,200 data in 1 h) were recorded, and the mean value of RAP was calculated as the analysis index.

After obtaining the patient's CT scan within 1 h postoperatively, three VOI with the size of $5 \times 5 \times 5$ mm were extracted from the hippocampal gyrus, brainstem, and thalamus of the injured side by pydicom module in the Python 3.8. At the same time, the radiomics module was used to extract 93 radiomics features in these three VOIs, respectively. Next, we performed feature selection based on SHAP values. SHAP value could be used to measure the contribution of each feature in the model to the prediction results. By calculating SHAP, the ranking of the importance of features in the model could be obtained, and the top five important features are selected as the analysis index. Finally, according to the features selected for three VOI, three random forest models were established to evaluate the RAP level of patients. According to previous studies, $RAP > 0.4$ was considered to be an indicator of poor prognosis. In this study, 0.4 was used as the threshold value, and the dichotomous judgment was made with RAP. The whole research process is shown in Figure 1.



Statistical analysis

Python 3.8 was used for the statistical analysis of the data. Numpy module and Pandas module were used for data operation and sorting, SHAP module was used for feature selection, RandomForestClassifier module of Sklearn was used for the model establishment, and the Matplotlib module is used for drawing. Continuous variables subject to normal distribution were expressed as the mean (M) \pm SD, continuous variables not subject to normal distribution were expressed as the median and interquartile range (IQR), and categorical variables were expressed as the frequency and percentage. Accuracy, precision, recall, and F1 score were used to evaluate

the performance of each model. The area under the receiver operator characteristic (ROC) curve was used in all four models to assess discrimination.

Results

From January 2019 to December 2020, a total of 36 patients with sTBI were included in this study, among which 25 were men (69.44%) and 11 were women (30.56%). Participants were between 18 and 65 years old, and the median age was 47 (IQR: 29–54) years old. The median Glasgow Coma Score (GCS) was 6 (IQR: 4–7) at the time of emergency admission;

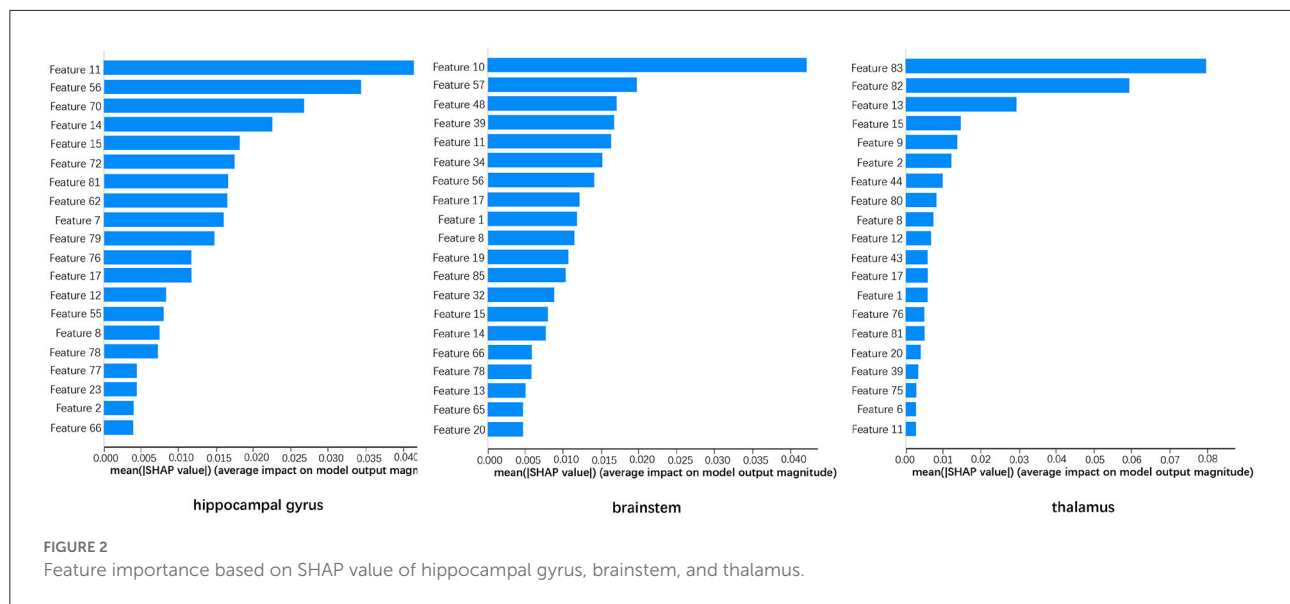


TABLE 1 RAP and selected radiomics features.

Patients with sTBI (<i>n</i> = 36)	
RAP	0.24 (−0.02–0.51)
>0.4	9 (25%)
Hippocampus (5 features)	
Minimum	14 (12–16)
Root Mean Squared	35.5732 (34.0433–37.6606)
Skewness	−0.0832 (−0.1991–0.0401)
Small dependence low gray level emphasis	0.0096 (0.0079–0.0117)
Short run emphasis	0.4424 (0.3950–0.4832)
Brainstem (5 features)	
Median	31 (29–33)
Minimum	10 (8–12)
Maximum probability	0.7005 (0.5994–0.8129)
Gray level variance	0.1452 (0.0966–0.1861)
Gray level non-uniformity	125.6637 (118.9920–130.9465)
Thalamus (5 features)	
Mean	34.4850 (32.8150–35.5325)
Robust mean absolute deviation	3.7269 (3.3536–3.9609)
Skewness	−0.1189 (−0.2629–0.1033)
Size zone non-uniformity normalized	0.2234 (0.1878–0.2800)
Small area emphasis	0.3710 (0.2771–0.4710)

27 patients (75%) had an abnormal light reflex in one or both pupils up-on arrival, among which postoperative pupil shrinkage was observed in 14 patients (51.85%). The order of feature importance based on the SHAP value is shown in Figure 2. Selected features of three VOI and collected RAP data was shown in Table 1.

TABLE 2 Performance of models based on textural features and morphological features.

	Hippocampus	Brainstem	Thalamus
Accuracy	77.78%	63.64%	81.82%
Precision	88.24%	58.33%	88.89%
Recall	60.00%	55.36%	75.00%
F1 Score	0.60	0.54	0.77
AUC	0.88	0.82	0.96

The optimal number of features for three predicting models of RAP was 5, respectively. The accuracy of predicting the model of the hippocampus was 77.78%, precision was 88.24%, the recall rate was 60%, the F1 score was 0.6, and AUC was 0.88. The accuracy of predicting the model of the brainstem was 63.64%, precision was 58.33%, the recall rate was 60%, the F1 score was 0.54, AUC was 0.82. The accuracy of predicting model of the thalamus was 81.82%, precision was 88.89%, the recall rate was 75%, the F1 score was 0.77, AUC was 0.96. These three models all had strong prediction ability and the model of the thalamus has the strongest prediction ability in discriminating RAP. The performance of three models in predicting RAP level is shown in Table 2 and Figure 3.

Discussion

This study retrospectively analyzed the CT images of patients with sTBI after operation treatment, conducted texture analysis, established three models to predict the RAP level according to the textural features obtained from selected morphological structure, and compared them with

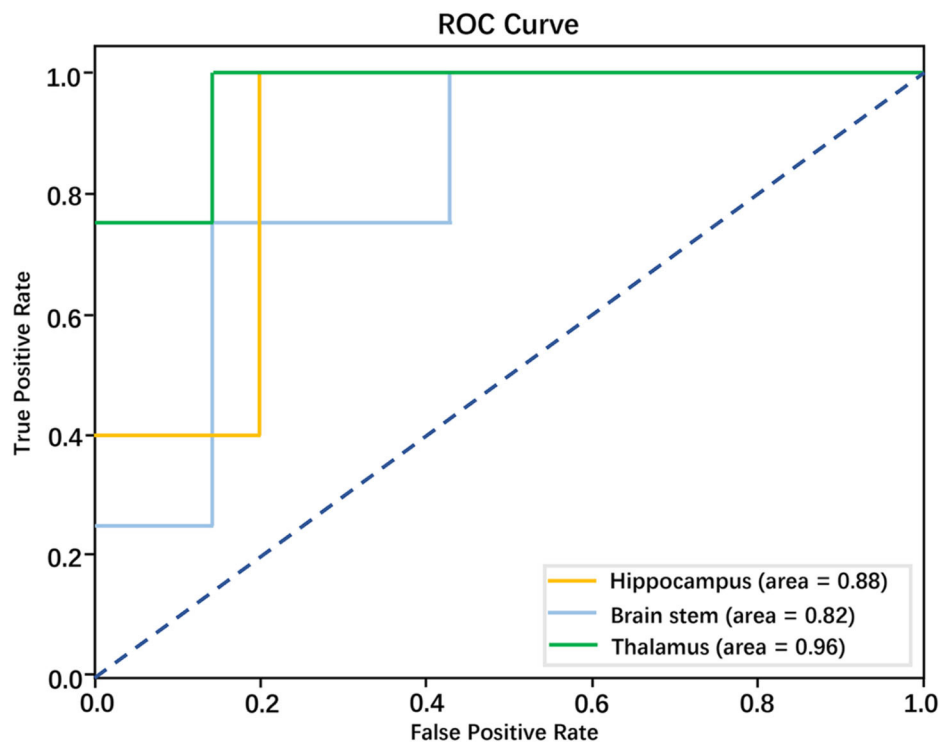


FIGURE 3
Performance of models based on radiomics features in discriminating RAP level; the AUCs for these models were 0.88, 0.82, and 0.96, respectively.

invasive ICP (I-ICP) monitoring. The results showed that three models all had strong prediction ability for the RAP level of patients with sTBI, the model of the thalamus has the strongest prediction ability in discriminating RAP. All of these results show CT radiomics has the potential to establish a method of non-invasive intracranial pressure (NI-ICP) monitoring.

Elevated ICP is the main pathophysiological change in patients with sTBI and the main cause of irreversible damage to brain function (7, 8). Early post-injury monitoring of sTBI patients with ICP and aggressive interventions based on changes are effective ways to reduce the mortality and disability rates (9, 10). Current ICP monitoring techniques are invasive and require the placement of ICP monitoring probes inside the patient's skull, which can lead to complications such as infection and bleeding (11, 12). Sometimes the time window for implantation of the ICP monitoring probe in the body does not meet the treatment needs, and monitoring has to be terminated to avoid the occurrence of infection, and the ICP monitoring needs for subsequent treatment cannot be met (13, 14). But, there is no established NI-ICP monitoring method that can serve as an alternative to the gold standards of I-ICP monitoring. To solve the above problems, Oliver et al. (15) evaluated a

new method of NI-ICP monitoring performed using algorithms to determine ICP based on acoustic properties of the brain. Bernhard et al. (16) attempted non-invasive assessment of ICP by using cerebral blood flow velocity (CBFV) and arterial blood pressure (ABP) based on a mathematical model. Andersen et al. propose a method to assess ICP by using retinal arteriole and venule diameter ratio (A/V-ratio), A/V-ratio can be measured using fundus photography, they correlated changes in the intracranial pressure with the diameter of vessels of the retina (17). However, none of these programs have been widely promoted in clinical practice. Although ICP monitoring is more than half a century old and its application techniques have changed considerably in the process, it still has a lot of space for improvement in itself compared to the development of other scientific advances.

With the increased awareness of the concept of non-invasive, more and more protocols are being proposed, among which the CT image-based ICP evaluation is the most superior (18). CT is usually the front-line imaging approach in sTBI (18, 19). In the past, the analysis of CT images was limited to the interpretation of structural information, despite the widespread use of CT, their diagnostic accuracy for detection of elevated ICP and their correlation with ICP measurement

are unknown. The analysis of CT texture features provides a perspective for establishing relevant assessment criteria and monitoring techniques (20). The morphological structural information alone is interpreted with a serious subjective bias (21). Texture features are quantifiable and can be analyzed to make abstract ICP monitoring data concrete, and provide a more objective basis for their interpretation. Here we analyzed texture features and then statistically integrated them to form a machine learning model to predict RAP in patients with sTBI. This is a complement to traditional machine learning models for predicting ICP and fills the gap in the direction of ICP-related parameter prediction by machine learning models.

The main damage after sTBI occurs is the destruction of important intracranial structures and functions (22). On top of these primary injuries, secondary injuries due to cerebral edema and hematoma further aggravate the damage to brain tissue and lead to deterioration of the condition. In our study, three important intracranial structures were selected for VOI extraction features to build models, in an attempt to fully explore the ability of CT imaging histology in machine learning to predict RAP. Among the three models, the thalamic model has the strongest predictive power, and we analyzed the reasons for this: (1) the thalamic structure is located in the deep part of the brain tissue, and its deformation and CT value changes are less subject to pressure changes, (2) the structural morphology of the thalamus is stable and is an ideal reservoir for texture feature extraction, and (3) the dense blood supply and blood flow in the thalamus are uniform. The above features are more universal in feature extraction and can fully reflect the internal changes of brain tissue. Building a machine learning model based on texture analysis for RAP capability is fully described in our study, while the feasibility of non-invasive ICP monitoring options can continue to be explored in future studies based on the above model. This provides potential options for the successful implementation of non-invasive ICP monitoring.

However, this study also had some limitations. Firstly, the number of cases is low. Secondly, studies focus on a single craniocerebral trauma type. Thirdly, retrospective patient past history should be considered in the study. The above issues will be addressed in subsequent studies, and further work will focus on expanding the capacity of the database and joint multicenter collaboration. The methods of CT impact histology quantification should be improved and more detailed and standardized criteria should be developed to fully take into account the impact of inter-case variation on the study, which should be assessed by a more sophisticated learning model.

Conclusions

In summary, the machine learning model based on texture feature analysis was constructed to be able to predict the RAP of patients with sTBI. At the same time, the construction of such analysis and prediction models has application value and facilitation to achieving non-invasive ICP monitoring.

Data availability statement

The original contributions presented in the study are included in the article/supplementary material, further inquiries can be directed to the corresponding author.

Ethics statement

The studies involving human participants were reviewed and approved by Ethics Committee of Shanghai General Hospital. The patients/participants provided their written informed consent to participate in this study. The animal study was reviewed and approved by Ethics Committee of Shanghai General Hospital.

Author contributions

JL, YS, and GG conceived the study. GG supervised and coordinated all aspects of the work and acquired the funding and administrated the project. JL and YS collected and analyzed the data and wrote the paper. All authors contributed to the article and approved the submitted version.

Conflict of interest

The authors declare that the research was conducted in the absence of any commercial or financial relationships that could be construed as a potential conflict of interest.

Publisher's note

All claims expressed in this article are solely those of the authors and do not necessarily represent those of their affiliated organizations, or those of the publisher, the editors and the reviewers. Any product that may be evaluated in this article, or claim that may be made by its manufacturer, is not guaranteed or endorsed by the publisher.

References

- Galgano M, Toshkezi G, Qiu X, Russell T, Chin L, Zhao LR. Traumatic brain injury: current treatment strategies and future endeavors. *Cell Transplant.* (2017) 26:1118–30. doi: 10.1177/0963689717714102
- Jiang JY, Gao GY, Feng JF, Mao Q, Chen LG, Yang XF, et al. Traumatic brain injury in China. *Lancet Neurol.* (2019) 18:286–95. doi: 10.1016/S1474-4422(18)30469-1
- Rakhit S, Nordness MF, Lombardo SR, Cook M, Smith L, Patel MB. Management and challenges of severe traumatic brain injury. *Semin Respir Crit Care Med.* (2021) 42:127–44. doi: 10.1055/s-0040-1716493
- Pan Y, Xue Y, Zhao P, Ding J, Ren Z, Xu J. Significance of ICP-related parameters for the treatment and outcome of severe traumatic brain injury. *J Int Med Res.* (2020) 48:300060520941291. doi: 10.1177/0300060520941291
- Jin SC, Choi BS, Kim JS. The RAP Index during intracranial pressure monitoring as a clinical guiding for surgically treated aneurysmal subarachnoid hemorrhage: consecutive series of single surgeon. *Acute Crit Care.* (2019) 34:71–8. doi: 10.4266/acc.2019.00437
- Hall A, O'Kane R. The best marker for guiding the clinical management of patients with raised intracranial pressure-the RAP index or the mean pulse amplitude? *Acta Neurochir.* (2016) 158:1997–2009. doi: 10.1007/s00701-016-2932-z
- Schaller B. Craniocerebral trauma—new pathophysiological and therapeutic viewpoints. 1: Management of the acute phase. *Swiss Surg.* (2002) 8:123–37. doi: 10.1024/1023-9332.8.4.145
- Potapov AA, Zakharova NE, Pronin IN, Kornienko VN, Gavrilov AG, Kravchuk AD, et al. Prognostic value of ICP, CPP and regional blood flow monitoring in diffuse and focal traumatic cerebral lesions. *Zh Vopr Neurokhir Im N N Burdenko.* (2011) 75:3–16.
- Alarcon JD, Rubiano AM, Okonkwo DO, Alarcon J, Martinez-Zapata MJ, Urrutia G, et al. Elevation of the head during intensive care management in people with severe traumatic brain injury. *Cochrane Database Syst Rev.* (2017) 12:CD009986. doi: 10.1002/14651858.CD009986.pub2
- Pedersen SH, Lilja-Cyron A, Astrand R, Juhler M. Monitoring and measurement of intracranial pressure in pediatric head trauma. *Front Neurol.* (2019) 10:1376. doi: 10.3389/fneur.2019.01376
- Tariq A, Aguilar-Salinas P, Hanel RA, Naval N, Chmayssani M. The role of ICP monitoring in meningitis. *Neurosurg Focus.* (2017) 43:E7. doi: 10.3171/2017.8.FOCUS17419
- Zhang X, Medow JE, Iskandar BJ, Wang F, Shokouinejad M, Koueik J, et al. Invasive and noninvasive means of measuring intracranial pressure: a review. *Physiol Meas.* (2017) 38:R143–R82. doi: 10.1088/1361-6579/aa7256
- Hawryluk GWJ, Aguilera S, Buki A, Bulger E, Citerio G, Cooper DJ, et al. A management algorithm for patients with intracranial pressure monitoring: the Seattle international severe traumatic brain injury consensus conference (SIBICC). *Intensive Care Med.* (2019) 45:1783–94. doi: 10.1007/s00134-019-05805-9
- Chesnut R, Aguilera S, Buki A, Bulger E, Citerio G, Cooper DJ, et al. A management algorithm for adult patients with both brain oxygen and intracranial pressure monitoring: the Seattle INTERNATIONAL SEVERE TRAUMATIC BRAIN INJURY CONSENSUS CONFERENCE (SIBICC). *Intensive Care Med.* (2020) 46:919–29. doi: 10.1007/s00134-019-05900-x
- Ganslandt O, Mourtzoukos S, Stadlbauer A, Sommer B, Rammensee R. Evaluation of a novel noninvasive ICP monitoring device in patients undergoing invasive ICP monitoring: preliminary results. *J Neurosurg.* (2018) 128:1653–60. doi: 10.3171/2016.11.JNS152268
- Schmidt B, Klingelhofer J, Perkes I, Czosnyka M. Cerebral autoregulatory response depends on the direction of change in perfusion pressure. *J Neurotrauma.* (2009) 26:651–6. doi: 10.1089/neu.2008.0784
- Andersen MS, Pedersen CB, Poulsen FR, A. A new novel method for assessing intracranial pressure using non-invasive fundus images: a pilot study. *Sci Rep.* (2020) 10:13062. doi: 10.1038/s41598-020-70084-0
- Brossard C, Lemasson B, Attie A, de Busschere JA, Payen JF, Barbier EL, et al. Contribution of CT-scan analysis by artificial intelligence to the clinical care of TBI patients. *Front Neurol.* (2021) 12:666875. doi: 10.3389/fneur.2021.666875
- Mutch CA, Talbott JF, Gean A. Imaging evaluation of acute traumatic brain injury. *Neurosurg Clin N Am.* (2016) 27:409–39. doi: 10.1016/j.nec.2016.05.011
- Dhar R, Sandler RH, Manwaring K, Kostick N, Mansy HA. Noninvasive detection of elevated ICP using spontaneous tympanic membrane pulsation. *Sci Rep.* (2021) 11:21957. doi: 10.1038/s41598-021-01079-8
- Chen W, Belle A, Cockrell C, Ward KR, Najarian K. Automated midline shift and intracranial pressure estimation based on brain CT images. *J Vis Exp.* (2013). doi: 10.3791/3871
- Mira RG, Lira M, Cerpa W. Traumatic brain injury: mechanisms of glial response. *Front Physiol.* (2021) 12:740939. doi: 10.3389/fphys.2021.740939



OPEN ACCESS

EDITED BY

Chengcheng Zhu,
University of Washington,
United States

REVIEWED BY

Alvin S. Das,
Massachusetts General Hospital and
Harvard Medical School, United States
Laura Lull,
Hospital Clinic of Barcelona, Spain

*CORRESPONDENCE

Praneeta Konduri
p.r.konduri@amsterdamumc.nl

SPECIALTY SECTION

This article was submitted to
Stroke,
a section of the journal
Frontiers in Neurology

RECEIVED 24 June 2022

ACCEPTED 01 September 2022

PUBLISHED 05 October 2022

CITATION

Konduri P, Buckner A, Boers A, Dutra B,
Samuels N, Treurniet K, Berkhemer O,
Yoo A, van Zwam W, van
Oostenbrugge R, van der Lugt A,
Dippel D, Roos Y, Bot J, Majoie C,
Marquering H and the MR CLEAN Trial
Investigators (Multicenter Randomized
Clinical Trial of Endovascular
Treatment for Acute Ischemic Stroke in
the Netherlands) (2022) Risk factors of
late lesion growth after acute ischemic
stroke treatment.
Front. Neurol. 13:977608.
doi: 10.3389/fneur.2022.977608

COPYRIGHT

© 2022 Konduri, Buckner, Boers, Dutra,
Samuels, Treurniet, Berkhemer, Yoo,
van Zwam, van Oostenbrugge, van der
Lugt, Dippel, Roos, Bot, Majoie,
Marquering and the MR CLEAN Trial
Investigators (Multicenter Randomized
Clinical Trial of Endovascular
Treatment for Acute Ischemic Stroke in
the Netherlands). This is an
open-access article distributed under
the terms of the [Creative Commons
Attribution License \(CC BY\)](#). The use,
distribution or reproduction in other
forums is permitted, provided the
original author(s) and the copyright
owner(s) are credited and that the
original publication in this journal is
cited, in accordance with accepted
academic practice. No use, distribution
or reproduction is permitted which
does not comply with these terms.

Risk factors of late lesion growth after acute ischemic stroke treatment

Praneeta Konduri^{1,2*}, Amber Buckner³, Anna Boers^{1,4},
Bruna Dutra^{1,2}, Noor Samuels^{5,6,7}, Kilian Treurniet^{2,8},
Olvert Berkhemer^{2,5,6}, Albert Yoo⁹, Wim van Zwam¹⁰,
Robert van Oostenbrugge¹¹, Aad van der Lugt⁵,
Diederik Dippel⁶, Yvo Roos¹², Joost Bot¹³, Charles Majoie²,
Henk Marquering^{1,2} and the MR CLEAN Trial Investigators
(Multicenter Randomized Clinical Trial of Endovascular
Treatment for Acute Ischemic Stroke in the Netherlands)

¹Department of Biomedical Engineering and Physics, Amsterdam UMC, Location AMC, Amsterdam, Netherlands, ²Department of Radiology and Nuclear Medicine, Amsterdam UMC, Location AMC, Amsterdam, Netherlands, ³Department of Radiology, University Medical Center Groningen, Groningen, Netherlands, ⁴Nico-Lab, Amsterdam, Netherlands, ⁵Department of Radiology and Nuclear Medicine, Erasmus MC, University Medical Center, Rotterdam, Netherlands, ⁶Department of Neurology, Erasmus MC University Medical Center, Rotterdam, Netherlands, ⁷Department of Public Health, Erasmus MC, University Medical Center, Rotterdam, Netherlands, ⁸Department of Radiology, Haaglanden Medisch Centrum, The Hague, Netherlands, ⁹Department of Radiology, Texas Stroke Institute, Dallas-Fort Worth, Dallas, TX, United States, ¹⁰Department of Radiology and Nuclear Medicine, Maastricht University Medical Center and Cardiovascular Research Institute Maastricht (CARIM), Maastricht, Netherlands, ¹¹Department of Neurology, Maastricht University Medical Center and Cardiovascular Research Institute Maastricht (CARIM), Maastricht, Netherlands, ¹²Department of Neurology, Amsterdam UMC, Location AMC, Amsterdam, Netherlands, ¹³Department of Radiology and Nuclear Medicine, Amsterdam UMC, Vrije Universiteit van Amsterdam, Amsterdam, Netherlands

Background: Even days after treatment of acute ischemic stroke due to a large vessel occlusion, the infarct lesion continues to grow. This late, subacute growth is associated with unfavorable functional outcome. In this study, we aim to identify patient characteristics that are risk factors of late, subacute lesion growth.

Methods: Patients from the MR CLEAN trial cohort with good quality 24h and 1-week follow up non-contrast CT scans were included. Late Lesion growth was defined as the difference between the ischemic lesion volume assessed after 1-week and 24-h. To identify risk factors, patient characteristics associated with lesion growth (categorized in quartiles) in univariable ordinal analysis ($p < 0.1$) were included in a multivariable ordinal regression model.

Results: In the 226 patients that were included, the median lesion growth was 22 (IQR 10–45) ml. In the multivariable model, lower collateral capacity [aOR: 0.62 (95% CI: 0.44–0.87); $p = 0.01$], longer time to treatment [aOR: 1.04 (1–1.08); $p = 0.04$], unsuccessful recanalization [aOR: 0.57 (95% CI: 0.34–0.97); $p = 0.04$], and larger midline shift [aOR: 1.18 (95% CI: 1.02–1.36); $p = 0.02$] were associated with late lesion growth.

Conclusion: Late, subacute, lesion growth occurring between 1 day and 1 week after ischemic stroke treatment is influenced by lower collateral capacity, longer time to treatment, unsuccessful recanalization, and larger midline shift. Notably, these risk factors are similar to the risk factors of acute lesion growth, suggesting that understanding and minimizing the effects of the predictors for late lesion growth could be beneficial to mitigate the effects of ischemia.

KEYWORDS

risk factors, predictors, post-treatment, subacute, lesion evolution, infarct growth, acute ischemic stroke

Introduction

Treatment of acute ischemic stroke (AIS) is strongly focused on the acute phase. However, even after treatment, both successful and unsuccessful, the volumetric increase of infarct related lesions, occurs between 24 h and 1 week after treatment. Although commonly unrecognized, this late lesion growth in the subacute period (i.e., after 24 h of stroke onset) is associated with unfavorable functional outcome (1–6). This suggests that secondary treatment even 24 h after stroke onset can be beneficial to alleviate the effects of ischemia. Infarct-related lesion growth is caused by a combination of edema formation and true infarct progression. Lesion growth is a dynamic and often an irreversible process (7, 8). Both ischemia and post-ischemic reperfusion lead to a cascade of pathophysiological processes, which results in poor prognosis (9). Although several risk factors for early, acute lesion growth between pre and post treatment time-points have been identified in literature (10–13), risk factors for late lesion growth after treatment are understudied.

The aim of this study is to perform an exploratory analysis of associations between baseline, imaging, and (post-) treatment characteristics and late lesion growth after treatment in patients with acute ischemic stroke due to a large vessel occlusion.

Methods

Patient population

For this study, we included data from patients included in the Multicenter Randomized Clinical Trial of Endovascular Treatment for Acute Ischemic Stroke in the Netherlands (MR CLEAN). A comprehensive description of the methodology of the MR CLEAN trial has been reported previously (14). In the MR CLEAN trial, patients with AIS due to a proximal arterial occlusion in the anterior circulation, aged 18 years or older with the possibility to treat with endovascular thrombectomy (EVT) within 6 h of symptom onset were randomized between standard with intravenous treatment (IVT) or standard care with IVT followed by EVT. Patients (allocated to intervention or control group) with Non-Contrast Computed Tomography (NCCT) scans between 24 h and 7 days after stroke onset were included. Patients whose scans had movement artifacts, partial volume effects and other technical errors were excluded. Further details of the inclusion and exclusion criterion of this study are provided in the online [Supplemental Material Figure 1](#) (1). The study protocol was approved by a central medical ethics committee and the research board of each participating center. All included patients or their legal representatives provided written informed consent.

Image analysis

In this study, lesion was defined as recent (i.e., early subacute) ischemic tissue as visualized on NCCT. Lesion was delineated to include infarcted tissue, hemorrhage and edema as described in a previous study (1). In short, the segmentations on 24-h NCCT scan were manually delineated using ITK-SNAP by two trained observers (A.B and P.K) (15). To prevent disparities while assessing the lesion, a fixed window-level setting with a window width 30 HU and center level 35 HU was used. Hyper-densities next to or within the hypodense areas including edema extending into the contra-lateral hemisphere or causing

Abbreviations: aOR, adjusted odds ratio; ASPECTS, Alberta Stroke Program Early Computed Tomography Score; CT, computed tomography; CI, confidence interval; EVT, endovascular treatment; IQR, inter quartile range; mAOL, modified Arterial Occlusion Lesion; mRS, modified Rankin Scale; MR CLEAN, Multicenter Randomized Clinical Trial of Endovascular Treatment for Acute Ischemic Stroke in the Netherlands; NIHSS, NIS Stroke Scale; NCCT, non-contrast CT; OR, odds ratio.

ventricular and/or sulcal effacement were considered to be part of the lesion. The observers were informed about the affected hemisphere. Old ipsilateral lesions, which were more hypodense with distinct borders and/or with no mass effect were not included in the segmentation. Lesion volume after 1 week (5–7 days) of stroke onset was automatically identified on NCCT scans using a previously validated software (16). The segmentations were verified and adjusted if necessary by one of two experienced neuro-radiologists (C.B.L.M. and J.C.J.B.) who were blinded to baseline and outcome characteristics. The lesions are more discernible on the 1-week NCCT scans compared to the 24-h NCCT scans and our software performed better in segmenting the lesions on the 1-week. Hence, we used the software for identifying lesions on the 1-week scans and manually delineated the 24-h lesions, often presented as subtle changes on the 24-h scans.

The lesion volume was calculated by multiplying the number of voxels in the segmentation with the image voxel size. Late lesion growth was the difference between lesions volumes calculated after 1 week and 24 h.

Midline shift, known as the gold standard to assess the extent of edema, was defined as the horizontal displacement (in mm) of midline structures and was measured by a neuroradiologist at the level of the septum pellucidum as described in a previous study (17). A central blinded core lab scored other radiological parameters like the Alberta Stroke Program Early Computed Tomography Score (ASPECTS) (18), Collateral Score (CS) (19), and modified Arterial Occlusion Lesion (mAOL) score (20). In this study, successful recanalization was assessed on the 24-h follow up CT Angiography scan and was defined as mAOL score of 3 points.

Statistical analysis

Visual inspection of the histogram of late lesion growth before and after log transformation and the Shapiro Wilk test indicated that it was not normally distributed (Supplemental material Figure II). Given the proof-of-concept and exploratory nature of this study, we modeled the late lesion growth by dividing the variable into quartiles instead of modeling it as a continuous variable for comprehensibility. Baseline, imaging and (post) treatment characteristics of the study population are tabulated according to quartiles of late lesion growth. Continuous variables are expressed as or medians (interquartile ranges, IQR), where applicable. Categorical variables are expressed as numbers of patients and percentages.

To identify risk factors for late lesion growth, we performed ordinal logistic regression, which is also known as shift analysis. The resulting common odds ratios represent a shift toward the higher quartile of late lesion growth after assuming proportional odds between different quartiles. To understand the effect of different variables we first performed univariable

ordinal regression with baseline, image, and (post-) treatment characteristics with late lesion growth (as a categorical variable). A multivariable ordinal regression was performed including all variables that were associated with late lesion growth in the univariable analysis with a p -value of < 0.10 . To visualize the association of the risk factors with late lesion growth identified in the multivariable ordinal regression, this relation was plotted while setting the other variables in the multivariable model to their mean values (21).

Patients with missing information were excluded from the analysis. Statistical analyses were performed using SPSS (IBM SPSS Statistics, version 26, 2019) and R [Version 4.0.2 (2020-06-22)] using RStudio (Version 1.2.5033–© 2009-2019 RStudio, Inc.). A p -value ≤ 0.05 was considered statistically significant.

Results

Patient characteristics

A total of 226 patients met the inclusion criterion for this study (Supplemental material Figure I). The median age of the population was 67 (IQR: 57–76) years and 132 (58%) were male. Nineteen (8.4%) patients suffered from a previous ischemic stroke, and 67 (30%) patients were using statins. Baseline median NIHSS was 17 (IQR: 13–21) and 63 (28%) patients had a proximal occlusion in the Intracranial Carotid Artery (ICA) or the ICA-terminus, while 163 patients had a distal occlusion in the middle cerebral artery [M1 segment: 144 (64%), M2 segment: 18 (8%)] and anterior cerebral artery (A2 segment: 1). Two-hundred-four (90%) patients received intravenous thrombolysis, 106 (47%) were allocated to endovascular treatment, and 110 (54%) patients in our study population achieved successful recanalization. Furthermore, of the patients allocated to EVT, 60 patients (57%) achieved a modified thrombolysis in cerebral infarction score of 2b-3 as assessed on the procedural digital subtraction angiography scans. Patient characteristics of the population are provided in Table 1 and patient characteristics categorized in quartiles of late infarct growth are provided in the (Supplementary Material Table I).

Lesion characteristics

Figure 1 shows an example of the delineation of the lesions on the 24-h and 1-week NCCT scans. The median lesion volume after 24 h was 43 (IQR: 21–99) ml and after 1 week was 79 (IQR: 33–140) ml. Median midline shift measured on the 24-h NCCT scans was 0 (IQR: 0–2.8) mm and 140 (62%) patients had no midline shift. The median late lesion growth was 22 (IQR: 10–45) ml. Patients were categorized into minimal growth (up to 10 ml), low growth (10–22 ml), moderate growth (22–45 ml), and large growth

TABLE 1 Baseline, radiological and treatment characteristics of the study population and univariable ordinal regression of these characteristics with subacute lesion evolution.

Variable	Population	Common odds ratio (95% CI)	p-value
Age	67 (57–76)	1.00 (0.98–1.02)	0.96
Sex	132 (58%)	0.94 (0.59–1.51)	0.81
Previous medical history			
Previous ischemic stroke	19 (8.4%)	1.3 (0.53–3.20)	0.57
Myocardial infarction	27 (12%)	0.71 (0.35–1.42)	0.33
Diabetes mellitus	25 (11%)	1.50 (0.71–3.20)	0.29
Hypertension	113 (50%)	0.96 (0.60–1.53)	0.86
Atrial fibrillation	64 (28%)	1.23 (0.73–2.07)	0.43
Hypercholesterolemia	54 (24%)	0.93 (0.54–1.59)	0.78
Current smoking	66 (29%)	0.76 (0.46–1.27)	0.30
Previous medication			
Antiplatelet drugs	63 (28%)	0.77 (0.46–1.29)	0.32
Coumarins	15 (6.6%)	1.18 (0.47–2.98)	0.72
Statins	67 (30%)	0.92 (0.56–1.52)	0.74
Anti-hypertensive drugs	114 (50%)	1.06 (0.66–1.69)	0.81
Clinical parameters			
Pre-stroke modified Rankin Scale (0–2)	216 (96%)	1.00 (0.31–3.25)	1.00
Systolic blood pressure (mmHg)	140 (130–160)	1.01 (1.00–1.02)	0.04*
Clinical hemisphere side left	123 (54%)	0.93 (0.58–1.49)	0.77
Baseline NIHSS	17 (13–21)	1.07 (1.03–1.12)	<0.01**
Radiological parameters			
ASPECT score	9 (8–10); 2 (0.88%)	0.81 (0.70–0.94)	0.01**
Proximal occlusion (ICA or ICA-T)	63 (28%)	1.76 (1.03–3.00)	0.04*
Collateral score	2 (1–3); 2 (0.88%)	0.61 (0.46–0.82)	<0.01**
Treatment characteristics			
Received iv Thrombolysis	204 (90%)	0.92 (0.41–2.07)	0.84
Allocated to endovascular treatment	106 (47%)	0.77 (0.48–1.24)	0.28
Time to randomization	200 (150–260)	1.04 (1.01–1.08)	0.01**
24-h follow up characteristics			
Successful recanalization	110 (54%); 23 (10%)	0.59 (0.36–0.97)	0.04*
Lesion volume (ml)	43 (21–99)	1.01 (1.01–1.02)	<0.01**
Midline shift (mm)	0 (0–2.8)	1.27 (1.12–1.44)	<0.01**

All data in the “Population” column are displayed as median (interquartile range) or number (percentage of population). When required number of missing patients (percentage of population) is also provided in the “Population” column. All variables significant at the level of $p < 0.10$ have been selected in the multivariable regression model. ASPECTS, Alberta Stroke Program Early Computed Tomography Score; ICA, Intracranial carotid artery; ICA-T, Intracranial carotid artery-T junction; NIHSS, NIH Stroke Scale/Score. ** $p \leq 0.01$ * $p \leq 0.05$.

(>45 ml). The median lesion growth for the categories were: minimal 1.6 (IQR: –2.9 to 6.3) ml; low 16 (IQR: 14–19) ml; moderate 32 (IQR: 26–36) ml; and large 73 (IQR: 60–95) ml, respectively.

Regression analysis

Results of the univariable ordinal regression analysis are provided in [Table 1](#). In summary, pre-treatment characteristics such as higher systolic blood pressure ($p = 0.04$), higher NIHSS ($p < 0.01$), lower ASPECTS ($p = 0.01$), lower collateral

score ($p < 0.01$), longer time to randomization ($p = 0.01$) were associated with lesion growth in the univariable analyses. Furthermore, unsuccessful recanalization ($p = 0.04$), larger 24-h lesion volume ($p < 0.01$) and 24-h midline shift ($p < 0.01$) were associated with late lesion growth. Administering intravenous thrombolysis ($p = 0.84$) and allocation to endovascular treatment ($p = 0.28$) were not associated with late lesion growth.

In multivariable ordinal regression analysis, lower collateral score [aOR: 0.62 (0.44–0.87); $p = 0.01$], longer time to treatment [aOR: 1.04 (1.00–1.08); $p = 0.04$], unsuccessful recanalization [aOR: 0.57 (0.34–0.97); $p = 0.01$] and larger

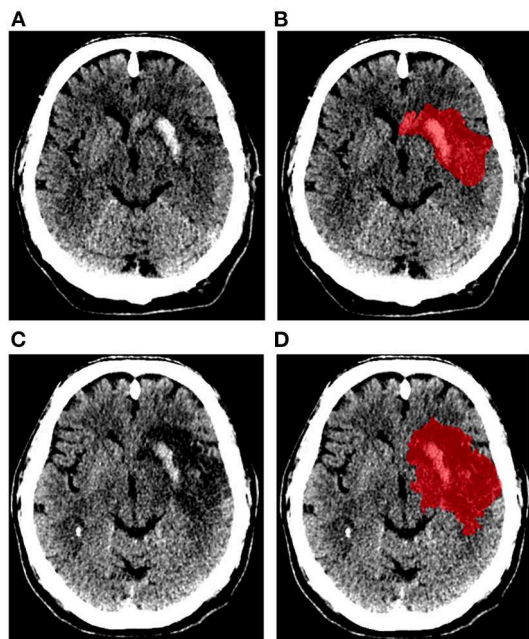


FIGURE 1
Example of ischemic lesion segmentation (represented in red).
Non-contrast CT scans and segmentation of ischemic lesion
obtained after 24 h (A,B), and 1 week (C,D) of stroke onset.

TABLE 2 Multivariable ordinal regression of subacute lesion evolution modeled in quartiles with baseline, imaging, and post-treatment characteristics.

Variable	Adjusted common odds ratio (95% CI)	p-value
Systolic blood pressure (mmHg)	1.00 (0.99–1.01)	0.57
Baseline NIHSS	1.05 (1.00–1.10)	0.06†
ASPECT score	1.00 (0.83–1.20)	0.99
Proximal occlusion (ICA or ICA-T)	1.70 (0.94–3.1)	0.08†
Baseline collateral score	0.62 (0.44–0.87)	0.01*
Time to randomization (per 10 min)	1.04 (1.00–1.08)	0.04*
Successful recanalization	0.57 (0.34–0.97)	0.04*
Midline shift (mm)	1.18 (1.02–1.36)	0.02*

ASPECTS, Alberta Stroke Program Early Computed Tomography Score; ICA, Intracranial carotid artery; ICA-T, Intracranial carotid artery-T junction; NIHSS, NIH Stroke Scale/Score. * $p \leq 0.05$ † $p < 0.1$.

24-h midline shift [aOR: 1.18 (1.02–1.36); $p = 0.02$] were independently associated with late lesion growth. Higher NIHSS on hospital admission [aOR: 1.05 (1.00–1.10); $p = 0.06$] and presence of a proximal occlusion [aOR: 1.70 (0.94–3.1); $p = 0.08$] showed a non-significant trend to be associated with late lesion growth (Table 2). The association of these variables on the predicted probability

of the late lesion growth category is visualized in the (Supplementary Material Figure III).

Discussion

In this exploratory study, we identified lower collateral score, longer time between onset and treatment, unsuccessful recanalization, and larger midline shift to be risk factors of subacute late lesion growth after treatment.

In literature, risk factors have been identified for lesion growth expansion between baseline and follow up at acute (6–24 h) (10, 12, 22), subacute (24 h to 7 days) (11, 23–29), or chronic (more than 7 days) (13) time points. In these studies, lesion growth was assessed on different modalities using various thresholds. Nevertheless, it is interesting to note that in line with our findings, unsuccessful reperfusion was associated with lesion growth between baseline and follow-up at acute (10, 12, 22) and subacute (11, 26) time points by several other studies, except by Haussen et al. (29). Our finding of lack of reperfusion to be a risk factor for late lesion growth in the subacute period is consistent with the results of previous studies that assessed lesion growth in the subacute period on MRI (4). It is well acknowledged that successful restoration of blood flow salvages the at-risk tissue in the down-stream territory and limits post-treatment lesion expansion in the acute situation. But, lesion progression continues possibly due to thrombus fragmentation to new or to the downstream territories, formation of micro-emboli or damage to the capillaries and smaller vasculature that could result from incomplete reperfusion, especially in cases with unsuccessful recanalization (12, 29). In contrast, Sah et al. did not find similar influence of reperfusion on lesion growth between 5 and 24 h after treatment, probably owing to their small sample size (5). In our study, successful recanalization is assessed in patients that were and in the patients that were not allocated to receive EVT. Since the recanalization rates are higher in the patients allocated to receive EVT (74%) compared to those that did not receive EVT (27%), it is possible that our observations may be biased to the control arm of the trial. Nevertheless, unsuccessful recanalization, irrespective of treatment arm, is associated with late lesion growth and treatment allocation was not. In this exploratory study we aimed to identify potential risk factors of late lesion growth and not to build an optimal association or prediction model. We, therefore, did not account for possible collinearities between the independent variables in the multivariable analysis.

In our study, we found that lower baseline collateral capacity is a risk factor for late lesion growth. Man et al. also identified low collateral supply to be associated with lesion growth between baseline and follow-up at a sub-acute time point (11). However, in a subpopulation of the DEFUSE3 patients that received an unscheduled MRI or CT scan after 5 days, Tate et al.

found a statistically insignificant trend between good collateral circulation and larger lesion growth in the subacute period (30). Consistent with Campbell et al., they suggest that a better baseline collateral supply leads to a smaller lesion in the early time window, which can expand if the collaterals fail in the later time window, especially in patients with unsuccessful reperfusion (23). This discrepancy in findings could be because Tate et al. compared lesions measured mainly on MRI after 24 h and NCCT after 5 days, unlike in our study where we used NCCT at both time points. This could also explain the lower median lesion growth compared to that observed in our study. Moreover, in the MR CLEAN trial, obtaining NCCT after 24 h and 1 week was standard practice unlike the DEFUSE 3 trial, which performed an unscheduled scan at 5 days only in the patients with a worse outcome. Studying collateral circulation in the subacute period would help to better understand the influence of collaterals on late lesion growth (14, 30).

Some of the (plausible) risk factors of the late lesion growth identified in this study, like longer time to randomization, poorer collaterals, higher baseline NIHSS, presence of a proximal occlusion are known to also be associated with larger lesion growth between baseline and acute time points, leading to larger 24-h lesion volumes (10). Furthermore, recanalization status was assessed on the follow-up CT Angiography scans, which is generally acquired after 24 h. Including time to randomization (as a proxy for time to treatment) instead of time to recanalization as an independent variable in the regression models captures the variability of time to treatment and its influence on late lesion growth better in our population. It is likely that influence of the risk factors on late lesion growth is due to the associated 24-h ischemic lesion volumes and the ensuing deterioration. But, incorporating the 24-h lesion volume in the multivariable model could obscure the influence of the other risk factors on the late lesion growth, especially because of the correlation (collinearity) between these risk factors and the 24-h lesion volume. Simard et al. have found that ischemia leads to the deterioration of the blood brain barrier, loss of capillary integrity and development of edema which leads to swelling of tissue. Swelling increases tissue pressure and exerts further mechanical force on the adjacent tissues, thereby reducing capillary flow. This further foster infarct growth and development of edema. The effect of edema is most pronounced between 24 and 72 h after an ischemic event (9). Presence and extent of midline shift is an indicator for mass effect. In our study, we use midline shift as a proxy for the 24-h lesion volume in the multivariable model to identify risk factors of late lesion growth. Midline shift is a surrogate marker for edema, especially for lesions large enough to cause a displacement in the midline structures (17). Our observation that increased midline shift is associated with late lesion growth is most likely due to

the prominent effect of a large 24-h lesion volume and the subsequent deterioration of the blood brain barrier and loss of capillary integrity, which also promotes the formation of vasogenic edema.

Our study has some limitations. In our study, we use NCCT imaging to assess the affected tissue 24 h and 1 week after stroke. It is important to note that lesions identified on NCCT scans include infarcted tissue, edema (cytotoxic and/or vasogenic) and even hemorrhagic regions. Furthermore, they are rather subtle on the 24-h scans further complicating the delineation of the lesions. Nevertheless, a recent study showed that the lesion is discernible in 89% of the patients on the 24-h NCCT scan (31). Still, NCCT was used in the trial since NCCT is a more commonly available imaging modality in most hospitals, especially when multiple scans are acquired at different timepoints. Furthermore, use of MRI imaging can lead to loss of inclusions because of contraindications to MRI and patients' uncooperativeness (possibly due to claustrophobia) to undergo an MRI. Since the effect of edema is maximal in the subacute period after an ischemic event (1), future studies focused on identifying risk factors for progression of the lesion after distinguishing edema and lesion are necessary to gain a better insight into the pathophysiology of lesion progression. DWI and MR FLAIR are better imaging techniques for assessing lesion status and its constituents especially in the early subacute window (after 24 h) compared to CT. Hence, we advocate that studying late lesion growth assessed on MRI would also aid in better understanding this phenomenon. The 1-week follow-up NCCT scan was obtained 3–9 days after stroke onset, which further necessitates the identification of edema and true infarcted regions within the lesions (14). It is known that reperfusion is a more commonly used marker for treatment success compared to recanalization. Since reperfusion is generally assessed on digital subtraction angiography images that are only available for patients in the intervention arm, in this study, treatment success was determined on the 24-h follow up CT angiography scan. Further studies distinguishing lesion progression into downstream and new territories after considering the influence of reperfusion are also required.

Conclusion

Lesion growth in patients treated for an AIS is not restricted to the acute phase between stroke onset and (successful) reperfusion. We identified lower collateral capacity, longer time between stroke onset and treatment, unsuccessful recanalization, and larger midline shift as risk factors for late, subacute lesion growth. Furthermore, higher baseline NIHSS and presence of a proximal occlusion showed a trend to be associated with more subacute lesion

evolution. Further research should be directed toward understanding and minimizing the effects of the predictors for late lesion growth.

Data availability statement

The data analyzed in this study was obtained from the Multicenter Randomized Clinical Trial of Endovascular Treatment for Acute Ischemic Stroke in the Netherlands (MR CLEAN; <https://www.mrclean-trial.org/home.html>), the following licenses/restrictions apply: Due to the sensitive nature of the data these datasets are not readily available. Requests to access these datasets should be directed to the MR CLEAN executive committee, mrclean@erasmusmc.nl.

Ethics statement

The studies involving human participants were reviewed and approved by MR CLEAN trial Committee. The patients/participants provided their written informed consent to participate in this study.

Author contributions

WZ, AL, RO, DD, YR, and CM: designed the MR CLEAN trial. OB: collected and prepared the data for the trial. PK, OB, BD, ABu, ABo, JB, and CM: prepared data for this study. PK: performed the statistical analysis, interpreted the results, and drafted the paper. HM: assisted with the statistical analysis, interpretation of the results, and drafting the paper. NS, ABu, KT, OB, AY, WZ, RO, AL, DD, YR, JB, and CM: critically revised the paper. All authors contributed to the article and approved the submitted version.

Funding

MR CLEAN is partly funded by the Dutch Heart Foundation (2008 T030). MR CLEAN is also funded by unrestricted grants from: AngioCare BV, Covidien/EV3®, MEDAC GmbH/LAMEPRO, Penumbra Inc., and Concentric Medical/TOP Medical BV. The study is designed, conducted, analyzed, and interpreted by the investigators independently of all. This sub-study is also funded by INSIST (www.insist-h2020.eu): a European Union's Horizon 2020 research and innovation program (grant agreement number: 777072).

Conflict of interest

PK is funded by INSIST (www.insist-h2020.eu): a European Union's Horizon 2020 research and innovation program (grant agreement number: 777072). ABo is a shareholder of Nico.Lab. AY reports grants from Cerenovus Neurovascular, Medtronic, Stryker, Penumbra, and Genentech for investigator-initiated studies; funds from Stryker, Cerenovus Neurovascular and Penumbra (core imaging lab activities) and Genentech (consultation); and declares to have equity ownership from Inera Therapeutics. WZ reports speaker fees from Stryker and Cerenovus (paid to the institution). AL and DD report funds from the Cerenovus Neurovascular, Dutch Heart Foundation, Brain Foundation Netherlands, Organization for Health Research and Development, Health Holland Top Sector Life Sciences & Health, and unrestricted grants paid to the institution from AngioCare BV, Covidien/EV3, MEDAC GmbH/LAMEPRO, PenumbraInc., Top Medical/Concentric, Stryker, Stryker European Operations BV, Medtronic, Thrombolytic Science and LLC for research. AL further reports grants paid to the institution from the Siemens Healthineers, GE Healthcare and Philips Healthcare. YR is a shareholder at Nico-Lab. CM reports grants from European Commission, during the conduct of the study; grants from CVON/Dutch Heart Foundation, grants from TWIN Foundation, grants from Stryker, outside the submitted work; and owns stock in Nico.lab. HM is a Co-founder and shareholder of Nico.lab.

The remaining authors declare that the research was conducted in the absence of any commercial or financial relationships that could be construed as a potential conflict of interest.

Publisher's note

All claims expressed in this article are solely those of the authors and do not necessarily represent those of their affiliated organizations, or those of the publisher, the editors and the reviewers. Any product that may be evaluated in this article, or claim that may be made by its manufacturer, is not guaranteed or endorsed by the publisher.

Supplementary material

The Supplementary Material for this article can be found online at: <https://www.frontiersin.org/articles/10.3389/fneur.2022.977608/full#supplementary-material>

References

- Bucker A, Boers AM, Bot JCJ, Berkhemer OA, Lingsma HF, Yoo AJ, et al. Associations of ischemic lesion volume with functional outcome in patients with acute ischemic stroke 24-h vs. 1-week imaging on behalf of the MR CLEAN trial investigators (Multicenter Randomized Clinical Trial of Endovascular Treatment for Acute Ischemic Stroke in the Netherlands). doi: 10.1161/STROKEAHA.116.015156
- Konduri P, Voorst H Van, Bucker A, Kranendonk K Van, Boers A. Post treatment ischemic lesion evolution is associated with reduced favorable functional outcome in patients with stroke. *Stroke*. (2021) 52:3523–31. doi: 10.1161/STROKEAHA.120.032331
- Krongold M, Almekhlafi MA, Demchuk AM, Coutts SB, Frayne R, Eilaghi A. Final infarct volume estimation on 1-week follow-up MR imaging is feasible and is dependent on recanalization status. *NeuroImage Clin*. (2015) 7:1–6. doi: 10.1016/j.nicl.2014.10.010
- Federau C, Mlynash M, Christensen S, Zaharchuk G, Cha B, Lansberg MG, et al. Evolution of volume and signal intensity on fluid-attenuated inversion recovery MR images after endovascular stroke therapy. *Radiology*. (2016) 280:184–92. doi: 10.1148/radiol.2015151586
- Sah RG, d'Este CD, Hill MD, Hafeez M, Tariq S, Forkert ND, et al. Diffusion-weighted imaging lesion growth occurs despite recanalization in acute ischemic stroke: Implications for future treatment trials. *Int J Stroke*. (2019) 14:257–64. doi: 10.1177/1747493018798550
- Blauenfeldt RA, Hougaard KD, Mouridsen K, Andersen G. High prestroke physical activity is associated with reduced infarct growth in acute ischemic stroke patients treated with intravenous tPA and randomized to remote ischemic preconditioning. *Cerebrovasc Dis*. (2017) 44:88–95. doi: 10.1159/000477359
- Barrett KM, Ding YH, Wagner DP, Kallmes DF, Johnston KC. Change in diffusion-weighted imaging infarct volume predicts neurologic outcome at 90 days results of the acute stroke accurate prediction (ASAP) trial serial imaging substudy. *Stroke*. (2009) 40:2422–27. doi: 10.1161/STROKEAHA.109.548933
- Cho KH, Kwon SU, Lee DH, Shim W, Choi C, Kim SJ, Suh DC, Kim JS, Kang DW. Early infarct growth predicts long-term clinical outcome after thrombolysis. *J Neurol Sci*. (2012) 316:99–103. doi: 10.1016/j.jns.2012.01.015
- Simard JM, Kent TA, Chen M, Tarasov K V, Gerzanich V. Brain oedema in focal ischaemia: molecular pathophysiology and theoretical implications. *Lancet Neurol*. (2007) 6:258–68. doi: 10.1016/S1474-4422(07)70055-8
- Simonsen CZ, Mikkelsen IK, Karabegovic S, Kristensen PK, Yoo AJ, Andersen G. Predictors of infarct growth in patients with large vessel occlusion treated with endovascular therapy. *Front Neurol*. (2017) 8:6–11. doi: 10.3389/fneur.2017.00574
- Man S, Aoki J, Hussain MS, Wisco D, Tateishi Y, Toth G, et al. Predictors of infarct growth after endovascular therapy for acute ischemic stroke. *J Stroke Cerebrovasc Dis*. (2015) 24:401–7. doi: 10.1016/j.jstrokecerebrovasdis.2014.09.004
- Cho TH, Nighoghossian N, Mikkelsen IK, Derex L, Hermier M, Pedraza S, et al. Reperfusion within 6 h outperforms recanalization in predicting penumbra salvage, lesion growth, final infarct, and clinical outcome. *Stroke*. (2015) 46:1582–89. doi: 10.1161/STROKEAHA.114.007964
- Hong CT, Sun Y, Lu CJ, Shin HC, Chen RC. Prediction of infarct growth and neurologic deterioration in patients with positive perfusion-diffusion mismatch. *Clin Neurol Neurosurg*. (2012) 114:376–80. doi: 10.1016/j.clineuro.2011.11.019
- Berkhemer OA, Fransen PSS, Beumer D, van den Berg LA, Lingsma HF, Yoo AJ, et al. A randomized trial of intraarterial treatment for acute ischemic stroke. *N Engl J Med*. (2015) 372:11–20. doi: 10.1056/NEJMoa1411587
- Yushkevich PA, Piven J, Hazlett HC, Smith RG, Ho S, Gee JC, et al. User-guided 3D active contour segmentation of anatomical structures: significantly improved efficiency and reliability. *Neuroimage*. (2006) 31:1116–28. doi: 10.1016/j.neuroimage.2006.01.015
- Boers AM, Marquering HA, Jochem JJ, Besselink NJ, Berkhemer OA, Van Der Lugt A, et al. Automated cerebral infarct volume measurement in follow-up noncontrast CT scans of patients with acute ischemic stroke. *Am J Neuroradiol*. (2013) 34:1522–7. doi: 10.3174/ajnr.A3463
- Kimberly WT, Dutra BG, Boers AMM, Alves HCB, Berkhemer OA, Van Den Berg L, et al. Association of reperfusion with brain edema in patients with acute ischemic stroke: a secondary analysis of the MR CLEAN Trial. *JAMA Neurol*. (2018) 75:453–61. doi: 10.1001/jamaneurol.2017.5162
- Barber PA, Demchuk AM, Zhang J, Buchan AM. Validity and reliability of a quantitative computed tomography score in predicting outcome of hyperacute stroke before thrombolytic therapy. *Lancet*. (2000) 355:1670–4. doi: 10.1016/S0140-6736(00)02237-6
- Tan IYL, Demchuk AM, Hopyan J, Zhang L, Gladstone D, Wong K, et al. CT angiography clot burden score and collateral score: correlation with clinical and radiologic outcomes in acute middle cerebral artery infarct. *Am J Neuroradiol*. (2009) 30:525–31. doi: 10.3174/ajnr.A1408
- Zaidat OO, Yoo AJ, Khatri P, Tomsick TA, Von Kummer R, Saver JL, et al. Recommendations on angiographic revascularization grading standards for acute ischemic stroke: a consensus statement and for the cerebral angiographic revascularization, grading (CARG) collaborators, STIR revascularization working group, and STIR thrombol. *Stroke*. (2013) 44:2630–63. doi: 10.1161/STROKEAHA.113.001972
- Fox J, Hong J. Effect displays in R for multinomial and proportional-odds logit models: extensions to the effects package. *J Stat Softw*. (2009) 32:1–24. doi: 10.18637/jss.v032.i01
- Deng W, Teng J, Liebeskind D, Miao W, Du R. Predictors of infarct growth measured by apparent diffusion coefficient quantification in patients with acute ischemic stroke. *World Neurosurg*. (2019) 123:e797–02. doi: 10.1016/j.wneu.2018.12.051
- Campbell BC, Christensen S, Tress BM, Churilov L, Desmond PM, Parsons MW, et al. Failure of collateral blood flow is associated with infarct growth in ischemic stroke. *J Cereb Blood Flow Metab*. (2013) 33:1168–72. doi: 10.1038/jcbfm.2013.77
- Albers GW, Goyal M, Jahan R, Bonafe A, Diener HC, Levy EI, et al. Relationships between imaging assessments and outcomes in solitaire with the intention for thrombectomy as primary endovascular treatment for acute ischemic stroke. *Stroke*. (2015) 46:2786–94. doi: 10.1161/STROKEAHA.115.010710
- Wheeler HM, Mlynash M, Inoue M, Tipiririni A, Liggins J, Bammer R, et al. The growth rate of early DWI lesions is highly variable and associated with penumbral salvage and clinical outcomes following endovascular reperfusion. *Int J Stroke*. (2015) 10:723–29. doi: 10.1111/ijss.12436
- Marks MP, Lansberg MG, Mlynash M, Kemp S, McTaggart R, Zaharchuk G, et al. Correlation of AOL recanalization, TIMI reperfusion and TIC1 reperfusion with infarct growth and clinical outcome. *J Neurointerv Surg*. (2014) 6:724–28. doi: 10.1136/neurintsurg-2013-010973
- Van Ginneken V, Gierhake D, Audebert HJ, Fiebach JB. Distal middle cerebral artery branch recanalization does not affect final lesion volume in ischemic stroke. *Cerebrovasc Dis*. (2017) 43:200–5. doi: 10.1159/000457811
- Darwish EAF, Abdelhameed-El-Nouby M, Geneidy E. Mapping the ischemic penumbra and predicting stroke progression in acute ischemic stroke: the overlooked role of susceptibility weighted imaging. *Insights Imaging*. (2020) 11:1–12. doi: 10.1186/s13244-019-0810-y
- Haussen DC, Nogueira RG, Elhammady MS, Yavagal DR, Aziz-Sultan MA, Johnson JN, et al. Infarct growth despite full reperfusion in endovascular therapy for acute ischemic stroke. *J Neurointerv Surg*. (2016) 8:117–21. doi: 10.1136/neurintsurg-2014-011497
- Tate WJ, Polding LC, Christensen S, Mlynash M, Kemp S, Heit JJ, et al. Predictors of early and late infarct growth in DEFUSE 3. *Front Neurol*. (2021) 12:1–6. doi: 10.3389/fneur.2021.699153
- Ospel JM, Menon BK, Qiu W, Kashani N, Mayank A, Singh N, et al. A detailed analysis of infarct patterns and volumes at 24-h noncontrast CT and diffusion-weighted MRI in acute ischemic stroke due to large vessel occlusion: results from the ESCAPE-NA1 trial. *Radiology*. (2021) 300:152–9. doi: 10.1148/radiol.2021203964



OPEN ACCESS

EDITED BY

Christopher Blair,
Liverpool Hospital, Australia

REVIEWED BY

Li Ma,
Capital Medical University, China
Junlin Lu,
Sichuan University, China

*CORRESPONDENCE

Lin Wang
dr_wang@zju.edu.cn

[†]These authors have contributed
equally to this work

SPECIALTY SECTION

This article was submitted to
Stroke,
a section of the journal
Frontiers in Neurology

RECEIVED 02 June 2022

ACCEPTED 12 August 2022

PUBLISHED 26 October 2022

CITATION

Li Y, Hu J-w, He X-c, Cao Y, Yu X-b,
Fu X-j, Zhou H, Hu L-b, Xu L, Xu C-r,
Wang Y-j and Wang L (2022) Bloody
fluids located between the temporal
muscle and targeted cerebral cortex
affect the establishment of indirect
collaterals in Moyamoya disease with
surgical bypass: A case-control study.
Front. Neurol. 13:960199.
doi: 10.3389/fneur.2022.960199

COPYRIGHT

© 2022 Li, Hu, He, Cao, Yu, Fu, Zhou,
Hu, Xu, Xu, Wang and Wang. This is an
open-access article distributed under
the terms of the [Creative Commons
Attribution License \(CC BY\)](#). The use,
distribution or reproduction in other
forums is permitted, provided the
original author(s) and the copyright
owner(s) are credited and that the
original publication in this journal is
cited, in accordance with accepted
academic practice. No use, distribution
or reproduction is permitted which
does not comply with these terms.

Bloody fluids located between the temporal muscle and targeted cerebral cortex affect the establishment of indirect collaterals in Moyamoya disease with surgical bypass: A case-control study

Yin Li^{1,2†}, Jun-wen Hu^{1,2†}, Xu-chao He^{1,2}, Yang Cao^{1,2},
Xiao-bo Yu^{1,2}, Xiong-jie Fu^{1,2}, Hang Zhou^{1,2}, Li-bin Hu^{1,2},
Liang Xu^{1,2}, Chao-ran Xu^{1,2}, Yong-jie Wang^{1,2} and Lin Wang^{1,2*}

¹Department of Neurosurgery, Second Affiliated Hospital, School of Medicine, Zhejiang University, Hangzhou, China, ²Clinical Research Center for Neurological Diseases of Zhejiang Province, Hangzhou, China

Objective: Bypass yields favorable outcomes in the treatment of Moyamoya disease (MMD). Bloody fluids accumulate between the targeted cortex and the temporal muscle after surgical bypass. These fluids are handled empirically *via* subcutaneous tubes or conservative treatments. However, substances located in certain positions may adversely affect the establishment of indirect collaterals (ICs) from muscular grafts.

Methods: Patients in our hospital from January 2014 to December 2019 were eligible for inclusion. Digital subtraction angiography (DSA) and radiological examinations were used during the perioperative and follow-up periods. Bloody fluid volumes were calculated using computed tomography- (CT-) based 3D Slicer software. The characteristics of bloody fluids, patient demographics, and clinical data were retrospectively analyzed.

Results: In total, 110 patients underwent indirect or combined bypass with follow-up DSA. The mean age of the enrolled patients was 42.4 ± 11.8 years. Previous ischemia ($p = 0.001$), previous hemorrhage ($p = 0.013$), bloody fluid volume ($p = 0.049$), and the time of imaging ($p = 0.081$) were associated with indirect outcomes. Ordinal regression analysis confirmed that good indirect outcomes were associated with previous ischemia ($p < 0.001$) and a large bloody fluid volume ($p = 0.013$). Further subgroups based on fluid volume were significantly correlated with IC establishment ($p = 0.030$).

Conclusions: A large bloody fluid volume and previous ischemic history were associated with good indirect outcomes. The presence of bloody fluids may reflect impaired degrees of muscular donors due to bipolar electrocoagulation, thus highlighting the importance of appropriate application of bipolar forceps.

KEYWORDS

Moyamoya disease, angiogenesis, bloody fluids, temporal muscle, digital subtraction angiography (DSA)

Introduction

Moyamoya disease (MMD) is a chronic cerebrovascular disease characterized by progressive steno-occlusive changes in bilateral intracranial carotid arteries and their proximal branches (1). Surgery can effectively improve cerebral hemodynamic status (2). Indirect bypass remains a high priority for pediatric patients because of its simplicity and patients' satisfactory improvements (3). Indirect bypass is also performed separately or as part of a combined bypass for treating adult patients with MMD (4). A recent study found that dual collateral establishment of direct and indirect parts occurred in only 47% of adult patients, and good indirect partial collaterals were likely to occur in patients at Suzuki stage IV or greater (5). Although strong angiogenic effects help indirect collaterals (ICs) develop toward favorable outcomes in younger patients (6), the temporal muscle takes a long time to establish valid connections with targeted brain regions. Therefore, incipient relationships must be established between the donor muscle and recipient cortices before the period when the deep temporal artery communicates further with the pial vasculature.

The initial contact between muscular grafts and brain surfaces occurs from errhysis of temporal muscles on the first post-operative day. Studies on the post-surgical accumulation of bloody fluids are lacking in evidence-based medicine. In most cases, subcutaneous tubes are empirically placed to drain residual bloody fluids. A previous study revealed that decreased levels of serum caveolin-1 and high concentrations of angiopoietin correlated with neovascularization in adults with MMD (7). Within various angiogenic factors, these fluids may affect the angiogenic interaction between the donor muscle and the arachnoid membrane. Here, we describe the role of bloody fluids in establishing ICs from the deep temporal artery and discuss the appropriate perioperative management of MMD.

Materials and methods

Study participants

After excluding 220 patients, 110 patients with MMD who underwent combined or indirect bypass were consecutively enrolled between January 2014 and December 2019 (Supplementary Figure 1). MMD was diagnosed as per the guidelines for MMD diagnosis and treatment published by the Research Committee on the Pathology and Treatment of Spontaneous Occlusion of the Circle of Willis (8).

Inclusion criteria were as follows: (1) MMD was definitively diagnosed *via* digital subtraction angiography (DSA). (2) Patients underwent either indirect bypass of the encephalo-duro-myo-synangiosis (EDMS) or combined bypass, of which the indirect part was EDMS. (3) Patients underwent either computed tomography (CT) or CT angiography (CTA) within 3 days post-surgery. (4) Follow-up DSA was conducted at ≥ 6 months post-surgery.

Exclusion criteria were as follows: (1) Neither CT nor CTA was performed within 3 days post-surgery. (2) No DSA was performed during the follow-up period. (3) Intracranial hemorrhage occurred in the acute post-operative stage.

Surgical revascularization modalities

Surgical revascularization procedures performed in the enrolled patients were categorized as indirect or combined bypass. Criteria for surgery included the presence of transient ischemic attack or infarct, subarachnoid or intracranial hemorrhage, epilepsy, and dizziness. Indirect bypass was referred to as EDMS. Combined bypass has been described previously and consists of the superficial temporal artery (STA) to middle cerebral artery (MCA) bypass and EDMS (9). Graft patency was confirmed by intraoperative emission of indocyanine green. The temporal muscle covered the brain surface without manual splitting.

Bloody fluid evaluation and divisions

Bloody fluid volume was calculated using 3D Slicer software (<https://www.slicer.org/>) after performing CT or

Abbreviations: CT, computed tomography; DSA, digital subtraction angiography; EDMS, encephalo-duro-myo-synangiosis; ICs, indirect collaterals; MCA, middle cerebral artery; MMD, Moyamoya disease; STA, superficial temporal artery; VEGF, vascular endothelial growth factor.

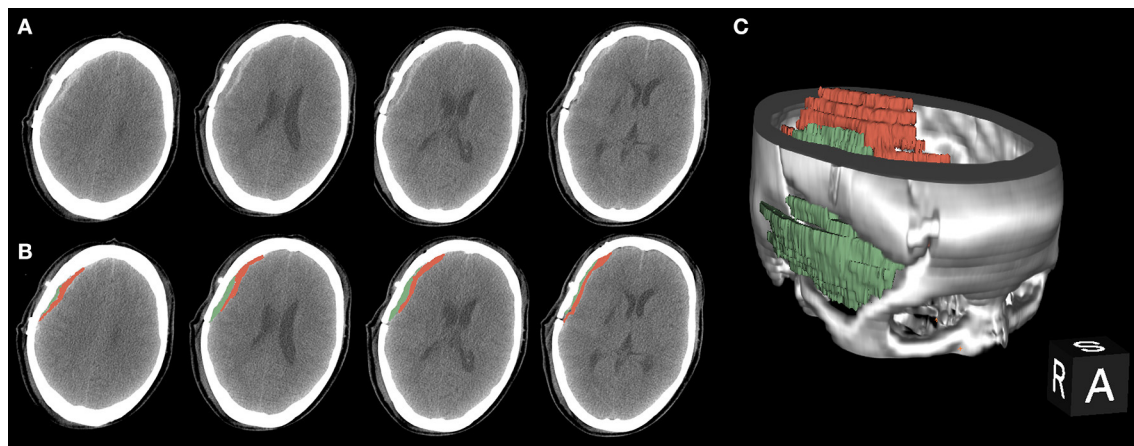


FIGURE 1

A procedure for typical bloody fluids around the operative area. (A) Original presentation of bloody fluids on post-operative computed tomography (CT) examinations. Black arrows indicate the separated temporal muscle. The graph shows different CT values with adjacent bloody fluids. (B) Bloody fluids are marked in red and the temporal muscle is marked in green using the 3D Slicer software. (C) The location of bloody fluids and the temporal muscle via 3D rebuilding.

TABLE 1 The interrater reliability in the calculation involved with bloody fluids.

	Surgeon 1	Surgeon 2	<i>P</i> -value ^y	ICC (95% CI)
Volume of bloody fluids, ml	7.0 ± 4.1	7.0 ± 4.4	<0.001	0.936 (0.908, 0.956)
Surface area, cm ²	25.5 ± 33.1	26.4 ± 37.2	<0.001	0.973 (0.961, 0.982)

^y*p* < 0.05 are bolded.

ICC, interclass correlation coefficient.

CTA within 3 days post-surgery (Figure 1). This software enables the measurement of intracranial hemorrhage more accurately than the conventional Tada formula (10). The calculated threshold range was set as the signal range of hematomas [i.e., 50–100 Hounsfield units (HU)]. The working process went as described previously (10). The separated temporal muscle showed slight high-density signal changes on CT in the acute post-operative stage, but the signal values of the muscles did not meet the abovementioned threshold range.

Enrolled patients were grouped by bloody fluid volume as a minimum: ≤4 ml; small: >4–≤8 ml; medium: >8–≤2 ml; or large: <12 ml.

The interrater reliability of the bloody fluid volume calculation by two independent surgeons was determined and revealed that the volume and surface area of these fluids reached a near perfect agreement [interclass correlation coefficient (ICC) = 0.936 and =0.973, respectively, Table 1].

Outcome measures

The evaluation of collateral networks was graded using the angiographic Matsushima score (11) as follows: 0: no collaterals in the target revascularization; 1: collaterals in ≤1/3 of the MCA territory; 2: collaterals in 1/3–2/3 of the MCA territory; and 3: collaterals in >2/3 of the MCA territory (9). Identification of collaterals provides an overall evaluation of the compensatory area derived from either direct bypass or EDMS (Supplementary Figure 2).

This cohort was then categorized into groups based on the indirect Matsushima score as follows: (1) poor IC group: indirect Matsushima score = 0; (2) minimal IC group: indirect Matsushima score = 1; and (3) good IC group: indirect Matsushima score = 2 or 3.

Data analysis

SPSS 24.0 (SPSS, Inc., Chicago, IL, USA) was used for statistical analysis. Differences in data between ordinal groups were compared using the Kruskal–Wallis *H*-test or Spearman's correlation as appropriate. Logistic regression analysis was conducted on factors achieving *p* < 0.10 in the univariate analysis. A *p* < 0.05 was considered statistically significant, and all tests were two-tailed.

Results

Demographics and clinical presentation

Of 330 consecutive patients with MMD who underwent surgery from January 2014 to December 2019, 110

TABLE 2 Baseline and clinical characteristics in patients with MMD who achieved surgical revascularization.

	Patients (<i>n</i> = 110)
Age, yrs [†]	42.4 ± 11.8 (11, 65)
Female, %	76 (69.1)
Smoking, %	20 (18.2)
Alcohol drinking, %	17 (15.4)
Hypertension, %	34 (30.9)
Diabetes, %	9 (8.2)
Moyamoya involved	
Bilateral	87 (79.1)
Left	12 (10.9)
Right	11 (10.0)
Type of onset	
Ischemia	59 (53.6)
TIA	20 (18.2)
Infarction	39 (35.5)
Hemorrhage	39 (35.5)
SAH	5 (4.5)
IVH	22 (20.0)
ICH	12 (10.9)
Epilepsy	2 (1.8)
Others	10 (9.1)
Angiographic suzuki stage	
I	15 (13.6)
II	14 (12.7)
III	54 (49.1)
IV	23 (20.9)
V	3 (2.7)
VI	1 (0.9)

[†]Values presented as mean ± standard deviation (SD) (minimum, maximum). MMD, Moyamoya disease; TIA, transient ischemic attack; SAH, subarachnoid hemorrhage; IVH, intraventricular hemorrhage; ICH, intracranial hemorrhage.

were identified as meeting the inclusion criteria. Eight patients with acute intracranial hemorrhage were excluded (Supplementary Figure 1). The mean patient age was 42.4 ± 11.8 years (range 11–65 years), and 76 enrolled patients were women. Of these patients, 80.6% presented with bilateral involvement. In total, 60 patients (54.5%) experienced ischemic onset. Table 2 summarizes the other clinical characteristics.

Surgical procedures and follow-up features

The median pre-operative disease course was 5 months (Table 3). Approximately half of the patients underwent surgery on the left side. Approximately 11 of 110 patients (10.0%) underwent indirect bypass, and 99

TABLE 3 Surgical and follow-up features in patients with surgical revascularization.

	Patients (<i>n</i> = 110)
Pre-op disease period (IQR), mos	5.0 (10.0)
Surgical type, %	
Indirect revascularization	11 (10.0)
Combined revascularization	99 (90.0)
Surgery on the left, %	56 (50.9)
Post-operative complications, %	28 (25.5)
Transient neurologic deficits	
Aphasia	22 (20.0)
Weakness	4 (3.6)
Cerebral infarction	2 (1.8)
Epilepsy	4 (3.6)
Length of stay (IQR), days	15.0 (5.0)
Follow-Up period (IQR), mos	11.5 (4.5)
Indirect matsushima score, %	
0	42 (38.2)
1	50 (45.5)
2	17 (15.5)
3	1 (0.9)
Direct matsushima score, %	
0	0 (0.0)
1	34 (34.3)
2	35 (45.5)
3	20 (20.2)

Pre-op, pre-operative; IQR, interquartile range.

(90.0%) underwent combined bypass. One-fourth of the enrolled patients experienced post-operative complications, of which the most common was transient aphasia (20.0%). Four patients had post-operative seizures. Eight excluded patients underwent acute intracranial hemorrhage (Supplementary Figure 1).

The radiographic follow-up period was 11.5 months. Angiographic angiogenesis was assessed for both indirect and direct parts, of which 18 of 110 (16.4%) patients had indirect scores ≥2, and 65.7% (55/99) had direct scores ≥2 on the Matsushima angiogenesis classification. Direct scores were more likely to grade favorably than indirect scores for all enrolled patients.

Factors related to establishing ICs

Patients were further categorized into poor, minimal, and good IC groups, as described in Section Outcome measures. Demographic characteristics were consistent and did not statistically differ among the groups (Table 4). In the good IC group, 88.9% experienced previous ischemic onset, which was positively correlated with indirect outcomes

TABLE 4 Factors related to the generation of indirect collaterals in MMDs after bypass.

	Univariate analysis				Ordinal regression analysis		
	Poor ICs (<i>n</i> = 42)	Minimal ICs (<i>n</i> = 50)	Good ICs (<i>n</i> = 18)	<i>P</i> -value ^Y	OR	95% CI	<i>P</i> -value ^Y
Age, yrs	41.7 ± 13.6	42.6 ± 11.7	43.1 ± 6.9	0.679 ^Z			
Female (%)	33 (78.6)	30 (60.0)	13 (72.2)	0.153 ^S			
Smoking (%)	5 (11.9)	12 (24.0)	3 (16.7)	0.323 ^S			
Bilateral involved	33 (78.6)	39 (78.0)	15 (83.3)	0.888 ^S			
Previous ischemia	15 (35.7)	28 (56.0)	16 (88.9)	0.001^S	4.724	2.161–10.327	<0.001
Previous hemorrhage	21 (50.0)	16 (32.0)	2 (11.1)	0.013^S			0.870
Initial suzuki stage (%)				0.157 ^Z			
I	9 (21.4)	6 (12.0)	0 (0.0)				
II	5 (11.9)	8 (16.0)	1 (7.1)				
III	19 (45.2)	22 (44.0)	13 (72.2)				
IV	6 (14.3)	13 (26.0)	4 (22.2)				
V	3 (7.1)	0 (0.0)	0 (0.0)				
VI	0 (0.0)	1 (2.0)	0 (0.0)				
Surgery on the left (%)	26 (61.9)	23 (46.0)	7 (38.9)	0.172 ^S			
Features of post-op blood fluids							
Volume, ml	5.9 ± 3.4	7.6 ± 4.5	7.9 ± 4.4	0.049^Z	1.122	1.025–1.228	0.013
Surface area, cm ²	27.5 ± 38.1	19.3 ± 25.6	40.9 ± 45.6	0.333 ^Z			
Time of imaging, days	1.9 ± 1.0	2.0 ± 1.0	2.4 ± 1.0	0.081 ^Z			0.159
Post-operative complications, %	10 (23.8)	10 (20.0)	8 (44.4)	0.121 ^S			
Follow-up period, mos	12.0 ± 5.9	14.3 ± 13.1	13.5 ± 5.7	0.221 ^Z			

^Y*p* < 0.05 are bolded.^ZSpearman's correlation.^SKruskal–Wallis H-test.

ICs, indirect collaterals; Ref, reference category; Post-op, post-operative.

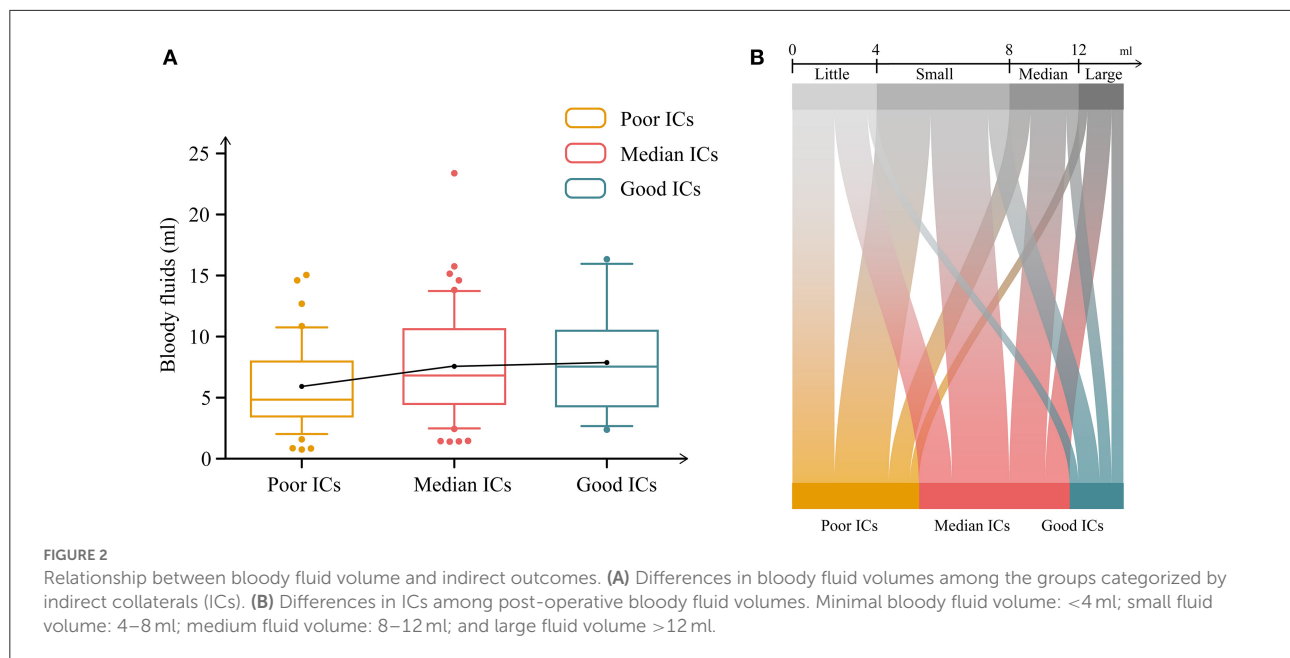
(*p* = 0.001). Conversely, initial hemorrhage was more common in the poor IC group than in the other two groups (*p* = 0.013). Surgery on the left side was less common in the good IC group than in the poor and minimal IC groups (38.9 vs. 61.9 and 46.0%, respectively, *p* = 0.172). Bloody fluid volume was significantly correlated with good indirect outcomes (*p* = 0.049). The average time points for post-operative imaging were similar, occurring ~2 days post-surgery. The mean follow-up periods for all groups exceeded 12 months.

All possible factors were included in the ordinal regression analysis, in which the parallel line test met the standard (Supplementary Table 1). Previous ischemia and bloody fluid volume were independent factors, which were related to indirect outcomes (Table 4). Imaging time was a potential confounding factor in the regression analysis, and no statistically significant differences were observed (*p* = 0.159). Increases in bloody fluid volume were correlated with good ICs [odds ratio (OR): 1.122, 95% confidence interval (CI): 1.025–1.228, *p* = 0.013, Table 4, Figure 2A]. Patients with previous ischemic histories were prone to favorable IC outcomes during a follow-up (OR: 4.724, 95% CI: 2.161–10.327, *p* < 0.001). Patients with hemorrhage at onset were more likely to have poor IC outcomes (*p* = 0.130); however,

the ordinal regression analysis showed no statistical differences (*p* = 0.870).

Bloody fluid features

We further explored clinical and follow-up differences among patients divided by bloody fluid volume grading (Section 2.3). In total, 28 patients had a minimal bloody fluid volume, 44 had a small volume, 23 had a medium volume, and 15 had a large volume. Table 5 compares the patient demographics, clinical features, surgeries, and follow-up characteristics. Only the IC grades differed significantly. The following subgroup analysis of initial onset was conducted in MMD based on the classification of post-operative bloody fluids (Supplementary Table 2). In the subgroup of ischemia, surgery on the left presented significant differences (*p* = 0.018). In contrast, post-operative bloody fluid volume showed statistical significance in the subgroup of hemorrhage (*p* = 0.009). Good IC grades were correlated with a large bloody fluid volume (*p* = 0.030; Figure 2B). Conversely, the direct Matsushima score was not associated with post-operative



bloody fluid volume and did not significantly differ among groups ($p = 0.550$). Postoperative imaging times did not significantly differ among the bloody fluid volume levels ($p = 0.376$).

Discussion

Single and combined bypass are used to treat MMD, and both yield satisfactory outcomes. Studies have explored the long-term patency of anastomotic sites or factors related to direct partial outcomes (12–14). Previous studies have confirmed the association between younger age and indirect partial outcomes (6). However, when establishing collateral networks among patients with MMD, the combination of STA-MCA bypass and EDMS may have opposite outcomes and yield opposite results. Furthermore, collateral cerebral development of single EDMS varies among patients. Here, we found that a large post-operative bloody fluid volume and previous ischemia were associated with good indirect outcomes.

Initial type of onset

The proportions of patients with previous ischemia increased from the poor to the good IC subgroups, with a decreasing trend in the initial hemorrhage (Table 4). After entering the ordinal regression, previous ischemia was a potential factor for good indirect outcomes. A multicenter study revealed that intracranial hemorrhage was an independent

predictor of poor neovascularization for patients with MMD undergoing indirect bypass (15). Subgroup analysis showed that bloody fluid volume was related to ICs in the hemorrhagic group (Supplementary Table 2). In contrast to those with hemorrhagic MMD, patients with ischemic onset exhibited favorable indirect outcomes. The hemodynamic status in ischemic MMD remained stable, and the pial vasculature in these patients did not suffer any hemorrhagic strikes. This may lay a foundation for a preliminary connection between the temporal muscle and the recipient vessels through the pial vasculature, further forming ICs from the deep temporal artery.

Post-operative bloody fluid volume

Postoperative bloody fluid volume was significantly correlated with indirect partial outcomes, which was supported by subsequent subgroup analysis (Table 4, Figure 2B). Unlike STA-MCA bypass, which reverses the impaired cerebral hemodynamic status immediately after surgery, it takes a long period for the temporal muscle to effectively associate with cortical regions *via* the leptomeningeal vessels (16). Hence, breaking down the barriers between the donor grafts and recipient arteries will help to further develop ICs. The specific location of bloody fluids greatly affects the contact between the separated temporal muscle and the pial vasculature (Figure 3).

Large volumes between the two layers may contain more angiogenesis-related cytokines, in contrast to the small volumes of bloody fluids. The specific allele of vascular

TABLE 5 Comparison of clinical features, surgical and follow-up characteristics in MMDs based on the classification of post-operative bloody fluids.

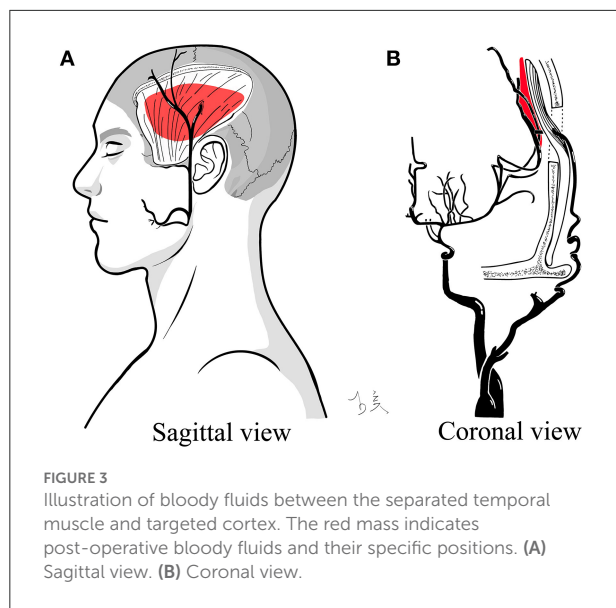
	Little (<i>n</i> = 28)	Small (<i>n</i> = 44)	Median (<i>n</i> = 23)	Large (<i>n</i> = 15)	<i>P</i> -value ^y
Age, yrs	41.4 ± 13.8	42.9 ± 11.4	40.1 ± 11.5	45.9 ± 8.9	0.864 ^z
Female (%)	20 (71.4)	33 (75.0)	15 (65.2)	8 (53.3)	0.445 [§]
Smoking (%)	3 (10.7)	8 (18.2)	5 (21.7)	4 (26.7)	0.582 [§]
Bilateral involved	23 (82.1)	35 (79.5)	17 (73.9)	12 (80.0)	0.910 [§]
Type of onset					0.536 [§]
Ischemia	16 (57.1)	23 (52.3)	13 (56.5)	1 (6.7)	
Hemorrhage	8 (28.6)	17 (38.6)	7 (30.4)	7 (46.7)	
Others	4 (14.3)	4 (9.1)	3 (13.0)	7 (46.7)	
Initial suzuki stage (%)					0.204 ^z
I	6 (21.4)	7 (15.9)	2 (8.7)	0 (0.0)	
II	2 (7.1)	5 (11.4)	5 (21.7)	2 (13.3)	
III	14 (50.0)	23 (52.3)	10 (43.5)	7 (46.7)	
IV	4 (14.3)	8 (18.2)	5 (21.7)	6 (40.0)	
V	2 (7.1)	0 (0.0)	1 (4.3)	0 (0.0)	
VI	0 (0.0)	1 (2.3)	0 (0.0)	0 (0.0)	
Surgery on the left (%)	14 (50.0)	22 (50.0)	10 (43.5)	10 (66.7)	0.572 [§]
Surface area, cm ²					
Time of post-op imaging, days	2.0 ± 1.0	2.0 ± 1.1	2. ± 1.0	2.270 ± 0.884	0.376 ^z
Post-operative complications, %	6 (21.4)	8 (18.2)	9 (39.1)	5 (33.3)	0.244 [§]
Follow-up period, mos	11.2 ± 3.9	15.5 ± 14.1	13.1 ± 6.4	11.1 ± 3.8	0.838 ^z
ICs grades, %					0.030[§]
Poor	14 (50.0)	18 (40.9)	7 (30.4)	3 (20.0)	
Minimal	11 (39.3)	19 (43.2)	12 (52.2)	8 (53.3)	
Good	3 (10.7)	7 (15.9)	4 (17.4)	4 (26.7)	
Direct matsushima score, %					0.550 ^z
1	8 (30.8)	11 (28.2)	10 (47.6)	5 (38.5)	
2	13 (50.0)	20 (51.3)	8 (38.1)	4 (30.8)	
3	5 (19.2)	8 (20.5)	3 (14.3)	4 (30.8)	

^y*p* < 0.05 are highlighted in bold.^zSpearman's correlation.[§]Kruskal–Wallis H-test.

Post-op, post-operative; ICs, indirect collaterals.

endothelial growth factor (VEGF) is associated with the poor collateral formation in MMD (17). Previous studies confirmed that the VEGF levels were nearly identical to those in healthy cohorts, confirming an active neovascularization state in patients with MMD (7) despite decreased serum caveolin-1 concentrations associated with negative arterial remodeling (18). Increased serum angiopoietin-2 levels have been described (19), and angiopoietins contained in these fluids may facilitate vascular responses that regulate angiogenesis *via* an autocrine release in patients with MMD (20). Additionally, surgical bypass can elevate VEGF-A₁₆₅ a/b ratios in MMD and intracranial atherosclerotic disease (21). These factors associated with neovascularization may be involved in initially establishing ICs, which contain these fluids between donor grafts and recipient encephalic regions.

Another hypothesis that may better account for this is that bloody fluid volume may be the epitome of donor muscular status. Bloody fluids inevitably accumulate after surgery, mostly because of errhysis of muscular grafts or from the outflow from anastomotic sites. During indirect or combined bypass, the temporal muscle is stripped from the skull and handled carefully *via* electrocoagulation, which may cause microvascular occlusion of the inner muscular side (22). Excessive application of bipolar forceps to the inner face of the separated muscle reduced the errhysis to a small volume in the first few hours after surgery. Conversely, a large volume of bloody fluids served as a possible indicator of well-preserved muscular grafts escaping immoderate electrocoagulation and implied a beneficial microvascular environment for collaterals through pia meningeal vessels in recipient encephalic regions. These



fluid volumes may reflect the impaired damage caused by electrocoagulation, suggesting that proper use of bipolar forceps is important when dealing with temporal muscles without severe arterial bleeding.

The large distance associated with large bloody fluid volumes may have blocked interactions between this donor muscle and recipient regions. Unfortunately, these results were not consistent with this trend. Medium and large volume of bloody fluids had similar results in the proportions of indirect outcomes (30.4 vs. 20.0, 52.2 vs. 53.3, and 17.4 vs. 26.7%; Table 5, Figure 2B). The largest volume was 23.4 ml from a patient in the minimal IC group. This may indicate that the inflection is reversed from positive to negative effects in ICs. The smallest size calculated by our software was 0.8 ml. The threshold range calculated by the software neglected the diluted portion mixed with subdural fluids, giving the illusion of minimal bloody fluids.

This study had several limitations. First, the threshold range calculated by the software may have neglected the dilute portion that is mixed with the subdural fluids, giving the illusion of minimal bloody fluids because the smallest size obtained was 0.761 ml. Second, operational factors, such as bipolar electrocoagulation frequency in the temporal muscle and integrity of the separated muscular grafts, could not be analyzed and might have resulted in a lack of evaluation criteria and data. Finally, there may be a selection bias between enrolled and excluded patients at baseline characteristics. Some cytokines possibly associated with collateral improvements in patients should also be confirmed. The conclusion requires further prospective studies with a larger MMD cohort to determine the critical point and mechanisms of MMD.

Conclusions

Bloody fluids between the temporal muscle and targeted brain regions are familiar manifestations in patients with MMD after surgery. In this study, the large volume of these fluids and previous ischemic history were associated with good indirect outcomes. The presence of bloody fluids reliably reflects muscle donor impairment due to bipolar electrocoagulation, which may indicate the active status of the temporal muscle, and highlights the need for appropriate application of the bipolar forceps. These findings also suggest that inadequate drainage may be acceptable, as this has occurred in patients undergoing EDMS and combined bypass. In summary, bloody fluids may have positive effects on long-term indirect outcomes.

Data availability statement

The raw data supporting the conclusions of this article will be made available by the authors, without undue reservation.

Ethics statement

The studies involving human participants were reviewed and approved by the Local Ethics Committee of the Second Affiliated Hospital of School of Medicine, Zhejiang University. Written informed consent to participate in this study was provided by the participants' legal guardian/next of kin.

Author contributions

Material preparation, data collection, and analysis were performed by YL and J-WH. The first draft of the manuscript was written by YL. All authors commented on previous versions of the manuscript, contributed to the study conception and design, read, and approved the final manuscript.

Funding

This work was supported by the National Science Foundation of China (Grant Nos. 81870910 and 82171271) and Natural Science Foundation of Zhejiang Province (LQ19H160039).

Acknowledgments

The volume of bloody fluids was calculated using 3D Slicer software (<https://www.slicer.org/>), which is a Free Open Source Software. In addition, we wish to thank the patients who participated in this study.

Conflict of interest

The authors declare that the research was conducted in the absence of any commercial or financial relationships that could be construed as a potential conflict of interest.

Publisher's note

All claims expressed in this article are solely those of the authors and do not necessarily represent those of their affiliated

organizations, or those of the publisher, the editors and the reviewers. Any product that may be evaluated in this article, or claim that may be made by its manufacturer, is not guaranteed or endorsed by the publisher.

Supplementary material

The Supplementary Material for this article can be found online at: <https://www.frontiersin.org/articles/10.3389/fneur.2022.960199/full#supplementary-material>

References

- Scott RM, Smith ER. Moyamoya disease and moyamoya syndrome. *N Engl J Med*. (2009) 360:1226–37. doi: 10.1056/NEJMra0804622
- Cho WS, Kim JE, Kim CH, Ban SP, Kang HS, Son YJ, et al. Long-term outcomes after combined revascularization surgery in adult Moyamoya disease. *Stroke*. (2014) 45:3025–31. doi: 10.1161/STROKEAHA.114.005624
- Ha EJ, Kim KH, Wang KC, Phi JH, Lee JY, Choi JW, et al. Long-Term outcomes of indirect bypass for 629 children with Moyamoya disease: longitudinal and cross-sectional analysis. *Stroke*. (2019) 50:3177–83. doi: 10.1161/STROKEAHA.119.025609
- Acker G, Fekonja L, Vajkoczy P. Surgical management of Moyamoya disease. *Stroke*. (2018) 49:476–82. doi: 10.1161/STROKEAHA.117.018563
- Uchino H, Kim JH, Fujima N, Kazumata K, Ito M, Nakayama N, et al. Synergistic interactions between direct and indirect bypasses in combined procedures: the significance of indirect bypasses in Moyamoya disease. *Neurosurgery*. (2017) 80:201–9. doi: 10.1227/NEU.00000000000001201
- Czabanka M, Vajkoczy P, Schmiedek P, Horn P. Age-dependent revascularization patterns in the treatment of moyamoya disease in a European patient population. *Neurosurg Focus*. (2009) 26:E9. doi: 10.3171/2009.1.FOCUS08298
- Bang OY, Chung JW, Kim SJ, Oh MJ, Kim SY, Cho YH, et al. Caveolin-1, ring finger protein 213, and endothelial function in Moyamoya disease. *Int J Stroke*. (2016) 11:999–1008. doi: 10.1177/174749301662039
- Research Committee on the Pathology and Treatment of Spontaneous Occlusion of the Circle of Willis, Health Labour Sciences Research Grant for Research on Measures for Infractable Diseases. Guidelines for diagnosis and treatment of Moyamoya disease (spontaneous occlusion of the circle of Willis). *Neurol Med Chir*. (2012) 52:245–66. doi: 10.2176/nmc.52.245
- Zhao J, Liu H, Zou Y, Zhang W, He S. Clinical and angiographic outcomes after combined direct and indirect bypass in adult patients with Moyamoya disease: a retrospective study of 76 procedures. *Exp Ther Med*. (2018) 15:3570–6. doi: 10.3892/etm.2018.5850
- Xu X, Chen X, Zhang J, Zheng Y, Sun G, Yu X, et al. Comparison of the tada formula with software slicer: precise and low-cost method for volume assessment of intracerebral hematoma. *Stroke*. (2014) 45:3433–5. doi: 10.1161/STROKEAHA.114.007095
- Matsushima T, Inoue T, Suzuki SO, Fujii K, Fukui M, Hasuo K. Surgical treatment of Moyamoya disease in pediatric patients—comparison between the results of indirect and direct revascularization procedures. *Neurosurgery*. (1992) 31:401–5. doi: 10.1097/00006123-199209000-00003
- Bremmer JP, Verweij BH, Klijn CJ, van der Zwan A, Kappelle LJ, Tulleken CA. Predictors of patency of excimer laser-assisted nonocclusive extracranial-to-intracranial bypasses. *J Neurosurg*. (2009) 110:887–95. doi: 10.3171/2008.9.JNS08646
- Matano F, Murai Y, Tateyama K, Tamaki T, Mizunari T, Matsukawa H, et al. Long-term patency of superficial temporal artery to middle cerebral artery bypass for cerebral atherosclerotic disease: factors determining the bypass patent. *Neurosurg Rev*. (2016) 39:655–61. doi: 10.1007/s10143-016-0736-5
- Kim JH, Ha SK, Jin SW, Lee HB, Kim SD, Kim SH, et al. Color doppler ultrasonography for predicting the patency of anastomosis after superficial temporal to middle cerebral artery bypass surgery. *Acta Neurochir*. (2021) 163:1503–13. doi: 10.1007/s00701-020-04669-z
- Zhao Y, Li J, Lu J, Zhang Q, Zhang D, Wang R, et al. Predictors of neoangiogenesis after indirect revascularization in Moyamoya disease: a multicenter retrospective study. *J Neurosurg*. (2019) 1–11. doi: 10.3171/2018.9.JNS181562
- Zhao Y, Lu J, Zhang Q, Zhang Y, Zhang D, Wang R, et al. Time course of neoangiogenesis after indirect bypass surgery for Moyamoya disease: comparison of short-term and long-term follow-up angiography. *Clin Neuroradiol*. (2020) 30:91–9. doi: 10.1007/s00062-018-0748-3
- Park YS, Jeon YJ, Kim HS, Chae KY, Oh SH, Han IB, et al. The role of VEGF and KDR polymorphisms in Moyamoya disease and collateral revascularization. *PLoS ONE*. (2012) 7:e47158. doi: 10.1371/journal.pone.0047158
- Chung JW, Kim DH, Oh MJ, Cho YH, Kim EH, Moon GJ, et al. Cav-1 (Caveolin-1) and arterial remodeling in adult Moyamoya disease. *Stroke*. (2018) 49:2597–604. doi: 10.1161/STROKEAHA.118.021888
- Yu J, Huang K, Pan J, Shen J, Zhan R. Significance of serum angiopoietin-2 in patients with hemorrhage in adult-onset Moyamoya disease. *Biomed Res Int*. (2020) 2020:8209313. doi: 10.1155/2020/8209313
- Blecharz KG, Frey D, Schenkel T, Prinz V, Bedini G, Krug SM, et al. Autocrine release of angiopoietin-2 mediates cerebrovascular disintegration in Moyamoya disease. *J Cereb Blood Flow Metab*. (2017) 37:1527–39. doi: 10.1177/0271678X16658301
- Jiang H, Toscano JF, Schiraldi M, Song SS, Schlick KH, Dumitrascu OM, et al. Differential expression of vascular endothelial growth factor-A165 isoforms between intracranial atherosclerosis and Moyamoya disease. *J Stroke Cerebrovasc Dis*. (2019) 28:360–8. doi: 10.1016/j.jstrokecerebrovasdis.2018.10.004
- Brill AI. Bipolar electrosurgery: convention and innovation. *Clin Obstet Gynecol*. (2008) 51:153–8. doi: 10.1097/GRF.0b013e318161e7ee



OPEN ACCESS

EDITED BY

Chengcheng Zhu,
University of Washington,
United States

REVIEWED BY

Yang Wang,
Capital Medical University, China
Rajat Dhar,
Washington University in St. Louis,
United States

*CORRESPONDENCE

Shaoshan Hu
shaoshanhu421@126.com
Jianjun Wang
1499@sdsdhospital.com.cn

[†]These authors have contributed
equally to this work

SPECIALTY SECTION

This article was submitted to
Applied Neuroimaging,
a section of the journal
Frontiers in Neurology

RECEIVED 30 June 2022

ACCEPTED 24 October 2022

PUBLISHED 08 November 2022

CITATION

Zhou P, Sun Q, Song G, Liu Z, Qi J,
Yuan X, Wang X, Yan S, Du J, Dai Z,
Wang J and Hu S (2022) Radiomics
features from perihematomal edema
for prediction of prognosis in the
patients with basal ganglia
hemorrhage. *Front. Neurol.* 13:982928.
doi: 10.3389/fneur.2022.982928

COPYRIGHT

© 2022 Zhou, Sun, Song, Liu, Qi, Yuan,
Wang, Yan, Du, Dai, Wang and Hu. This
is an open-access article distributed
under the terms of the [Creative
Commons Attribution License \(CC BY\)](#).
The use, distribution or reproduction
in other forums is permitted, provided
the original author(s) and the copyright
owner(s) are credited and that the
original publication in this journal is
cited, in accordance with accepted
academic practice. No use, distribution
or reproduction is permitted which
does not comply with these terms.

Radiomics features from perihematomal edema for prediction of prognosis in the patients with basal ganglia hemorrhage

Peng Zhou^{1†}, Quanye Sun^{2†}, Gesheng Song^{3†}, Zexiang Liu¹,
Jianfeng Qi¹, Xuhui Yuan¹, Xu Wang¹, Shaofeng Yan¹,
Jianyang Du⁴, Zhengjun Dai⁵, Jianjun Wang^{1*} and
Shaoshan Hu^{6*}

¹Department of Neurosurgery, The First Affiliated Hospital of Shandong First Medical University & Shandong Provincial Qianfoshan Hospital, Jinan, China, ²Research Center of Translational Medicine, Central Hospital Affiliated to Shandong First Medical University, Jinan, China, ³Department of Radiology, The First Affiliated Hospital of Shandong First Medical University & Shandong Provincial Qianfoshan Hospital, Jinan, China, ⁴Department of Neurosurgery, Shandong Provincial Hospital Affiliated to Shandong First Medical University, Jinan, China, ⁵Scientific Research Department, Huiying Medical Technology Co., Ltd, Beijing, China, ⁶Department of Neurosurgery, Emergency Medicine Center, Hangzhou Medical College, Zhejiang Provincial People's Hospital, Hangzhou, China

Objective: We developed and validated a clinical-radiomics nomogram to predict the prognosis of basal ganglia hemorrhage patients.

Methods: Retrospective analyses were conducted in 197 patients with basal ganglia hemorrhage (training cohort: $n = 136$, test cohort: $n = 61$) who were admitted to The First Affiliated Hospital of Shandong First Medical University (Shandong Provincial Qianfoshan Hospital) and underwent computed tomography (CT) scan. According to different prognoses, patients with basal ganglia hemorrhage were divided into two groups. Independent clinical risk factors were derived with univariate and multivariate regression analysis. Radiomics signatures were obtained using least absolute shrinkage and selection operator. A radiomics score (Rad-score) was generated by 12 radiomics signatures of perihematomal edema (PHE) from CT images that were correlated with the prognosis of basal ganglia hemorrhage patients. A clinical-radiomics nomogram was conducted by combining the Rad-score and clinical risk factors using logistic regression analysis. The prediction performance of the nomogram was tested in the training cohort and verified in the test cohort.

Results: The clinical model conducted by four clinical risk factors and 12 radiomics features were used to establish the Rad-score. The clinical-radiomics nomogram outperformed the clinical model in the training cohort [area under the curve (AUC), 0.92 vs. 0.85] and the test cohort (AUC, 0.91 vs. 0.85). The clinical-radiomics nomogram showed good calibration and clinical benefit in both the training and test cohorts.

Conclusion: Radiomics features of PHE in patients with basal ganglia hemorrhage could contribute to the outcome prediction. The clinical-radiomics nomogram may help first-line clinicians to make individual clinical treatment decisions for patients with basal ganglia hemorrhage.

KEYWORDS

radiomics, perihematomal edema, machine learning model, prognosis, basal ganglia hemorrhage

Introduction

Spontaneous intracerebral hemorrhage (ICH) accounts for 10% of all strokes and has a high mortality rate of ~40% (1). The basal ganglia are the most common site of ICH. Globally, ICH leads to 2.8 million deaths per year (2, 3), and only 12–39% of ICH patients could live independently without disabilities (4). Because ICH usually leads to death, morbidity, and disability, early and accurate prediction of clinical prognosis is important to guide the development of clinical treatment plans and observe the effect of treatment.

Perihematomal edema (PHE) is caused by damage to the blood-brain barrier (BBB) and neuronal ion channel disruption and is an important secondary injury following ICH (5, 6). It is the primary cause of increased intracranial pressure, brain hernia, and death in ICH patients and contributes to poor clinical prognosis (7, 8). Many studies have shown that increased PHE volume around the hematoma after ICH was an independent risk factor in ICH patients for poor prognosis (9–12). Computed tomography (CT) is the most common examination method for diagnosing PHE. During the early stage, the characteristics of PHE are not typical in CT images, and accurate interpretations rely on radiologists' experience (13–15). It is difficult for clinicians to quantify early cerebral edema following ICH. Therefore, developing a more objective and convenient method for volume and severity assessment of the PHE in CT scans will significantly benefit prognosis predictions and could contribute to clinical intervention decision-making.

Radiomics is a rapidly developing method based on computer-aided detection or diagnosis and combines quantitative image analysis and machine learning algorithms (16–19). Radiomics overcomes the limitation of image interpretation, which usually relies on the experience of doctors (20, 21). At present, radiomics is used primarily for screening and quantitative analysis of the most valuable imaging features, which are used to develop machine learning models for either diagnosis or prognosis prediction (22–24).

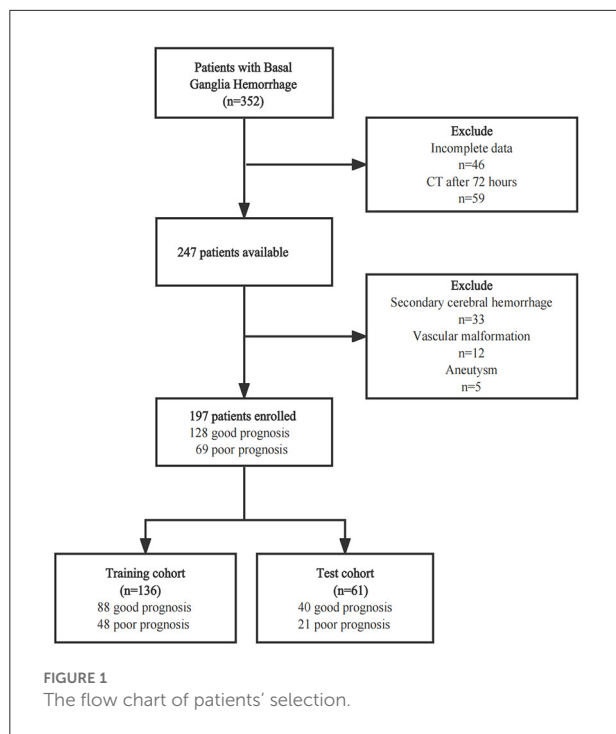
Although previous studies have suggested that PHE is a predictor of functional outcomes in ICH patients, the impact of PHE on the prognosis of ICH is controversial (25–28). Currently, the association between the radiomics features of PHE in CT scans and the outcome of ICH patients remains unclear.

In this study, we aimed to establish and validate a combined nomogram for predicting the prognosis of basal ganglia hemorrhage patients using the radiomics features of PHE and clinical characteristics.

Materials and methods

Collection and selection of patient data

This single-center retrospective study was approved by the Medical Ethics Committee of The First Affiliated Hospital of Shandong First Medical University (Shandong Provincial Qianfoshan Hospital), and the informed consent was waived. 352 ICH patients were recruited between January 2016 and March 2022. For this study, the inclusion criteria were as follows: (1) patients aged over 18 years with a spontaneous ICH in the basal ganglia; (2) CT examination performed within 72 h of disease onset; (3) admission assessment using the National Institute of Health Stroke Scale (NIHSS). Patients with the following conditions were excluded: (1) patients with a tumor, vascular malformation, aneurysm, or trauma, and those who had undergone thrombolytic therapy or cerebral arteriovenous thrombosis; (2) patients pretreated with anticoagulants or those with coagulopathy; (3) pregnant women; (4) patients with multiple organ failure. Finally, a total of 197 patients were enrolled. This patient database was divided into a training cohort ($n = 136$) and a test cohort ($n = 61$) at a 7:3 ratio, with the random seed of 186 (Figure 1). The Glasgow Outcome Scale (GOS) was used for assessing the clinical outcome of patients when they were discharged from the hospital, which was usually 7–10 days after admission. A GOS score of 4–5 represented a good prognosis, while a score of 1–3 was regarded as a poor prognosis (Figure 1).



Images acquisition and region of interest segmentation

The first CT scans of patients after ICH onset were acquired on two types of CT scanners (Discovery CT750 HD and Optima CT660, General Electric Company, USA) using standardized scanning protocols: tube voltage and current of 120 kV and 350 mA, the field of view of 32 cm, matrix size of 512×512 , and slice thickness of 5 mm. The scanning range was from the skull base to the cranium.

The region of interest (ROI) segmentation of the PHE and hematoma were performed by a neuroradiologist with 10 years of experience using Radcloud (Huiying Medical Technology Co., Ltd., China). The validation of segmentation results was conducted by a senior neuroradiologist with 20 years of experience in 19 randomly selected patients. All radiologists were blind to the clinical information of the patients.

Feature extraction and selection

Using the Radcloud platform, we extracted 1,409 quantitative imaging features of PHE from the CT images. These features contained first-order statistics and texture, shape, and size features. The feature extraction was conducted using a “pyradiomics” package (<https://pyradiomics.readthedocs.io/en/latest/>).

We first conducted the intraclass correlation coefficient test in 19 patients, and 1,225 features with a $p > 0.75$ were screened for the subsequent analysis. The variance threshold method reduced the number of features to 1,178, of which 131 were retained after applying the SelectKBest method. Finally, using the least absolute shrinkage and selection operator (LASSO) regression model, 12 radiomics signatures were selected for machine model building (Figure 2). The features of hematoma were extracted in the same way as for PHE and were combined with the features of PHE for selection. The combined feature selection was conducted using the variance threshold (variance threshold = 0.8), SelectKBest ($p < 0.05$), and the LASSO, and 12 combined features were obtained (Supplementary materials). PHE volume and hematoma volume were calculated using the Radcloud platform.

Machine learning model building

Clinical characteristics were screened using univariate and multivariate logistic regression analyses. Factors with a $p < 0.05$ were considered single risk factors for prognosis in basal ganglia hemorrhage patients by univariate logistic regression analyses in the training cohort. These single factors were then analyzed by multivariate logistic regression analyses, and factors with a $p < 0.1$ were considered independent risk factors for prognosis. Using these factors, we built a clinical model using logistic regression in the training cohort and verified in the test cohort.

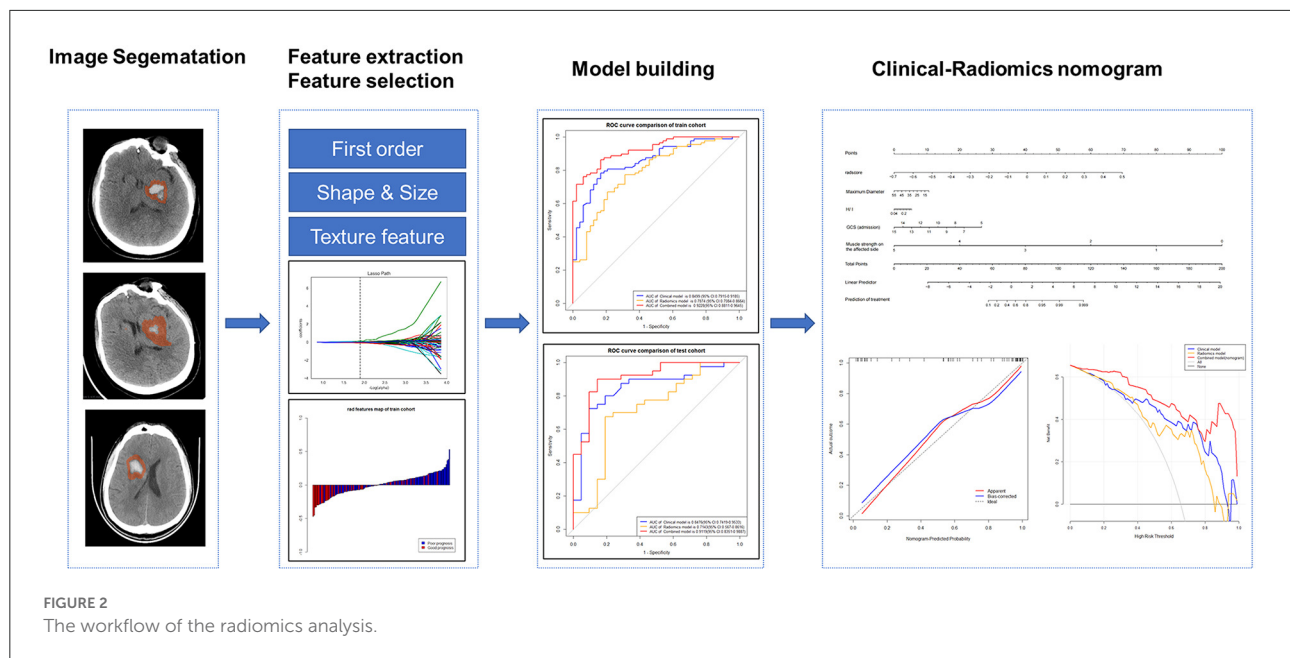
PHE volume-clinical model was conducted with the PHE volume and the four independent clinical features by logistic regression in the training cohort and verified in the test cohort.

The radiomics score (Rad-score) was calculated for each patient by a formula using the selected 12 radiomics signatures. The rad-score formula was obtained as follows: $\text{Rad-score} = \alpha + \sum_{i=1}^n \beta_i X_i$, and α is the intercept ($\alpha = 0.647$), β_i is the value of radiomics feature; X_i is the corresponding coefficient (Supplementary materials).

Based on the selected features of PHE, we constructed radiomics models with three classifiers, including Logistic Regression (LR), Decision tree (DT), and Support Vector Machine (SVM). The effectiveness of the model was improved using the validation method.

The clinical-radiomics nomogram was derived using the rad-score and the independent clinical risk factors in the training cohort and verified in the test cohort using logistic regression analysis.

The PHE-hematoma-clinical model was conducted with four independent clinical risk factors and the 12 selected combined radiomics features using LR analysis in the training cohort and verified in the test cohort (Supplementary materials).



Model evaluation

The receiver operating characteristic (ROC) curve was used to assess the predictive efficacy of machine learning models in the training and test cohort. Delong test was used to evaluate the differences of the area under curves (AUCs). The nomogram was evaluated by calibration curves and Hosmer-Lemeshow test in the training and test cohorts. Decision curve analysis (DCA) was conducted to determine the clinical benefit of the machine learning models by calculating the net benefits at different threshold probabilities.

Statistical analysis

Statistical analyses were conducted with R software (version 3.4.4) and the SPSS software (version 22.0). Clinical characteristics are described as medians (interquartile ranges) or means \pm standard deviations according to the results of the Shapiro-Wilk test. Categorical data, such as sex, are expressed as percentages. The chi-squared test, Fisher's exact test, and Mann-Whitney U test were used for univariate analysis. A $p < 0.05$ was considered statistically significant.

Results

Characteristics of basal ganglia hemorrhage patients

There were no significant differences in clinical characteristics between the training and test cohorts

(Table 1). Univariate analysis indicated that maximum diameter, hematoma/intracranial diameter (H/I), Glasgow Coma Scale (GCS) score, Mg (magnesium), hematoma volume, D-dimer (DD2), NIHSS score, and muscle strength on the affected side were potential risk factors for prognosis in basal ganglia hemorrhage (Table 2, $p < 0.05$). These eight clinical features were subsequently analyzed using multivariate logistic regression and obtained four independent predictors of prognosis: GCS score ($p = 0.013$), muscle strength on the affected side ($p < 0.001$), hematoma volume ($p = 0.092$), and DD2 ($p = 0.047$).

Clinical and radiomics models for prognosis prediction in patients with basal ganglia hemorrhage

The clinical model comprising four independent risk factors had an AUC of 0.85 [95% confidence interval (CI), 0.79–0.92] in the training cohort, and the AUC was 0.85 (95% CI, 0.74–0.95) in the test cohort (Figure 3).

The radiomics model comprised three different classifiers using the 12 radiomics features. As shown in Supplementary Figure 2, in the training cohort, the AUC of the SVM model was 0.79 (95% CI, 0.71–0.87), the AUC of the LR model was 0.79 (95% CI, 0.71–0.87), and the AUC of the DT model was 0.74 (95% CI, 0.67–0.81). In the test cohort, the AUC of the SVM model was 0.70 (95% CI, 0.56–0.85), the AUC of the LR model was 0.71 (95% CI, 0.57–0.86), and the

TABLE 1 Patients' characteristics in the training and test cohorts.

Variables	Training cohort (<i>n</i> = 136)	Test cohort (<i>n</i> = 61)	<i>P</i>
Age, years	60 ± 11.8	59.5 ± 12.9	0.372
Sex (male), <i>n</i> (%)	78 (57)	44 (72)	0.057
Muscle strength on the affected side	3 (1,4)	2 (1,4)	0.484
Minimum diameter, mm	16.81 (14.51, 20.98)	18.52 (13.05, 21.65)	0.088
Maximum diameter, mm	31.36 ± 10.77	29.93 ± 8.5	0.718
Roundness, mm	12.2 (6.45, 19.5)	11.4 (5.7, 18.9)	0.337
Intracranial diameter, mm	127.31 ± 7.28	128.6 ± 7.5	0.485
Hematoma diameter, mm	19.94 (15.65, 24.29)	21.65 (14.67, 26.76)	0.275
H/I	0.16 ± 0.05	0.17 ± 0.05	0.189
GCS score	11(9,13)	10 (9,13)	0.879
Alkaline phosphatase	75 (64, 90.15)	71.6 (62.6, 88)	0.751
K, mmol/L	3.88 (3.52, 4.07)	3.91 (3.57, 4.3)	0.413
Na, mmol/L	141.06 (137, 143)	141.1 (138, 143)	0.307
Ca, mmol/L	2.23 (2.11, 2.33)	2.21 (2.16, 2.29)	0.799
Mg, mmol/L	0.88 (0.84, 0.91)	0.89 (0.85, 0.92)	0.095
Blood glucose at admission, mmol/L	5.97 (4.94, 6.91)	5.9 (5.06, 7.3)	0.710
WBC, 10 ⁹ /L	7.66 (6.38, 9.49)	8.09 (6.06, 9.58)	0.884
Neutrophils, 10 ⁹ /L	6.03 (4.44, 7.68)	5.77 (4.38, 7.96)	0.613
Lymphocyte, 10 ⁹ /L	1.16 (0.77, 1.55)	1.3 (0.78, 1.73)	0.448
NLR	5.08 (3.14, 9.63)	4.54 (2.77, 7.36)	0.471
Hb, g/L	137.2 ± 15.46	137.98 ± 14.57	0.842
HCT	0.41 ± 0.04	0.42 ± 0.04	0.497
RDW–CV	12.5 (12,13)	12.7 (12.1, 13.2)	0.346
PLT, 10 ⁹ /L	218 (185, 251.75)	213 (171, 265)	0.299
PDW, fL	12 (10.47, 13.43)	11.9 (10.7, 12.9)	0.569
PT, sec	11.2 (10.7, 11.6)	11.3 (10.6, 11.7)	0.914
INR	0.96 (0.91, 1.01)	0.97 (0.90, 1.03)	0.689
APTT, sec	25.4 (23.45, 27.13)	25.6 (21.73, 29.43)	0.456
TT, sec	17.05 (16.38, 17.8)	17.1 (16.5, 17.9)	0.621
DD2, mg/L	0.35 (0.2, 0.69)	0.35 (0.22, 0.75)	0.657
Systolic pressure at hospital admission	164 ± 27.4	162.3 ± 23.6	0.745
Diastolic pressure at hospital admission	95.4 ± 15.8	93 ± 13.0	0.054
Hematoma volume, mL	16.64 (9.9, 27.83)	15.23 (6.47, 23.38)	0.149
NIHSS score	7 (4,11)	6 (4,11)	0.429
First CT (hour)	19 (12,30)	20 (12,33)	0.672

H/I, hematoma/intracranial diameter; GCS, Glasgow Coma Scale; NIHSS, National Institute of Health stroke scale. Data are shown as median (interquartile ranges) or mean ± standard deviations.

AUC of the DT model was 0.67 (95% CI, 0.50–0.76). The LR model got better performance than the SVM and DT models (Supplementary Table 1). The results of Delong test showed that although the clinical model had higher AUCs than the LR radiomics model, no significant difference was found between these models in the training cohort ($p = 0.152$) and the test cohort ($p = 0.159$).

To verify whether the PHE volume contributes to the enhanced prediction of prognosis, we combined

the four independent clinical risk factors and the PHE volume to build a model to predict the prognosis of basal ganglia hemorrhage patients. Results showed that PHE volume-clinical model had an AUC of 0.91 (95% CI, 0.87–0.96) in the training cohort and an AUC of 0.84 (95% CI, 0.74–0.95) in the test cohort (Supplementary Figure 3). This PHE volume-clinical model did not show a better performance than the clinical model in prognosis prediction.

TABLE 2 Univariate analyses of predictors of prognosis in training cohorts.

Variables	Good prognosis (<i>n</i> = 88)	Poor prognosis (<i>n</i> = 48)	<i>P</i>
Age, years	62.5 ± 13.1	59.1 ± 10.1	0.203
Sex (male), <i>n</i> (%)	52 (59)	26 (54)	0.709
Muscle strength on the affected side	4 (2-4)	0 (0-2)	<0.001
Minimum diameter, mm	16.63 (13.84, 18.79)	17.66 (15.13, 22.37)	0.060
Maximum diameter, mm	29.81 ± 9.93	34.22 ± 11.74	0.021
Roundness, mm	10.3 (6.31, 17.44)	13.48 (6.9, 21.93)	0.116
Intracranial diameter, mm	127.74 ± 7.71	126.53 ± 6.41	0.355
Hematoma diameter, mm	8.16 (14.9, 23.37)	21.04 (17.14, 25.64)	0.067
H/I, median	0.15 ± 0.06	0.17 ± 0.05	0.048
GCS score	12 (10,13)	9 (7.75, 10)	<0.001
Alkaline phosphatase	75.55 (64.38, 90.15)	72.3 (63.25, 88.75)	0.609
K, mmol/L	3.84 (3.54, 4.05)	3.9 (3.49, 4.11)	0.460
Na, mmol/L	141.18 ± 3.95	140.86 ± 3.95	0.651
Ca, mmol/L	2.22 ± 0.1	2.25 ± 0.11	0.104
Mg, mmol/L	0.91 ± 0.1	0.86 ± 0.1	0.009
Blood glucose at admission, mmol/L	6.26 (5.46–7.15)	5.36 (4.79–6.02)	0.163
WBC, 10 ⁹ /L	7.5 (6.32, 8.95)	8.16 (6.49, 9.72)	0.084
Neutrophils, 10 ⁹ /L	5.74 (4.42, 7.6)	6.22 (4.62, 8.29)	0.084
Lymphocyte, 10 ⁹ /L	1.17 (0.8, 1.54)	1.09 (0.75, 1.61)	0.432
NLR	5 (3.04, 8.47)	5.6 (3.49, 10.89)	0.344
Hb, g/L	138.35 ± 14.76	135.08 ± 16.62	0.240
HCT	0.41 ± 0.04	0.4 ± 0.05	0.108
RDW–CV	12.9 (12.0–13.4)	12.2 (11.9–13.0)	0.331
PLT, 10 ⁹ /L	219.5 (188.5, 256.5)	215.5 (167.25, 248)	0.595
PDW, fL	11.75 (10.47, 13.53)	12.2 (10.45, 13.25)	0.917
PT, sec	11.1 (10.7, 11.43)	11.2 (10.67, 11.7)	0.080
INR	0.96 (0.92, 1)	0.96 (0.9, 1.02)	0.149
APTT, sec	25.4 (23.7, 26.85)	25.25 (23.03, 27.45)	0.069
TT, sec	17.2 (16.6, 17.83)	16.8 (16.17, 17.4)	0.872
DD2, mg/L	0.29 (0.18, 0.54)	0.5 (0.24, 0.88)	0.027
Systolic pressure at hospital admission	165.6 ± 27.5	161.3 ± 27.1	0.727
Diastolic pressure at hospital admission	96.3 ± 16.4	93.8 ± 14.8	0.934
Hematoma volume, mL	13.97 (8.18, 24.98)	26.82 (16.23, 35.1)	<0.001
NIHSS score	5 (3,8)	10 (7,14)	<0.001
First CT (hour)	20 (12, 29.25)	19 (12, 31.25)	0.655

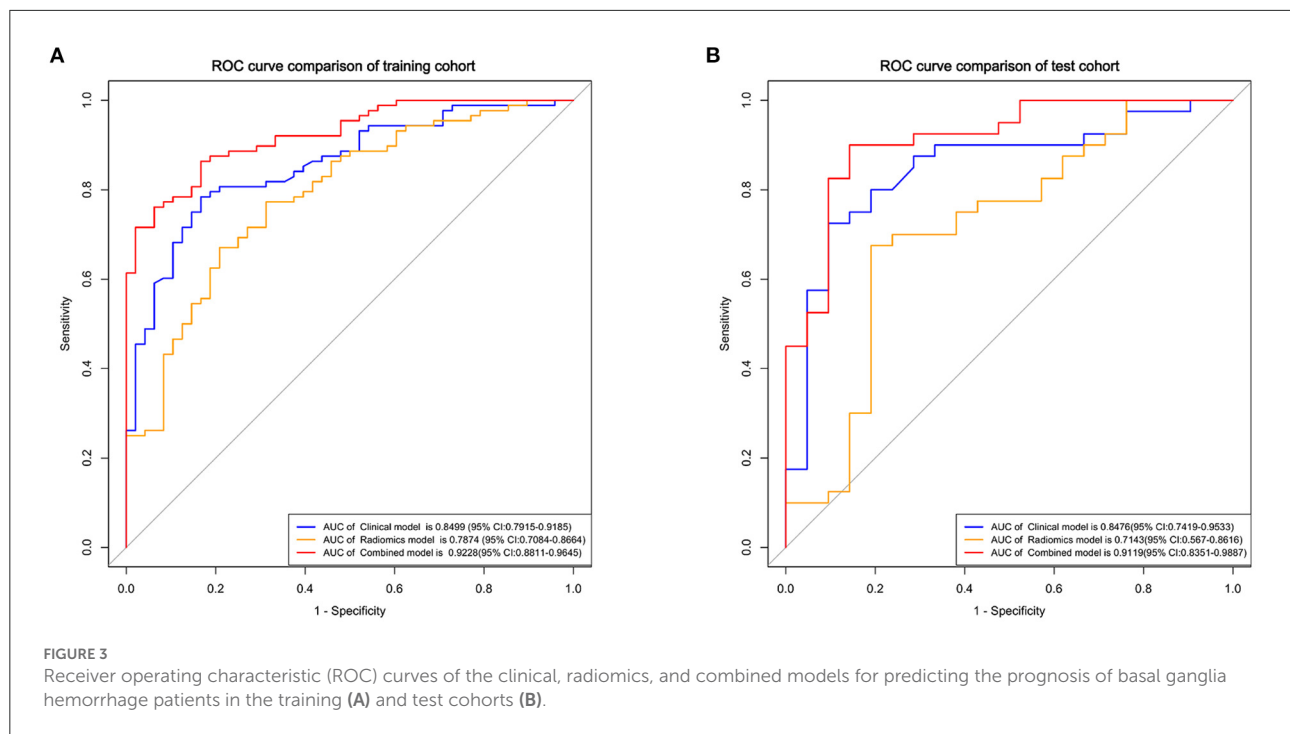
H/I, hematoma/intracranial diameter; GCS, Glasgow Coma Scale; NIHSS, National Institute of Health stroke scale. Data are shown as median (interquartile ranges) or mean ± standard deviations.

Development of the clinical-radiomics nomogram

Using the four clinical independent risk factors and the Rad-score, a clinical-radiomics combined model was built using a logistic regression classifier. As shown in Figure 3, the AUC of the combined model was 0.92 (95% CI, 0.88–0.96) in the training cohort and 0.91 (95% CI, 0.84–0.99) in the test cohort. The clinical-radiomics model showed a better performance in

prognosis prediction than the clinical ($p = 0.006$, Delong test) and radiomics models ($p < 0.001$, Delong test) in the training cohort. In the test cohort, although the clinical-radiomics model did not perform significantly differently from the clinical ($p = 0.203$), but had a better performance in prognosis prediction than the radiomics model ($p = 0.002$).

The clinical-radiomics nomogram for determining the prognosis of basal ganglia hemorrhage patients was shown in Figure 4. The calibration curves indicated the prediction



probabilities of the nomogram were well-aligned with the actual outcome in both the training ($p = 0.154$) and test cohorts ($p = 0.860$).

We also developed a PHE-hematoma-clinical model using 12 combined radiomics features of PHE and hematoma and the four independent clinical features for prognosis prediction. The PHE-hematoma-clinical model showed AUCs of 0.91 and 0.90 in the training and test cohort (Supplementary Figure 4). This PHE-hematoma-clinical model did not show a better performance in prognosis prediction than the clinical-radiomics model (Supplementary Table 2).

Finally, we used DCA analysis to compare the clinical benefits of different prediction models. As shown in Figure 5, the decision curves graphically displayed that the clinical-radiomics model had a better benefit than the clinical and radiomics models, indicating the superiority of the combined model.

Discussion

In this research, we confirmed that radiomics features of PHE from CT images combined with clinical features are valuable for prognosis prediction of patients with basal ganglia hemorrhage. Compared with the clinical model, the clinical-radiomics model showed a better performance for prognosis prediction. The nomogram derived from this clinical-radiomics model will enable first-line clinicians to evaluate ICH patients and develop individual treatment strategies without relying on substantial experience in diagnostic imaging.

At present, most clinicians predict the prognosis of ICH patients using clinical characteristics. Therefore, we first analyzed the clinical data of patients. Statistical results showed that DD2, GCS score, hematoma volume, and muscle strength on the affected side were independent predictors of prognosis in basal ganglia hemorrhage patients. The GCS has been widely used in clinical research to assess and calculate the level of consciousness of patients (29–31). In line with our results, the GCS score has been shown to be strongly associated with the outcome of basal ganglia hemorrhage patients and is an independent predictor of critical care (32, 33). Similar to the previous studies, plasma DD2 could predict poor outcome and mortality in ICH patients (34–36). We used these four risk factors to build a clinical model using logistic regression and yielded in the test cohort (AUC: 0.85), which indicated that the clinical model does not provide sufficient accuracy for predicting prognosis in basal ganglia hemorrhage patients. Combining these clinical features with other variables would likely improve the predictive ability of this machine learning model.

PHE is associated with secondary injury in ICH (5, 36). Volbers et al. (37) showed that the volume of PHE is an independent predictive factor for ICH patients at 90 days post-onset. However, it has controversy for the connection between PHE and the ICH patients' outcome (38). Loan et al. (39) reported the volume of PHE was not independently associated with death or dependence 1 year after ICH, as well as the total volume of ICH and PHE are independent risk factors. As shown in this research, the AUC of PHE volume-clinical model was

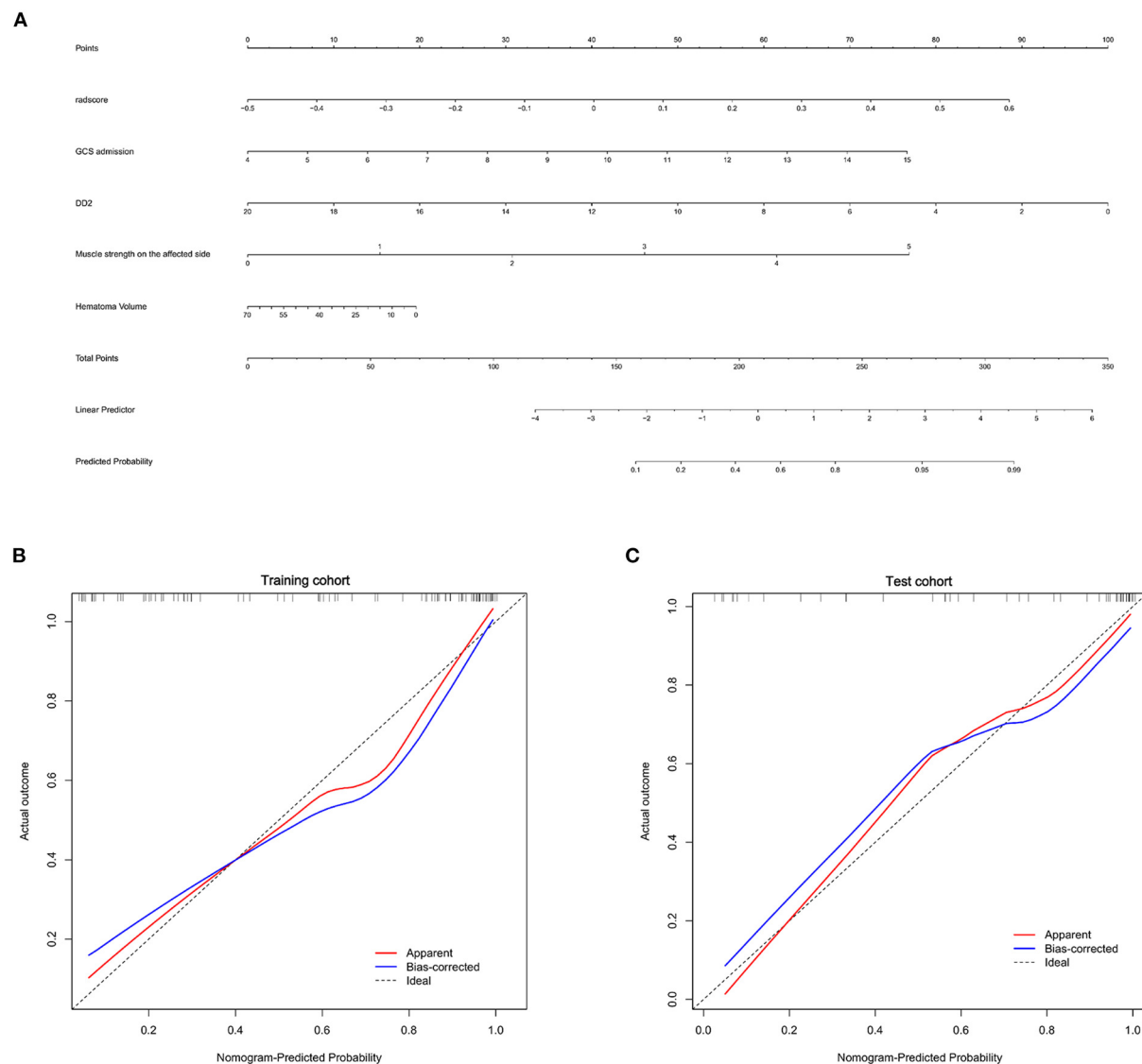


FIGURE 4

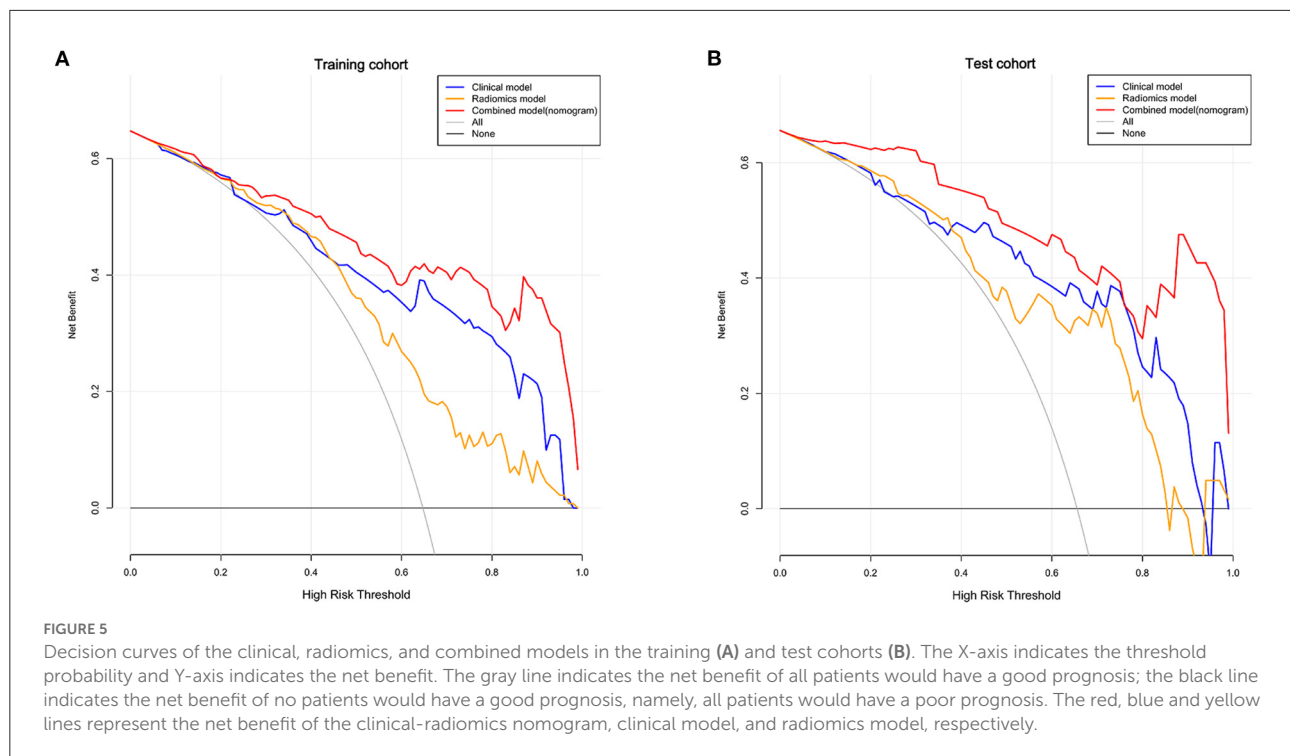
Nomogram for prognosis prediction and the calibration of the nomogram in the patients with basal ganglia hemorrhage. (A) The clinical-radiomics nomogram for the prediction of prognosis of basal ganglia hemorrhage patients. Calibration curves of the radiomics nomogram in the training (B) and test cohorts (C).

0.84 in the test cohort, suggesting that PHE volume could not improve the prediction ability of the clinical model. Radiomics features of PHE may have a better-discriminating efficacy for the prognosis of basal ganglia hemorrhage patients.

Although radiomics features enable the quantification of medical imaging characteristics, they are difficult to reproduce and validate according to published studies because of the lack of standardized definitions. The Image Biomarker Standardization Initiative formed in 2016 allows the validation of different radiomics software (40). This finding contributed to the repeatability of medical imaging research. We standardized

image processing and feature extraction according to this standard. The Rad-score in our study was derived from 12 radiomics features of PHE in CT images associated with prognoses and included eight texture features (three GLRLM and five GLSZM), three shape features, and one first-order feature.

In our study, the clinical model showed an AUC of 0.85 and radiomics model showed an AUC of 0.71, which indicated the use of only one of these modalities would not offer sufficient accuracy. Thus, we combined these two models, which yielded a much higher AUC



(0.91) in the test cohort, which suggested radiomics could improve prognosis prediction in basal ganglia hemorrhage patients.

Since hematoma is a critical factor related to the prognosis of ICH, we added the radiomics features of hematoma for analysis. Results showed an AUC of 0.90 of the PHE-hematoma-clinical model in the test cohort, which did not have a better performance in prognosis prediction compared with the clinical-radiomics model. These results suggested that the clinical-radiomics model contained features of PHE combined with independent clinical features (including hematoma volume) already had a good performance in prognosis prediction of basal ganglia hemorrhage patients. There was no need to add the radiomics features of hematoma for model building.

There are some limitations in our research. First, the data of the patients were obtained from a single center with relatively small sample size. We plan to conduct a multi-center study with a larger patient sample size in the future. Second, we used GOS scores to evaluate the prognosis of basal ganglia hemorrhage patients when they were discharged from the hospital (~7–10 days following ICH onset). We plan to include additional time points, including long-term prognoses, in future studies. Third, the results of DeLong test suggested that the clinical-radiomics model had a higher AUC than the clinical and radiomics models in the test cohort;

however, the difference was not significant. We considered the relatively small sample size and segmentation errors might be responsible for this result. Finally, this was a retrospective study, and diagnostic, detection, and evaluation criteria were not standardized. Therefore, several variables could not be analyzed, which may have impacted the predictive ability of the radiomics model.

Conclusion

We built a clinical-radiomics nomogram (model) comprising clinical independent risk factors and radiomics features of PHE derived from CT images, and this nomogram showed good accuracy for prognosis prediction in basal ganglia hemorrhage patients. Our findings suggested the radiomics features of PHE could contribute to the outcomes prediction of patients with basal ganglia hemorrhage. The clinical-radiomics nomogram may help first-line clinicians in clinical treatment decision-making for basal ganglia hemorrhage patients.

Data availability statement

The original contributions presented in the study are included in the article/[Supplementary material](#),

further inquiries can be directed to the corresponding authors.

Author contributions

PZ, QS, and GS: writing original draft. ZL, JQ, and JD: organization. ZL, PZ, QS, GS, JQ, and JD: statistical analysis. XY, XW, and SY: data collection. JW, SH, and JD: conceptualization, funding acquisition, and review. JW, SH, PZ, QS, GS, and JD: study design. All authors contributed to the article and approved the submitted version.

Funding

This study was funded by Clinical Scientific Research Fund of Shandong Medical Association (No. YXH2022ZX02179) and Natural Science Foundation of Shandong Province (No. ZR2020MH153).

Acknowledgments

The authors thank Dr. Aiyin Li for reviewing the CT images and Ms. Ran Zhang for analyzing the datasets.

References

- Schrag M, Kirshner H. Management of intracerebral hemorrhage: JACC focus seminar. *J Am Coll Cardiol*. (2020) 75:1819–31. doi: 10.1016/j.jacc.2019.10.066
- Hostettler IC, Seiffge DJ, Werring DJ. Intracerebral hemorrhage: an update on diagnosis and treatment. *Expert Rev Neurother*. (2019) 19:679–94. doi: 10.1080/14737175.2019.1623671
- Wang SS, Yang Y, Velz J, Keller E, Luft A, Regli L, et al. Management of brainstem haemorrhages. *Swiss Med Wkly*. (2019) 149:w20062. doi: 10.4414/smww.2019.20062
- Li Y, Fang W, Tao L, Li M, Yang Y, Gao Y, et al. Efficacy and safety of intravenous nimodipine administration for treatment of hypertension in patients with intracerebral hemorrhage. *Neuropsychiatr Dis Treat*. (2015) 11:1231–8. doi: 10.2147/NDT.S76882
- Selim M, Norton C. Perihematomal edema: implications for intracerebral hemorrhage research and therapeutic advances. *J Neurosci Res*. (2020) 98:212–8. doi: 10.1002/jnr.24372
- Gusdon AM, Gialdini G, Kone G, Baradaran H, Merkler A, et al. Neutrophil-lymphocyte ratio and perihematomal edema growth in intracerebral hemorrhage. *Stroke*. (2017) 48:2589–92. doi: 10.1161/STROKEAHA.117.018120
- Wang X, Arima H, Yang J, Zhang S, Wu G, Woodward M, et al. Mannitol and outcome in intracerebral hemorrhage: propensity score and multivariable intensive blood pressure reduction in acute cerebral hemorrhage trial 2 results. *Stroke*. (2015) 46:2762–7. doi: 10.1161/STROKEAHA.115.009357
- Lim-Hing K, Rincon F. Secondary hematoma expansion and perihemorrhagic edema after intracerebral hemorrhage: from bench work to practical aspects. *Front Neurol*. (2017) 8:74. doi: 10.3389/fneur.2017.00074
- Hall AN, Weaver B, Liotta E, Maas MB, Faigle R, Mroczek DK, et al. Identifying modifiable predictors of patient outcomes after

Conflict of interest

Author ZD was employed by Huiying Medical Technology Co., Ltd.

The remaining authors declare that the research was conducted in the absence of any commercial or financial relationships that could be construed as a potential conflict of interest.

Publisher's note

All claims expressed in this article are solely those of the authors and do not necessarily represent those of their affiliated organizations, or those of the publisher, the editors and the reviewers. Any product that may be evaluated in this article, or claim that may be made by its manufacturer, is not guaranteed or endorsed by the publisher.

Supplementary material

The Supplementary Material for this article can be found online at: <https://www.frontiersin.org/articles/10.3389/fneur.2022.982928/full#supplementary-material>

- intracerebral hemorrhage with machine learning. *Neurocrit Care*. (2021) 34:73–84. doi: 10.1007/s12028-020-00982-8
- Pasi M, Casolla B, Kyheng M, Boulouis G, Kuchcinski G, Moulin S, et al. Long-term functional decline of spontaneous intracerebral haemorrhage survivors. *J Neurol Neurosurg Psychiatry*. (2021) 92:249–54. doi: 10.1136/jnnp-2020-324741
- Zou J, Chen H, Liu C, Cai Z, Yang J, Zhang Y, et al. Development and validation of a nomogram to predict the 30-day mortality risk of patients with intracerebral hemorrhage. *Front Neurosci*. (2022) 16:942100. doi: 10.3389/fnins.2022.942100
- Kang H, Cai Q, Gong L, Wang Y. Nomogram prediction of short-term outcome after intracerebral hemorrhage. *Int J Gen Med*. (2021) 14:5333–43. doi: 10.2147/IJGM.S330742
- Yu J, Yuan Q, Sun YR, Wu X, Du Z, Li Z, et al. Effects of deferoxamine mesylate on hematoma and perihematomal edema after traumatic intracerebral hemorrhage. *J Neurotrauma*. (2017) 34:2753–9. doi: 10.1089/neu.2017.5033
- Wu TY, Sharma G, Strbian D, Putaala J, Desmond P, Tatlisumak T, et al. Natural history of perihematomal edema and impact on outcome after intracerebral hemorrhage. *Stroke*. (2017) 48:873–9. doi: 10.1161/STROKEAHA.116.014416
- Urday S, Beslow LA, Dai F, Zhang F, Battery T, Vashkevich A, et al. Rate of perihematomal edema expansion predicts outcome after intracerebral hemorrhage. *Crit Care Med*. (2016) 44:790–7. doi: 10.1097/CCM.0000000000001553
- Gillies RJ, Kinahan PE, Hricak H. Radiomics: images are more than pictures, they are data. *Radiology*. (2016) 278:563–77. doi: 10.1148/radiol.2015151169
- Porcu M, Solinas C, Mannelli L, Micheletti G, Lambertini M, Willard-Gallo K, et al. Radiomics and “radi-omics” in cancer immunotherapy: a guide for clinicians. *Crit Rev Oncol Hematol*. (2020) 154:103068. doi: 10.1016/j.critrevonc.2020.103068

18. Mayerhoefer ME, Materka A, Langs G, Häggström I, Szczypiński P, Gibbs P, et al. Introduction to radiomics. *J Nucl Med.* (2020) 61:488–95. doi: 10.2967/jnumed.118.222893
19. Yang L, Gu D, Wei J, Yang C, Rao S, Wang W, et al. A radiomics nomogram for preoperative prediction of microvascular invasion in hepatocellular carcinoma. *Liver Cancer.* (2019) 8:373–86. doi: 10.1159/000494099
20. Lambin P, Leijenaar RTH, Deist TM, Peerlings J, de Jong EEC, van Timmeren J, et al. Radiomics: the bridge between medical imaging and personalized medicine. *Nat Rev Clin Oncol.* (2017) 14:749–62. doi: 10.1038/nrclinonc.2017.141
21. Vernuccio F, Cannella R, Comelli A, Salvaggio G, Lagalla R, Midiri M. [Radiomics and artificial intelligence: new frontiers in medicine]. *Recenti Prog Med.* (2020) 111:130–5. doi: 10.1701/3315.32853
22. Rudie JD, Rauschecker AM, Bryan RN, Davatzikos C, Mohan S. Emerging applications of artificial intelligence in neuro-oncology. *Radiology.* (2019) 290:607–18. doi: 10.1148/radiol.2018181928
23. Bruixola G, Remacha E, Jiménez-Pastor A, Dualde D, Viala A, Montón J, et al. Radiomics and radiogenomics in head and neck squamous cell carcinoma: potential contribution to patient management and challenges. *Cancer Treat Rev.* (2021) 99:102263. doi: 10.1016/j.ctrv.2021.102263
24. Guiot J, Vaidyanathan A, Deprez L, Zerka F, Danthine D, Frix A, et al. A review in radiomics: making personalized medicine a reality via routine imaging. *Med Res Rev.* (2022) 42:426–40. doi: 10.1002/med.21846
25. Rodriguez-Luna D, Stewart T, Dowlatshahi D, Kosior JC, Aviv R, Molina C, et al. Perihematomal edema is greater in the presence of a spot sign but does not predict intracerebral hematoma expansion. *Stroke.* (2016) 47:350–5. doi: 10.1161/STROKEAHA.115.011295
26. Grunwald Z, Beslow LA, Urday S, Vashkevich A, Ayres A, Greenberg M, et al. Perihematomal edema expansion rates and patient outcomes in deep and lobar intracerebral hemorrhage. *Neurocrit Care.* (2017) 26:205–12. doi: 10.1007/s12028-016-0321-3
27. Carcel C, Sato S, Zheng D, Heeley E, Arima H, Yang J, et al. Prognostic significance of hyponatremia in acute intracerebral hemorrhage: pooled analysis of the intensive blood pressure reduction in acute cerebral hemorrhage trial studies. *Crit Care Med.* (2016) 44:1388–94. doi: 10.1097/CCM.0000000000001628
28. Appelboom G, Bruce SS, Hickman ZL, Zacharia BE, Carpenter AM, Vaughan KA, et al. Volume-dependent effect of perihematomal oedema on outcome for spontaneous intracerebral haemorrhages. *J Neurol Neurosurg Psychiatry.* (2013) 84:488–93. doi: 10.1136/jnnp-2012-303160
29. Teasdale G, Maas A, Lecky F, Manley G, Stocchetti N, Murray G. The glasgow coma scale at 40 years: standing the test of time. *Lancet Neurol.* (2014) 13:844–54. doi: 10.1016/S1474-4422(14)70120-6
30. Mehta R, Chinthapalli K. Glasgow coma scale explained. *BMJ.* (2019) 365:l1296. doi: 10.1136/bmj.l1296
31. Song Z, Tang Z, Liu H, Guo D, Cai J, Zhou Z. A clinical-radiomics nomogram may provide a personalized 90-day functional outcome assessment for spontaneous intracerebral hemorrhage. *Eur Radiol.* (2021) 31:4949–59. doi: 10.1007/s00330-021-07828-7
32. Faigle R, Chen BJ, Krieger R, Marsh EB, Alkhachroum A, Xiong W, et al. Novel score for stratifying risk of critical care needs in patients with intracerebral hemorrhage. *Neurology.* (2021) 96:e2458–68. doi: 10.1212/WNL.00000000000012682
33. Maas MB, Francis BA, Sangha RS, Lizza BD, Liotta EM, Naidech AM. Refining prognosis for intracerebral hemorrhage by early reassessment. *Cerebrovasc Dis.* (2017) 43:110–6. doi: 10.1159/000452679
34. Johansson K, Jansson JH, Johansson L, Wiklund PG, Nilsson TK, Lind M. D-dimer is associated with first-ever intracerebral hemorrhage. *Stroke.* (2018) 49:2034–9. doi: 10.1161/STROKEAHA.118.021751
35. Zhou Z, Liang Y, Zhang X, Xu J, Kang K, Qu H, et al. Plasma D-dimer concentrations and risk of intracerebral hemorrhage: a systematic review and meta-analysis. *Front Neurol.* (2018) 9:1114. doi: 10.3389/fneur.2018.01114
36. Yao X, Liao L, Han Y, Wei T, Wu H, Wang Y, et al. Computerized tomography radiomics features analysis for evaluation of perihematomal edema in basal ganglia hemorrhage. *J Craniofac Surg.* (2019) 30:e768–71. doi: 10.1097/SCS.00000000000005765
37. Volbers B, Giede-Jeppe A, Gerner ST, Sembill JA, Kuramatsu JB, Lang S, et al. Peak perihemorrhagic edema correlates with functional outcome in intracerebral hemorrhage. *Neurology.* (2018) 90:e1005–12. doi: 10.1212/WNL.00000000000006272
38. Jiang C, Guo H, Zhang Z, Wang Y, Liu S, Lai J, et al. Pathological, clinical, and therapeutic aspects of perihematomal edema in different stages of intracerebral hemorrhage. *Oxid Med Cell Longev.* (2022) 2022:3948921. doi: 10.1155/2022/3948921
39. Loan JJ, Gane AB, Middleton L, Sargent B, Moullaali TJ, Rodrigues MA, et al. Association of baseline hematoma and edema volumes with one-year outcome and long-term survival after spontaneous intracerebral hemorrhage: a community-based inception cohort study. *Int J Stroke.* (2020) 16:828–39. doi: 10.1177/1747493020974282
40. Zwanenburg A, Vallières M, Abdalah MA, Aerts H, Lck S. The image biomarker standardization initiative: standardized quantitative radiomics for high-throughput image-based phenotyping. *Radiology.* (2020) 295:328–38. doi: 10.1148/radiol.2020191145



OPEN ACCESS

EDITED BY

Sheng Zhang,
Zhejiang Provincial People's
Hospital, China

REVIEWED BY

Faheem G. Sherif,
Texas Tech University Health Science
Center, United States
Ayham Alkhachroum,
University of Miami Health System,
United States

*CORRESPONDENCE

Charlene J. Ong
Cjong@bu.edu

†These authors have contributed
equally to this work and share first
authorship

SPECIALTY SECTION

This article was submitted to
Applied Neuroimaging,
a section of the journal
Frontiers in Neurology

RECEIVED 16 September 2022

ACCEPTED 20 October 2022

PUBLISHED 06 December 2022






CITATION

Kim ISY, Balogun OO, Prescott BR,
Saglam H, Olson DM, Speir K,
Stutzman SE, Schneider N, Aguilera V,
Lussier BL, Smirnakis SM, Dupuis J,
Mian A, Greer DM and Ong CJ (2022)
Quantitative pupillometry and
radiographic markers of intracranial
midline shift: A pilot study.
Front. Neurol. 13:1046548.
doi: 10.3389/fneur.2022.1046548

COPYRIGHT

© 2022 Kim, Balogun, Prescott,
Saglam, Olson, Speir, Stutzman,
Schneider, Aguilera, Lussier, Smirnakis,
Dupuis, Mian, Greer and Ong. This is
an open-access article distributed
under the terms of the [Creative
Commons Attribution License \(CC BY\)](#).
The use, distribution or reproduction
in other forums is permitted, provided
the original author(s) and the copyright
owner(s) are credited and that the
original publication in this journal is
cited, in accordance with accepted
academic practice. No use, distribution
or reproduction is permitted which
does not comply with these terms.

Quantitative pupillometry and radiographic markers of intracranial midline shift: A pilot study

Ivy So Yeon Kim^{1,2,3†}, Oluwafemi O. Balogun^{1,2,3†},
Brenton R. Prescott^{1,2,3}, Hanife Saglam^{3,4}, DaiWai M. Olson ⁵,
Kinley Speir⁵, Sonja E. Stutzman ⁵, Nathan Schneider ⁵,
Veronica Aguilera ⁵, Bethany L. Lussier⁵,
Stelios M. Smirnakis^{3,6}, Josée Dupuis^{7,8}, Asim Mian^{1,2},
David M. Greer^{1,2} and Charlene J. Ong ^{1,2,3,4*}

¹Boston University School of Medicine, Boston, MA, United States, ²Boston Medical Center, Boston, MA, United States, ³Mass General Brigham, Boston, MA, United States, ⁴Harvard Medical School, Boston, MA, United States, ⁵University of Texas Southwestern Medical Center, Dallas, TX, United States, ⁶Jamaica Plain Veterans Administration Medical Center, Boston, MA, United States, ⁷Boston University School of Public Health, Boston, MA, United States, ⁸Department of Epidemiology, Biostatistics and Occupational Health, McGill University, Montreal, QC, Canada

Background: Asymmetric pupil reactivity or size can be early clinical indicators of midbrain compression due to supratentorial ischemic stroke or primary intraparenchymal hemorrhage (IPH). Radiographic midline shift is associated with worse functional outcomes and life-saving interventions. Better understanding of quantitative pupil characteristics would be a non-invasive, safe, and cost-effective way to improve identification of life-threatening mass effect and resource utilization of emergent radiographic imaging. We aimed to better characterize the association between midline shift at various anatomic levels and quantitative pupil characteristics.

Methods: We conducted a multicenter retrospective study of brain CT images within 75 min of a quantitative pupil observation from patients admitted to Neuro-ICUs between 2016 and 2020 with large (>1/3 of the middle cerebral artery territory) acute supratentorial ischemic stroke or primary IPH > 30 mm³. For each image, we measured midline shift at the septum pellucidum (MLS-SP), pineal gland shift (PGS), the ratio of the ipsilateral to contralateral midbrain width (IMW/CMW), and other exploratory markers of radiographic shift/compression. Pupil reactivity was measured using an automated infrared pupillometer (NeuroOptics[®], Inc.), specifically the proprietary algorithm for Neurological Pupil Index[®] (NPi). We used rank-normalization and linear mixed-effects models, stratified by diagnosis and hemorrhagic conversion, to test associations of radiographic markers of shift and asymmetric pupil reactivity (Diff NPi), adjusting for age, lesion volume, Glasgow Coma Scale, and osmotic medications.

Results: Of 53 patients with 74 CT images, 26 (49.1%) were female, and median age was 67 years. MLS-SP and PGS were greater in patients with IPH, compared to patients with ischemic stroke (6.2 v. 4.0 mm, 5.6 v. 3.4 mm,

respectively). We found no significant associations between pupil reactivity and the radiographic markers of shift when adjusting for confounders. However, we found potentially relevant relationships between MLS-SP and Diff NPi in our IPH cohort ($\beta = 0.11$, SE 0.04, $P = 0.01$), and PGS and Diff NPi in the ischemic stroke cohort ($\beta = 0.16$, SE 0.09, $P = 0.07$).

Conclusion: We found the relationship between midline shift and asymmetric pupil reactivity may differ between IPH and ischemic stroke. Our study may serve as necessary preliminary data to guide further prospective investigation into how clinical manifestations of radiographic midline shift differ by diagnosis and proximity to the midbrain.

KEYWORDS

pupillometry, neurocritical care, herniation, radiology, midline shift

Introduction

One of the most feared early complications of acute ischemic stroke and intraparenchymal hemorrhage (IPH) is anatomic shift of midline structures (1). Mass effect on midline structures can cause secondary and life-threatening injury (1) and is therefore closely monitored clinically and radiographically. In critically ill patients with acute intracranial injury, mass effect is best visualized through serial radiographic imaging, particularly head Computed Tomography (CT) due to its speed and accessibility. Midline shift, often measured at the septum pellucidum, is a quantitative marker used to assess severity and track mass effect trajectory over time. However, even with CTs serial imaging is logistically limited by scanner and transport availability, timing, and radiation concerns (2, 3). Other modalities, including ultrasound, are dependent on adequate temporal windows, which are not present in a large percentage of patients.

Therefore, current clinical pathways rely on recognition of non-specific clinical signs of deterioration such as decreased arousal, which is also associated with fever, medications, or metabolic abnormalities (4, 5). More objective signs of impending herniation occur late, including ipsilateral or contralateral motor impairment, or subjective recognition of pronounced absence of pupil reactivity and large pupil diameter (size), traditionally referred to as “a fixed and dilated pupil”.

While pupil size and reactivity has historically been assessed qualitatively, the increasing use of automated infrared

pupillometers in neurocritical care offers the opportunity to study the association of both evolving brain injury and evolving *quantitative* pupil characteristics, including constriction velocity, dilation velocity, latency, pupil size, and pupil reactivity *via* the Neurological Pupil Index[®] (NPi) (6). While the use of the device is growing, few studies have rigorously examined the presence and effect sizes of quantitative pupil asymmetry or difference in NPi (**Diff NPi**) and multiple radiographic markers of midline shift or compression.

Understanding the relationship between asymmetric pupil changes and radiographic midline shift has potential high clinical utility. Pupil checks are frequent, non-invasive, and safe. If certain characteristics can identify the presence, relative location, and degree of mass effect, clinicians can more expeditiously and specifically order confirmational radiographic imaging to inform management and prognosis.

To address the need for non-invasive and reproducible bedside indicators of evolving intracranial injury, a better understanding of the relation between quantitative pupil characteristics and radiographic markers of midline shift and compression are needed. Other studies and case series suggest that there is an association between pupil reactivity and midline shift at the level of the septum pellucidum (7) and pineal gland (8). Because pupillary pathways traverse the midbrain, we hypothesized that differences in pupil reactivity would be significantly associated with compression of midline structures, including midline shift at the septum pellucidum (MLS-SP), pineal gland shift (PGS), and unilateral midbrain compression, defined as the ratio of the ipsilateral midbrain width to the contralateral midbrain width (IMW/CMW). A more comprehensive understanding of the relation between midline structure displacement and pupil characteristics could provide clinicians with non-invasive and accessible information to assist in localizing injury and guiding treatment decisions for evolving intracranial pathology.

Abbreviations: CT, Computed Tomography; Diff Npi, Difference in Npi; GCS, Glasgow Coma Scale; IA, Interpeduncular Angle; IMW/CMW, Ratio of The Ipsilateral Midbrain Width/Contralateral Midbrain Width; IPH, Intraparenchymal Hemorrhage; IPS, Interpeduncular Shift; MCA, Middle Cerebral Artery; MLS-SP, Midline Shift at The Septum Pellucidum; MW/ML, Ratio of Midbrain Width to Midbrain Length; NPi, Neurological Pupil Index; PGS, Pineal Gland Shift.

Materials and methods

We conducted a four-center retrospective cohort study of patients with large acute supratentorial ischemic stroke or primary IPH from the Brigham and Women's Hospital (BWH), Massachusetts General Hospital (MGH), Boston Medical Center (BMC), and University of Texas Southwestern Medical Center (UTSW) Neurointensive Care Units admitted between 2016 and 2020. Study participants were selected as a convenience sample of adult patients with radiographic evidence of stroke larger than one third of the Middle Cerebral Artery (MCA) or IPH volume $>30 \text{ mm}^3$ on head CT performed within 75 min of quantitative pupillometry. Seventy-five min was chosen because it provided the best opportunity to obtain quantitatively collected pupil measurements at a close time-period to either emergent or scheduled imaging. CT images are typically obtained by treating clinicians at their discretion. Typical reasons include neurologic decline (including anisocoria), or surveillance imaging in the absence of neurologic decline. At these institutions quantitative pupillometry is standard practice at 2-h (MGB), and at the time of any neurological checks which includes every one, two, or 4 h depending on the frequency of neuro checks ordered (BMC and UTSW). Images were excluded from the analysis if they had significant acute contralateral or posterior fossa injury ($> 1/3$ any vascular territory), had incomplete pupil measurements (missing right or left pupil observations), or were performed after surgical decompression, external ventricular drain placement, or had greater than trace intraventricular hemorrhage.

Data collection

We collected demographic, procedural, Glasgow Coma Scale (GCS) (9), and osmotic medications [including mannitol or hypertonic saline (23.4 or 3%)] from the electronic medical record at home institutions. Quantitative pupillometry data were recorded and collected using the NeuroOptics NPi-200 (NeuroOptics Inc.,) pupillometer. Trained nursing staff conducted quantitative pupillometry as standard of care every 1–2 h in participating neurocritical care units. In addition to recording pupil size and constriction velocity, the pupillometer calculates the Neurological Pupil index (NPi), an algorithm that uses resting and constricted pupil size, percent change, constriction and dilation velocity, and latency (10, 11). NPi values range between 0 and 5. Values <3 are considered “abnormal” and values ≥ 3 normal based on studies of normal populations. Its relation to constriction velocity has been externally examined in prior studies (11). There is no standard practice for administering osmotic medication or image collection following abnormal NPis alone at these institutions.

Digital Imaging and Communications in Medicine (DICOM) head CT images were obtained from each of the

four collaborating centers and were stored in a centralized database (Figure 1). A trained M.D. (FB) standardized head CT images from eligible study participants using semi-automatic registration on AnalyzePro14.0 using the sagittal view as the reference image (Supplementary Figure 1). MLS-SP was measured at the level of the Septum Pellucidum at its maximal deviation from the midline (12). PGS was measured at the level where the pineal gland at its point of maximal deviation as it had the best inter-rater reliability for measurement purposes. Moreover, authors felt that any bias introduced by measuring at the maximal deviation would most likely err toward the null, as some pineal calcifications are significantly larger at baseline than others and less likely result in a spurious positive association. To measure IMW, a straight line was drawn connecting the ipsilateral side of the cerebral peduncle (nearest to the associated temporal lobe) to the midbrain midline defined as the perpendicular line connecting the interpeduncular cistern with the quadrigeminal cistern. CMW was measured by connecting the midbrain midline to the contralateral cerebral peduncle, and the ratio between the two (IMW/CMW) was subsequently calculated. Information on other radiographic markers of midline shift and compression are included in the Supplementary Methods. A two-way intraclass correlation coefficient (ICC) was used to measure the reliability of ratings of radiographic markers that were measured by assigned investigators (IK, OB, and BP). Reliability was interpreted based on the 95% confident interval of the ICC values: <0.5 (poor), $0.5\text{--}0.75$ (moderate), $0.75\text{--}0.9$ (good), and >0.9 (excellent).

The study was approved by our local Institutional Review Boards (H-37699, 2016P002718). The study was exempt from requiring consent because pupillometry assessment remains standard of care and no intervention was introduced to research participants. We prepared this report according to Strengthening the Reporting of Observational Studies in Epidemiology (STROBE) reporting guidelines.

Variables

Our primary outcome was the continuous absolute difference in pupil reactivity between left and right eye (Diff NPi). A description and abbreviations of all quantitative pupil metrics collected and analyzed are included in Supplementary Table 1. Our three primary exposures included MLS-SP, PGS, and IMW/CMW. MLS-SP and PGS were chosen as these markers are frequently quantified and have prior evidence suggesting they are associated with pupillary changes. We selected IMW/CMW as our marker of intrinsic midbrain involvement as we postulated that a marker of midbrain compression would most affect asymmetric pupil reactivity and be less subject to natural variations in baseline configurations of the midbrain than midbrain shift. For our multivariable models, we selected hypothesized confounders

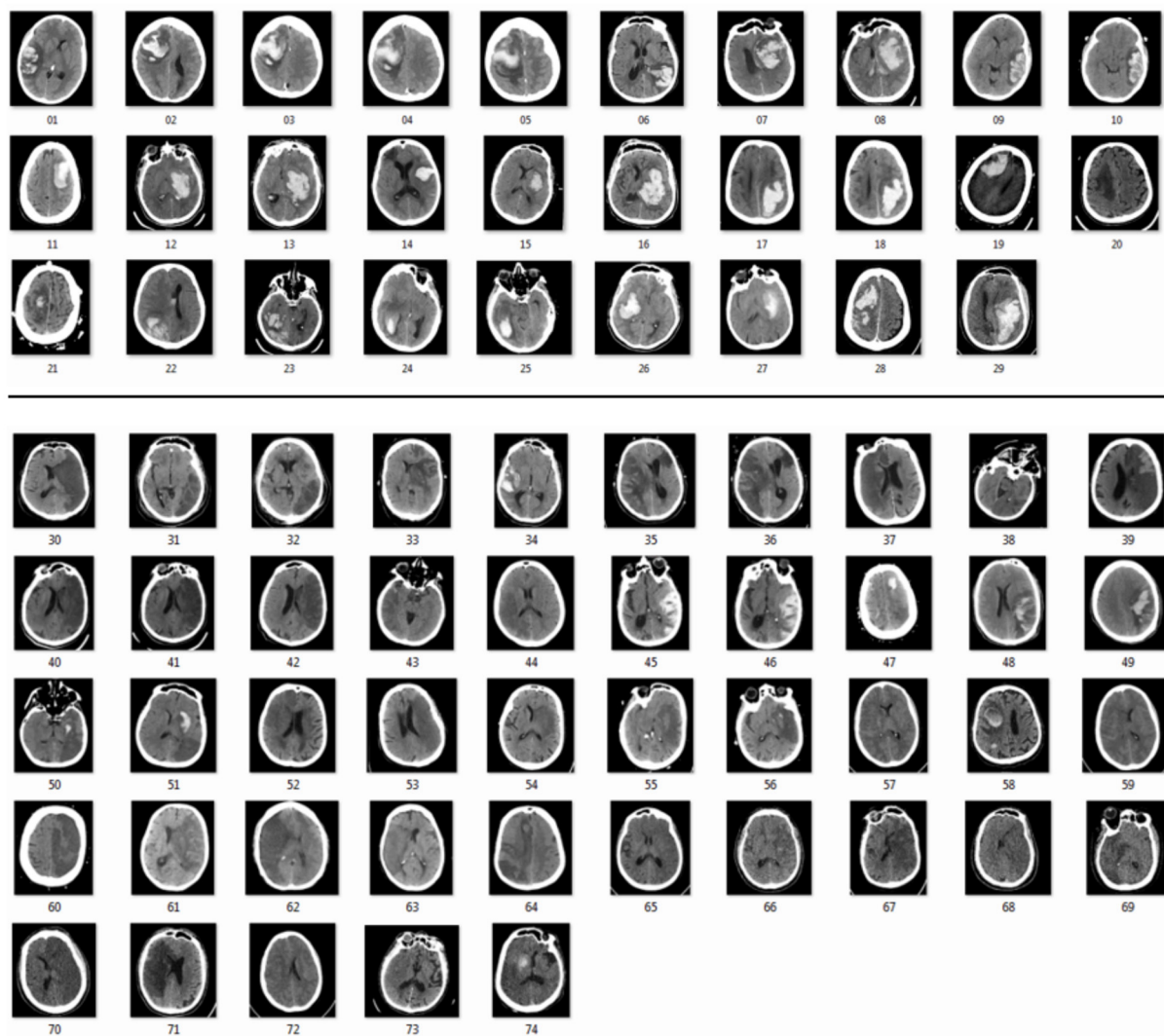


FIGURE 1
Head computed tomography of intraparenchymal hemorrhage patients (01–29) and ischemic stroke patients (30–74) from four different sites from 2016 to 2020.

that affect both pupil reactivity/size and midline shift based on the literature including age (13), lesion volume, arousal *via* the GCS score (14), and osmotic medications (15). Because other pupil influencing medications are not necessarily causally related to radiographic midline shift, these were not included as covariates. However, we have included a list of potentially pupil-influencing medications (Supplementary Table 2) prior to pupil observation in Supplementary Table 3.

Exploratory markers of midline shift and compression included Interpeduncular Shift (IPS)—measured on the axial slice in which the interpeduncular cistern was most visible, as a perpendicular line from the midline connecting the Crista Galli and the Posterior occipital protuberance), the ratio of Midbrain width to midbrain length (MW/ML—defined by the

ratio of the width of the midbrain from cerebral peduncles over the length of the midbrain from the interpeduncular to intercollicular cistern), and the interpeduncular angle (IA—defined as the minimum measured angle between the cerebral peduncles). More information on our protocols are included in Supplementary Methods.

Statistical analysis

Baseline characteristics are reported in Table 1, with median or proportions and interquartile range (IQR) as appropriate. We transformed our pupil variables using rank normalization to satisfy the normality assumption (16). To test the association

TABLE 1 Baseline patient and observation characteristics.

Patient characteristics	Total <i>N</i> = 53 (100%)	Ischemic stroke <i>N</i> = 34 (64.2%)	IPH <i>N</i> = 19 (35.8%)
Demographics and outcomes			
Age	67.0 (62.0–77.0)	66.5 (62.0–79.0)	67.0 (63.0–71.0)
Female	26 (49.1%)	17 (50.0%)	9 (47.4%)
Race			
White	23 (43.4%)	14 (41.2%)	9 (47.4%)
Black	9 (17.0%)	6 (17.7%)	3 (15.8%)
Asian	5 (9.43%)	4 (11.8%)	1 (5.3%)
Unknown*	16 (30.2%)	10 (29.3%)	6 (31.6%)
Ethnicity			
Hispanic	9 (17.0%)	7 (20.6%)	2 (10.5%)
Non-hispanic	42 (79.3%)	26 (76.5%)	16 (84.2%)
Unknown	2 (3.7%)	1 (2.9%)	1 (5.3%)
Medical Institution			
Massachusetts General	23 (43.4%)	12 (35.3%)	11 (57.9%)
Brigham Women's	8 (15.1%)	4 (11.8%)	4 (21.1%)
Boston Medical Center	14 (26.4%)	12 (35.3%)	2 (10.5%)
University of Texas Southwestern	8 (15.1%)	6 (17.6%)	2 (10.5%)
Death at discharge	35 (47.3%)	23 (51.1%)	12 (41.4%)
Observation characteristics	Total <i>M</i> = 74 (100%)	Ischemic stroke <i>M</i> = 45 (60.8%)	IPH <i>M</i> = 29 (39.2%)
Medical institutions			
Massachusetts General Hospital	38 (40.5%)	20 (44.4%)	18 (62.1%)
Brigham Women's Hospital	14 (18.9%)	7 (15.6%)	7 (24.1%)
Boston Medical Center	14 (18.9%)	12 (26.7%)	2 (7.0%)
University of Texas Southwestern	8 (10.8%)	6 (13.3%)	2 (7.0%)
Imaging characteristics			
Lesion volume** (mm ³)	91.8 (53.1–183.0)	115.0 (60.6–248.8)	66.5 (47.0–135.0)
MLS-SP (mm)	4.9 (2.4–8.7)	4.0 (2.2–6.9)	6.2 (3.4–12.1)
PGS (mm)	4.1 (2.7–6.0)	3.4 (2.5–5.1)	5.6 (2.5–6.5)
Quantitative pupil characteristics			
Pupil Obs to head CT (min)	29.0 (21.0–47.8)	30.0 (22.0–50.0)	28.0 (21.0–45.0)
R/L NPi difference	0.2 (0.1–0.5)	0.2 (0.1–0.6)	0.2 (0.1–0.3)
R/L resting diff size (mm)	0.5 (0.2–0.7)	0.5 (0.3–0.7)	0.3 (0.2–0.5)
Average NPi	4.4 (3.7–4.8)	4.5 (3.4–4.8)	4.4 (3.9–4.8)
Covariate characteristics			
GCS within 60 min ¹	10.0 (7.7–12.0)	10.0 (7.0–13.0)	9.0 (8.0–12.0)
Osmotic Med within 60 min	13 (17.6%)	7 (15.6%)	6 (20.7%)

Medians (Q1–Q3) or *N* (%).

IPH, Intraparenchymal Hemorrhage; *M*, Number of head Computed Tomography images; *N*, Number of patients; NPi, Neurological Pupil Index; Obs, Observations; R/L, Right/Left.

*Unknown, Native American, or Hawaiian Pacific Islander.

**Average lesion volume was used if there were more than one Head CT for a given patient.

¹For patients with multiple head CTs, we reported the average of Glasgow Coma Scale closest to imaging.

between our primary outcome, the continuous difference in pupil reactivity (Diff NPi) and radiographic exposures, we first conducted univariate linear mixed effects models accounting

for correlations between patients with multiple scans using a random effect. To assess collinearity between our radiographic markers of interest, we tested correlation based on the Spearman

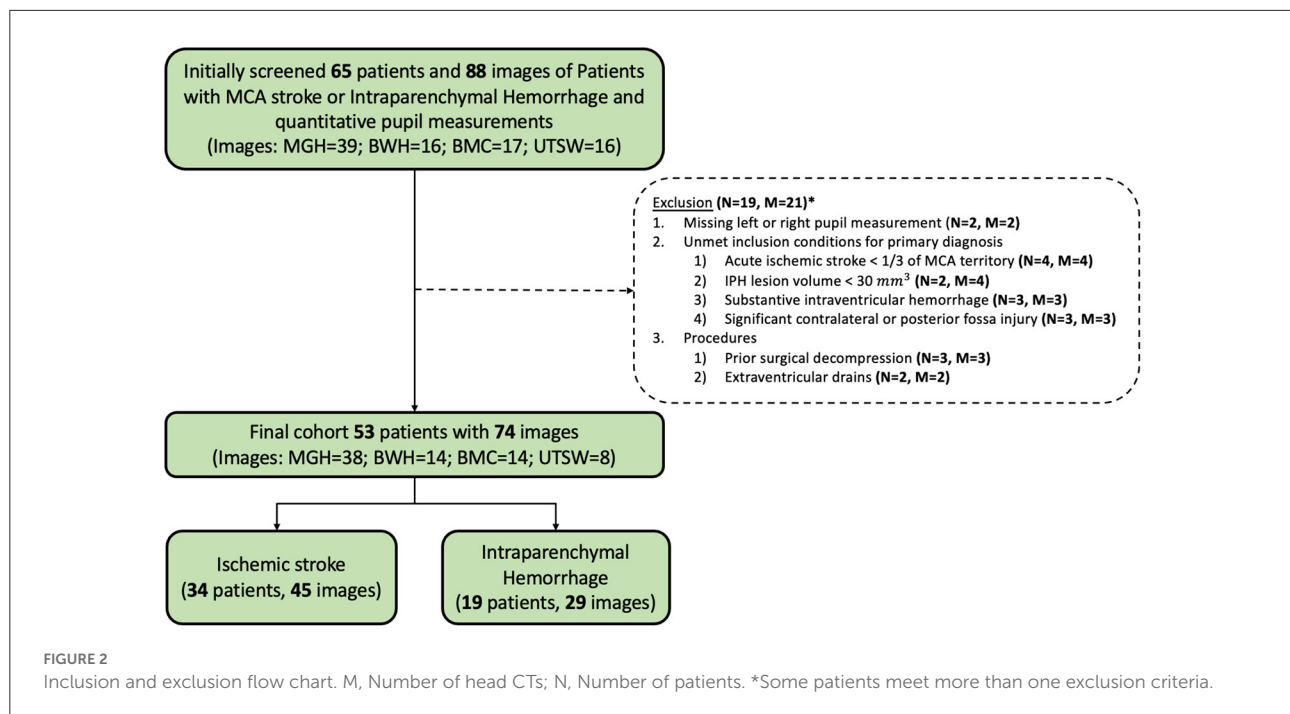


TABLE 2 Univariate models accounting for inter-patient correlation.

	MLS-SP		PGS Max		IMW/CMW	
	Beta (SE)	P	Beta (SE)	P	Beta (SE)	P
Full patient cohort (N = 53, M = 74)						
Diff NPi	0.04 (0.03)	0.11	0.09 (0.05)	0.05	0.41 (0.30)	0.18
Diff size	0.04 (0.03)	0.16	0.02 (0.05)	0.62	0.30 (0.33)	0.37
Min NPi	−0.04 (0.03)	0.15	−0.07 (0.05)	0.12	−0.19 (0.31)	0.55
Ischemic stroke cohort (N = 34, M = 45)						
Diff NPi	0.00 (0.04)	0.93	0.13 (0.06)	0.06	0.65 (0.44)	0.14
Diff size	0.00 (0.04)	0.92	0.06 (0.06)	0.37	0.69 (0.40)	0.09
Min NPi	−0.01 (0.04)	0.75	−0.09 (0.07)	0.16	0.07 (0.45)	0.88
Intraparenchymal hemorrhage cohort (N = 19, M = 29)						
Diff NPi	0.09 (0.03)	<0.01	0.11 (0.06)	0.11	0.19 (0.40)	0.63
Diff size	0.10 (0.04)	0.01	0.08 (0.08)	0.32	−0.07 (0.55)	0.90
Min NPi	−0.08 (0.03)	<0.01	−0.09 (0.06)	0.14	−0.62 (0.42)	0.15

Diff NPi, Absolute difference in left and right Neurologic Pupil Index; Diff Size, Absolute difference in left and right resting pupil size; M, Number of head Computed Tomography images; Min NPi, Minimum NPi of the left and right eye; MLS, Midline Shift at septum pellucidum; N, Number of patients; NPi, Neurological Pupil index; PGS, Pineal Gland Shift; SE, Standard Error.

β coefficients are reported as an increase in one unit of transformed pupil outcome.

coefficient (17). We constructed a multivariable model testing the association of MLS-SP, PGS, and IMW/CMW adjusting for potential confounders. We used two-sided tests and a Benjamini-Hochberg correction with a False Detection Rate of 0.10 to assess significance for our hypotheses that markers of midline shift and compression including MLS-SP, PGS, and IMW/CMW are significantly associated with Diff NPi in our total cohort and ischemic and IPH subgroups (18).

We also conducted exploratory analyses of the association of quantitative pupil characteristics and a comprehensive list of potential radiographic markers of midline shift using similar univariate linear mixed effects models. We used RStudio Version 1.3.959 [(19). RStudio: Integrated Development for R. RStudio, PBC] for statistical analyses. Further details are available in [Supplementary Methods](#).

TABLE 3 Multivariable model assessing Diff NPi and radiographic markers of midline shift.

	Beta (SE)	P
Full patient cohort (N = 53, M = 74)		
MLS-SP	0.01 (0.04)	0.69
PGS	0.07 (0.04)	0.24
IMW/CMW	0.65 (0.37)	0.08
Age	0.01 (0.01)	0.46
Lesion volume	0.00 (0.00)	0.04
GCS	−0.00 (0.05)	0.98
Osmotic medications	0.22 (0.31)	0.48
Ischemic stroke cohort (N = 34, M = 45)		
MLS-SP	−0.05 (0.06)	0.40
PGS	0.17 (0.09)	0.07
IMW/CMW	0.84 (0.52)	0.12
Age	−0.00 (0.02)	0.96
Lesion volume	0.00 (0.00)	0.15
GCS	−0.00 (0.06)	0.99
Osmotic medications	0.20 (0.45)	0.66
Intraparenchymal hemorrhage cohort (N = 19, M = 29)		
MLS-SP	0.11 (0.04)	0.01
PGS	−0.11 (0.08)	0.20
IMW/CMW	0.16 (0.47)	0.74
Age	0.03 (0.02)	0.10
Lesion volume	0.01 (0.00)	0.04
GCS	0.08 (0.07)	0.29
Osmotic medications	0.16 (0.36)	0.67

GCS, Glasgow Coma Scale; IMW/CMW, Ipsilateral Midbrain Width/Contralateral Midbrain Width; MLS-SP, Midline Shift at Septum Pellucidum; PGS, Pineal Gland Shift.

Results

Fifty-three patients with 74 CT scans met our final eligibility criteria. Nineteen patients with 25 scans were excluded for <1/3 MCA territory or <30 cc IPH ($N = 6$), significant contralateral or posterior fossa brain injury ($N = 3$), substantive intraventricular hemorrhage ($N = 3$), external ventricular drains ($N = 2$), prior surgical decompression ($N = 3$), or missing left or right pupil measurements ($N = 2$; [Figure 2](#)). The final cohort consisted of patients with a median age of 67 (IQR: 62–77) years. Twenty-six (49.1%) patients were female, 8 were admitted to BWH, 23 to MGH, 14 to BMC, and 8 to UTSW. Nineteen patients (35.8%) had IPH and 34 patients (64.2%) had ischemic stroke ([Table 1](#)). Ten patients had 2 CTs, four had 3 CTs, and one had 4 CTs used for data analysis.

Of 74 CT scans, the median MLS-SP was 4.9 (2.4–8.7) mm, PGS was 4.1 (1.6–3.4) mm, and IMW/CMW was 0.93 (0.75–1.12). In our cohort, patients with IPH had larger shift and/or compression in midline structures as evidenced by MLS-SP (6.2 v. 4.0 mm), PGS (5.6 v. 3.4 mm),

and IMW/CMW (0.92 v. 0.93). There was moderate correlation between the three primary radiographic outcomes (Spearman coefficient 0.11 for MLS-SP and IMW/CMW, 0.37 for PGS and IMW/CMW, and 0.58 for MLS-SP and PGS, respectively). The intercorrelation coefficients showed good reliability for MLS-SP (0.78; IQR: 0.58–0.88) and IMW/CMW (0.72; IQR: 0.33–0.94), and excellent reliability for PGS (0.90; IQR: 0.81–0.95).

Median Diff NPi among our 74 observations was 0.2 (IQR: 0.1–0.48), median Diff Size was 0.45 (IQR: 0.25, 0.65) mm, and median Min NPi was 4.3 (IQR: 3.4, 4.7). The ischemic stroke group had a median Diff NPi of 0.2, (IQR: 0.1, 0.6), median Diff Size of 0.65 mm (IQR: 0.3–0.74), and median Min NPi of 4.3 (IQR: 3.1–4.7), while the IPH group had a median Diff NPi of 0.2 (IQR: 0.1–0.3), median Diff Size of 0.5 mm (IQR: 0.18–0.5), and median Min NPi of 4.3 (IQR: 3.7–4.7). Median time between pupil observation and imaging was 29 min (IQR: 21–47.8; [Table 1](#), [Supplementary Table 3](#)).

In our linear mixed effect univariate model accounting for intra-patient correlation, we found that PGS was associated with Diff NPi ($P = 0.05$) in the full patient cohort, and MLS-SP was associated with Diff NPi, Diff Size, and min NPi in the IPH Cohort ($p < 0.01$) ([Table 2](#)). A comprehensive list of our univariate associations is included in [Supplementary Tables 4–7](#). After adjusting for confounders in our multivariable model, associations between Diff NPi and radiographic markers of midline shift did not meet the threshold for significance ([Table 3](#)) However, we found an intriguing relationship between Diff NPi and MLS-SP in our IPH subgroup, after adjusting for other markers of midline shift and midbrain compression ($\beta = 0.11$ increase in rank-normalized Diff NPi for every 1 mm increase in MLS-SP, SE 0.04, $P = 0.01$). Similarly, Diff Size was also significantly associated with MLS-SP in our IPH subgroup ($\beta = 0.18$ increase in rank-normalized Diff Size for every 1 mm increase in MLS-SP, SE 0.05, $P < 0.01$) ([Supplementary Table 4](#)). In our ischemic stroke cohort, PGS appeared to have the strongest relation with Diff NPi compared to other radiographic markers ($\beta = 0.17$ increase in rank-normalized Diff NPi for every 1 mm increase in PGS, SE 0.09, $P = 0.07$; [Table 3](#)). In a further subgroup analysis including only ischemic stroke scans with no hemorrhagic conversion, we also found a strong association between PGS and Diff NPi ($\beta = 0.30$, SE 0.12, $P = 0.02$; [Supplementary Table 8](#)).

In our exploratory analyses, we assessed potential relationships between quantitative pupil values and radiographic markers of MLS ([Supplementary Table 9](#)). On further analysis of the association of NPi and MLS-SP in the IPH subgroup, we found that MLS-SP and contralateral NPi appeared to be related ($\beta = -0.08$, SE 0.03, $P = 0.02$). We also observed that in our full cohort, our ratio of IMW/CMW appeared to be significantly and negatively associated with contralateral resting pupil size ($\beta = -0.88$, SE 0.3, $P < 0.01$) and contralateral constriction velocity ($\beta = -0.80$, SE 0.29, $P = 0.01$) suggesting that as the

ipsilateral width decreases in comparison to contralateral width, can affect the opposite pupil ([Supplementary Tables 4–7](#)).

Discussion

Among the constellation of symptoms associated with herniation, asymmetric pupil reactivity and size are perhaps the most classic. Plum and Posner (20) expressed the view that in certain cases the diencephalon would not be the first structure compressed but that pupil signs might be an earlier feature than others in uncal herniation. Ropper and Shafran (21) found that the first indication of oculomotor (third) nerve compression is usually a sluggish or absent light reaction on the side of the mass, which may persist for hours or longer before the pupil actually enlarges.

Building on this background, modern studies have sought to confirm the relationship between quantitative measurement of pupil reactivity/size and evidence of mass effect. Mass effect is commonly clinically quantified by radiographic midline shift, and increased midline shift at various levels including the septum pellucidum and pineal gland have been associated with drowsiness, stupor, and pupil changes in seminal case series (8). In modern investigations, Osman et al. found significant associations in their study of 134 patients with MLS-SP and NPi (7). However, midline shift was associated with the ipsilateral pupil only in the rightward but not leftward direction.

In our study, we present preliminary data seeking further clarification of the relationship between radiographic shift/compression prior to herniation and asymmetric pupil reactivity, or the difference in NPi. Characterizing this relationship can help clinicians better interpret non-invasively measured physiologic characteristics that signify early neurological worsening in acutely ill patients. We hypothesized that like Osman, et al. there is a significant relationship between MLS-SP and difference in NPi. Further, we also hypothesized that there would be a significant association with PGS, as others have found that the pineal gland is more closely associated with diminished arousal. Finally, we explored whether there was a reliable relationship between other radiographic markers of midbrain compression and asymmetric pupil reactivity.

Unlike Osman, et al. (7) we did not find a significant association between markers of radiographic shift and Diff NPi when adjusting for other confounders including age, lesion volume, GCS, and osmotic medications. However, MLS-SP appeared to have a stronger association with asymmetric pupil reactivity in IPH patients than in ischemic stroke patients. We also found that PGS, while also not meeting our predetermined threshold for statistical significance, appeared more strongly associated with Diff NPi in our ischemic stroke cohort than in patients with IPH. PGS continued to appear more strongly associated with Diff NPi in patients with no hemorrhagic transformation. Our findings raise the question of whether

the clinical significance and manifestations of radiographic midline shift at different anatomic levels varies by diagnosis and intracerebral hemorrhage.

One possible hypothesis for why MLS-SP might have a stronger association with IPH may be because of more substantial disruption of cortical pathways responsible for attention that modulate pupil reactivity and size. A recent study showed that pupillary responses and differences in size can be elicited when no differential light is presented nor expected, when participants were asked to recall dark or bright objects, suggesting that attention can play a role in pupil modulation independent of external visual sources (22). While there is no literature that we are aware of studying IPH location and pupil dysfunction, Peinkhofer, et al. (23) evaluated the pupillary light reflex in 25 ischemic stroke patients with insular cortex or prefrontal eye field involvement and compared them to controls. They failed to find a correlation between the pupillary light reflex in the prefrontal eye field or insula (23). If patients with ischemic stroke have less disruption of cortical pupil-modulating pathways compared to patients with IPH when controlling for size, it may be a reason why we observed that MLS-SP is less strongly associated with asymmetric pupil reactivity in the ischemic stroke group.

PGS on the other hand, has been shown in qualitative case series to be strongly associated with decreased level of consciousness, which often but not always accompanies asymmetric change in pupil reactivity (8). However, similar to the discrepancy between the strength of the association of asymmetric pupil reactivity and MLS at the septum pellucidum, we also found that the extent of the association between PGS and Diff NPi also differed between ischemic stroke and IPH cohorts. One possibility for our observation may be related to the dynamic nature of pupillary change.

In our prior work on anisocoria, we found that up to 63% of patients experienced new onset anisocoria (pupil size difference of ≥ 1 mm) at least once during their hospitalization, and that it occurred up to 10% of all pupillary measurements (24). However, after new onset anisocoria occurred, it was often transient. Of the 45 MGH and BMC patients, 28 of the 29 patients who had a Diff NPi of >0.7 (considered abnormal by the manufacturer), normalized within an average of 2.7 h. Whether these values normalized in response to targeted therapy was out of scope for the present study, but these observations demonstrate that pupil characteristics can fluctuate between abnormal and normal values. Others posited that fluctuations in pupil size and shape may be a transtentorial sign before frank pupillary enlargement, and also transient features during recovery of light reaction may represent incomplete stages of compression of the pupilloconstrictor fibers of the third nerve (25). One possible reason for why PGS and Diff NPi did not appear to strongly correlate in the IPH cohort compared to the ischemic stroke cohort may be because Diff NPi may be optimally detected at the time of the more rostral

increase in MLS-SP (which typically occurs prior to PGS) and potentially normalized by the time PGS occurred. While the clinical significance of fluctuating pupil abnormalities is still unclear, foundational work including our methodological and preliminary examination of the relation between radiographic shift and pupil observations close in time is a necessary step toward a better understanding of how to interpret quantitative pupil characteristics.

We did not find meaningful associations between radiographic markers of midbrain compression and pupil reactivity. One reason for why we may not have observed significant associations for some of our markers of midbrain compression include variation in the size and configuration of tentorial openings. Because of wide ranges in the width of the incisura (2–4 cm), and from the edge of the midbrain to the tentorial margin (0–6.6 mm) (26), age-related atrophy may play a role in changing the outline of the opening between patients (27, 28), and almost certainly plays a role in how mass effect shifts rather than compresses neuronal pathways.

Our primary marker, IMW/CMW, appears to have an inverse relationship with both contralateral NPi and constriction velocity (Supplementary Table 3). While it has been reported that initial pupil involvement contralateral to the injury has been seen in up to 10% of pupillary changes due to subdural hematoma (29), there has been no unifying theory to adequately explain its occurrence. Some suggest that contralateral pupil impairment may be due to uncus herniation on the opposite side, while others believe this is almost impossible once the midbrain has shifted over and perimesencephalic cisterns are closed off (25). An alternative mechanism is that the posterior cerebral artery on the side of the mass may be higher than its opposite (resulting in less stretching of the ipsilateral third nerve in comparison to the contralateral side). Ultimately, we agree that different configurations are likely responsible for pupil enlargement (ipsilateral or contralateral) in individual cases due to difference in the shape and size of tentorial openings and in the course of the third nerves (25). Our findings suggest that as the ipsilateral midbrain width decreases in comparison to the contralateral midbrain width, subtle contralateral pupil changes may occur. Whether our observations are simply a product of multiple tests of association, or hints at irritation of the contralaterally running tract of the afferent pupillary light reflex pathway at the level of the midbrain is unclear. Further work would be needed to clarify the association between quantitative contralateral pupil response to acute injury locations.

Limitations and strengths

We acknowledge several limitations to our study. Our sample size is small, limiting how definitively we could assess potentially significant associations. Moreover, in

the measurement of our radiographic markers of interest, differences in imaging angle could impact how data was collected within one axial plane. We also did not have a baseline scan on each patient to use as a comparison. We attempted to mitigate these limitations by a comprehensive protocol for normalization and measurement and included patients who had multiple scans that met criteria adjusting for correlation using linear mixed effects regression. However, though interrater reliability of MLS-SP and PGS was good to excellent, we acknowledge that inter-rater reliability, especially of IMW/CMW, may have limited our ability to accurately observe some relationships. We conducted multiple tests of association, increasing the potential for false positive findings. We attempted to allay the limitation by selecting three primary hypotheses and an appropriate statistical correction. The remainder of our analyses are hypothesis-generating for more definitive studies. Given the transformations that were required to normalize our data, we caution any interpretations concerning effect size. Because our study was observational and retrospective, we cannot exclude residual confounding or establish causal relations. We did not have information on cognitive load, pain, or ambient light levels, which have been reported to affect pupil characteristics (14). We were unable to adjust for all potential residual confounders including potential pupil influencing medications (15, 30), which can affect pupil size and reactivity. However, we have included data that occurred prior to pupil measurements and prior to imaging in Supplementary Table 3.

Despite limitations, our study has the following strengths. We conducted a four-center study with pupil observations conducted within 75 min of a radiographic image to assess the relation between quantitative pupil markers and radiographic markers of midline shift. Other work in this area has previously used larger time windows (6 h) (7), which limits the study of the associations between immediate pupillary reaction in response to mass effect. We comprehensively measured both established and novel markers of shift and compression. We adjusted for patient- and pupil-level covariates including radiographic markers of MLS and compression at various anatomic levels, demographics, osmotic medications, and arousal state. We believe that our results can provide important information for further prospective studies.

Conclusion

Our work describes the methodology and potential associations between radiographic markers of midline shift and quantitative pupil characteristics. The results suggest that the relation between midline shift at various levels and asymmetric pupil reactivity may differ for different diagnoses. Our study may serve as necessary preliminary data to guide further prospective investigation into how clinical manifestations of

radiographic midline shift differ by diagnosis and proximity to the mid.

Data availability statement

Due to protected health information, all data will be made available upon request after appropriate data use agreements with the participating institutions.

Ethics statement

The studies involving human participants were reviewed and approved by Partners Human Research Committee; Harvard Medical Center Integrated Network for Subject Protection In Research; Boston University. Written informed consent for participation was not required for this study in accordance with the national legislation and the institutional requirements.

Author contributions

SMS, DO, and CO conceived and designed the overall study. IK, OB, BP, HS, KS, SES, NS, VA, and BL organized and administered collected data for modeling. AM reviewed interrater reliability. IK, BP, and CO performed statistical analysis. JD reviewed analysis and interpretation. IK, OB, BP, and CO wrote the manuscript. HS, DO, KS, SES, NS, VA, BL, SMS, JD, AM, DG, and CO helped with reviews and revision. CO provided overall study direction and critical

review. All authors contributed to the article and approved the submitted version.

Funding

This study was funded by National Institute of Neurological Disorders and Stroke (NINDS) Research Program Award (NIH/NINDS K23NS116033).

Conflict of interest

The authors declare that the research was conducted in the absence of any commercial or financial relationships that could be construed as a potential conflict of interest.

Publisher's note

All claims expressed in this article are solely those of the authors and do not necessarily represent those of their affiliated organizations, or those of the publisher, the editors and the reviewers. Any product that may be evaluated in this article, or claim that may be made by its manufacturer, is not guaranteed or endorsed by the publisher.

Supplementary material

The Supplementary Material for this article can be found online at: <https://www.frontiersin.org/articles/10.3389/fneur.2022.1046548/full#supplementary-material>

References

- Ong CJ, Gluckstein J, Laurido-Soto O, Yan Y, Dhar R, Lee JM. Enhanced detection of edema in malignant anterior circulation stroke (EDEMA) score: a risk prediction tool. *Stroke*. (2017) 48:1969–72. doi: 10.1161/STROKEAHA.117.016733
- Waydhas C. Intrahospital transport of critically ill patients. *Crit Care*. (1999) 3:R83–9. doi: 10.1186/cc362
- Mettler FA, Huda W, Yoshizumi TT, Mahesh M. Effective doses in radiology and diagnostic nuclear medicine: a catalog. *Radiology*. (2008) 248:254–63. doi: 10.1148/radiol.2481071451
- Khan S, Guerra C, Khandji A, Bauer RM, Claassen J, Wunsch H. Frequency of acute changes found on head computed tomographies in critically ill patients: a retrospective cohort study. *J Crit Care*. (2014) 29:884 e7–12. doi: 10.1016/j.jcrc.2014.05.001
- Sporer KA, Solares M, Durant EJ, Wang W, Wu AH, Rodriguez RM. Accuracy of the initial diagnosis among patients with an acutely altered mental status. *Emerg Med J*. (2013) 30:243–6. doi: 10.1136/emermed-2011-200452
- Olson DM, Fishel M. The use of automated pupillometry in critical care. *Crit Care Nurs Clin North Am*. (2016) 28:101–7. doi: 10.1016/j.cnc.2015.09.003
- Osman M, Stutzman SE, Atem F, Olson D, Hicks AD, Ortega-Perez S, et al. Correlation of objective pupillometry to midline shift in acute stroke patients. *J Stroke Cerebrovasc Dis*. (2019) 28:1902–10. doi: 10.1016/j.jstrokecerebrovasdis.2019.03.055
- Ropper AH. Lateral displacement of the brain and level of consciousness in patients with an acute hemispherical mass. *N Engl J Med*. (1986) 314:953–8. doi: 10.1056/NEJM198604103141504
- Teasdale G, Jennett B. Assessment of coma and impaired consciousness. A practical scale. *Lancet*. (1974) 2:81–4. doi: 10.1016/S0140-6736(74)91639-0
- Olson DM, Stutzman SE, Atem F, Kincaide JD, Ho TT, Carlisle BA, et al. Establishing normative data for pupillometer assessment in neuroscience intensive care: the “END-PANIC” registry. *J Neurosci Nurs*. (2017) 49:251–4. doi: 10.1097/JNN.00000000000000296
- Shoyombo I, Aiyagari V, Stutzman SE, Atem F, Hill M, Figueroa SA, et al. Understanding the relationship between the neurologic pupil index and constriction velocity values. *Sci Rep*. (2018) 8:6992. doi: 10.1038/s41598-018-25477-7
- Kimberly WT, Bevers MB, von Kummer R, Demchuk AM, Romero JM, Elm JJ, et al. Effect of IV glyburide on adjudicated edema endpoints in the GAMES-RP Trial. *Neurology*. (2018) 91:e2163–9. doi: 10.1212/WNL.0000000000000618
- Watson AB, Yellott JJ, A. unified formula for light-adapted pupil size. *J Vision*. (2012) 12:12. doi: 10.1167/12.10.12

14. Larson MD, Behrends M. Portable infrared pupillometry: a review. *Anesth Analg.* (2015) 120:1242–53. doi: 10.1213/ANE.0000000000000314
15. Ong C, Hutch M, Barra M, Kim A, Zafar S, Smirnakis S. Effects of osmotic therapy on pupil reactivity: quantification using pupillometry in critically ill neurologic patients. *Neurocrit Care.* (2019) 30:307–15. doi: 10.1007/s12028-018-0620-y
16. Qiu X, Wu H, Hu R. The impact of quantile and rank normalization procedures on the testing power of gene differential expression analysis. *BMC Bioinformatics.* (2013) 14:124. doi: 10.1186/1471-2105-14-124
17. Dancey CP, Reidy J. *Statistics Without Maths for Psychology: Using Spss for Windows*. Prentice-Hall, Inc.; (2004).
18. Benjamini Y, Hochberg Y. Controlling the false discovery rate: a practical and powerful approach to multiple testing. *J Royal Stat Soc Series B (Methodol).* (1995) 57:289–300. doi: 10.1111/j.2517-6161.1995.tb02031.x
19. RStudio Team (2020). *RStudio: Integrated Development for R*. Boston, MA: RStudio, PBC. Available online at: <http://www.rstudio.com/>
20. Plum F, Posner JB, ebrary Inc. *Plum and Posner's Diagnosis of Stupor and Coma*. New York, Oxford: Oxford University Press.; (2007).
21. Ropper AH, Shafran B. Brain edema after stroke. Clinical syndrome and intracranial pressure. *Arch Neurol.* (1984) 41:26–9. doi: 10.1001/archneur.1984.04050130032017
22. Zokaei N, Board AG, Manohar SG, Nobre AC. Modulation of the pupillary response by the content of visual working memory. *Proceed Nat Acad Sci.* (2019) 116:22802–10. doi: 10.1073/pnas.1909959116
23. Peinkhofer C, Martens P, Grand J, Truelsen T, Knudsen GM, Kjaergaard J, et al. Influence of strategic cortical infarctions on pupillary function. *Front Neurol.* (2018) 9:916. doi: 10.3389/fneur.2018.00916
24. Prescott BR, Saglam H, Duskin JA, Miller MI, Thakur AS, Gholap EA, et al. Anisocoria and poor pupil reactivity by quantitative pupillometry in patients with intracranial pathology. *Crit Care Med.* (2022) 50:e143–53. doi: 10.1097/CCM.0000000000005272
25. Ropper AH. Herniation. In: Wijdicks EF, editor *Handbook of Clinical Neurology* Elsevier. (2008).
26. Ono M, Ono M, Rhoton AL, Barry M. Microsurgical anatomy of the region of the tentorial incisura. *J Neurosurg.* (1984) 60:365–99. doi: 10.3171/jns.1984.60.2.0365
27. Corsellis F. Individual variation in the size of the tentorial opening. *J Neurol Neurosurg Psychiatry.* (1958) 21:279. doi: 10.1136/jnnp.21.4.279
28. Plaut H. Size of the tentorial incisura related to cerebral herniation. *Acta Radiol.* (1963) 1:916–28. doi: 10.1177/028418516300100346
29. Pevehouse B, Bowman W, McKissock W. Ophthalmologic aspects of diagnosis and localization of subdural hematomas. *Neurology.* (1960) 10:1037–41. doi: 10.1212/WNL.10.11.1037
30. Chan WP, Prescott BR, Barra ME, Chung DY, Kim IS, Saglam H, et al. Dexmedetomidine and other analgesedatives alter pupil characteristics in critically ill patients. *Crit Care Explor.* (2022) 4:e0691. doi: 10.1097/CCE.0000000000000691



OPEN ACCESS

EDITED BY

Gabriel Broocks,
University of Hamburg, Germany

REVIEWED BY

Donald Lobsien,
Helios Hospital Erfurt, Germany
Jun Yu,
University of Florida, United States
Jiangyong M. D.,
Spectrum Health, United States

*CORRESPONDENCE

Yu Geng
✉ gengyu@hmc.edu.cn

†These authors have contributed
equally to this work and share first
authorship

SPECIALTY SECTION

This article was submitted to
Applied Neuroimaging,
a section of the journal
Frontiers in Neurology

RECEIVED 30 June 2022

ACCEPTED 05 December 2022

PUBLISHED 04 January 2023

CITATION

Shao Y, Chen X, Wang H, Shang Y,
Xu J, Zhang J, Wang P and Geng Y
(2023) Large mismatch profile predicts
rapidly progressing brain edema in
acute anterior circulation large vessel
occlusion patients undergoing
endovascular thrombectomy.
Front. Neurol. 13:982911.
doi: 10.3389/fneur.2022.982911

COPYRIGHT

© 2023 Shao, Chen, Wang, Shang, Xu,
Zhang, Wang and Geng. This is an
open-access article distributed under
the terms of the [Creative Commons
Attribution License \(CC BY\)](#). The use,
distribution or reproduction in other
forums is permitted, provided the
original author(s) and the copyright
owner(s) are credited and that the
original publication in this journal is
cited, in accordance with accepted
academic practice. No use, distribution
or reproduction is permitted which
does not comply with these terms.

Large mismatch profile predicts rapidly progressing brain edema in acute anterior circulation large vessel occlusion patients undergoing endovascular thrombectomy

Yanqi Shao^{1†}, Xinyi Chen^{2†}, Huiyuan Wang^{1,3}, Yafei Shang^{1,3},
Jie Xu^{1,2}, Jinshi Zhang⁴, Peng Wang¹ and Yu Geng^{1*}

¹Department of Neurology, Center for Rehabilitation Medicine, Zhejiang Provincial People's Hospital, Affiliated People's Hospital, Hangzhou Medical College, Hangzhou, Zhejiang, China,

²Second Clinical Medical College, Zhejiang Chinese Medical University, Hangzhou, China,

³Department of Clinical Medicine, Bengbu Medical College, Bengbu, China, ⁴Department of Nephrology, Urology and Nephrology Center, Zhejiang Provincial People's Hospital, Affiliated People's Hospital, Hangzhou Medical College, Hangzhou, Zhejiang, China

Background: Brain edema is a severe complication in patients with large vessel occlusion (LVO) that can reduce the effectiveness of endovascular therapy (EVT). This study aimed to investigate the association of the perfusion profile at baseline computed tomography (CT) perfusion with rapidly progressing brain edema (RPBE) after EVT in patients with acute anterior LVO.

Methods: We retrospectively reviewed consecutive data collected from 149 patients with anterior LVO who underwent EVT at our center. Brain edema was measured by the swelling score (0–6 score), and RPBE was defined as the swelling score increased by more than 2 scores within 24 h after EVT. We investigated the effect of RPBE on poor outcomes [National Institute of Health Stroke Scale (NIHSS) score and modified Rankin scale (mRS) score at discharge, the occurrence of hemorrhagic transformation, and mortality rate in the hospital] using the Mann–Whitney *U*-test and chi-square test. A multivariate logistic regression model was used to assess the relationship between perfusion imaging parameters and RPBE occurrence.

Results: Overall, 39 patients (26.2%) experienced RPBE after EVT. At discharge, RPBE was associated with higher NIHSS scores ($Z = 3.52$, 95% CI 2.0–12.0, $P < 0.001$) and higher mRS scores ($Z = 3.67$, 95% CI 0.0–1.0, $P < 0.001$) including the more frequent occurrence of hemorrhagic transformation ($\chi^2 = 22.17$, 95% CI 0.29–0.59, $P < 0.001$) and higher mortality rates in hospital ($\chi^2 = 9.54$, 95% CI 0.06–0.36, $P = 0.002$). Univariate analysis showed that intravenous thrombolysis, baseline ischemic core volume, and baseline mismatch ratio correlated with RPBE (all $P < 0.05$). After dividing the mismatch ratio into quartiles and performing a chi-square test between quartiles, we found that the occurrence of RPBE in Q4 (mismatch ratio > 11.3) was significantly lower than that in Q1 (mismatch ratio ≤ 3.0) ($P < 0.05$). The result of multivariate logistic

regression analysis showed that compared with baseline mismatch ratio <5.1 , baseline mismatch ratio between 5.1 and 11.3 (OR:3.85, 95% CI 1.06–14.29, $P = 0.040$), and mismatch ratio >11.3 (OR:5.26, 95% CI 1.28–20.00, $P = 0.021$) were independent protective factors for RPBE.

Conclusion: In patients with anterior circulation LVO stroke undergoing successful EVT, a large mismatch ratio at baseline is a protective factor for RPBE, which is associated with poor outcomes.

KEYWORDS

brain edema, acute ischemic stroke, endovascular thrombectomy, CT-perfusion, ischemic core, penumbra, mismatch ratio

1. Introduction

Brain edema is a devastating complication of acute ischemic stroke, especially with large vessel occlusion (LVO); despite conservative intensive care, the mortality rate of malignant brain edema is still as high as 80% (1). Although endovascular thrombectomy (EVT) based on imaging screening has been shown to be effective and safe in patients with anterior circulation LVO stroke (2–6), approximately 45% of patients still experience poor functional outcomes after EVT (4), among whom recurrent edema is prevalent and might reduce the benefit of EVT (7, 8). Despite the limited treatments for cerebral edema, early decompressive hemicraniectomy can help reduce mortality and increase the possibility of a good functional outcome (9). Therefore, it is important to identify the risk factors for brain edema after stroke to determine the correct perioperative management.

The interaction between reperfusion and cerebral edema remains inconclusive. Experimental and clinical studies yield conflicting results. Cerebral edema deteriorates after reperfusion treatment in animal models (10–12). Nevertheless, in clinical studies, brain edema has been alleviated after recanalization (7, 8, 13). These contradictory results may indicate a complex interaction between reperfusion and edema.

A recent clinical study focused on patients with large hemispheric infarction (core volume 80–300 ml) demonstrated that when the ischemic core volume was <130 ml, reperfusion did not affect midline shift (MLS). Conversely, when the ischemic core volume exceeded 130 ml, recanalization treatment was associated with the prevalent occurrence of MLS because of the intracranial mass effect of cerebral edema (14). Another study showed that when perfusion profiles displayed a large penumbra volume, recanalization treatment was associated with reduced brain edema, but this effect was not detected in patients with a smaller penumbra volume. Whether reperfusion therapy may reduce brain edema when the perfusion profiles showed that the ischemic core volume was minimal to moderate, depends on the penumbral volume (15). These results indicate

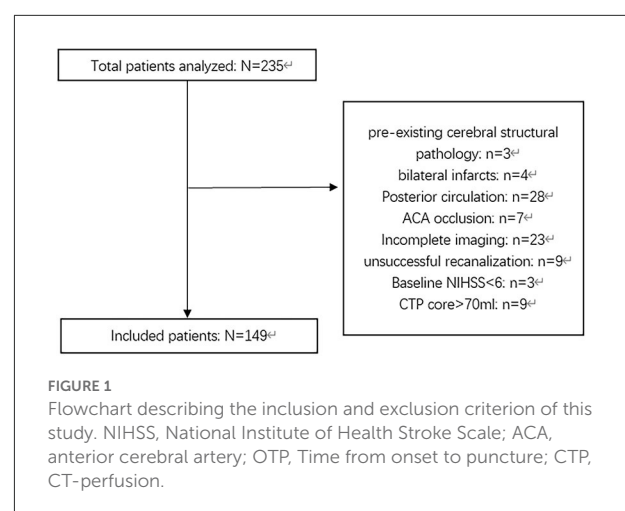
that there seems to be a complicated correlation between perfusion status and cerebral edema, which may be influenced by a combination of factors.

There is currently limited evidence regarding the relationship between the mismatch ratio (penumbra volume/core volume) and cerebral edema in small to moderate ischemic core volume subpopulations. This study aimed to investigate the impact of the mismatch ratio at baseline computed tomography (CT) perfusion on rapidly progressing brain edema (RPBE) within 24 h after successful reperfusion in patients with anterior circulation LVO stroke.

2. Materials and methods

2.1. Patient population

In this study, we retrospectively recruited patients with anterior circulation LVO stroke who underwent successful EVT at a single comprehensive stroke center (Zhejiang Provincial People's Hospital) between January 2020 and December 2021.



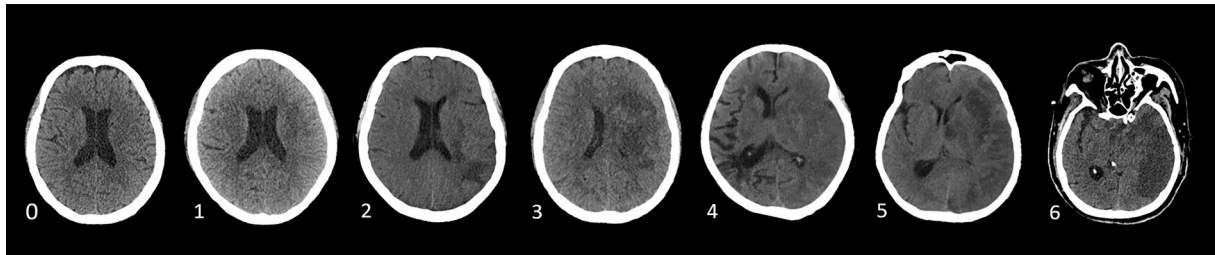


FIGURE 2

Swelling Score (0 score illustrates no swelling; a score of 1 indicates the disappearance of cortical sulci; a score of 2 implies minor effacement of the ipsilateral lateral ventricle; a score of 3 indicates the complete disappearance of the ipsilateral lateral ventricle; a score of 4 indicates the disappearance of the third ventricle; a score of 5 illustrates the shift away of the midline; and a score of 6 indicates the disappearance of basal cisterns) (20).

Patients who met the following inclusion criteria were recruited: (a) age ≥ 18 years old; (b) time from stroke onset to puncture (OTP) ≤ 16 h (stroke onset is defined as the time the patient was last known to be at their neurologic baseline); (c) National Institute of Health Stroke Scale (NIHSS) score at baseline ≥ 6 and modified Rankin Scale score (mRS) before stroke < 2 ; (d) baseline CT angiography confirming the occlusion of the internal carotid artery (ICA) and/or proximal segment (M1 or M2) of the middle cerebral artery (MCA); and (e) for patients with OTP ≥ 6 h, baseline CT perfusion (CTP) confirming an ischemic core volume < 70 ml, and a mismatch ratio (penumbra volume/core volume) > 1.8 . Patients with pre-existing cerebral structural pathology, bilateral infarcts, incomplete images, known allergy to iodine, pregnancy, severe sustained hypertension (defined as systolic blood pressure > 185 mmHg or diastolic blood pressure > 110 mmHg), platelet count $< 50 \times 10^9/L$, known hereditary or acquired hemorrhagic diathesis, coagulation factor deficiency, baseline blood glucose of < 2.78 mmol/L or > 22.20 mmol, modified treatment in cerebral infarction (mTICI) score $< 2b$, and patients who underwent neurosurgical treatments before a 24-h CT or MR scan during the follow-up period were excluded. Figure 1 shows the inclusion and exclusion criteria used in this study.

This study was reviewed and approved by the Ethical Committee of Zhejiang Provincial People's Hospital. All patients or their legal representatives (of patients suffering from severe stroke or who were unable to speak or sign) who were suitable for reperfusion therapy were informed about the study and asked to consent for enrollment at the same time that the informed consent for treatment was provided before the reperfusion treatment. The physician informed the patients or their legal representatives that the patient's clinical and image data would be recorded for analysis and research, but no identifying information would be disclosed and no additional intervening measures would be conducted. All patients or their legal representatives signed the consent without dropping out.

All the procedures were conducted in accordance with the principles of the Declaration of Helsinki. Patient data were stored confidentially in Zhejiang Provincial People's Hospital.

2.2. Image analysis

At baseline, whole-brain dynamic CT angiography and perfusion imaging were performed on a Toshiba Aquilion 320-slice CT scanner (Toshiba Medical Systems, Tokyo, Japan), including a non-contrast CT (NCCT) head scan (120 kV, 320 mA, contiguous 5 mm axial slices) and volume perfusion CT (VPCT) (100 mm in the z-axis, 4 s delay after start of contrast medium injection, 74.5 s total imaging duration, 80 kV, 120 mA, effective dose = 3.68 mSv, slice thickness 10 mm, collimation 32×1.2 mm). A total of 19 consecutive spiral acquisitions were performed. Approximately, 45 ml of iohexol (MEDRAD Stellant D SCT-212; Bayer HealthCare, Berlin, Germany) was injected at a flow rate of 5 ml/s, followed by 30 ml of saline at 4 ml/s.

We used automated commercial software (MISTar; Apollo Medical Imaging Technology, Australia) to reconstruct images and obtain ischemic core volumes, penumbra volumes, and T_{max} maps. Ischemic core volume was defined as baseline relative cerebral blood flow (rCBF) $< 30\%$ (18). The penumbra volume was defined as $T_{max} > 6$ s. The mismatch ratio was calculated by dividing the penumbra volume by the core volume. The collateral index was calculated by dividing the volume of delay time > 6 s by the volume of delay time > 2 s (16). The mTICI score classified the degree of reperfusion (17), and a score of 2b–3 after the EVT procedure was considered a successful recanalization (19).

According to Wardlaw and Sellar (20), brain edema was assessed on a 7-point swelling scale and 0–6 points based

TABLE 1 Baseline characteristics of the study population compared between participants with and without RPBE.

Characteristics		Patients without RPBE (<i>n</i> = 110)	Patients with RPBE (<i>n</i> = 39)	<i>P</i> -value
Age, ys		68 (56, 79)	70 (60, 84)	0.168
Male		65 (59.1)	22 (56.4)	0.770
Admission NIHSS		16 (12, 20)	15 (13, 19)	0.907
Admission mRS		4 (4, 5)	5 (4, 5)	0.247
SBP, mmHg		155.8 ± 28.1	154.3 ± 22.2	0.768
DBP, mmHg		90.4 ± 18.3	89.3 ± 15.4	0.732
Baseline glucose, mmol/L		7.0 (6.1, 8.7)	7.3 (6.5, 9.9)	0.380
Prothrombin time, s		11.9 (11.5, 12.8)	12.0 (11.4, 12.8)	0.841
Platelet count, 10 ⁹ /L		177.5 (147.5, 213.0)	175.0 (117.0, 203.0)	0.260
Hemoglobin, g/L		139.0 ± 20.6	136.0 ± 14.7	0.403
Received thrombolysis		36 (32.7)	20 (51.3)	0.029*
Time from onset to recanalization, min		554.5 (358.0, 870.5)	393.0 (286.8, 585.8)	0.031*
Hypertension		49 (44.5)	20 (51.3)	0.468
Diabetes mellitus		22 (20)	8 (20.5)	0.945
History of stroke		11 (10)	4 (10.3)	0.964
Atrial fibrillation		42 (38.2)	21 (53.8)	0.097
Anticoagulant drugs		30 (27.3)	12 (30.8)	0.677
Antiplatelet drugs		13 (11.8)	8 (20.5)	0.180
TOAST classification	CE	47 (42.7)	20 (51.3)	0.290
	LAA	47 (42.7)	14 (35.9)	
	Others (mainly dissection)	10 (9.1)	1 (2.6)	
	Unknown	6 (5.5)	4 (10.3)	
Baseline brain edema scale	0	41 (37.3)	23 (59.0)	0.051
	1	45 (40.9)	9 (23.1)	
	2	24 (21.8)	7 (17.9)	
ASPECTS		8.0 (6.0, 9.0)	7.0 (6.0, 9.0)	0.219
CTP penumbra volume, ml		102.5 (68.8, 154.3)	116.0 (75.0, 186.0)	0.394
CTP core volume, ml		14.0 (6.0, 31.25)	31.0 (12.0, 65.0)	0.003*
CTP core volume Q1		33 (30)	5 (12.8)	0.029*
CTP core volume Q2		29 (26.4)	9 (23.1)	
CTP core volume Q3		27 (24.5)	9 (23.1)	
CTP core volume Q4		21 (19.1)	16 (41)	
DT + 2 s, ml		161.0 (107.8, 222.0)	167.0 (106.0, 254.0)	0.699
DT + 6 s, ml		27.5 (5.0, 59.0)	38.0 (9.0, 90.0)	0.284
Collateral index		17.5 (4.0, 31.1)	21.7 (7.8, 37.6)	0.300
Collateral index Q1		30 (27.3)	8 (20.5)	0.246
Collateral index Q2		27 (24.5)	10 (25.6)	

(Continued)

TABLE 1 (Continued)

Characteristics		Patients without RPBE (n = 110)	Patients with RPBE (n = 39)	P-value
Collateral index Q3		30 (27.3)	7 (17.9)	
Collateral index Q4		23 (20.9)	14 (35.9)	
Mismatch ratio		5.9 (3.5, 16.6)	3.6 (1.8, 6.9)	<0.001*
Mismatch ratio Q1		23 (20.9)	16 (41.0)	0.005*
Mismatch ratio Q2		23 (20.9)	13 (33.3)	
Mismatch ratio Q3		31 (28.2)	6 (15.4)	
Mismatch ratio Q4		33 (30.0)	4 (10.3)	

Data are demonstrated as mean \pm SD, median (interquartile range), and number (percentage). The chi-Square test/Fisher test and the t-test/Mann-Whitney U-test were conducted to compare categorical and continuous variables between the RPBE and no RPBE groups as appropriate. CTP core volume (ml) in the first through fourth quartiles were ≤ 7 , 7–17, 17–42, and > 42 , respectively; Collateral Index in the first through fourth quartiles were ≤ 4.5 , 4.5–17.9, 17.9–32.4, and > 32.4 , respectively; mismatch ratios in the first through fourth quartiles were ≤ 3.0 , 3.0–5.1, 5.1–11.3, and > 11.3 , respectively.

NIHSS, National Institute of Health Stroke Scale; mRS, modified Rankin scale; TOAST, Trial of Org 10172 in Acute Stroke Treatment; CE, cardio embolism; LAA, large artery atherosclerosis; DBP, diastolic blood pressure; SBP, systolic blood pressure; ASPECTS, Alberta Stroke Program Early CT Score; CTP, computed tomography perfusion; DT, delay time.

* $p < 0.05$.

TABLE 2 The effect of RPBE on poor outcomes in hospital.

Outcomes	Patients without RPBE (n = 110)	Patients with RPBE (n = 39)	Z or χ^2	P-value
Discharge NIHSS, median (IQR)	6.50 (2.00, 15.25)	13.00 (6.00, 40.00)	3.52	<0.001
Discharge mRS, median (IQR)	3.50 (2.00, 4.00)	5.00 (4.00, 5.00)	3.67	<0.001
Hemorrhagic transformation (%)	42 (38.2)	32 (82.1)	22.17	<0.001
Mortality in hospital (%)	8 (7.3)	11 (28.2)	9.54	0.002

Data are demonstrated as median (interquartile range) or number (percentage). The chi-Square test and the Mann-Whitney U-test were conducted to compare categorical and continuous variables between the patients with RPBE and those without RPBE as appropriate.

on NCCT or MRI, which is shown in Figure 2 independently by two trained neurologists (CXY and WHY) blinded to clinical information. RPBE was defined as an increase in the swelling score by more than 2 points on follow-up NCCT or MRI performed 24 h after EVT compared with that at baseline.

2.3. Statistical analysis

All statistical analyses were conducted using statistical software (IBM SPSS Statistics, version 25.0). Two-sided $P < 0.05$ were regarded as statistically significant. Continuous variables were expressed as median or mean, while categorical variables were expressed as numbers with percentages. We performed a univariate logistic regression analysis to investigate the impact of the perfusion profile at baseline CTP on RPBE, including adjustments for potential confounders. Demographic, clinical, laboratory, and imaging variables associated with RPBE at a significance level of $p < 0.05$ were enrolled in the multivariate logistic regression analysis. Results were given as odds ratio (OR) with relative risks of 95% confidence interval (CI).

3. Results

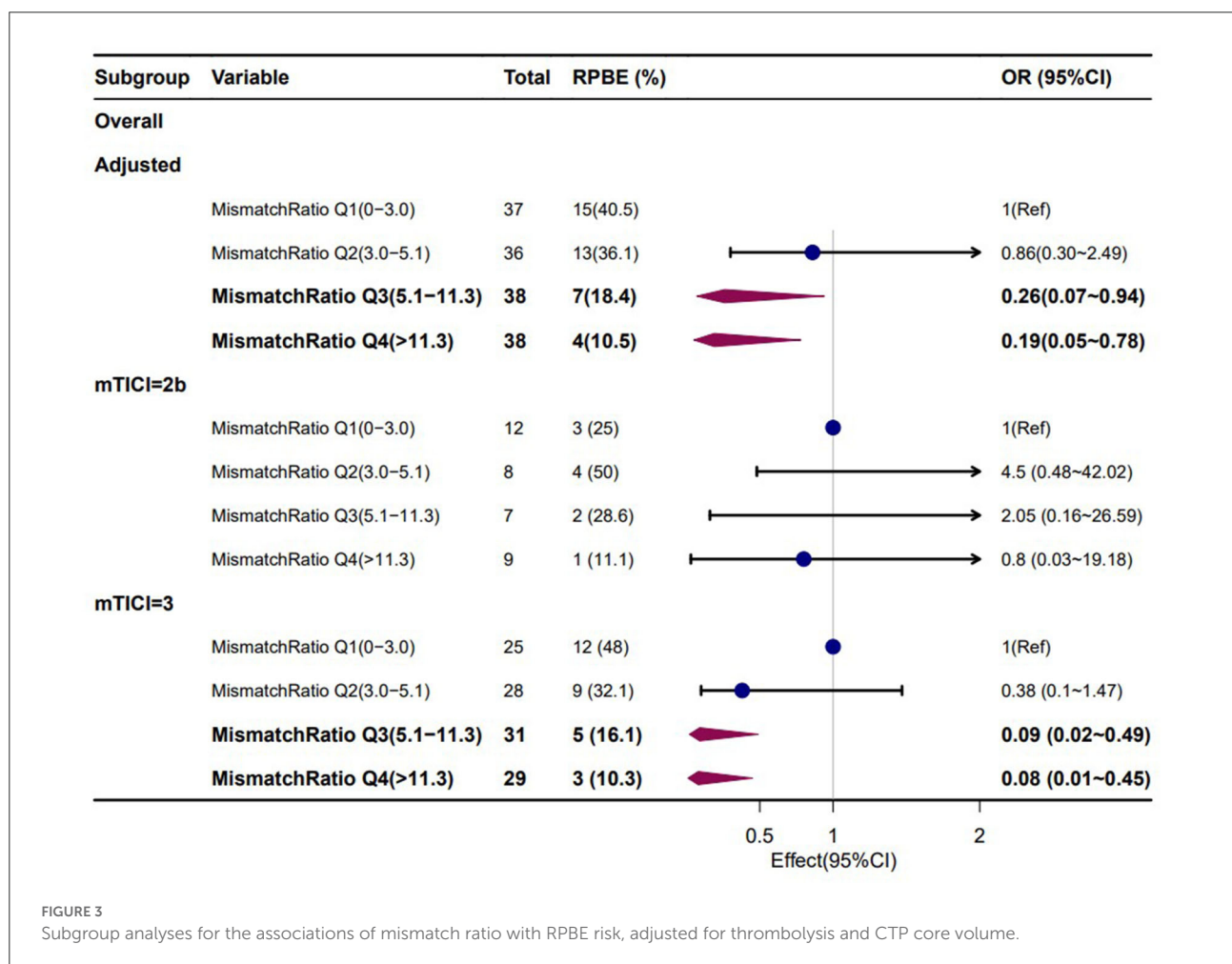
Among 235 patients who underwent EVT, 149 were included in the study (Figure 1). The median age was 68 [interquartile range (IQR) 57.5–80.0] years, and 58.4% of the patients were male. The median values of NIHSS score (at baseline), core volume, and penumbra volume were 16.0 (IQR 12.5–20.0), 17.0 ml (IQR 7.0–43.0), and 107.0 ml (IQR 69.5–167.5), respectively. Overall, 26.2% (39/149) of patients who underwent successful recanalization experienced RPBE after EVT. Table 1 presents the baseline characteristics of the study population compared between the participants with and without RPBE. There were significant differences in the NIHSS ($Z = 3.52$, 95% CI 2.0–12.0, $P < 0.001$) and mRS scores ($Z = 3.67$, 95% CI 0.0–1.0, $P < 0.001$) at discharge between patients with and without RPBE. In addition, the occurrence of hemorrhagic transformation ($\chi^2 = 22.17$, 95% CI 0.29–0.59, $P < 0.001$) and mortality in hospital ($\chi^2 = 9.54$, 95% CI 0.06–0.36, $P = 0.002$) were significantly more prevalent in patients with RPBE (Table 2).

Furthermore, a univariate logistic regression analysis was conducted to observe the correlations between demographic, clinical, and laboratory indicators; ASPECTS at baseline CT;

TABLE 3 Univariate and multivariate logistic regression analyses between demographic, clinical, laboratory indicators, perfusion profile at baseline CT perfusion, and RPBE.

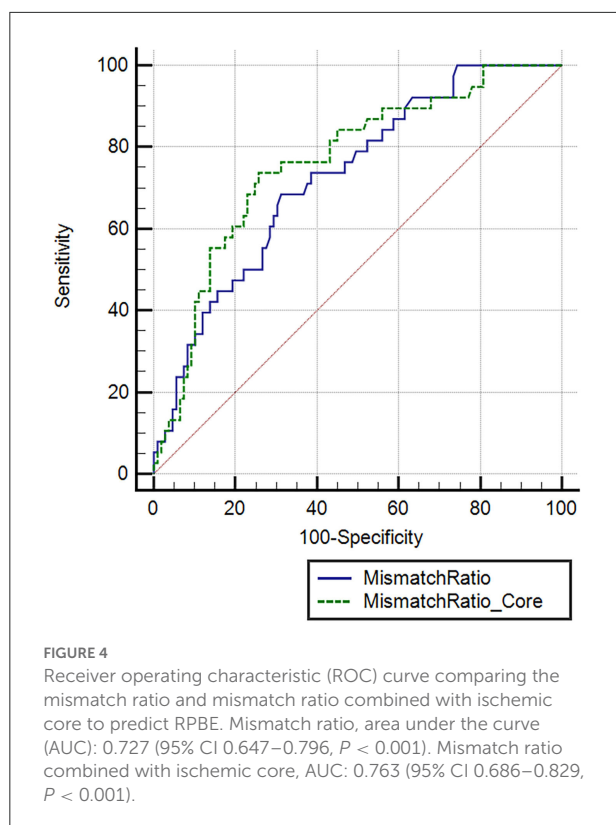
Variables	Univariate logistic regression		Multivariate logistic regression	
	Odds ratio (95% CI)	P-value	Odds ratio (95% CI)	P-value
Received IV thrombolysis	2.28 (1.08–4.84)	0.031*	2.72 (1.20–6.20)	0.017*
CTP core volume	1.01 (1.00–1.02)	0.019*	1.00 (0.99–1.01)	0.644
Mismatch ratio Q3 (5.1–11.3)	0.28 (0.09–0.82)	0.021*	0.26 (0.07–0.94)	0.040*
Mismatch ratio Q4 (>11.3)	0.17 (0.05–0.59)	0.005**	0.19 (0.05–0.78)	0.021*

**p < 0.01; *p < 0.05.



perfusion profile at baseline CTP; and RPBE. The result showed a significant correlation among RPBE and thrombolysis ($P = 0.031$), CTP core volume ($p = 0.019$), mismatch ratio Q3 (IQR 5.1–11.3, $P = 0.021$), and mismatch ratio Q4 (IQR > 11.3, $P = 0.005$). These variables were incorporated into multivariate logistic regression analysis, which revealed that mismatch ratio Q3 (OR 0.26, 95% CI 0.07–0.94, $P = 0.040$) and mismatch ratio Q4 (OR 0.19, 95% CI 0.05–0.78, $P = 0.021$) were the independent protective factors for RPBE (Table 3). A subgroup

analysis indicated that among patients with mTICI 3 scores, mismatch ratio Q3 (OR 0.09, 95% CI 0.02–0.49, $P = 0.005$) and mismatch ratio Q4 (OR 0.08, 95% CI 0.01–0.45, $P = 0.005$) were independent protective factors for RPBE (Figure 3). The area under the curve (AUC) of the receiver operator characteristics (ROC) curve was 0.727 (95% CI 0.647–0.796, $P < 0.001$). Additionally, we found that when the mismatch ratio is >5.1 and the core volume is <42, the protective effect of RPBE was stronger than the mismatch ratio alone;



and the AUC was 0.763 (95% CI 0.686–0.829, $P < 0.001$; Figure 4).

4. Discussion

The primary finding of our study is that RPBE after successful EVT in patients with LVO stroke is related to poor NIHSS and mRS scores at discharge, a more frequent incidence of hemorrhagic transformation, and a higher in-hospital mortality rate. Furthermore, we demonstrated that the mismatch ratio and intravenous thrombolysis were independently associated with RPBE after reperfusion therapy. Our study reveals that a large mismatch ratio is a protective factor for RPBE, which implies that a higher mismatch ratio is related to a lower possibility of RPBE. Specifically, we observed that when the mismatch ratio was >5.1 as the core volume was <42 ml, the protective effect of RPBE was stronger than that of the mismatch ratio alone (AUC 0.763 vs. 0.727).

Many studies suggest that core volume and mismatch volume are associated with brain edema (21–23), which is consistent with the conventional understanding that serious stroke is associated with severe edema (24). Nevertheless, some of these studies did not include patients who

underwent reperfusion therapy and defined brain edema by qualitative measurements, such as midline shift >5 mm or occurrence of cerebral hernia requiring hemicraniectomy. These measurements are not sensitive to mild or moderate edema; therefore, they are unsuitable for accurately monitoring a patient's condition. Identifying patients with a high risk of brain edema early is critical. This study provides a new way to assess the RPBE (an increase of more than two points in cerebral edema mass effect within 24 h). The occurrence of RPBE observed in this study (26.2%) is comparable with the 24 h net water uptake observed in previous research (20.6–22.0%) (25, 26). Although RPBE is a semi-quantitative assessment, it shows the predictive value for poor early clinical outcomes (Table 2), which is consistent with previous studies (7, 8, 27).

Considering reperfusion's effect on cerebral edema may be complicated and dependent on the perfusion profile of the ischemic tissue. Ng et al. found that recanalization was associated with reduced cerebral edema when the mismatched volume was larger than 102 ml. However, this interaction between recanalization and edema was not observed in patients with smaller mismatch volumes. A large mismatch volume indicated increased brain edema in patients who underwent unsuccessful reperfusion therapy but not in those with successful reperfusion (15). A recent clinical study focused on patients with large hemispheric infarction (core volume 80–300 ml) demonstrated that reperfusion did not affect MLS when the ischemic core volume was smaller than 130 ml. Conversely, recanalization treatment was associated with the prevalent occurrence of MLS because of the intracranial mass effect of cerebral edema when the ischemic core volume exceeded 130 ml of edema (14). These results indicate that there is a seemingly complicated correlation between perfusion status and cerebral edema, which may be influenced by a combination of factors. In contrast to previous studies, our study focused on populations with small to moderate ischemic core volume (median 17.0 ml, IQR 7.0–43.0) who underwent successful recanalization with mTICI scores of 2b to 3. Univariate analysis showed that the baseline ischemic core volume and baseline mismatch ratio were correlated with RPBE ($P < 0.05$). After dividing the mismatch ratio into quartiles and performing a chi-square test between quartiles, we found that the occurrence of RPBE in Q4 (mismatch ratio > 11.3) was significantly lower than that in Q1 (mismatch ratio ≤ 3.0) ($P < 0.05$). Multivariate logistic regression analysis revealed that mismatch ratio Q3 (OR 0.26, 95% CI 0.07–0.94, $P = 0.040$) and mismatch ratio Q4 (OR 0.19, 95% CI 0.05–0.78, $P = 0.021$) were the independent protective factors for RPBE (Table 3); the AUC-ROC curve was 0.727 (95% CI 0.647–0.796, $P < 0.001$). Furthermore, we observed that when the mismatch ratio was >5.1 and core volume was < 42 ml, the protective effect of RPBE was stronger than that of the mismatch ratio

alone. The AUC was 0.763 (95% CI 0.686–0.829, $P < 0.001$; Figure 3).

The primary mechanism of cerebral edema is microvascular dysfunction and blood–brain barrier (BBB) disruption. Increased CBF volume during reperfusion is correlated with aggravation of BBB disruption (11). Approximately 26.7% of patients after endovascular treatment were found to have early BBB disruption on CT (28). Animal experiments have shown that rapidly progressing cerebral edema may occur after LVO, and increased BBB permeability was observed 20–155 min after MCA occlusion (29). A recent study reported that a larger edema volume within 24 h was associated with more edema and lesion progression (25). The mismatch ratio is the ratio of the penumbra volume to the infarct core volume, combining the infarct core with the mismatched volume. A high mismatch ratio indicates a large penumbra with a comparatively small infarct core, which is equivalent to a higher proportion of salvageable tissue. To our knowledge, this is the first study to assess early-phase edema progression with semi-quantified measurement and to reveal an interaction between RPBE with combined perfusion profiles of the ischemic core and mismatch ratio. These findings have several potential clinical implications, according to these results. Assessment of the ischemic core volume and mismatch ratio could provide prognostic information for predicting RPBE and help identify patients who are at high risk for edema and may require particular intervention.

Our study has some limitations. First, brain edema was classified into seven grades, and an increase in edema score of more than 2 points was defined as edema progression, which is a categorical variable. More accurate quantitative research is required in future. Second, the edema score is related to the degree of lateral ventricle compression; hence, patients with infarction foci close to the cortex are less likely to improve the edema score later, which may lead to bias. Third, as the implementation of mechanical thrombectomy referred to the DEFUSE 3 criteria, which required relatively small infarct cores (<70 ml), the median core volume in our study was as small as 17.0 ml (IQR 7.0–43.0). Therefore, this may lead to selection bias; thus, the progress of brain edema after thrombectomy in patients with large infarct cores is unclear.

5. Conclusion

For anterior circulation LVO stroke patients with successful EVT, RPBE is associated with poor outcomes. A large mismatch ratio at baseline is a protective factor for RPBE in patients with mild-to-moderate core volume. Furthermore, these results could help identify patients

with a high risk of edema and who probably require appropriate intervention.

Data availability statement

The raw data supporting the conclusions of this article will be made available by the authors, without undue reservation.

Ethics statement

The studies involving human participants were reviewed and approved by the Ethical Committee of Zhejiang Provincial Peoples' Hospital. The patients/participants provided their written informed consent to participate in this study.

Author contributions

YShao and YG designed the study. XC, HW, JX, and YShan collected the data. YShao, XC, and JZ performed the statistical analysis, interpreted the results, and drafted the article. YShao, XC, YG, and PW critically revised the article. All authors contributed to the article and approved the submitted version.

Funding

This study was supported by the Medical Health Science and Technology Project of Zhejiang Provincial Health Commission under Grant Nos. 2020KY415 and 2021KY489.

Conflict of interest

The authors declare that the research was conducted in the absence of any commercial or financial relationships that could be construed as a potential conflict of interest.

Publisher's note

All claims expressed in this article are solely those of the authors and do not necessarily represent those of their affiliated organizations, or those of the publisher, the editors and the reviewers. Any product that may be evaluated in this article, or claim that may be made by its manufacturer, is not guaranteed or endorsed by the publisher.

References

- Hofmeijer J, Algra A, Kappelle LJ, van der Worp HB. Predictors of life-threatening brain edema in middle cerebral artery infarction. *Cerebrovasc Dis.* (2008) 25:176–84. doi: 10.1159/000113736
- Saver JL, Goyal M, Bonafe A, Diener HC, Levy EI, Pereira VM, et al. Stent-retriever thrombectomy after intravenous t-PA vs. t-PA alone in stroke. *N Engl J Med.* (2015) 372:2285–95. doi: 10.1056/NEJMoa1415061
- Campbell BC, Mitchell PJ, Kleinig TJ, Dewey HM, Churilov L, Yassi N, et al. Endovascular therapy for ischemic stroke with perfusion-imaging selection. *N Engl J Med.* (2015) 372:1009–18. doi: 10.1056/NEJMoa1414792
- Goyal M, Demchuk AM, Menon BK, Eesa M, Rempel JL, Thornton J, et al. Randomized assessment of rapid endovascular treatment of ischemic stroke. *N Engl J Med.* (2015) 372:1019–30. doi: 10.1056/NEJMoa1414905
- Berkhemer OA, Fransen PS, Beumer D, van den Berg LA, Lingsma HF, Yoo AJ, et al. A randomized trial of intraarterial treatment for acute ischemic stroke. *N Engl J Med.* (2015) 372:11–20. doi: 10.1056/NEJMoa1411587
- Jovin TG, Chamorro A, Cobo E, de Miquel MA, Molina CA, Rovira A, et al. Thrombectomy within 8 hours after symptom onset in ischemic stroke. *N Engl J Med.* (2015) 372:2296–306. doi: 10.1056/NEJMoa1503780
- Kimberly WT, Dutra BG, Boers AMM, Alves HCBR, Berkhemer OA, van den Berg L, et al. Association of reperfusion with brain edema in patients with acute ischemic stroke: a secondary analysis of the mrc clean trial. *JAMA Neurol.* (2018) 75:453–61. doi: 10.1001/jamaneurol.2017.5162
- Thorén M, Dixit A, Escudero-Martínez I, Gdovinová Z, Klecka L, Rand VM, et al. Effect of recanalization on cerebral edema in ischemic stroke treated with thrombolysis and/or endovascular therapy. *Stroke.* (2020) 51:216–23. doi: 10.1161/STROKEAHA.119.026692
- Dower A, Mulcahy M, Maharaj M, Chen H, Lim CED, Li Y, et al. Surgical decompression for malignant cerebral oedema after ischaemic stroke. *Cochrane Database Syst Rev.* (2022) 11:CD014989. doi: 10.1002/14651858.CD014989.pub2
- Dzialowski I, Klotz E, Goericke S, Doerfler A, Forsting M, Kummer RV. Ischemic brain tissue water content: CT monitoring during middle cerebral artery occlusion and reperfusion in rats. *Radiology.* (2007) 243:720–6. doi: 10.1148/radiol.2432060137
- Yang GY, Betz AL. Reperfusion-induced injury to the blood-brain barrier after middle cerebral artery occlusion in rats. *Stroke.* (1994) 25:1658–64. doi: 10.1161/01.STR.25.8.1658
- Pillai DR, Dittmar MS, Baldaranov D, Heidemann RM, Henning EC, Schuierer G, et al. Cerebral ischemia-reperfusion injury in rats—A 3 T Mri study on biphasic blood-brain barrier opening and the dynamics of edema formation. *J Cereb Blood Flow Metab.* (2009) 29:1846–55. doi: 10.1038/jcbfm.2009.106
- Broocks G, Hanning U, Flottmann F, Schönfeld M, Faizy TD, Sporns P, et al. Clinical benefit of thrombectomy in stroke patients with low aspects is mediated by oedema reduction. *Brain.* (2019) 142:1399–407. doi: 10.1093/brain/awz057
- Ng FC, Yassi N, Sharma G, Brown SB, Goyal M, Majoie CBLM, et al. Cerebral edema in patients with large hemispheric infarct undergoing reperfusion treatment: a Hermes meta-analysis. *Stroke.* (2021) 52:3450–8. doi: 10.1161/STROKEAHA.120.033246
- Ng FC, Churilov L, Yassi N, Kleinig TJ, Thijs V, Wu TY, et al. Association between pre-treatment perfusion profile and cerebral edema after reperfusion therapies in ischemic stroke. *J Cereb Blood Flow Metab.* (2021) 41:2887–96. doi: 10.1177/0271678X211017696
- Campbell BC, Christensen S, Levi CR, Desmond PM, Donnan GA, Davis SM, et al. Cerebral blood flow is the optimal Ct perfusion parameter for assessing infarct core. *Stroke.* (2011) 42:3435–40. doi: 10.1161/STROKEAHA.111.618355
- Nael K, Sakai Y, Larson J, Goldstein J, Deutsch J, Awad AJ, et al. Ct perfusion collateral index in assessment of collaterals in acute ischemic stroke with delayed presentation: comparison to single phase Cta. *J Neuroradiol.* (2022) 49:198–204. doi: 10.1016/j.neurad.2021.11.002
- Osama O, Albert J, Pooja K, Thomas A, Rüdiger V, Jeffrey L, et al. Recommendations on angiographic revascularization grading standards for acute ischemic stroke: a consensus statement. *J Cereb Circulat.* (2013) 44:2650–63. doi: 10.1161/STROKEAHA.113.001972
- Liebeskind DS, Bracard S, Guillemin F, Jahan R, Jovin TG, Majoie CB, et al. Ertic reperfusion: defining success in endovascular stroke therapy. *J Neurointerv Surg.* (2019) 11:433–8. doi: 10.1136/neurintsurg-2018-014127
- Wardlaw JM, Sellar A. A simple practical classification of cerebral infarcts on Ct and its interobserver reliability. *AJNR Am J Neuroradiol.* (1994) 15:1933–9.
- Bektas H, Wu TC, Kasam M, Harun N, Sitton CW, Grotta JC, et al. Increased blood-brain barrier permeability on perfusion Ct might predict malignant middle cerebral artery infarction. *Stroke.* (2010) 41:2539–44. doi: 10.1161/STROKEAHA.110.591362
- Minnerup J, Wersching H, Ringelstein EB, Heindel W, Niederstadt T, Schilling M, et al. Prediction of malignant middle cerebral artery infarction using computed tomography-based intracranial volume reserve measurements. *Stroke.* (2011) 42:3403–9. doi: 10.1161/STROKEAHA.111.619734
- Firlik AD, Yonas H, Kaufmann AM, Wechsler LR, Jungreis CA, Fukui MB, et al. Relationship between cerebral blood flow and the development of swelling and life-threatening herniation in acute ischemic stroke. *J Neurosurg.* (1998) 89:243–9. doi: 10.3171/jns.1998.89.2.0243
- Wu S, Yuan R, Wang Y, Wei C, Zhang S, Yang X, et al. Early prediction of malignant brain edema after ischemic stroke. *Stroke.* (2018) 49:2918–27. doi: 10.1161/STROKEAHA.118.022001
- Konduri P, van Kranendonk K, Boers A, Treurniet K, Berkhemer O, Yoo AJ, et al. The role of edema in subacute lesion progression after treatment of acute ischemic stroke. *Front Neurol.* (2021) 12:705221. doi: 10.3389/fneur.2021.705221
- Broocks G, Hanning U, Faizy TD, Scheibel A, Nawabi J, Schön G, et al. Ischemic lesion growth in acute stroke: water uptake quantification distinguishes between edema and tissue infarct. *J Cereb Blood Flow Metab.* (2020) 40:823–32. doi: 10.1177/0271678X19848505
- Strbian D, Meretoja A, Putaala J, Kaste M, Tatlisumak T, Helsinki Stroke Thrombolysis Registry Group. Cerebral edema in acute ischemic stroke patients treated with intravenous thrombolysis. *Int J Stroke.* (2013) 8:529–34. doi: 10.1111/j.1747-4949.2012.00781.x
- Shi ZS, Duckwiler GR, Jahan R, Tateshima S, Szeder V, Saver JL, et al. Early blood-brain barrier disruption after mechanical thrombectomy in acute ischemic stroke. *J Neuroimaging.* (2018) 28:283–8. doi: 10.1111/jon.12504
- Gerriets T, Walberer M, Ritschel N, Tschernatsch M, Mueller C, Bachmann G, et al. Edema formation in the hyperacute phase of ischemic stroke. Laboratory investigation. *J Neurosurg.* (2009) 111:1036–42. doi: 10.3171/2009.3.JNS081040

Frontiers in Neurology

Explores neurological illness to improve patient care

The third most-cited clinical neurology journal explores the diagnosis, causes, treatment, and public health aspects of neurological illnesses. Its ultimate aim is to inform improvements in patient care.

Discover the latest Research Topics

[See more →](#)

Frontiers

Avenue du Tribunal-Fédéral 34
1005 Lausanne, Switzerland
frontiersin.org

Contact us

+41 (0)21 510 17 00
frontiersin.org/about/contact

